Modeling and information reconstruction from landslide monitoring data

Mohit Mishra

Université Grenoble Alpes

THÈSE

Pour obtenir le grade de

DOCTEUR DE L'UNIVERSITÉ GRENOBLE ALPES

Spécialité : **Automatique-Productique (AP)**

Arrêtée ministériel : 25 mai 2016

Présentée par

Mohit MISHRA

Thèse dirigée par **Gildas BESANÇON (Grenoble INP) et Guillaume CHAMBON (INRAE)**
Codirigéee par **Laurent BAILLET (ISTerre)**

préparée au sein du **Laboratoire GIPSA-lab**
dans **l'École Doctorale EEATS**

Modeling and information reconstruction from landslide monitoring data

Thèse soutenue publiquement le **25/04/2022**,
devant le jury composé de :

M. Didier GEORGES
Grenoble INP, Président

Mme Stéphanie GAUTIER
Université de Montpellier, Rapporteure

M. Romain POSTOYAN
CNRS CRAN, Rapporteur

Mme Séverine BERNARDIE
Bureau de Rercherches Géologiques et Minières, Examinatrice

M. Gildas BESANCON
Grenoble INP, Directeur de thèse

M. Guillaume CHAMBON
INRAE, Co-Directeur de thèse

M. Laurent BAILLET
ISTerre, Co-Directeur de thèse, Invité

"To my Grandmother"

Acknowledgments

This work has been supported by the French National Research Agency in the framework of the Investissements d'Avenir program (ANR-15-IDEX-02) and Cross-Disciplinary project RISK@UGA.

Working as a Ph.D. student has been a long journey with an immersion into the life of a young researcher. During this period, I have met many friendly people who made this experience special. It is a humbling experience to acknowledge those people who have, mostly out of kindness, helped along my Ph.D. journey. I am indebted to so many for encouragement and support.

First of all, from the bottom of my heart, I would like to say a big thank you to my supervisors Prof. Gildas Besançon, Prof. Guillaume Chambon, and Prof. Laurent Baillet, for their kindness, noble guidance, availability, and support with full encouragement and enthusiasm all along with the thesis duration. I am grateful for the opportunity to work with them and learn from their insights.

I am extremely thankful to the whole CDP Risk team for their insightful suggestions and contributions to the research project. I would like to recognize the invaluable assistance that Prof. Denis Jongmans, Prof. Christophe Bérenguer, and Prof. Julien Baroth provided during my study. It is wholeheartedly appreciated that your great advice for my study proved monumental towards the success of this study.

I would like to show my gratitude to the whole GIPSA-lab team. Their kind help and support have made my study and life in the Grenoble a wonderful time. I am indebted to the administrative, human resources, and informatics team of the GIPSA-lab for their assistance at every stage of the research project.

Finally, big thanks to my family and friends for your continuous support and encouragement. Thank you, everyone, for always being there with a word of encouragement and a listening ear.

Abstract

Landslide is a gravity-driven downslope movement of soil, debris, or rock near the earth's surface. It can display heterogeneity in rates and movement types, ranging from creeping motion to catastrophic acceleration. Both scenarios pose a threat to the exposed region's people, infrastructure, ecosystem, and economy. Traditional landslide risk management strategy suggests avoiding building new infrastructure in such a region based on hazard maps. However, with climate change and rapid urbanization, this strategy seems challenging to implement. Therefore, Early Warning Systems (EWS) are way forward to take timely corrective measures to reduce life and economic losses. These EWS's rely on landslide monitoring systems, landslide models, and information reconstruction schemes.

In this challenging context of landslide monitoring and forecasting, the present work aims to define a physics-based dynamical model of landslides, unknown parameters identification, and observer-based hazard evaluation from available measurements. This requires a multi-disciplinary approach, i.e., concepts from geophysics on the one hand and control theory on the other hand, for model structure definition and solution methods for observer problems (or parameter identification), respectively. In short, the idea is to analyze the changes in landslide variables and mechanical parameters prior to or while in a motion.

In the first part of our study, we formulated state and parameter estimation issues in an ODE-PDE landslide model (with Ordinary and Partial Differential Equations) as an optimization problem with discrete-time asynchronous synthetic measurements. The calculus of variation based *adjoint method* (iterative approach) is then utilized to solve the problem. Secondly, we address a similar state and parameter estimation problem in a coupled ODE-PDE landslide model by designing a *state observer* again for synthetic measurements (continuous approach). The observer consists of a copy of the PDE part of the system and a Kalman-like design for the ODE. It is shown to ensure exponential convergence of the state and parameter estimates employing the Lyapunov tool. Finally, we present an approach for reconstructing displacement patterns and some unknown soil properties of slow-moving landslides, using a special form of the so-called Kalman filter or observer. This approach is validated for Super-Sauze landslide data from the literature with an extension of the observer to forecast landslide displacement.

Keywords: Landslide dynamics, Coupled ODE-PDE system, State and parameter estimation, Optimization, Discrete-time asynchronous measurements, Observer design, Kalman filter, Observer tuning, Displacement forecasting.

Résumé

Un glissement de terrain est un mouvement sur pente descendante d'une partie du sol, de débris, ou de roche de surface, entraîné par la gravité. On peut trouver une certaine hétérogénéité dans les mouvements de ce type, comme dans leurs vitesses d'évolution, allant du glissement lent à l'accélération catastrophique. Ces deux scénarios constituent une menace pour la population, les infrastructures, l'écosystème et l'économie de la région exposée. La stratégie traditionnelle de gestion des risques de glissement de terrain suggère d'éviter de construire de nouvelles infrastructures dans une telle région sur la base de cartes des aléas. Cependant, avec le changement climatique et l'urbanisation rapide, cette stratégie semble difficile à tenir. Par conséquent, les Systèmes d'Alerte Précoce (SAP) sont la voie à suivre pour prendre des mesures correctives en temps opportun afin de réduire les pertes en vies humaines et économiques. Ces SAP s'appuient sur des systèmes de surveillance des glissements de terrain, des modèles de glissements de terrain, et des algorithmes de reconstruction d'informations.

Dans ce contexte difficile de surveillance et de prévision des glissements de terrain, le travail présenté dans cette thèse vise à définir un modèle dynamique des glissements de terrain basé sur la physique, développer des méthodes d'identification des paramètres inconnus, et contribuer à l'évaluation des risques par des techniques d'observateurs à partir des mesures disponibles. Cela nécessite une approche multidisciplinaire, s'appuyant ici sur des concepts issus d'une part de la géophysique et d'autre part de la théorie du contrôle, pour la définition d la structure du modèle et les méthodes de résolution des problèmes d'observateurs (ou d'identification des paramètres), respectivement. En bref, l'idée est d'analyser les changements dans les variables de glissement de terrain et dans les paramètres mécaniques avant ou pendant un mouvement.

Dans la première partie de notre étude, nous avons formulé des problèmes d'estimation d'état et de paramètres dans un modèle de glissement de terrain ODE-PDE (combinant Equations Différentielles Ordinaires et à dérivées Partielles), comme un problème d'optimisation avec des mesures synthétiques asynchrones à temps discret. La *méthode adjointe* basée sur le calcul variationnel est ensuite utilisée pour résoudre le problème (approche itérative). Dans un deuxième temps, nous abordons un problème similaire d'estimation d'état et de paramètres dans un modèle de glissement de terrain couplé ODE-PDE en concevant cette fois un *observateur*, à nouveau pour des mesures synthétiques (approche continue). L'observateur se compose d'une copie de la partie PDE du système, et d'une synthèse de type Kalman pour l'ODE. Il est montré qu'il assure une convergence exponentielle des estimations d'état et de paramètres en utilisant l'outil de Lyapunov. Enfin, nous présentons une approche pour reconstruire les schémas de déplacement et certaines propriétés inconnues du sol dans le cas des glissements de terrain lents, en utilisant une forme spéciale du filtre (ou observateur) de Kalman. Cette approche est validée avec des données de glissement de terrain issues de la littérature pour le cas de Super-Sauze, et une extension de l'observateur pour prédire l'évolution du glissement est proposée.

Mots-clefs: Dynamique des glissements de terrain, Système ODE-PDE couplé, Estimation d'état et de paramètres, Optimisation, Mesures asynchrones en temps discret, Filtre de Kalman, Conception d'observateur, Réglage d'observateur, Prédiction de déplacement.

Contents

List of Abbreviations

AE Acoustic Emission

AEWG Acoustic Emission monitoring using active Waveguides

CHASM Combined Hydrology And Stability Model

CPT Coherence Pixel Technique

D-InSAR Differential Interferometric Synthetic Aperture

DEM Digital Elevation Model

DGPS-RTK Differential Global Positioning System in Real-Time Kinematic

DP Digital Photogrammetry

ED Event-Duration

EI Event-Intensity

EO Earth Observation

ERT Electrical Resistivity Tomography

EWS Early Warning System

FCC False Color Composites

FLaIR Forecasting of Landslides Induced by Rainfall

FoS Factor of Safety

FOSM First-Order Second-Moment

GB-SAR Ground-based Synthetic Aperture Radar

GB-LiDAR Ground-based Light Detection And Ranging

GIS Geographic Information System

GPM Global Precipitation Mission

GPR Ground Penetrating Radar

GPS Global Positioning System

HIRESSS High-Resolution Slope Stability Simulator

InSAR Interferometric Synthetic Aperture Radar

IPTA Interferometric Point Target Analysis

IRT Infrared Thermography

JAXA Japan Aerospace and Exploration Agency

LiDAR Light Detection And Ranging

LoS Line of Sight

MIT Milti-temporal Interferometric Technique

NASA National Aeronautics and Space Administration, US

NLP Nonlinear Programming

NDVI Normalized Difference Vegetation Index Radar

ODE Ordinary Differential Equation

PDE Partial Differential Equation

PDF Probability Density Function

PEM Point Estimate Method

PSP Persistent Scatterer Pairs

QP Quadratic Programming

QPS Quasi Persistent Scatterer

RFID Radio Frequency Identification

RTI Rainfall Triggering Index

RMSE Root Mean Square Error

SAA Shape Acceleration Array

SAR Synthetic Aperture Radar

SBAS Small Baseline Subset

SHALSTAB Shallow Landslide Stability

SI Stability Index

SINMAP Stability Index Mapping

SPN Stable Point Network

SQP Sequential Quadratic Programming

SWCC Soil-Water Characteristic Curve

TDR Time Domain Reflectometers

TIN Triangulated Irregular Network

TLS Terrestrial Laser Scanning

tRIBS Triangulated irregular network-based Real-time Integrated Basin Simulator

TRIGRS Transient Rainfall Infiltration and Grid-based Regional Slope Stability

TRMM Tropical Rainfall Measuring Mission

UAV Unmanned Aerial Vehicle

VHR Very High Resolution

VWC Volumetric Water Content

1 General Introduction

1.1 Thesis context

1.1.1 Landslide modeling and information reconstruction

A landslide, also characterized as slope destabilization, is a gravity-driven downslope movement of rock, debris, or soil near the earth's surface resulting from severe precipitation, floods, earthquakes, substantial snowmelt, or human activities like construction (Fig. 1.1). Landslides have become more common in recent years due to climate change and growing urbanization. They can have severe socio-economic effects, including significant costs in terms of human lives, infrastructure, the economy, and the region's ecosystem. Landslides have various movement types and rates, from slow creeping to rapid catastrophic acceleration. In the most destructive catastrophes, rocks, debris, or soil can flow at speeds of several tens of meters per year, wreaking havoc on the region's infrastructure, economy, and ecosystem.

Figure 1.1: A landslide covers a circuit course in Nihonmatsu city, Fukushima prefecture, northeastern Japan, Sunday, Feb. 14, 2021. The strong earthquake shook the quake-prone areas of Fukushima and Miyagi prefectures late Saturday, setting off landslides and causing power blackouts for thousands of people. [Hironori Asakawa/Kyodo News]

On the other hand, slow-moving landslides can have typical velocities ranging from a few millimeters to several meters per year. Slow-moving landslides seldom result in fatalities, although they can damage public and private infrastructure significantly. Slow, persistent landslides can sometimes lead to catastrophic acceleration; clayey landslides, for example, are prone to these transitions. Traditional landslide risk management solutions focus on avoiding infrastructure construction in vulnerable areas based on landslide hazard maps, stabilizing unstable slopes (landslide geometry modifications, water drainage), and erecting protective structures. However, infrastructure is still being built on or near major landslides due to a lack of risk awareness. Slope stabilization can be costly in such instances, and relocating the population to more stable places might generate significant socio-economic problems. Implementing an Early Warning System (EWS) under these scenarios can assist in taking prompt interventions to reduce life and economic losses prior to hazardous events. The monitoring and warning service is an essential part of EWS. For anticipation/estimation of the hazards associated with landslide physics-based dynamical model, landslide monitoring and data assimilation play a vital role.

Our starting point is then that, the physics-based dynamical models are susceptible to the initial conditions and parameters of the system. Simulating a model and iteratively modifying the initial conditions and parameter values to achieve consistency with measured data can account for these sensitivities. Another effective method can be to run a model over time and fine-tune it to synchronize with updated measurements. Landslide models can then assist in forecasting once these sensitivities have been addressed. *As a result, this manuscript proposes a cross-disciplinary approach for landslides investigation which is general objective of the project Risk@UGA, associating landslide models from Geophysics and Control theoretical tools for information reconstruction.*

1.1.2 Cross-displinary Project 'Risk@UGA'

The Ph.D. work presented in this thesis was developped in the context of a "Risk" project of Université Grenoble Alpes. With the motto of *"Managing risk for a more resilient world"*, this project was started in 2018 to develop cross-disciplinary research and scientific innovation in the field of disaster and risk management, specifically in areas that are made vulnerable due to a strong interdependency between humans, natural or technological hazards. In addition to the Grenoble basin, the project has addressed on other vulnerable territories such as the Beirut area (Lebanon), Port-au-Prince (Haiti), and Peru and Nepal. The project also aimed at proposing a risk institute within Université Grenoble Alpes.

1.1.2.1 Challenges

The project's primary goal was to contribute to the proactive mitigation of disaster risks and develop a culture of risk. It was dedicated to a global and regional challenge, which is fundamental for the decades to come, due to the increase of the world population with often-anarchic densification of urbanized areas, the increasing human impact on ecosystems, but also the emergence of new risks induced by climate change and technological development.

1.1.2.2 Interdisciplinarity

The project federated a hundred researchers belonging to 15 research labs from Human and Social Sciences, Information and System Sciences, Geosciences, and Engineering Sciences. The scientific challenges of collecting and processing heterogeneous data, modeling complex and cascaded phenomena, multi-objective decision making, and assessing or defining risk governance schemes require genuinely global and interdisciplinary approaches.

1.1.2.3 Project organization

The project proposed an innovative scientific approach to address the following challenging issues:

- Managing data heterogeneity through a participatory approach
- Integrating rare or emergent events and cascading effects
- Moving from a static/reactive risk management approach to a proactive/dynamic approach
- On the one hand, designing appropriate strategies for disaster risk reduction (apart from a relevant assessment of vulnerabilities and local cultures) and for communications, on the other hand managing risk better and strengthening the culture of risk.

1.1.2.4 International visibility

The project was entirely in line with Sendai's United Nations conference framework on disaster risk prevention in 2015, which encourages countries to prevent better and anticipate disaster risks. It aimed to become a privileged interlocutor of the risk management stakeholders in France and abroad, particularly on the five selected study sites (economic sphere, public authorities, humanitarian organizations, academia, or risk center networks). The project offers a solid contribution for both the structure and visibility of Univ. Grenoble Alpes in risk assessment and management by proposing a unique risk management institute in France. The Risk project fosters the development of new interdisciplinary methodologies by research teams to better work together and transfer research results to relevant stakeholders and decision-makers. It also actively participates in reinforcing interdisciplinary curriculum in risk management.

1.2 Research Question and Objectives

The main guiding research question of this work has been formulated as:

> *"How to reconstruct missing information required for landslide models to forecast mass movement from available measurements?"*

To answer this question, the following sub-questions have been identified:

- What is the state of the art regarding various landslide monitoring techniques and their constraints in the sense of temporal and spatial resolution, different statistical and physically-based landslide modeling studies, and variety of tools that have been utilized for missing information reconstruction (back analysis) from measurements?
- What can control and systems tools bring in the context of this thesis: using optimization based off line appraoch, state observer based online techniques, and prediction tools?

Addressing research questions, the first objective of this thesis is to understand different landslide monitoring techniques and their constraints. The second objective is the

selection of mechanical models of landslides based on the available measurement in a dynamical system framework. These two objectives consitutes state-of-the-art for the work. Following state-of-the-art on the landslide monitoring and modeling, back anlysis (inverse problem) for unknown parameter identification from available data is to be investigated by optimization-based solution and observer design. Finally, observer-based approaches for dynamical monitoring and landslide motion evaluation are to be developed based on the available measurements and models.

1.3 Manuscript Outline

The structure of the manuscript is as follows:

- Current chapter 1 presents a brief overview of the context, cross-disciplinary project Risk@UGA, research question, and objectives of the thesis.
- Keeping overall objective of the thesis in mind, an overview of a conducted literature review on different landslide monitoring techniques with their constraints, landslide modeling studies from statistical to physically-based models, and inversion techniques for parameter identification is given in Chapter 2.
- Addressing the research question of information reconstruction, optimization-based adjoint method for estimation (unknown parameters and initial condition) in landslide models with discrete-time asynchronous synthetic measurements is proposed in Chapter 3. The system under investigation is presented as a pair of coupled Ordinary Differential Equation (ODE) and Partial Differential Equation (PDE). The Lagrangian multiplier is introduced to connect the dynamics of the system and the cost function formulated as the least square error between the simlation values and the available measurements. The adjoint method is used to obtain adjoint system and gradients with respect to parameters and inital state. Finally, cost fuctional is optimized using the steepest descent method. This chapter validates the proposed method for state and parameter estimation with the help of two landslide application examples: i) extended sliding-consolidation landslide model and ii) viscoplastic sliding-consolidation landslide model, and using synthetic data.
- In Chapter 4, as a "continuous" alternative to the optimization approach, an observer for state and parameter estimation in extended sliding-consolidation landslide model is designed. The observer consists of a copy of the PDE part of the system and Kalman-like observer for the ODE. In this chapter, Lyapunov tool is utilized to ensure exponential convergence of the state and parameter estimates. At the end of the Chapter, simulation results are presented to illustrate effectiveness of the designed observer, again based on synthetic data.
- Considering a simplified model, a Kalman filter approach for reconstruction and forecasting landslide displacement is presented in Chapter 5 with synthetic and real-field data (taken from literature). The proposed observer relies on a simplified viscoplastic sliding model of landslide. The observer's performance is improved by using a resetting method, and to overcome sensitivity to the observer coefficients, a novel tuning method is proposed, which considers both actual and synthetic test cases. The approach is also extended to landslide displacement forecasting. Using a similar approach, some preliminary results with the Hollin Hill landslide data are presented in Appendix A.1.
- General conclusions and future perspectives are finally given in Chapter 6.

1.4 List of Publications

1. Mishra, M., Besançon, G., Chambon, G., and Baillet, L. (2021). “Calculus of variations for estimation in ODE-PDE landslide models with discrete-time asynchronous measurements". (submitted in the International Journal of Control)

2. Mishra, M., Besançon, G., Chambon, G., and Baillet, L. (2021). “Reconstruction and forecasting of landslide displacement using a Kalman filter approach". (submitted in the Journal Landslides)

3. Mishra, M., Besançon, G., Chambon, G., and Baillet, L. (2021). “Combined state and parameter estimation for a landslide model using Kalman filter". 19th IFAC Symposium on System Identification SYSID 2021, 54(7), 304-309.

4. Mishra, M., Besançon, G., Chambon, G., Baillet, L., Watlet, A., Whiteley, J. S., Boyd, J. P., and Chambers, J. E. (2021). “Application of Kalman filter to reproduce displacement pattern along with the unknown soil properties of slow-moving landslides". EGU General Assembly 2021, Online, 19-30 Apr 2021, EGU21-9396, doi:10.5194/egusphere-egu21-9396.

5. Mishra, M., Besançon, G., Chambon, G., and Baillet, L. (2020). “Observer design for state and parameter estimation in a landslide model". 21th IFAC World Congress, 53(2), 16709-16714, doi:10.1016/j.ifacol.2020.12.1116.

6. Mishra, M., Besançon, G., Chambon, G., and Baillet, L. (2020). “Optimal parameter estimation in a landslide motion model using the adjoint method". In 2020 European Control Conference (ECC), 226-231, doi:10.23919 ECC51009.2020.9143819.

Notice that chapters 3, 4, 5 being strongly based on some of the above papers, they are presented in a self-contained way.

2
State of the art

This chapter provides an overview on the context and tools for landslide monitoring issues. It takes the form of a state-of-the-art review about three items: landslide monitoring, landslide modeling, and information reconstruction. This review gives the opportunity to introduce basic motivations and ingredients for the developments proposed in the thesis, summarized at the end of each item.

2.1 Landslide monitoring

Landslide monitoring on marginally stable slopes is critical for identifying landslides occurrence and providing early warnings. It analyzes changes in attribute values of landslide triggering factors and observes slope displacements in possible landslide sites, allowing for early evacuation of vulnerable persons, timely repair, and maintenance of essential infrastructure. The construction of slope stability models relies heavily on the monitoring of kinematic, hydrological, and climatic characteristics [Chae2017]. Forecasting is impossible without first understanding movement patterns, and responses to climate events [Angeli2000a]. It necessitates the monitoring of not only actual movements but also environmental and geotechnical characteristics [Uhlemann2016]. Landslide monitoring aids in the understanding of the landslide mechanism as well as the development of valid criteria for landslide forecasts and early warnings. There has been a lot of research into landslide forecasting and early warning in recent years, and the need for landslide monitoring has been emphasized.

Landslide monitoring can be divided into three categories (Fig. 2.1). The first one is field observations of changing topography features, cracks, and surface water flow. It is a standard monitoring technique in which geologists take measurements of changing features in the field at regular intervals. However, because measuring changes at the site in a short time interval, such as a minute or hourly scale, is difficult, the method is limited in providing information on impending landslides or slope failures. The second category involves employing various in situ sensors to observe slope displacement, hydrological and physical qualities of the soil, and rainfall. Rain gauges for measuring precipitation, extensometers, inclinometers, tiltmeters, and a Global Positioning System (GPS) for monitoring slope displacement and deformation are the principal instruments deployed in the field. Total stations, laser scanners, Radio Frequency Identification (RFID), and Acoustic Emission (AE) sensors are also used to measure slope deformation, as well as Time Domain Reflectometers (TDR), Tensiometers, and Piezometers to measure changes in hydrological and physical properties of soils. Remote sensing approaches, such as satellite image analysis, Synthetic Aperture Radar (SAR) interferometry, optical reflectometry, and Light Detection And Ranging (LiDAR), fall into the third category. These approaches have been popular in recent years for landslide monitoring because they can quantify slope displacement with high resolution in large target regions in the field. They can also measure ground displacement in adverse weather and even at night. SAR interferometry and LiDAR monitoring have recently been carried out utilizing ground-based SAR (GB-SAR) and LiDAR (GB-LiDAR) as well as airborne satellites and planes. This section offers in situ ground-based monitoring and remote sensing methodologies to comprehend the current state-of-the-art landslide monitoring technologies.

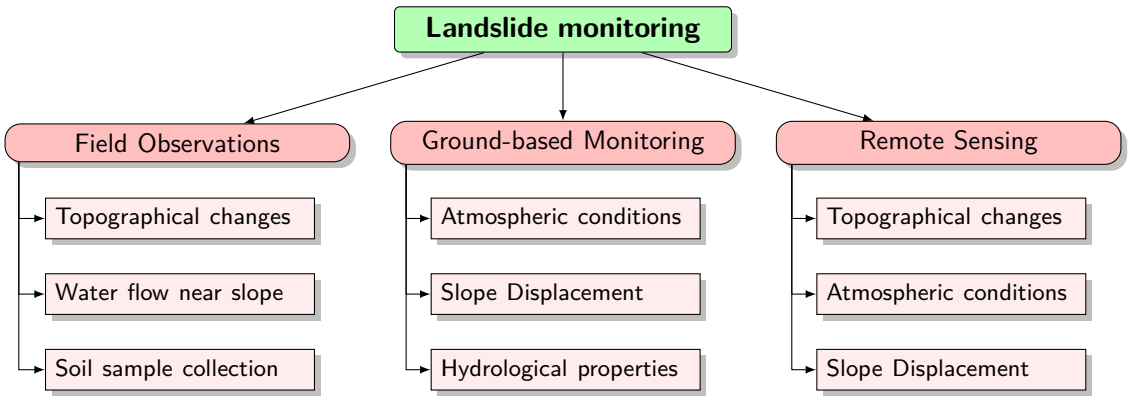

Figure 2.1: Landslide monitoring techniques

2.1.1 In Situ Ground-based monitoring

Precipitation, slope displacement, and hydrological/physical features of soils, such as groundwater level, Volumetric Water Content (VWC), and pore water pressure are all monitored in situ. Instruments installed in boreholes and on the surface of possible landslide areas measure the monitored entities. The instruments can track changes in observation factors in real-time or at regular intervals. Changes in observation factors can be measured in both short and long time intervals since the geologist can modify the measurement interval.

The monitoring data is evaluated primarily to detect slope displacements. Based on the monitoring data, it is possible to identify the depth of a sliding surface and understand the slope's sliding rates. Furthermore, the research findings reveal the relationship between slope motions and the hydrological or physical properties of the slope under a variety of geological and meteorological situations. As a result, in situ ground-based monitoring enables decision-making on landslide triggering variables and suggests landslide triggering factor thresholds at the monitoring site, such as rainfall and VWC. On the other hand, ground-based monitoring is site-specific since it can detect landslides inside the monitoring sensor zones. Effective landslide monitoring across a large area simultaneously has certain limitations.

The three types of in situ ground-based monitoring are: i) monitoring environmental conditions, ii) slope displacement and iii) hydrological and mechanical properties of soil (Fig. 2.2). Because rainfall is the most prevalent triggering element, it is critical to investigate the link between rainfall conditions and landslide triggering using rainfall measurement data. Some past studies used rain gauges in the field to determine empirical or statistical rainfall thresholds [Caine1980a, Aleotti2004, Guzzetti2008a, Brunetti2010, Martelloni2012]. It is emphasized that the locality and timing of rainfall control landslides generated by rainfall [Franks1999, Tsaparas2002].

[Corominas1999] performed a thorough investigation on the association between landslides and rainfall in the upper basin of the Llobregat River, Eastern Pyrenees, and discovered that two different rainfall patterns were associated with landslide occurrence [Keqiang2009]. According to [Guzzetti2007], the joint US-Japanese Tropical Rainfall Measuring Mission (TRMM), which was launched in November 1997 [Adler2003], and the planned co-operative United States National Aeronautics and Space Administration (NASA) and Japan Aerospace and Exploration Agency (JAXA) Global Precipitation Mission (GPM), could provide spatial and temporal precipitation information with sufficient detail to forecast the possible occurrence of landslides.

In recent years, most landslide monitoring involved rainfall measurements integrated with slope displacement, hydrological and physical properties of soils [Luo2008, Yin2010, Bittelli2012, Chae2011, Palis2016]. The integrated monitoring (e.g., Fig. 2.3 and Fig. 2.4) allows a better understanding of the relationships between the different triggering characteristics of landslides and more reliable warning thresholds prior to an occurrence or at the very early stage of landslide movement.

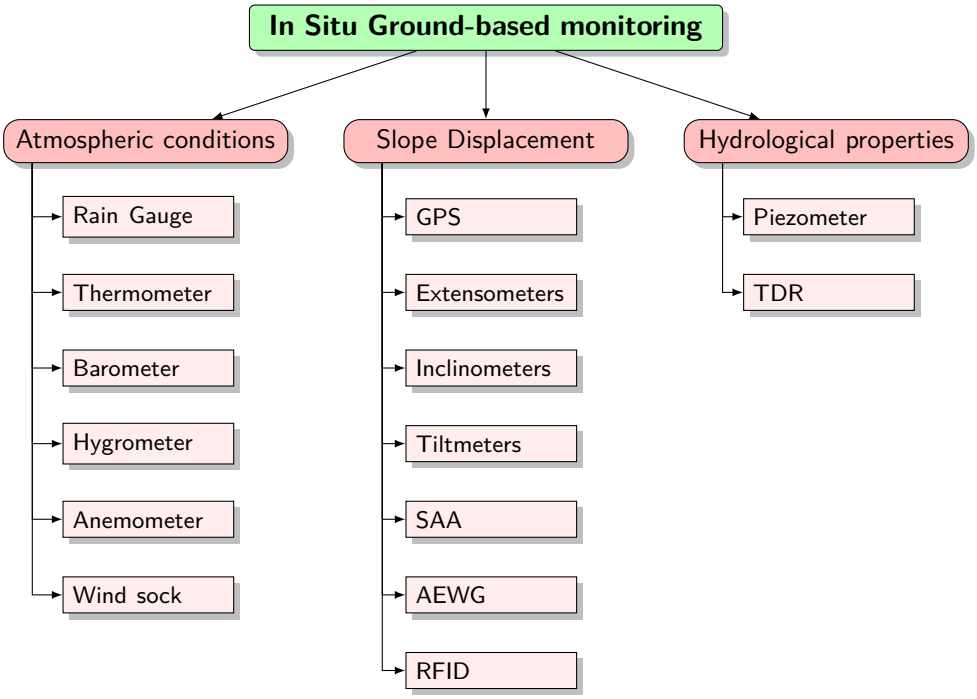

Figure 2.2: In Situ Ground-based monitoring techniques

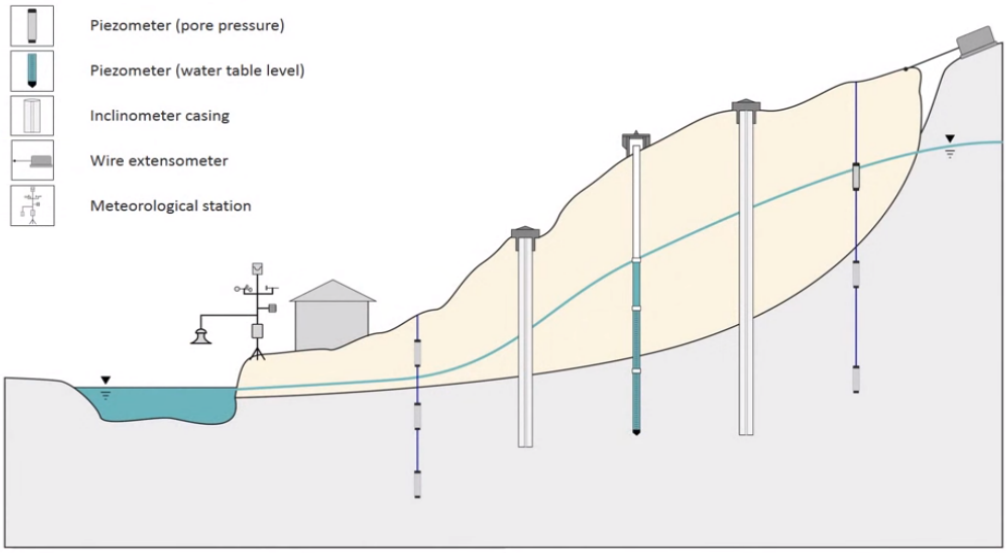

Figure 2.3: Natural slope monitoring system

Global Positioning System (GPS), tiltmeter, inclinometer, and extensometer are generally installed on the surface or in the subsurface of a slope to examine the deformation behavior of rainfall-triggered landslides in the notion of displacement monitoring. [Malet2002, Corsini2005, Brückl2013] examined measurements from two or three of the aforementioned traditional deformation monitoring approaches, finding a strong correlation between surface and subsurface deformations in terms of movement occurrences. In the top part of the landslide, [Chelli2006, Konak2004] placed a GPS, tiltmeter, and wire extensometer to determine the shape of the sliding masses and the depth of the sliding masses. They also used displacement monitoring to determine the absolute lateral and vertical movements and the rate of movement (velocity) of the various elements of the

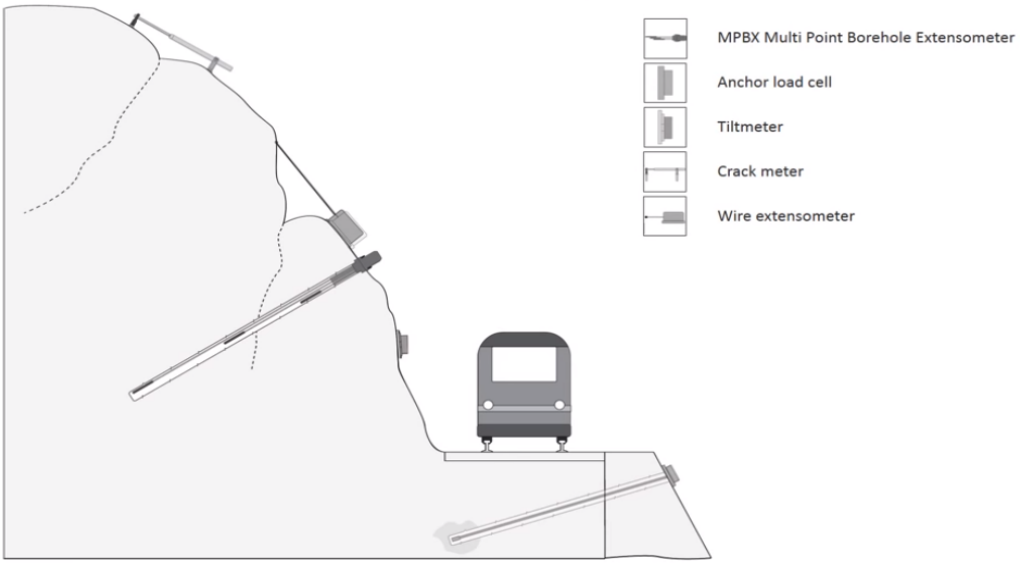

Figure 2.4: Earthwork slope monitoring system

complicated landslide.

[Stevens2000] analyzed 15 inclinometer datasets collected over six years. The goal of the monitoring was to find out if shear horizons existed, how deep they were, and how fast they moved. In recent years, high-resolution and high-accuracy movement measurements have been necessary to offer data that can be utilized to verify landslide theories and models, as well as landslide warning [Xie2004]. High-resolution tiltmeters provide the same type of data as inclinometers, but at a much greater resolution, ranging from 1 mrad (≈1 mm/m) to 1 nrad (≈1 nm/m), depending on the tiltmeter model. In two perpendicular orientations, tiltmeters measure the angle between the instrument body and the plumb line [García2010]. Tiltmeters were erected by [Chae2011] to monitor slope displacements caused by rainfall infiltration into the soil. As the sensors were set in a grid pattern both vertically and horizontally in the slope, they can detect small soil layer movements and changes in the wetting front behavior caused by rainwater penetration. In [Breton2019], radio-frequency identification (RFID) technology is presented as an alternative to traditional geodetic methods for measuring landslide displacements.

One of the goals of landslide monitoring is to identify a threshold for an influencing factor that can cause landslides in mountainsides, considering geologic conditions and rainfall. [Yin2010] monitored the Yuhuangge landslide in the Three Gorges Reservoir area in real-time. The monitoring system comprised TDR, a borehole inclinometer to monitor deep displacement, a piezometer to measure pore water pressure, precipitation, reservoir water level monitoring, and GPS with high accuracy double frequency for ground displacement monitoring. The early warning criteria for landslides were established based on the landslide monitoring experience at the Three Gorges Reservoir area, in which a catastrophic scenario was categorized into four tiers. On the Hollin Hill landslide (Fig. 2.5), [Uhlemann2016] coupled traditional techniques such as GPS, inclinometer, and tiltmeter with newly-applied deformation monitoring techniques such as AE monitoring using active waveguides (AEWG) and Shape Acceleration Array (SAA).

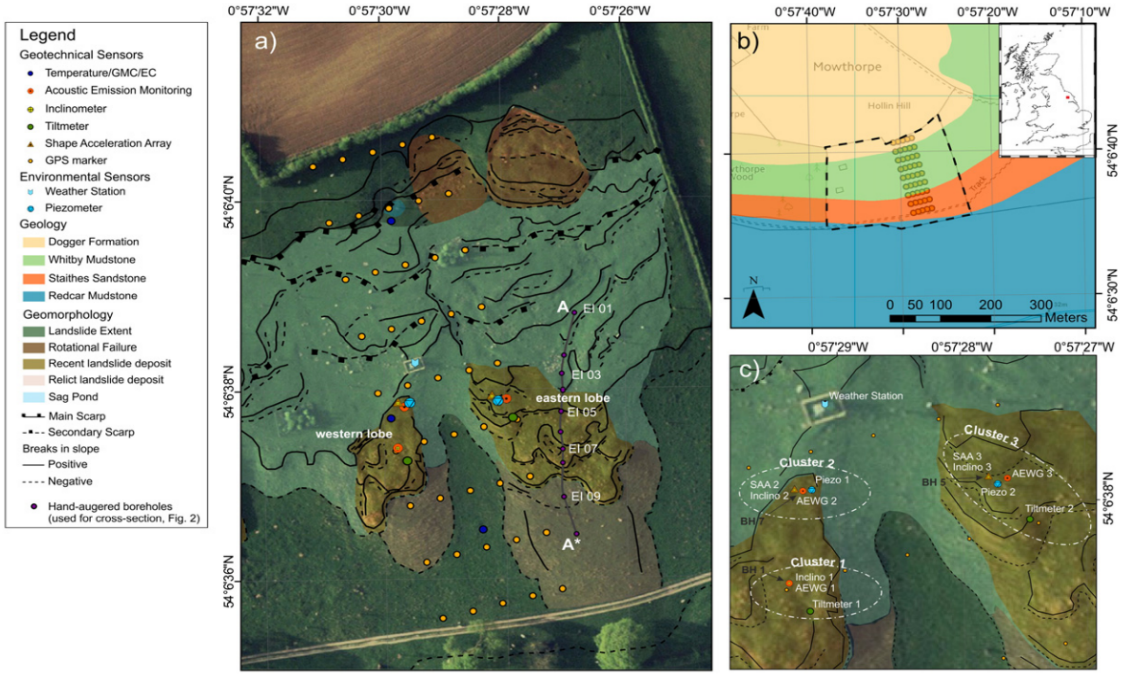

Figure 2.5: Overview maps of the study site. a) Geomorphological map of the landslide indicating different landslide bodies and features. Also shown are the locations of the monitoring equipment that are deployed at the site. b) Geological setting of the study site. c) A section of Fig. 2.5 a) at a larger scale showing the locations of sensor clusters comprising inclinometer, AEWG, SAA, piezometer, and tiltmeter deployed on the two lobes, as well as the location of the weather station. (after [Uhlemann2016])

S-shaped slope displacement time behavior, defined as periods of slope acceleration, deceleration, and stability in response to changes in pore-water pressures, was captured using high temporal resolution data. An array of displacement measuring systems, including GPS units, SAA, satellite (InSAR), and crack extensometers, as well as an array of piezometers targeting pore water pressures in the region of the shear surface, were used to monitor the Ripley landslide by [Macciotta2015]. During the active displacement period, the displacement monitoring system displays the annual cycle of slope deformations and average horizontal velocities. The system aims to provide landslide experts enough time to assess the hazard level linked with the Ripley landslide. To establish early warning displacement thresholds and associated hazard management protocols, analyses of landslide displacement patterns and near-real-time monitoring data are integrated with earlier studies of landslide-induced railway track deflections and track quality standards.

The third type of monitoring for rainfall-induced shallow landslides is continuous monitoring of the soil's hydrological and mechanical parameters. Many previous studies have shown that monitoring techniques can be used to identify the hydrological and mechanical conditions of the soil during the triggering of shallow landslides [Simoni2004, Matsushi2006, Godt2008, Godt2009, Leung2012, Bordoni2015, Springman2013a, Baum2010, Bittelli2012, Damiano2012].

Other earlier research has used the concept of hydrological and mechanical monitoring of landslides. For shallow landslide triggering, unsaturated soil hydrology is crucial [Lu2008, Tsai2009]. The most crucial cause of shallow landslides, according to some authors, is a decrease in matric suction following rainfall and the creation of positive pressures above the groundwater table. The stability study of an infinite slope was presented by [Lu2008], which considered the suction stress idea proposed by [Lu2006]). Previous

research has revealed that two potential mechanisms can cause rainfall-induced slope failures: i) a drop in matric suction [Ng1998, Collins2004, Rahardjo2007] and ii) an increase in the water table [Cho2002, Crosta2003]. [Li2013] demonstrated that slopes with an effective friction angle greater than the slope angle are unlikely to be driven by the loss of matric suction through analytical study. When infiltrating rainfall reaches an impermeable layer or the main groundwater table, the water table may rise. Moreover, [Montgomery2002, Jiao2005, Jiao2006] observed that the groundwater flow regime in a highly permeable layer overlain by a less permeable layer could result in an unusually high rise in pore water pressure compared to typical conditions. The equipment of piezometers was installed on the slope of the Yangbaodi landslide in China to connect the change in the hydraulic head with rainfall and investigate the effect of hydrological and mechanical factors initiating landslides [Li2015].

Time Domain Reflectometry (TDR) for mass deformation investigations is becoming more popular for landslide research among the existing techniques. [O'Connor2021] described the technique, and other articles describing applications in various circumstances have been published. The TDR approach is more often used for assessing soil water content and electrical conductivity [Topp1980, Robinson2003, Bittelli2012]. TDRs and tensiometers were installed to observe slope displacements caused by rainwater infiltration into the soil by [Chae2011] 2011. The sensors can monitor the velocity of rainfall infiltration into the soil since they were installed in a grid pattern both horizontally and vertically in the slope. They also investigate how rainfall penetration in the soil affects the monitored slope's Factor of Safety (FoS). In order to investigate the relationship between rainfall and pore water pressure and the occurrence of landslides and debris flows, [Berti2005] monitored rainfall and pore water pressure with sensors buried in a loose channel bed to investigate mechanisms and prediction methods for debris flow initiation by channel bed mobilization. In order to understand the mechanics of mudslides in Italy, [Comegna2007] tried long-term monitoring of landslide movements and pore water pressure.

2.1.2 Remote Sensing Techniques for Landslide Monitoring

Traditional direct field monitoring strategies have the disadvantage of physically placing the instrument in the landslides being monitored. As a result, measuring systems may face two issues: i) they may influence the system and, as a result, the measured quantities, and ii) the system may influence them. Remote sensing approaches almost entirely overcome this constraint by measuring geophysical ground variables from a distance and without direct contact. This, combined with recent significant advancements in space or airborne sensing platforms, has resulted in a significant rise in remote sensing's contribution to landslide hazard assessment, monitoring, and early warning. According to a recent review by [Tofani2013], based on a thorough survey conducted in Europe, remote sensing is employed as a standard technology for landslide detection, mapping, and monitoring in 83%. According to the report, 75% of users employ a combination of two or more strategies.

In the field of landslide analysis, the current availability of advanced remote sensing technologies allows for rapid and easily updatable data acquisitions, improving traditional detection, mapping, and monitoring capabilities, optimizing fieldwork, and investigating hazardous or inaccessible areas while ensuring the operators safety. Optical Very High-Resolution (VHR) and Synthetic Aperture Radar (SAR) imagery represent very effective tools for these implementations among Earth Observation (EO) techniques in the last decades because very high spatial resolution can be obtained using optical systems and new generations of sensors designed for interferometric applications. Even though these spaceborne platforms have revisiting times of a few days, they cannot match the spatial detail or time resolution achieved by Unmanned Aerial Vehicles (UAV), Digital Photogrammetry

(DP), and ground-based devices such as Ground-Based Interferometric SAR (GB-InSAR), Terrestrial Laser Scanning (TLS), and Infrared Thermography (IRT), which have seen a significant increase in usage in recent years due to technological advancements The potential of the methodologies mentioned above, as well as the efficacy of their synergistic application, is considered in this section.

Despite the benefits, there are still several important issues with remote sensing methods for landslide monitoring, including i) the lack of subterranean penetration capability, ii) the lower acquisition frequency compared to direct automated systems, and iii) atmospheric disturbances. The primary advantages and limitations of remote sensing approaches are driven by landslide typology, namely by two essential elements that come from the latter: landslide velocity and dimension, as revealed by the study of [Tofani2013]. Traditionally, space-borne, airborne, and ground-based sensors have been classified (Fig. 2.6), with the key distinction being the platform utilized to bring the sensor into place, hence the measurement frequency and distance from the target.

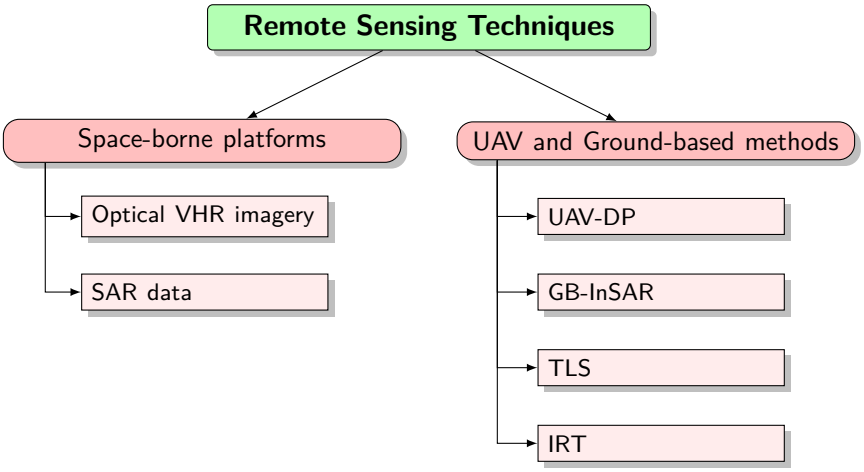

Figure 2.6: Remote Sensing Techniques for Landslide Monitoring

2.1.2.1 Space-borne platforms

Optical VHR imagery

Optical data is typically utilized for landslide detection and mapping via visual examination or analytical approaches [Metternicht2005, Fiorucci2011, Parker2014, Guzzetti2012, Mondini2014]. For example, several optical derivative products (panchromatic, pan sharpen, false-color composites, rationing) can assist in landslide mapping visualization [Casagli2005, Ma2016, Marcelino2009]. Multispectral channels, which have a lower spatial resolution than panchromatic channels, are downscaled in image fusion techniques using analytical models based on panchromatic-derived spatial information [Eyers1998, Chini2011, Martha2012, Kurtz2014]. The False Color Composites (FCCs) of VHR pictures are frequently employed to distinguish lithologies or terrain with distinct properties (weathering, water content, vegetation cover) [Ciampalini2012, Lamri2016]. Another index extensively used to map landslides by analyzing the plant cover rate is the Normalized Difference Vegetation Index (NDVI) developed from optical images [Lin2004]. Higher NDVI values indicate a dense vegetation cover, whereas lower values indicate areas affected by landslides. Furthermore, analytical methods based on the spectral features of the land surface and automatic approaches focusing on the classification of image pixels can be used to enhance multispectral pictures to detect landslides [Martha2010, Mondini2011]. Because most hyperspectral satellite sensors are still in development, few studies have addressed

the use of hyperspectral data to recognize and categorize landslides based on Earth surface characteristics [Scaioni2014].

SAR data

SAR satellites circle the Earth at altitudes ranging from 500 to 800 kilometers, following sun-synchronous, near-polar orbits that are slightly inclined with respect to Earth meridians. Pixels with different amplitude and phase values make up a SAR image. The vital ingredient for detecting ground displacement is the phase values of a single SAR image, which are partially dependent on the sensor-target distance. SAR Interferometry is a technique that analyzes at least two SAR images to measure changes in signal phase over time [Fruneau1996, Singhroy1998]. The Differential Interferometric SAR (D-InSAR) [Bamler1998] is an excellent way to exploit phase difference between two consecutive radar images recorded over the same object. The D-InSAR technique is less reliable due to geometrical and temporal decorrelation and atmospheric effects produced by variations in the phase reflectivity value of specific radar targets [Berardino2002]. To address these constraints, multi-temporal interferometric techniques (MIT) based on analysis of long stacks of coregistered SAR data can be used to improve InSAR-based information [Ferretti2001, Crosetto2016]. Several MIT approaches have been developed in recent years, including the Permanent Scatterers Interferometry, named PSInSARTM [Ferretti2011,Colesanti2003], the SqueeSARTM [Ferretti2011], the Stanford Method for Persistent Scatterers StaMPS [Hooper2004,Hooper2007], the Interferometric Point Target Analysis IPTA [Werner2003, Strozzi2006], the Coherence Pixel Technique CPT [Mora2003], the Small Baseline Subset SBAS [Lanari2004, Berardino2003], the Stable Point Network SPN [Casu2006, Crosetto2008], the Persistent Scatterer Pairs PSP [Herrera2010] and the Quasi PS technique QPS [Costantini2008]. The signal analysis of a network of coherent radar targets (Permanent Scatterers, PS) enables determining the displacement of each acquisition. The deformation rate of a Line of sight (LoS) can be estimated with a theoretical accuracy of better than 0.1 mm/yr. Each measurement is linked to a unique reference image and a stable reference location in both time and space. The MIT analysis aims to construct a time series of ground deformations for each PS based on different deformation models (e.g., linear, nonlinear, or hybrid). The potential of SAR data has been utilized at various scales in the field of landslide investigations, including national [Adam2011], regional [Meisina2008, Meisina2013, Ciampalini2015, Ciampalini2016], basin [Lu2011], slope [Frodella2016], and building scale [Ciampalini2014,Bianchini2015,Nolesini2016], as well as in different phases of landslide response [Canuti2007].

2.1.2.2 UAV and Ground-based methods

UAV-DP

DP is a well-known method for obtaining detailed 3D geometric information in slopes from stereoscopic overlaps of photo sequences taken with a calibrated digital camera [Chandler1999, Lane2000, Sturzenegger2009]. With the rapid development of DP techniques and the availability of easy-to-use, focusable, and relatively inexpensive digital cameras in recent years, this technique has found widespread use in various fields, including 3D building reconstruction, heritage protection, and landslide studies [Scaioni2015]. DP can be divided into two fields of activity [Gopi2007], depending on the camera lens setting: far range, which is usually more exploited for landslide characterization and general mapping [Wolter2014], and close range, which is widely used in high precision metrological and deformation monitoring applications [Liu2016, Scaioni2015]. [Colomina2014, James2012, Remondino2012, Eisenbeiss2011]. More recently, the combination of rapid development of

low-cost and small UAVs and improvements in conventional sensors in terms of cost and size led to new, promising scenarios in environmental remote sensing, surface modeling, and monitoring.

GB-InSAR

The GB-InSAR system comprises a computer-controlled microwave transceiver with transmitting and receiving antennas that can synthesize a linear aperture along the azimuth direction by moving along a mechanical linear rail [Tarchi1997,Rudolf1999,Pieraccini2003]. The obtained SAR image contains amplitude and phase information of the observed backscattered echo in the acquiring time interval (from little to less than 1 minute with the most advanced systems) [Luzi2004, Wang2021, Monserrat2014]. The displacement derived from the phase difference computation can be depicted in 2D maps in a GB-InSAR interferogram, with the chromatic scale covering a total value equal to half of the wavelength employed. Due to the periodic nature of the phase, it cyclically assumes the same values, causing image interpretation issues. This problem, known as phase ambiguity, can be overcome by employing appropriate phase unwrapping algorithms [Ghiglia1994], which count the number of cycles done by the wave and produce cumulated displacement maps. Because GB-InSAR apparatuses normally operate over short distances (less than 3 km), they function in the Ku band (1.67–2.5 cm). GB-primary InSAR's research applications quickly shifted to slope monitoring [Pieraccini2003, Tarchi2003] and civil protection [Ventisette2011, Intrieri2012, Bardi2014, Bardi2016, Lombardi2016].

TLS

A TLS device creates and emits a directed, coherent, and in-phase electromagnetic radiation beam [Jaboyedoff2010]. The laser scanner can acquire the exact position of a mesh of points (point cloud) described by (x, y, z) cartesian coordinates by measuring the backscattered laser signal with high accuracy (millimeter or centimeter) [Slob2005]. The device's fast capture rate (up to hundreds of thousands of points per second) allows for quick access to the object's detailed 3D geometry. It is possible to link the obtained high-resolution 3D surface digital model to a global reference system by defining the coordinates of specific laser reflectors within the surveyed area using a Differential Global Positioning System in Real-Time Kinematic mode (DGPS-RTK) [Morelli2012, Tapete2015, Pazzi2015]. TLS is increasingly being employed in landslide investigations for geometrical and geostructural characterization and monitoring unstable rock cliffs [Abellán2006, Abellán2011, Jaboyedoff2007, Ferrero2008, Gigli2012b]. Because of the excellent resolution of the laser scanning survey, even tiny details such as the structural crack pattern, crack opening direction [Gigli2009, Gigli2012a], and orientation of crucial discontinuities within the rock mass [Gigli2011,Rosser2005] may be extracted. Furthermore, this technique may estimate ground 3D temporal displacements by comparing sequential recordings from the same scenario [Abellán2011]. The intensity data can also provide information about the type of material and soil moisture content of the targets, which can be used to supplement information about the landslide's key geomorphologic features [Franceschi2009].

IRT

IRT is a type of remote sensing that involves monitoring the radiant temperature of Earth's surface characteristics from afar [Spampinato2011]. The result of an infrared thermographic survey is a pixel matrix (thermogram) collected by the thermal camera array detector, which represents a radiant temperature map of the investigated object after correction of the sensitive parameters (object emissivity, path length, air tem-

perature, and humidity). Fractures, subsurface voids, moisture, and seepage zones inside the observable surface will affect the material's thermal properties (density, thermal capacity, and conductivity), affecting heat transmission [Teza2012]. As a result, inhomogeneity within the observed scenario will be displayed as an abnormal thermal pattern about the surroundings ("thermal anomaly") in the related radiant temperature map [Frodella2017]. [Spampinato2011]. In recent years, IRT has seen substantial growth in applications in geosciences. Nonetheless, except for a few notable experimental investigations [Wu2005, Baroň2012, Frodella2017], it is still experimentally utilized in the study of slope instability processes. IRT (typically in conjunction with laser scanning) is used for the following purposes: i) collect data on rock mass fracturing; ii) detect shallow surface weakness in rock walls [Teza2012]; iii) assess rockfall/slide susceptibility [Teza2014]; iv) map ephemeral drainage patterns [Frodella2015]; v) combine traditional geo-structural and geomechanical surveys [Mineo2015, Mineo2016, Pappalardo2016].

Summary on landslide monitoring techniques

- No single technique or instrument can provide complete information about a landslide, and therefore, various combinations are usually employed. The primary parameters of interest are **precipitation, displacement, and pore-water pressure**.
- The performance of monitoring techniques and instruments is usually assessed in terms of accuracy and precision, **spatial and temporal resolutions**, sensitivity, and reliability. Another predominant factor driving the choice of instrumentation and techniques is their cost.
- The data collected with the help of landslide monitoring systems facilitates landslide modeling and information reconstruction which in turn helps in development of Early Warning System (EWS).

2.2 Landslide modeling

One's capacity to represent a complex system in mathematical form reflects its understanding. The lack of knowledge of physical circumstances, material qualities, and physical laws characterizing processes occurring on-site is the cause of landslides' complicated and unpredictable behavior. Landslides are caused by a variety of physical processes, including tectonics [Bennett2016], human activity [Petley2007, Herrera2013a], earthquakes [Marano2010], and climate [Moreiras2005]. More than 70% of fatal landslides are due to climate change, according to [Froude2018]. Landslides caused by climate change are caused by heavy rains, melting snow, or melting permafrost, all of which reduce ground rigidity and stress. Landslides can involve a wide range of movements (fall, topple, slide, spread, and flow), geological materials (from solid rock to soft clay), and velocity (from centimeters per year to meters per second) [Cruden1996a, Hungr2014, Iverson2005a]. Landslide models can be classified into data-driven/statistical and physically based models (Fig. 2.7). The section reviews different modeling studies carried out in the literature.

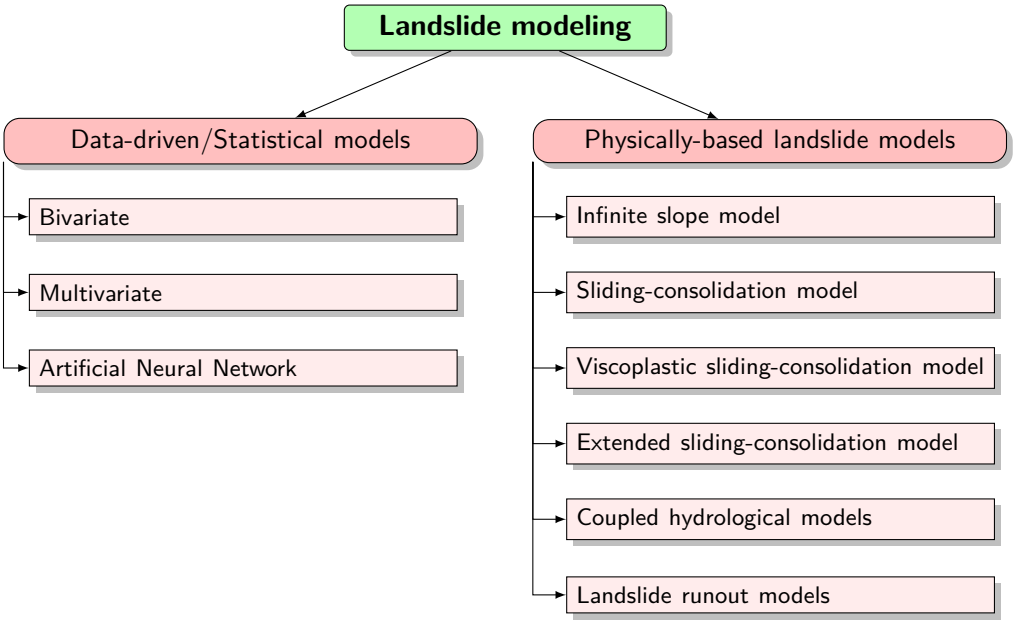

Figure 2.7: Landslide models

2.2.1 Data-driven/Statistical models

The statistical relationships between the positions of past landslides and landslide-inducing factors are analyzed in data-driven models, and then quantitative projections for landslide-free places with similar conditions are made. Since data on previous landslides is used to acquire information on the relative impact of each factor, these methods are known as data-driven approaches [Santoso2011]. This strategy presumes that conditions that have caused landslides in the past will continue to do so in the future. Bivariate statistical methods, multivariate statistical methods, and artificial neural network analysis are the three most frequent data-driven methodologies (Fig. 2.7). Each conditioning element, such as slope, geology, or land use, is integrated with the landslide occurrence sites in bivariate statistical analysis, and weight values are computed for each parameter class. Multivariate statistical approaches analyze the combined correlation between a dependent variable (landslide occurrence) and a series of independent variables (conditioning factors such as slope, geology) [Lu2003]. An artificial neural network is a computational device that can acquire, represent, and compute a map from one multivariate information space to another given set of data-defining relationships. A set of correlated input and output values is used to train an artificial neural network. Data-driven models help assess various spatially dispersed landslide-inducing elements across broad areas.

According to [Westen2000], collecting data on landslide distribution and factor maps over vast areas is the central issue in applying data-driven models. Furthermore, data-driven landslide models focus solely on the correlations between landslides and related factors rather than the failure mechanism [Park2013]. Furthermore, statistical models typically disregard the temporal elements of landslides and cannot forecast the influence of changes in landslide-controlling variables (e.g., water table fluctuations and land-use changes) [Westen2004a].

2.2.2 Physically-based models

Modeling the mechanism of landslide occurrence is the basis for physically based landslide models. Geometrical and geotechnical parameters are considered in these models for

estimating slope instability. Physically-based models, unlike data-driven models, may analyze slope stability regardless of landslide incidence by combining physical slope models with on-site or laboratory test results. Physical description is desirable for the following reasons: i) the quantitative thinking process is often more rewarding in terms of gaining much more in-depth insight into observable facts; ii) the practical need to predict future run-out, damage, and path of landslides or other gravity mass flow equations of motion of a landslide is a pre-requisite to any computer modeling. Physically-based models have recently been popular because of their improved prediction capability and suitability for quantitative evaluation of the effects of specific parameters that contribute to landslide onset [Corominas2013].

2.2.2.1 Infinite slope model

A physical slope model, such as an infinite slope model, is used to assess slope stability by analyzing the forces exerted on the slope. For shallow sliding on a slip surface parallel to the ground slope, the infinite slope model (Fig. 2.8) is basic but adequate. This model is best suited for analyzing shallow landslides with planar failure surfaces because it considers that landslides are indefinitely long but have a little depth compared to their length and width. Because the failure surfaces for rainfall-induced landslides are often shallow (a few meters) and parallel to the ground surface [Lu2013], the infinite slope model has been used to analyze susceptibility in several previous studies of shallow landslides [Ali2014a, Alvioli2014b, Griffiths2011, Tsai2014, Frattini2004, Huang2006, Rosso2006, Godt2008, Avanzi2009, Apip2010, Santoso2011, Park2013, Ho2012].

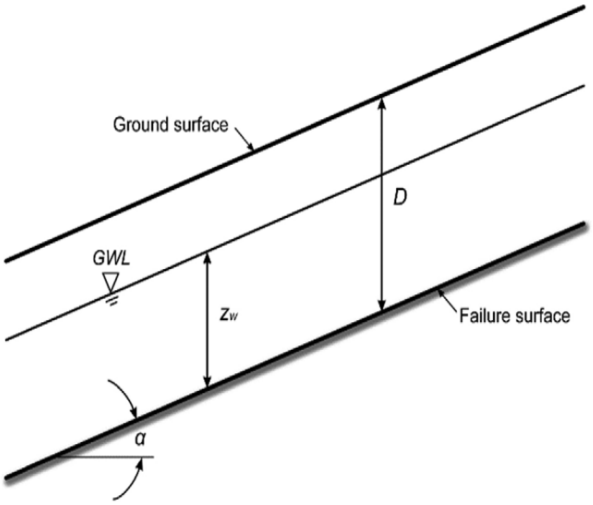

Figure 2.8: Infinite slope model

The infinite slope model is based on a limit equilibrium analysis that establishes the balance between shear stress and shear strength, which are the forces resisting movement along the presumed failure plane, and calculates a factor of safety (FoS). That is, assuming that the groundwater is situated at a distance from the failure surface and that groundwater flow is parallel to the slope (Fig. 2.8). The capacity of a system beyond the expected or actual load is known as FoS. It may be defined as the ratio of resistive to driving forces.

$$FoS = \frac{\text{Resistive forces}}{\text{Driving forces}} \tag{2.1}$$

The slope is unstable if $FoS \leq 1$, but steady if $FoS > 1$. However, if FoS is somewhat more than 1, even minor slope disequilibrium can result in slope failure. For instance, if

FoS is 1.05 and the slope is marginally steady, resistive forces are only 5% stronger than driving forces. Slight undercutting, excessive rainfall, seismicity, and other factors could lead the slope to fail in such situations. Resistive forces act in the opposing direction of the motion, tending to resist it. The resistive force is characterized by the material's shear strength, which is a function of cohesion and internal friction angle. The capacity of particles to stick together is referred to as cohesion. Clays and granites, for example, are cohesive, but dry sand is non-cohesive. The measure of frictional forces acting between constituent grains is the angle of internal friction. The driving force acts in the motion's direction, promoting downslope movement. Gravity is the primary driving factor, and it plays an important role in guiding or initiating mass wasting occurrences. Every material or body is pushed downward, towards the earth's center, by gravity. A gravitational force acts perpendicular to the ground on a flat surface, as shown Fig. 2.9. As a result, the ground-forming material will not move and remain intact. The gravitational force on a slope can be separated into two components (Fig. 2.9):

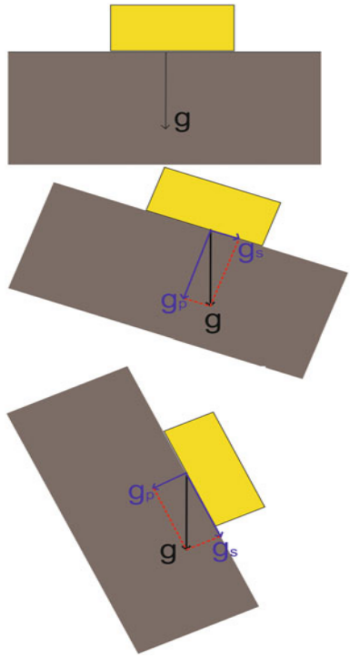

Figure 2.9: Gravitational force and its components [Pradhan2019]

1. Acting perpendicular to the slope (g_p): Resistive force or shear strength which hold the object and resist movement

2. Acting tangential to the slope (g_s): Driving force or shear stress that promote down slope movement of the object.

The slope forming material will break when the shear stress (driving force) surpasses the shear strength (resistive force). As a result, on higher slopes, the tangential component of gravity exceeds the resistive component, causing the mass to slide downhill. Other vital parameters that determine the size of the driving force include slope angle, slope height, climatic conditions, types of slope materials, runoff, and groundwater. The presence of water exacerbates slope instability when water is added to a slope. It produces slope failure due to the additional weight on the slope, which accelerates erosion rates and increases pore pressure, resulting in a drop in the slope forming material's shear strength. Considering the above parameters FoS can be calculated from Eq. (2.2) [Coduto2010]).

$$\text{FoS} = \frac{C + Hgcos^2\theta(\rho - \rho_w)tan\phi}{\rho Hgsin\theta cos\theta} \tag{2.2}$$

where, C is the effective cohesion, H is the thickness of potential slide, g acceleration due to gravity, θ is the dip angle of potential sliding plane, ρ is the material density of potential sliding plane, ρ_w is the density of water, ϕ is the internal friction angle.

Pore water pressure affects the effective normal stress and shear strength of soil in this model, resulting in slope failure; therefore, knowing the groundwater level is critical for forecasting and mitigating slope instability. However, measuring groundwater levels over a large area is almost impossible. As a result, past studies have employed a fixed or randomly chosen value for the groundwater level for the whole study area [Zhou2020, Griffiths2011]. On the other hand, the groundwater level varies depending on the soil type, rainfall intensity, and hydraulic conductivity; thus, applying for a fixed or randomly chosen number over a vast area is ineffective.

2.2.2.2 Sliding-consolidation model

A model for a single event behavior of flow slides in loose, cohesionless materials is proposed in [Hutchinson1986]. This model provides a possible mechanism for the event in which excess pore-fluid pressure is assumed to be generated by undrained loading. Resulting in the loss of shear strength and correspondingly the downslope motion of debris by basal sliding, consolidating by single, upward drainage. As a result, the pore pressure at the base decays to a value that brings the debris to rest.

The debris sheet is considered to be placed on the slope inclined at α (Fig. 2.10), with initial downslope velocity v_0 and initial distribution of pore-water pressure in a saturated basal layer of thickness $s\bar{h}$.

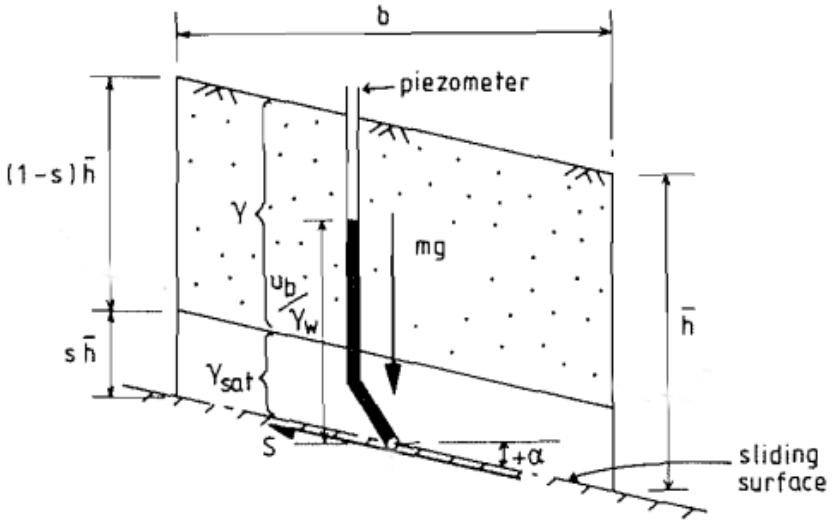

Figure 2.10: Sliding-consolidation model [Hutchinson1986]

The dynamics of the landslide are governed by the difference between destabilizing forces (F) and resisting forces (F_r). The momentum equation is given as,

$$F - F_r = ma = m\ddot{x} \tag{2.3}$$

where m is the mass and a or $\ddot{x}$ is the acceleration. Stability of slopes can be investigated by idealizing the slopes as infinite and uniform. Considering effective stresses acting on a

plane parallel to the surface of the slope and depth $\bar{h}$. Forces are computed over a unit surface, and therefore shear stresses are considered in what follows:

$$\tau - (\sigma - u_b)\, tan\phi = ma \tag{2.4}$$

where τ is the destabilising shear stress $= mgsin\alpha$,
σ is the normal shear stress $= mgcos\alpha$, and
$\sigma - u_b$ is the normal effective stress.
The equation of motion for the debris sheet expressed as, a Net driving force

$$m\ddot{d} = mgsin\alpha - (mgcos\alpha - u_b)\, tan\phi \tag{2.5}$$

where, $mg = b\bar{h}\,[(1-s)\,\gamma + s\gamma_{sat}]$,
d is the displacement,
u_b is the basal pore-water pressure at time t,
ϕ is the friction basal angle,
b is the basal area of the debris sheet,
$\bar{h}$ is the thickness of the debris sheet, and
γ & γ_{sat} are the unit weight of debris sheet material in non-saturated and saturated layer respectively.

Simplifying (2.5) gives the downslope acceleration/velocity/travel of the debris sheet,

$$\begin{aligned} \ddot{d} &= g\left\{ sin\alpha - \left(cos\alpha - \frac{u_b}{\bar{h}cos\alpha\,[(1-s)\,\gamma + s\gamma_{sat}]} \right) tan\phi \right\} \\ \dot{d} &= \ddot{d}t + v_0 \\ d &= \frac{\ddot{d}t^2}{2} + v_0 t \qquad at \quad t = 0, \quad d(0) = 0, \quad and \quad \dot{d}(0) = v_0 \end{aligned} \tag{2.6}$$

Another factor controlling the further progress of the debris sheet sliding is a process of consolidation. The collapse of a metastable structure generates excess pore-fluid pressure, a process of consolidation decays the basal excess pore-fluid pressure. Assuming that Tarzaghi's one-dimensional consolidation theory applies and that single, upward drainage is taking place, the time t_c required for the basal excess pore-water pressure to decay from initial value to a value that brings debris sheet at rest is given by [Hutchinson1986]

$$t_c = \frac{T\left(\bar{d}\right)^2}{c_v} \tag{2.7}$$

where T is the time factor for the degree of the basal excess pore-water pressure, $\bar{d} = s\bar{h}cos\alpha$ is the average length of drainage path, and c_v is the coefficient of consolidation of the material forming the layer $s\bar{h}$ of the debris sheet, for the appropriate pore fluid and stress level. For initial excess pore-water pressure u_{b_0} an approximate solution of equation governing one-dimensional consolidation is given by,

$$u_b = u_{b_0} e^{\frac{-t}{t_c}} \tag{2.8}$$

Note: If initial effective stress at the base of debris sheets is zero, the maximum value u_b can be (limiting condition or liquefaction limit)

$$u_b = [(1-s)\,\gamma + s\gamma_{sat}]\,\bar{h}cos^2\alpha \tag{2.9}$$

2.2.2.3 Viscoplastic sliding-consolidation model

The strength of resistance to downslope motion of debris/soil may also be caused by cohesion, which consists of soil cohesion and root strength ($c = c_s + c_r$) [Schmidt2008]. Root cohesion varies widely in space (land cover and land pattern) and time (growth period). Also, it is challenging to estimate c_r by sample laboratory tests quantitatively. In this work, neglecting the effect of root cohesion, and assuming that cohesive strength is due to soil particle cohesion only.

$$F_r = c + (\sigma - u_b)\, tan\phi \tag{2.10}$$

Sometimes nearly constant rates of displacement are observed in coincidence with steady groundwater levels, which suggests the development of viscous forces during movement [Corominas2005a]. Viscous forces are usually dependent on the strain rate of the shear zone and can be evaluated using a Bingham model,

$$F_v = \frac{\eta v}{z} \tag{2.11}$$

where η is the viscosity, v is the velocity, and z is the thickness of the shear zone. In the viscoplastic model, resisting force F_r resists destabilizing force (2.10), and the difference between these two forces leads to inertial force F and viscous force F_v (2.11). The momentum equation is,

$$F - F_r = F_i + F_v = ma + \frac{\eta v}{z} \tag{2.12}$$

$$\tau - [c + (\sigma - u_b)\, tan\phi] = ma + \frac{\eta v}{z} \tag{2.13}$$

If pore water pressure measurements are not available, it can be estimated from readings of the depth of groundwater level. Assuming parallel flow to the slope surface

$$u_b = z\gamma_w cos^2\alpha \tag{2.14}$$

where γ_w is the specific weight of pore water, z is the height of groundwater level. In [Herrera2013a] and [Bernardie2014a] changes in groundwater level assumed directly proportional to effective rainfall intensity:

$$\Delta z = \frac{I_{prep}}{n} \tag{2.15}$$

where I_{prep} is rainfall intensity in $mm^{-2}day^{-1}$ and n is the material porocity. This change in groundwater level leads to change in pore water pressure,

$$\Delta u_b = \Delta z \gamma_w cos^2\alpha \tag{2.16}$$

The dissipation of excess pore-fluid pressure in the saturated layer is computed using Terzaghi's one-dimensional consolidation theory (2.8) for [Herrera2013a]

$$t_c = \frac{4\left(\bar{d}\right)^2}{\pi^2 c_v} \tag{2.17}$$

And, in [Bernardie2014a] as

$$u_b = u_{b_0} e^{\frac{-k}{t_c}} \tag{2.18}$$

where k is the number of days since last recharge (or rainfall) and t_c (in days) is the time factor controlling the dissipation of the excess pore pressure, the initial excess pore-fluid pressure u_{b_0} is estimated as,

$$u_{b_0} = [z_{max} - z_0]\, \gamma_w cos^2\alpha \tag{2.19}$$

where, z_{max} is the highest groundwater level since the last recharge, and z_0 is the groundwater level when the landslide is at rest. The process of recharge and dissipation of excess pore pressure takes place simultaniously. Hence, the variation of the pore water pressure is given by (2.20) and variation of water table level by (2.21)

$$\begin{aligned}\Delta u_b &= \Delta u_{b_{recharge}} + \Delta u_{b_{dissipation}} \\ &= \frac{I_{prep}}{n}\gamma_w cos^2\alpha + u_{b_0} e^{\frac{-k}{t_c}}\left(1 - e^{\frac{1}{t_c}}\right)\end{aligned} \tag{2.20}$$

$$\Delta z = \frac{\Delta u_b}{\gamma_w cos^2\alpha} \tag{2.21}$$

2.2.2.4 Extented sliding-consolidation model

Motion of the slide block:
The extended sliding-consolidation clarifies how diverse styles and rates of landslide motion can result from regulation of Coulomb friction by dilation or contraction of the water-saturated basal shear zone. A model described in [Iverson2005a] is based on Newton's second law where landslide motion is resisted only by basal Coulomb friction. In this model, basal pore fluid pressure regulates rigid body translation of a landslide block with an added feature of pore pressure feedback. It is considered a solid, poroelastic block placed on a rigid, planner slope inclined at an angle θ and aligned to rectangular Cartesian coordinates in x-y. Also, forces at the base of the block are resolved using a coordinate system (x'-y') rotated by dilatancy angle ψ with respect to x-y system as shown in Fig. 2.11.

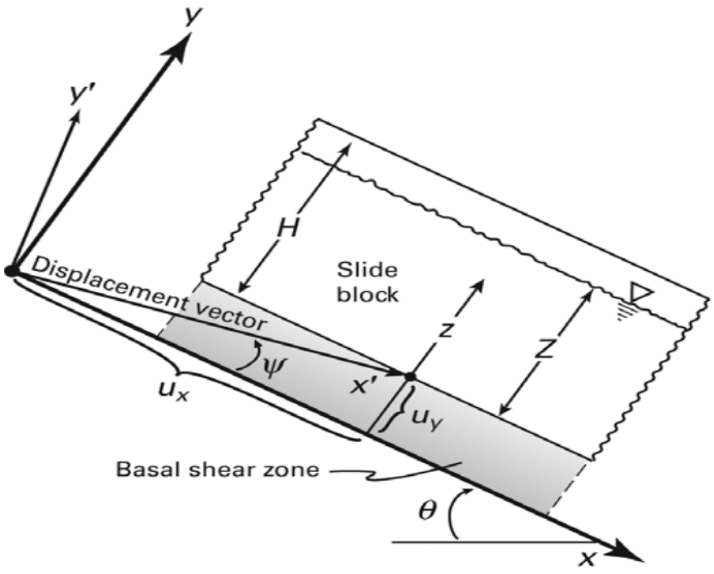

Figure 2.11: Extended sliding-consolidation model [Iverson2005a]

The forces acting at the base of the block mainly consist of three components: (i) gravity imposed driving force parallel to the slope (x' direction) is $\rho g H A sin(\theta - \psi)$ where ρ is the slide block mass density, g is the acceleration due to gravity, H is the thickness of the slide block, and A is the area of the slide block base, (ii) consequent frictional resistance equal to $-\rho g H A cos(\theta - \psi) tan\phi$ where ϕ is a basal frictional angle, and (iii) the component of the fluid pressure force acting in the direction reducing the basal frictional force acting uniformly along the base of the slide block equal to $p(0,t) A cos\psi \tan\phi$ where

$p(0,t)$ is the pore fluid pressure act at the base of the slide block. The net downslope force in the x' direction,

$$F_{x'} = \rho g H A sin(\theta - \psi) - \rho g H A cos(\theta - \psi) tan\phi + p(0,t) A cos\psi \tan\phi \tag{2.22}$$

The downslope movement of the side block initiates when $F_{x'} > 0$, therefore, the resultant momentum change in the x direction (which is smaller than momentum change in x' by a factor $cos\psi$) is given by,

$$\rho g H A \frac{\mathrm{d}^2 \mathrm{u_x}}{\mathrm{dt}^2} = cos\psi F_{x'} \tag{2.23}$$

where u_x is the rigid body displacement in the x-direction. Substituting (2.23) in (2.22) and dividing the result by ρHA, we get

$$\begin{aligned} \frac{d^2 u_x}{dt^2} &= g cos\psi \left[sin(\theta - \psi) - \left(cos(\theta - \psi) - \frac{p(0,t)}{\rho g H} cos\psi \right) tan\phi \right] \\ &= \frac{dv}{dt} \end{aligned} \tag{2.24}$$

which is a second-order ordinary differential equation describing the downslope movement of the slide block, where v is the slide block velocity.

Pore pressure diffusion:

Systems of conservation laws arise naturally in several areas of physics and mechanics, and landslide motion is one of them. Evolution of pore fluid pressure p is assumed to be governed by conventional linear diffusion equation (1-D hyperbolic PDE) that describes transient, one dimensional, saturated groundwater flow in a poroelastic medium that does not change total stress [Iverson2005a],

$$\frac{\partial p(z,t)}{\partial x} - D \frac{\partial^2 p(z,t)}{\partial z^2} = 0 \qquad z \in [0, Z], t \geq 0 \tag{2.25}$$

where D is the hydraulic diffusivity, and Z is the height of the water table. Eq. (2.25) is derived from the principles of mass conservation where the state of the system (pore pressure p) is a field that is a vector-valued function $p(z,t)$ of space variables z and the time t. For the analysis purpose, pore fluid pressure is split into two components: (i) the imposed pore pressure p_i due to processes such as rain infiltration and (ii) the excess pore pressure p_e which develops due to contraction or dilation of the basal shear zone.

$$p(z,t) = p_i(z,t) + p_e(z,t) \tag{2.26}$$

Both imposed, and excess pore pressure satisfies their linear diffusion equation (PDE).

$$\frac{\partial p_i(z,t)}{\partial x} - D \frac{\partial^2 p_i(z,t)}{\partial z^2} = 0 \qquad z \in [0, Z], t \geq 0 \tag{2.27}$$

$$\frac{\partial p_e(z,t)}{\partial x} - D \frac{\partial^2 p_e(z,t)}{\partial z^2} = 0 \qquad z \in [0, Z], t \geq 0 \tag{2.28}$$

Pressure gradient (boundary conditions) for imposed pore pressure derived by Darcy's law given as,

$$\frac{\partial p_i}{\partial z}(Z,t) = -\rho_w g \beta \tag{2.29}$$

$$\frac{\partial p_i}{\partial z}(0,t) = -\rho_w g \left(\beta + W \frac{K}{D} Z \right) \tag{2.30}$$

where, ρ_w is the pore water density, β and W are dimensionless constants, and K is the hydraulic conductivity. Imposed pore pressure serves to trigger slide block motion and

also influences post-failure sliding but does not facilitate feedback analysis. Therefore, (2.27), (2.29) and (2.30) are simplified to

$$p_i(z,t) = \rho_w g \left[\beta(Z-z) + WK\left(t + \frac{(Z-z)^2}{2D}\right)\right] \tag{2.31}$$

Since interest is in imposed pore pressure at the base of the slide block

$$p_i(0,t) = \rho_w g \left[\beta Z + WK\left(t + \frac{Z^2}{2D}\right)\right] \tag{2.32}$$

Pressure gradient (boundary conditions) for excess pore pressure derived by Darcy's law given as,

$$\frac{\partial p_e}{\partial z}(0,t) = \frac{\rho_w g}{K}\frac{du_y}{dt}, \quad p_e(Z,t) = 0 \tag{2.33}$$

For infinitesimal displacement dilatancy angle $tan\psi \approx \psi = du_y/du_x$ and $v = du_x/dt$ therefore, pressure gradients (boundary conditions) are given as,

$$\frac{\partial p_e}{\partial z}(0,t) = \frac{\rho_w g}{K}\psi v, \quad p_e(Z,t) = 0 \tag{2.34}$$

Combining (2.24), (2.26), (2.28), (2.32) and (2.34) yields governing equations and boundary conditions for the landslide dynamics in which downslope slide block velocity (v) and excess pore pressure (p_e) are the dependent variables (states):

$$\begin{aligned}
p_i(0,t) &= \rho_w g \left[\beta Z + WK\left(t + \frac{Z^2}{2D}\right)\right], \quad p_e(z,0) = 0 \\
p(z,t) &= p_i(z,t) + p_e(z,t) \\
\frac{d^2u_x}{dt^2} = \frac{dv}{dt} &= gcos\psi\left[sin(\theta-\psi) - \left(cos(\theta-\psi) - \frac{p(0,t)}{\rho g H}cos\psi\right)tan\phi\right] \\
\frac{\partial p_e(z,t)}{\partial x} &= D\frac{\partial^2 p_e(z,t)}{\partial z^2} \\
\frac{\partial p_e}{\partial z}(0,t) &= \frac{\rho_w g}{K}\psi v, \quad p_e(Z,t) = 0 \quad (b.c.)
\end{aligned} \tag{2.35}$$

2.2.2.5 Coupled hydrological models

Hydrogeological models can evaluate an increase in pore water pressure induced by rainfall infiltration; therefore, some physically-based models connect hydrogeological models to evaluate the impacts of pore water pressure with the infinite slope stability model for the computation of the FoS. As a result, by analyzing a drop in the shear strength of the soil produced by increased pore water pressure, physically-based models combined with a hydrogeological model can anticipate distributed shallow landslide initiation locations.

Based on the simplifying assumption, hydrogeological models can be divided into two categories: steady-state and transient-state models [Montgomery1994, Terlien1995, Wu1995, Pack1998, Baum2002, Crosta2003, Savage2004, Godt2008]. The steady-state shallow subsurface flow model described in TOPMODEL [Beven1979] and TOPOG [O'Loughlin1986] is the most often used hydrological model in slope stability studies [Montgomery1994, Wu1995]. The steady-state model assumes that rainfall infiltration is constant and saturated water flows parallel to the slope surface. As a result, rather than simulating the spatial groundwater level variation as a function of groundwater flow and rainfall intensity during a rainfall event, this model assumes a uniform recharge state that simulates the spatial groundwater level variation as a function of groundwater flow and

rainfall intensity over a long period. Due to continual rainfall infiltration, this model cannot analyze short-term temporal variations in pore pressure and temporal changes in FoS. By adding the infiltration process in an infinite slope using an estimated variant of Richard's equation [Iverson2000] sought to overcome the restricted assumptions of steady water table level [Arnone2011]. Using the linearized solution of Richard's equation [Iverson2000, Baum2002], the transient-state model performs transient seepage analysis and delivers more realistic findings. However, one of the challenges in using the transient hydrologic model in a physically-based analysis approach is that the transient hydrologic model necessitates a large amount of geographical data.

In recent years, a considerable number of physically-based models have been produced. The most extensively used slope stability analysis methods based on the physically-based model are SHALSTAB (Shallow Landsliding Stability model), SINMAP (Stability Index Mapping), and TRIGRS (Transient Rainfall Infiltration and Grid-based Regional Slope Stability). SHALSTAB is a coupled model that combines a stability model based on the infinite slope equation with a steady-state hydrological model, assuming that the subsurface flow is parallel to the slope [Beven1979, O'Loughlin1986]. Rainfall infiltration is assumed to be in equilibrium with steady-state, saturated water flow parallel to the slope surface above an impervious border in this model. The steady-state discharge is calculated for each cell as a function of the infiltration rate and a "contributing area," representing the upslope area that influences the subsurface flux through the cell. To estimate the relative water table depth and, as a result, the relative pore water pressure, the steady-state discharge is paired with a general form for groundwater flow parallel to the slope. SHALSTAB has been widely utilized in numerous research, including [Guimarães2003,Rosso2006,Huang2006,Sasso2014,Pradhan2014b,Fernandes2004,Gorsevski2006,Sorbino2009,Zizioli2013,de Luiz Rosito Listo2012] because of its simple hydrogeological model for the generation of steady-state pore water pressure.

SINMAP is based on the infinite slope stability model, which uses groundwater pore pressures from a topographically based steady-state hydrogeology model [Pack1998]. SINMAP uses topographic, hydrological, and soil factors to classify terrain stability. The input data (slope and specific catchment region) is derived from digital elevation models (DEMs) analysis. An interactive visual approach that updates these parameters based on observed landslides can be changed and calibrated. SINMAP provides for uncertainty in input parameters by defining uniform probability distributions with lower and upper bounds. The parameters are supposed to change at random between these boundaries for the probability distribution. This model generates the stability index (SI), defined as the chance that a place is stable, by assuming uniform distributions of the parameters over uncertainty ranges.

Because the ratio of the contributing area to the cross-sectional width will be evaluated, both SINMAP and SHALSTAB indicate that shallow landslides will concentrate in areas of topographic convergence. The two programs differ in several details, such as flow-routing algorithms, consideration of material attributes, and use of FoS calculations to find unstable slopes, but their fundamental approach to determining slope stability is comparable [Savage2004]. SINMAP and SHALSTAB are useful for preliminary stability assessment over large areas where the underlying models' assumptions are met. Under constant rainfall, both models examine a basic steady-state hydrogeological process. This means that both models are used to anticipate a spatially distributed slope stability, but due to the steady-state description of hydrological fluxes, they are confined to the temporal prediction of slope stability. Furthermore, steady-state models are restricted to a few implausible scenarios involving rainfall characteristics and in situ conditions [Iverson2000].

The TRIGRS model incorporates transient pressure responses to rainfall and downward infiltration to estimate the possible occurrence of shallow landslides [Baum2008]. TRIGRS

combines an infinite slope stability calculation with an analytic, one-dimensional solution for pore-pressure diffusion in a finite-depth soil layer in response to time-varying rainfall [Savage2004, Baum2002]. The infiltration models in TRIGRS are based on the solution of Richards' equation for an infinitely deep impervious basal boundary by [Iverson2000] and the surface condition of constant flux for a defined time and zero flux thereafter by [Salciarini2006]. [Iverson2000] presents a theoretical framework for understanding how hydrologic processes affect the location, timing, and rate of landslide occurrence based on a solution to the boundary problem provided by Richard's equation. [Baum2002] developed the TRIGRS software program by generalizing Iverson's initial infiltration model solution for unsaturated environments and variable rainfall intensity and duration scenarios. Many research, including [Baum2005, Salciarini2006, Godt2008, Zizioli2013, Vieira2010, Liao2010, Raia2014, Bordoni2015, Lee2015]. , have used TRIGRS to evaluate the Spatio-temporal prediction of landslide occurrence.

Transient models can improve the effectiveness of susceptibility analysis by accounting for the transient impacts of fluctuating rainfall on slope stability conditions, but they typically require a lot of detailed spatial data [Sorbino2009]. Furthermore, they are sensitive to some essential input variables, such as soil hydraulic characteristics, starting steady-state groundwater conditions, and soil depths, which can only be accurately evaluated using empirical models or inverse deterministic analyses [Salciarini2006, Godt2008]. Comparative analyses using different physical slope models were undertaken since multiple physically-based models have been developed and used to create shallow landslide susceptibility maps. [Meisina2007] used the SINMAP and SHALSTAB models to analyze slope stability and compared the results to the locations of shallow landslides in Oltrepo Pavese's area (Northern Apennines) in November 2002. In May 1998, in the Campania Region of Italy, [Sorbino2009] used SHALSTAB and TRIGRS to investigate the source locations of major rainfall-induced, shallow landslides. [Zizioli2013] employed SINMAP, SHALSTAB, and TRIGRS to create landslide susceptibility maps for a region in the northern Apennines where landslides inflict significant infrastructure and agricultural damage. SINMAP and SHALSTAB were compared by mapping landslide-prone areas in Brazil in [Michel2014]. The comparison of the various methodologies helps identify the most significant.

Several novel physically-based landslide susceptibility study methods have been presented in recent years. The triangulated irregular network (TIN)-based real-time integrated basin simulator (tRIBS) model was developed by [Arnone2011] and [Lepore2013] that allows simulation of most spatial-temporal hydrologic processes (infiltration, evapotranspiration, groundwater dynamics, and soil moisture conditions) that can influence landslide occurrence. To account for heterogeneous and anisotropic soil impacts, this model considers the spatial variability in precipitation fields, land-surface descriptors, and the related moisture. [Montrasio2008] and [Montrasio2009] suggested a SLIP model that focuses on the destabilizing forces created by the water downflow and the contribution of partial saturation to the soil shear strength [Montrasio2011]. This model includes the partial saturation contribution to soil shear strength using total soil cohesion. The practical and apparent cohesion connected to the matrix suction proposed by [Fredlund1996] is included in total cohesion. Based on experimental data, [Montrasio2008] estimated suction-related cohesiveness as a mathematical function of saturation degree. To assess the slope stability change linked with rainfall on a slope, [Chae2011] proposed the modified infinite slope model based on the concept of the saturation depth ratio. To investigate the influence of the saturation depth ratio following rainfall infiltration, a rainfall infiltration test on unsaturated soil was performed using a column. The proposed approach was tested on real-world instances to determine its viability and construct a Geographic Information Systems (GIS) regional landslide susceptibility map.

2.2.2.6 Landslide runout models

In the case of a catastrophic failure, landslide runout is defined as the total distance covered by a landslide [McDougall2017]. It can refer to a distance measured downstream of a given point (runout length) or the complete horizontal path length measured on a map (travel distance) [Rickenmann2005]. Both cases suggest that a landslide can move much further than simple frictional models predict [Corominas1996, Johnson2016]. Although various landslides in a variety of materials can move over long distances and display flow-like behavior [Hungr2001], the word "runout" is usually used to describe the mobility of fast landslides that travel at exceptionally high speeds (> 5 m/s; [Cruden1996b]). Rockfalls, debris flows, and rock/soil avalanches are examples of fast landslides that rapidly accelerate the original collapse, resulting in large displacements. Fast landslides have severe destructive consequences and many causalities due to their speed and lack of predictability (see [Guzzetti2000, Petley2012]). According to [Dai2002], landslide runout modeling is critical at all levels of hazard and risk zoning.

How can we tell if a landslide has the potential to become exceedingly rapid? Primarily based on previous experience and precedence. The majority of shallow slides that occur on steep slopes can become relatively rapid. They usually involve a stable substrate and loose granular regolith. Such collapses almost invariably occur during heavy rain, guaranteeing that the loose layer is saturated. As the initial failure moves faster, the soil downslope is over-ridden, liquefied by rapid undrained loading, and integrated into an expanding debris avalanche [Sassa1985]. When loose sediment is abundant, debris mobilization can also occur in established steep stream channels [Kean2013]. The surging, extremely rapid debris flow is caused by the moving mixture of water and debris entrapping more material. Debris flows are common occurrences that contribute to forming a fan with its deposits.

Slides that do not evolve faster than quick (3 m/min) movement are frequently found in soils dominated by fine clayey material. According to [Ter-Stepanian2000], clay flow slides that are extra-sensitive ("quick") are a significant and well-known exception. When mixing with surface water is sufficiently rapid, clay slopes can also create shallow collapses that evolve into extremely rapid mudflows [Hungr2001]. After a sudden failure, rock slides, rockfalls, and rock topple in good-quality rock can become exceedingly quick. The movement can take on a flow-like quality when a rock mass is broken, resulting in exceptionally rapid rock avalanches [Melosh1987]. The failure behavior of numerous landslides is described in [Hungr2005], which can be used as a guideline.

Rapid gravitational processes are common and the most dangerous type of landslide, regardless of the material involved. The capacity to forecast their travel distance and possibly other factors such as velocity or peak discharge has significant implications for hazard assessment and mitigation design. Several methods for calculating fast-moving landslides' travel distances and velocities have been developed. They range from empirical-statistical methods to dynamic methods, continuum-based models that allow simulation of the flow and related parameters along the slope, including a deposition [Rickenmann2005].

Since early attempts to constrain the relationship between landslide travel distance (L) and the elevation difference between the starting and ending points of deposition (H), it has been clear that the volume of the mass movement (V) has a significant impact on its mobility [Corominas1996, Rickenmann1999]. According to a plot of the tangent of the trip angle (H/L) against landslide volume (Fig. 2.12), large landslides have lower travel angles than smaller ones. Differences in material characteristics and mobility mechanisms and the shape of the deposition sites or impediments are frequently linked with high scatter in such interactions [Corominas1996, Rickenmann1999]. Their application must consider a homogeneous set of data reflective of the specific landslide type. On the other hand, using mean values can produce overly optimistic findings; instead, use the lower envelope

or the line corresponding to a given confidence level (e.g., 90%) [Hungr2005].

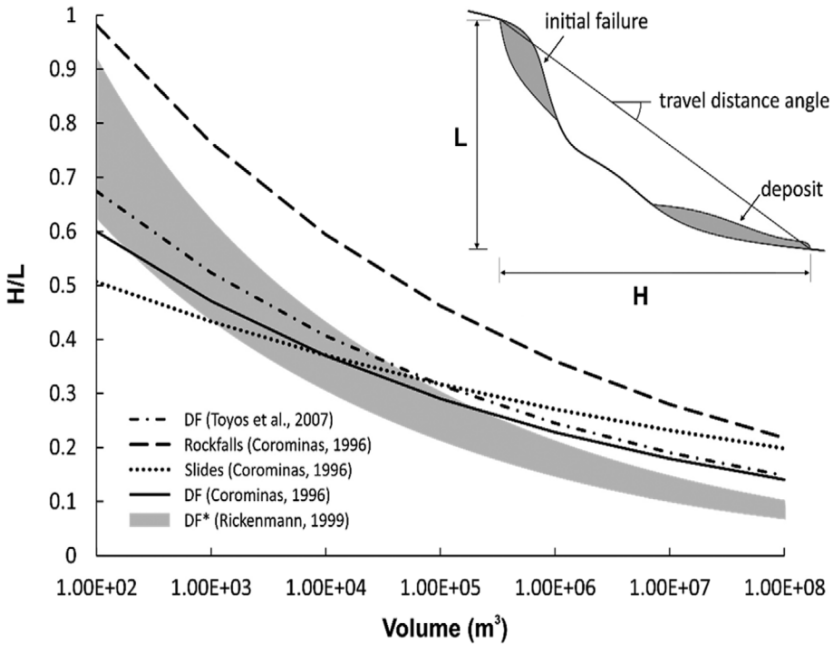

*Figure 2.12: Relationship between landslide mobility (H/L) and volume as described by various authors for different types of mass movements. *H ranging from 200 to 2000 m (after [Chae2017])*

For preliminary hazard mapping purposes, most empirical methodologies are simple enough to use GIS to outline the extent of possibly affected areas [Toyos2007]. [Zimmermann1997] defined a lower envelope of tan (H/L) as a function of the catchment area for preliminary evaluations when volume estimates are lacking in the case of debris flows. Alternatively, [Prochaska2008] proposes using the average channel slope to forecast runout for small and medium-sized debris flows in constrained channels. [Fannin2001] advocated using a sediment budget along the flow path to estimate the total travel distance, recognizing the role of sediment entrainment for debris flows. Their method works regardless of whether or not the projected debris-flow volume is known, and it is mainly reliant on the quality of field data [Miller2008].

For lahars, [Iverson1998] suggested a method that links event volume (V) with a flooded area (B) and cross-sectional flow area (A) (Fig. 2.13). It is founded on scaling considerations and statistical data analysis from previous events. It may be used to a variety of fast-moving landslides as long as the semi-empirical scaling relationships between volumes V, B, and A are adjusted. Many researchers have proved its applicability to debris flows [Crosta2003, Simoni2011] and other phenomena [Griswold2008]. Certain beneficial modifications have been offered to improve the method's capabilities or meet specific situations. [Scheidl2009] added a module to their TopRunDF for automated flow path prediction on the fan while expressing the mobility coefficient (V-B relationship constant) as a function of the gradient of the deposition area. The prediction model DFLOWZ [Berti2014] provides for the simulation of both confined and unconfined flows and the consideration of scaling relationship uncertainties and their impact on outcomes. [Griswold2008] included a module for defining likely debris flow source regions to the GIS tool LAHARZ [Schilling1998] and, more recently, [Reid2016] incorporated the effects of debris-flow expansion along the channel due to entrainment into the same method.

Through frequency-magnitude connections, empirical, volume-based models allow the

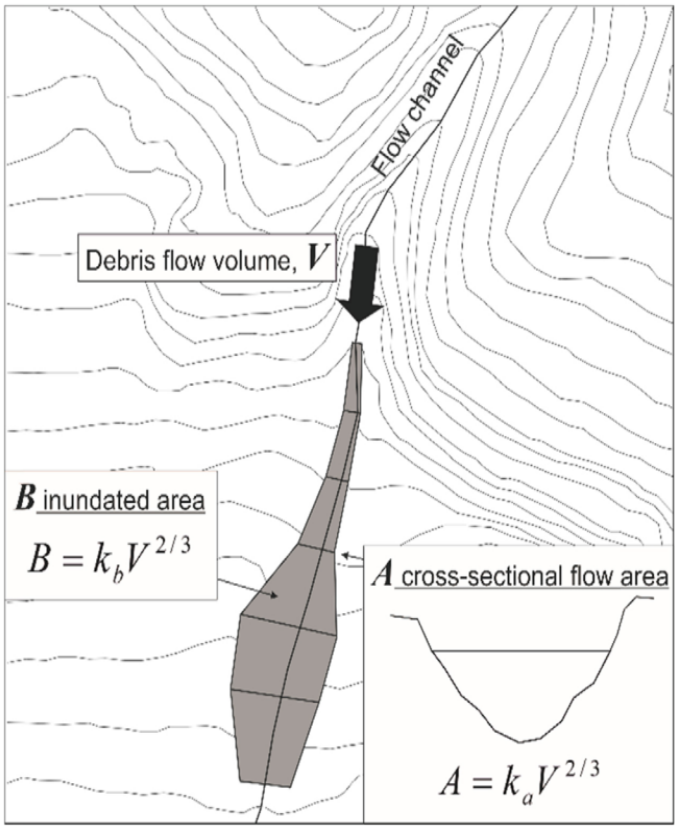

Figure 2.13: Definition of empirical scaling relationships describing the relation between event volume (V), inundated area (B) and cross-sectional flow area (A). Mobility coefficients k_a and k_b can be obtained based on statistical analysis of past events (after [Chae2017])

likelihood of alternative debris-flow runout lengths or inundated areas to be assessed. While mapping hazard zones as a function of event volume would be advantageous, estimating a likely range of flow volumes for a given channel or location can be problematic [Riley2013, Corominas2014]. On the other hand, empirical methods retain their relevance and can be utilized for preliminary hazard assessment due to their simplicity, speed, and ease of use.

Dynamic approaches use one-, two-, or three-dimensional models to simulate debris flow propagation utilizing mass, momentum, and energy conservation. [McDougall2004, Hungr1995, O'Brien1993a]. The majority of approaches treat debris flow as a continuous system with superficial constitutive relationships capable of recreating a material's macroscopic behavior. Even though a propagating gravity flow is nearly always a non-homogeneous and multi-phase mixture, several single-phase rheological models have been devised for simulating its behavior [Iverson2000]. Due to the complexity and abundance of needed parameters, more rigorous, physically-based multi-phase models have been proposed [Iverson2001], although their application is limited [Liu2016]. Because natural materials contain coarse, irregular particles in a wide range of sizes and a variable quantity of water, determining their rheological behavior remains difficult.

Gravitational flows are typically described using three dimensions as a non-Newtonian fluid flowing using dynamic methods. A Bingham fluid, or, more broadly, a Coulomb viscous [Johnson2016] or Herschel-Bulkley fluid, is a flow resistance term that is frequently used. These models are more suitable for relatively fine-grained "mudflows" than for "stony debris flows," which require a dilatant or inertial grain shearing model to account for the grain collisions that dominate the flow behavior [O'Brien1993a]. Some intermediate models describe the combined influence of viscous, inertial, and turbulent flow regimes. Despite its origins as a snow avalanche model, the Voellmy frictional model has been successfully and widely adapted to debris flows [Revellino2004, Naef2006]. A Coulomb-type friction term scales with normal stress and a turbulent drag coefficient that scales with velocity squared are included.

However, because mono-phase models do not represent the physics of flowing materials and full-scale direct measurement is impractical, the parameters of a specific rheological model are usually obtained through back-analysis of similar events [Sosio2007]. This is a significant limitation of dynamic methods because actual debris flows, or mudflows, exhibit significant variability in behavior during successive surges of a single event [Berti2000, McCoy2010] and, even more so, between events that occur within the same catchment [Kean2013, Navratil2013]. Rheological parameters generated from back-analysis of documented historical events are often employed for prediction purposes [Jakob2012, Pirulli2010]. Though such an approach seeks to handle the choice of rheological parameters effectively, it inevitably adds uncertainty to the outcomes due to the above-mentioned inter-event variability. Back analysis appears to be the only realistic choice because no systematic effort has been made to constrain the ranges of rheological parameters as a function of the many variables that influence flow behavior (e.g., volume, particle size, solid concentration).

In general, predictive application of dynamic methods necessitates a thorough understanding of the physical phenomena to be recreated and the rheological model. To correlate hazard values to simulation results of a specific catchment, the design volume or, better still, the volume-frequency relationship is necessary, similar to empirical approaches [Jakob2007]. Alternatively, the flow's erosion and deposition dynamics must be considered. By injecting a user-specified quantity of entrainment (e.g., bed-normal depth eroded per unit flow and unit displacement) along the course, [Hungr2001] attempted to model the entrainment process, and several instances recently appeared in the literature [Hussin2012, Frank2015]. When entrainment is included in a model, the entrainment

region and depth become extra input parameters, making them more difficult to limit. Field-based geological observations can be utilized to estimate these parameters; however, dynamic approaches are needed to replicate the entrainment process effectively [Asch2007].

FLOW-2D (3-D integrated Eulerian model) is one of the most extensively used dynamic models for analyzing debris flows and mudflows on colluvial fans [Sosio2007, Marchi2010]. The model is based on the quadratic rheological technique presented earlier in this section [O'Brien1993b]. An incoming water hydrograph is combined with a time-dependent sediment-concentration graph to depict the inflow volume. To account for changes in surface coverage, the Manning coefficient should be assigned to each grid element to account for the hydraulic roughness of the terrain surface.

In the case of studies, several different debris-flow simulation models were used and compared to actual debris flows. DAN-3D [Hungr1995, McDougall2004], RAMMS [Christen2010, Christen2012, Hussin2012], and RASH-3D [Pirulli2010] are only a few of them. Runout distance inundation patterns, flow heights, and velocities can be investigated using dynamic numerical models. Given that the local terrain mostly dictates the runout pattern, several writers concur on the importance of an accurate digital elevation model of the prospective depositional area [Rickenmann2016, Hürlimann2008]. [Rickenmann2006] conducted comparative research on the performance of simulation models. Because of the large spectrum of physical processes that can be simulated, generalizations are impossible. Some forms of flow (e.g., rocky turbulent debris flows) may be better reproduced by a simulation model, whereas others may be reproduced less correctly (e.g., muddy viscous flows). Because most simulation models' rheologies do not define the physics of the process, tracing boundaries is difficult. It is not unexpected, for example, that the Voellmy rheology, which was created to mimic snow avalanches [Christen2010], can also be used to simulate debris flows [Hussin2012] and rock avalanches [Deline2010, Sosio2008]. To permit successful calibration based on a sufficient number of control factors (e.g., inundated area, velocities, depths), maybe more than one event, rheological relationships should be simple with few, readily constrained parameters [Hungr2005].

Collecting field observations that can be utilized to systematically back-analyze past events is the most desirable development in the fast-moving landslide propagation study. This will allow for the establishment of much-needed standards for the selection of rheological parameters and the evaluation of model performance in terms of landslide typology.

Summary on landslide models

- In most of the models discussed above, for instance, threshold-based models, many of these are defined without rigorous mathematical or physical criterion.
- Then models like depth-averaged landslide model are very complex to solve parameter estimation problems, as well as they require extensive spatial data.
- Therefore, we stick to **relatively simple physics-based dynamical models** of landslide for the further investigation, e.g. sliding-consolidation, extended sliding-consolidation, viscoplastic sliding-consolidation model of landslide.

2.3 Information Reconstruction

To produce effective landslide forecasts using the physically-based model, adequate and precise data is required. As a result, the quality and amount of input parameters have been the primary considerations in landslide forecasting. In actuality, such data are frequently limited in scope, have flaws, and are of varying quality [van Westen2005]. As a natural process creates the slope material, the strength parameters of slope materials, such as cohesion and friction angle, are fundamentally spatially heterogeneous [Baecher2003, Carrara2008, Chowdhury2010]. Furthermore, the input parameters for the physically-based approach should be collected from a large study area, with presumably limited sampling; consequently, uncertainties are invariably present in the physically-based model analysis. The disparity between simulated and observed landslide occurrence distributions has been identified as an essential driver of uncertainty in model parameter evaluation [Burton1998]. As a result, when using physically-based models to perform susceptibility analysis, geographical variability and uncertainty in ground conditions must be considered. As a result, using some model/parameter identification tools, it is vital to address such uncertainties. We briefly review such strategies from the literature in this section.

2.3.1 Probabilistic approach

The majority of physically-based model studies have employed a deterministic technique to evaluate slopes' potential or relative instability across a vast area without considering input parameter uncertainty. The deterministic methodology is not adequate for analyzing uncertainties and variability because just a single fixed value is given for an unknown parameter. Because of the uncertainties and difficulty gathering, checking, and processing big spatial data sets, applying the deterministic technique to a wide study area might be extremely difficult or impossible [Zhou2003, Zhou2020]. Probabilistic analysis can be used to account for variability and uncertainty in a quantitative way. As a result, probabilistic analysis has gained popularity as a powerful technique for dealing with uncertainty. To account for the uncertainties associated with determining strength parameters, they should be treated as random variables in probabilistic analysis. In addition, the available field or laboratory data is used to calculate the statistical parameters (such as mean and standard deviation) and probability density function (PDF) of unknown variables. The probabilistic analysis is then performed utilizing the statistical parameters and the PDF of uncertain parameters with the performance function (i.e., a physically-based model in this study).

The first-order second-moment method (FOSM), the point estimate method (PEM), and Monte Carlo simulations are the three most often utilized probabilistic analysis approaches. Even when additional information about the random variables is absent, FOSM and PEM have the advantage of providing an approximate estimation of the chance of failure using only the means and standard deviations. When the performance functions are complex, however, the computations become impossible. Furthermore, because these methods can only be used to estimate the likelihood of failure, they cannot calculate the distributions for FSs, which are also treated as random variables [Harr1987, Park2001]. On the other hand, Monte Carlo simulations are one of the most extensively used probabilistic analysis approaches that, in theory, may be used to any model that can be analyzed deterministically. Because all random variables and the likelihood of failure arising from the reliability analysis are represented by their PDFs through repeated calculations, Monte Carlo simulations are regarded as a complete probabilistic analysis technique [Park2013]. Monte Carlo simulations are simple to set up on a computer and may accept a wide range of functions, even ones that are difficult to define explicitly [Baecher2003]. Several works [Harr1987, Baecher2003, Chowdhury2010] provide extensive explanations for the various probabilistic analyses.

As many reports have pointed out, probabilistic analysis has been adopted in site-specific slope stability analyses at hillslope scale [Christian1994, Gokceoglu2000, Park2001, El-Ramly2002, Park2005, Li2014, Zhang2007, Cho2010, Ali2014a, Zhu2013, qiang Dou2014] The use of geographic information system (GIS) methodologies has lately permitted a probabilistic approach to spatially distributed study and physically-based modeling of landslide susceptibility over large areas. [Santoso2011] used a probabilistic analysis approach in the physically-based model method, but the strength parameters were not treated as random variables. In certain research, probabilistic analytic methodologies were employed in physically-based model assessments, but the hydrogeological model was not used; therefore, a constant groundwater level was assumed for the entire study area [Zhou2003, Shou2005, Shou2009]. Other scholars have used uniformly distributed strength parameters with upper and lower bounds to model the uncertainties in input parameters, which is the most basic type of probabilistic analysis [Dietrich2001, Meisina2007, Terhorst2009, Yilmaz2009].

Recently, more extensive probabilistic techniques for landslide susceptibility analysis that are regionally dispersed and physically-based have been presented. Using Monte Carlo simulation, [Raia2014] proposed a probabilistic version of the TRIGRS code. The qualities of the slope material, such as strength and hydraulic parameters, are treated as uniformly distributed random variables in this study. The proposed method was then tested on a study area, with the probabilistic and deterministic analyses being contrasted. According to the study, the predictive power of the probabilistic analysis was around 10% higher than that of the deterministic analysis. High-resolution slope stability simulator (HIRESSS), a physically-based slope stability simulator incorporating Monte Carlo simulation, was proposed by [Rossi2013]. The probabilistic technique was employed to control uncertainty in typical geotechnical parameters, which is a common weakness of the deterministic model. The proposed simulator was tested in three different regions, with good results in managing unpredictable input data over a vast area and on a vast scale. In a physically based and spatially distributed landslide susceptibility analysis coupled with the hydrological infiltration model, [Park2013] and [Lee2015] used Monte Carlo simulation as the probabilistic approach. The proposed model was used to investigate locations with numerous landslides, and the probabilistic analysis outperformed the deterministic analysis.

2.3.2 Determination of triggering thresholds

2.3.2.1 Rainfall thresholds

Landslide early warning is critical for recognizing landslide indications early or in advance so that inhabitants can be evacuated from potential landslide locations and minimize the damage caused by landslides. Early identification of landslides in a vast natural terrain is achievable by real-time or near-real-time monitoring of rainfall and changes in the soil's physical properties. The majority of landslide warning systems use triggering levels set by rainfall and the soil's physical qualities. A threshold is the lowest or highest quantity required for a process or a state to change [White1996]. As a result, securing feasible and reliable triggering criteria for landslide early warning is critical.

Because landslides frequently occur during periods of heavy rainfall, a landslide triggering threshold is linked to the rainfall and hydrological conditions in the soil. According to [Corominas2000, Aleotti2004, Wieczorek2005, Guzzetti2007], a rainfall threshold can be established either empirically (statistically) or physically (deterministically). Physical thresholds are based on numerical models that evaluate the relationship between rainfall, pore water pressure, VWC, suction stress, and slope stability, whereas empirical thresholds are developed by collecting rainfall data for meteorological events

with and without landslides. Empirical rainfall thresholds were divided into three categories by [Guzzetti2008a]: i) thresholds that combine precipitation measurements obtained for specific rainfall events, ii) thresholds that include the antecedent conditions [Terlien1998, Crozier1999, Chleborad2003, Aleotti2004], and iii) other thresholds, such as hydrological [Reichenbach1998, Jakob2003]. Thresholds based on precipitation data from a single or several rainfall events can be further classified into intensity-duration (ID) thresholds, total event rainfall (E), rainfall event-duration thresholds (ED), and rainfall event-intensity (EI) thresholds, according to [Guzzetti2007]. These thresholds are usually calculated by plotting lower bound lines in Cartesian, semi-logarithmic, or logarithmic coordinates on the rainfall conditions that caused landslides [Iverson2000, Capparelli2011]. Deterministic-based models seek to expand the slope stability models used in geotechnical engineering spatially. Deterministic-based models can be used to global, regional, and local thresholds. Furthermore, deterministic-based models can predict the quantity of precipitation required to cause slope collapses and the location and timing of projected landslides, making them useful for landslide warning systems [Chung2016].

Global, regional, and local rainfall thresholds have been established for the start of landslides. A global threshold establishes a minimal level beyond which landslides are unlikely to occur, regardless of local morphological, lithological, and land-use constraints, as well as local or regional rainfall patterns and histories [Caine1980a, J.E.2005]. Regional thresholds are developed for areas ranging from a few to several thousand square kilometers with similar meteorological and physiographic characteristics and are possibly suitable for landslide warning systems based on quantitative spatial rainfall forecasts, estimations, or observations. The authors of [Salciarini2006] and [Melchiorre2011] recommended regional thresholds. Local thresholds apply to single landslides or groups of landslides in areas ranging from a few square kilometers to hundreds of square kilometers and take into account the local meteorological regime, geomorphologic context, and geological parameters directly or implicitly.

[Wang2021] proposed a rainfall-based debris flow warning model based on the link between rainfall and debris flow. A way to describe a rainfall event and its antecedent rainfall were presented to assess the risk of debris flows induced by rainstorms. This method defined rainfall parameters such as rainfall intensity, duration, accumulated rainfall, and effective accumulated rainfall. The rainfall triggering index (RTI), which set up a rainfall-based debris flow warning model, was defined as the hourly rainfall intensity and effective accumulated rainfall. Based on the RTI values of historical rainfall occurrences, they suggested a method for determining the lower critical RTI value and the higher critical RTI value. After determining the two crucial RTI values in a rainfall event, a diagram with instant RTI values at time t on the ordinate and the variation of time t on the abscissa can be used to estimate the immediate debris flow occurrence potential.

2.3.2.2 Physical and mechanical thresholds

As mentioned earlier, rainfall is the most crucial landslide early warning threshold. However, there can be variances in landslide triggering under the same rainfall conditions. Rain data obtained by rain gauges in landslide-prone locations is required for early warning of shallow and deep landslides. Nonetheless, the impact of rainfall is difficult to quantify because it is dependent on several factors, including soil heterogeneity. As a result, based on each scenario's physical and mechanical thresholds, it is required to investigate the links between soil parameters and landslide triggering [Chae2011].

Because of the variability in conditions relevant to each significant component, physical thresholds have various limits for applicability to large areas. Cite as an example of how to get around these limits. [Rupp2018] provided a model of antecedent soil water status

that took into account empirical thresholds like antecedent rainfall and physical properties like soil moisture and potential evaporation. [Huggel2009] used an empirical rainfall threshold function, which took ten years and divided it into six-hour periods.Within a hydrological conceptual modeling framework, [Sirangelo1996] created the forecasting of landslides induced by rainfalls (FLaIR) model to forecast landslide movements activated by a rainstorm. The relationship between the mobility function and landslide likelihood as a function of antecedent rainfall is considered in this model. The FLaIR model is partly based on physical approaches because the mobility function is specified as a function of the infiltration rate, directly related to soil and topographical conditions. The system comprises two modules: a monitoring module that uses previous rainfall data and a warning module that uses anticipated rainfall data. This fourth module, in particular, evaluates the information offered by meteorological models, which provide rainfall estimates for the next 6, 12, 18, and 24 hours. According to [Capparelli2010a], the system can forecast likely developments over the next 24 hours using these values. The FLaIR model was later expanded to mudflow movement [Sirangelo1996], leading to the MoniFLaIR early warning system [Sirangelo2002, Capparelli2010a].

The relationship between slope failure and the VWC gradient as a function of rainfall circumstances was investigated by [Chae2011]. In the Deoksan research region in Korea, the VWC gradient was distributed in the range of 0.107-0.249 in cases of slope failure, but field monitoring results without slope failure showed a gradient range of VWC between 0.003 and 0.073. The findings show that slope failure is caused by a considerable amount of rainfall and a steep VWC gradient. Based on the findings, they proposed a VWC gradient threshold for early warning of landslides produced by rainfall. The findings revealed that a landslide is more likely to occur in the study area when the VWC gradient is greater than 0.1.

A limit equilibrium model was integrated into a landslide early warning system by [Thiebes2014]. The combined hydrology and stability model (CHASM), a physically-based slope stability model, was first used to analyze stability conditions on a reactivated landslide in the Swabian Alps and was then integrated into a prototype of a semi-automated landslide early warning system. The CHASM combines the simulation of saturated and unsaturated hydrological processes to calculate pore water pressures, which are then incorporated into the computation of slope stability using limit equilibrium analysis for assessing slope stability and early warning modeling. The results of the CHASM program show that the FoS is relatively low for various potential shear surfaces, and additional rainfall occurrences could create instability. International geospatial standards were employed to assure the interoperability of system components and the transferability of the implemented system as a whole while integrating and automating CHASM within an early warning system. The CHASM algorithm is executed automatically as a web processing service, with fixed, planned input data and changing input data, such as hydrological monitoring and quantitative rainfall forecasts. When pre-defined modeling or monitoring criteria are crossed, a web notification service sends text and email messages to relevant specialists, who decide to provide an early warning to local and regional stakeholders and offer action suggestions.

The characterization of hydrological and mechanical behavior of unsaturated soils is possible using the soil-water characteristic curve (SWCC), which is connected to pore water pressure and water content. The hysteretic nature of SWCC [Lu2006,Fredlund2011, Likos2014,Lu2013], linked to in situ processes resulting from different drying and wetting cycles that the soils suffer under natural conditions, determines the development of the drying and wetting curve. Thus it can have practical implications on water movement in soils and mechanical behavior of unsaturated soils in terms of deformation and shear strength [Wheeler2003,Likos2014,Bordoni2015]. The stability of an unsaturated slope on

natural terrain was assessed using the fluctuation in suction stress caused in the soil by rainfall infiltration over time, according to [Song2016]. The SWCC and the suction stress characteristic curve of the unsaturated soil acquired from the study area were evaluated using the [van Genuchten1980] and [Lu2006] models to apply the slope stability analysis considering suction stress unsaturated soil. Because of changes in suction stress generated by evaporation and infiltration of water in the unsaturated soil layer, the FoS of the natural slope fluctuated continuously. As a result, when the VWC or matric suction in the soil is being monitored in the field, the infinite slope stability of a slope in natural terrain can be evaluated in real-time by measuring the suction stress induced by rainfall in the unsaturated soil.

2.3.2.3 Back analysis and ground motion prediction for landslide forecasting

The shape of landslides, material qualities, and time change of groundwater level (or pore pressure) can be used to solve physically-based model equations to anticipate ground motion [Herrera2013a]. Field observations, in-situ tests, and laboratory experiments can all be used to get the parameters. Back analysis can estimate any of these characteristics in a fixed period if unavailable; however, the prediction must be made for a different time. To minimize disparities between observed and computed displacements, unknown material parameters (viscous parameter and friction angle) were estimated using nonlinear regression in [Corominas2005a]. In [Herrera2013a], a similar strategy is employed.

Nonlinear regression

The relationship between a variable of interest Y and one or more explanatory or predictor variables x_j is studied using regression.. The general model is

$$Y_i = h\langle x_i^{(1)}, x_i^{(2)}, ..., x_i^{(m)}; \theta_1, \theta_2, ..., \theta_p\rangle + E_i \tag{2.36}$$

where h is an appropriate function that depends on the explanatory variables and parameters, that we want to summarize with vectors $\bar{x} = \left[x_i^{(1)}, x_i^{(2)}, ..., x_i^{(m)}\right]^T$ and $\bar{\theta} = [\theta_1, \theta_2, ..., \theta_p]^T$. The random errors E_i characterize the unstructured departures from the function h. For the distribution of this random error, a normal distribution is assumed, so

$$E_i \sim \mathcal{N}\langle 0, \sigma^2\rangle$$

[Bernardie2014a] computed displacements by solving combined statistical-mechanics-based model equations using Sequential Quadratic Programming (SQP) algorithm to optimize some geometrical parameters and material properties for chosen range. The main objective was to predict daily displacement from the precipitation time series. Therefore, the calibration procedure has been performed over several time windows using the SQP optimization algorithm. The models were then tested for any day of the period of interest. Before a given day D, an optimal calibration window size among a period of 60 and 180 days was looked for. Results indicate that most of the optimized windows are around 90 days [Bernardie2014a]. Then the model was calibrated, and the displacements were computed during this period (Fig. 2.14). The next day of the calibration was then shifted at $D+1$, and the procedure was iterated.

In order to test the ability of the methodology to be used in an operational early warning system delivering daily warnings in near real-time, a prediction procedure was developed and tested in [Bernardie2014a]. The method was applied as if the new data were received each morning and processed in real-time daily. Hence, the "new" received data

were added to the historical time series for each day. The calibration was performed over time windows of different durations (Fig. 2.14). The optimal calibration was then used to predict the displacement for the three following days, based on the meteorological data of these three subsequent days, assumed to be meteorological forecasts. The procedure was then repeated for the next day, with a completely new calibration. In order to test the 3-day prediction procedure, the daily predicted displacements were compared with the observed displacements for the three predicted days. Consistency between model output and observation was observed with some discrepancies.

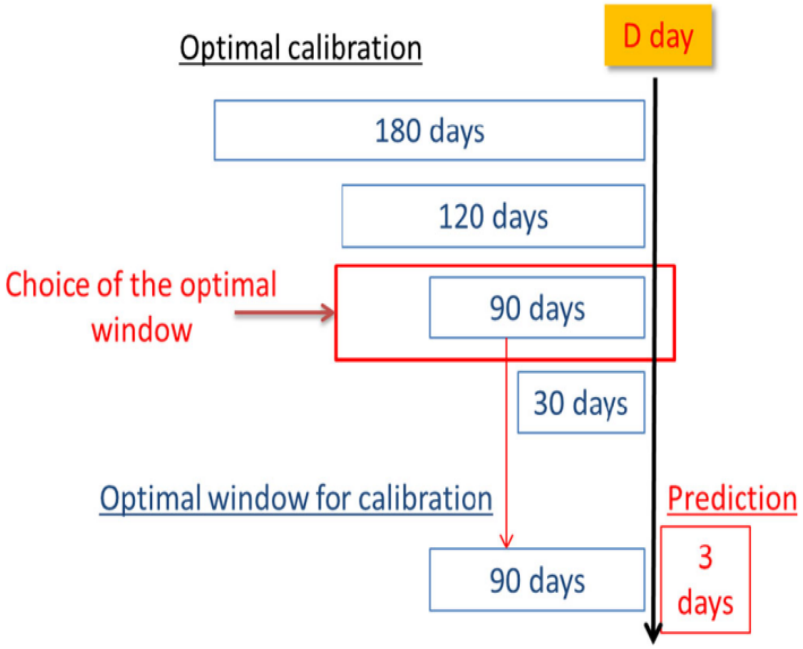

Figure 2.14: Schematic framework of the forecasting procedure (after [Bernardie2014a])

Based on the results, first, inverse velocity criteria was analyzed to predict a catastrophic fluidization event (as already applied in other studies [Petley2002, Petley2005, Rose2007]. However, it was found that this parameter was not suitable for the prediction as inverse velocity was found to be decreasing even if no fluidization phenomenon occurred. Another approach used was based on the evolution of some estimated parameters (optimized each day), for instance, viscosity. Results suggested that viscosity vastly increases during the period preceding the occurrence of a fluidization event. However, this trend was observed for non-fluidization events. Thus, even these criteria were found non-suitable for the prediction purpose.

In the results based on Root Mean Square Error (RMSE) computed on the three predicted days, it was observed that the model could not reproduce the accurate displacement preceding the occurrence of a fluidization event. It indicated an important change in mechanical behavior and the kinematic regime of the landslide. Thus, the RMSE variation was considered a good indicator of the occurrence of fluidization. Out of three proposed thresholds, the first two were based on the normal law distribution of the RMSE values, with the use of a threshold equal to the mean of the RMSE plus three standard deviation values of the RMSE and the second one equal to the mean of the RMSE plus one standard deviation values of the RMSE:

$$T_1 = \text{mean}(x) + 3\sigma_x$$
$$T_2 = \text{mean}(x) + \sigma_x$$

A third threshold was defined based on the historical RMSE curve. The threshold was then chosen as the RMSE values prior to the past fluidization events.

Sequential Quadratic Programming (SQP)

SQP is one of the most used approaches for solving constrained nonlinear optimization problems numerically. It has a strong theoretical foundation and sophisticated algorithmic tools for solving large-scale technologically relevant problems. Consider the use of the SQP methodology to solve NLPs (Nonlinear Optimization Problems) of the form

$$\begin{aligned} \min_{x} \quad & f(x) \quad \forall x \in \mathbb{R}^n \\ \text{s.t.} \quad & h(x) = 0 \\ & g(x) \leq 0 \end{aligned} \tag{2.37}$$

where $f : \mathbb{R}^n \to \mathbb{R}$ is the objective functional, the functions $h : \mathbb{R}^n \to \mathbb{R}^m$ and $g : \mathbb{R}^n \to \mathbb{R}^p$ describe the equality and inequality constraints.
SQP is an iterative procedure which models the NLP for a given iterate $x^k, k \in \mathbb{N}_0$ by a Quadratic Programming (QP) subproblem, solves that QP subproblem, and then uses the solution to construct a new iterate x^{k+1}. This construction is done in such a way that the sequence $(x^k)_{k\in\mathbb{N}_0}$ converges to a local minimum x^* of the NLP (2.37) as $k \to \infty$. In this sense, the NLP resembles the Newton and quasi-Newton methods for the numerical solution of nonlinear algebraic systems of equations. However, the presence of constraints renders both the analysis and the implementation of SQP methods much more complicated.

Our work is mainly motivated by research work on landslide displacement/velocity forecasting [Bernardie2014a, Corominas2005a, Herrera2013a], in which beforehand foreacasting process, unknown parameters are estimated first (back analysis) from past data. In that regard, we propose systems and control theoretical tools to acheive the goal of parameter identification.

2.3.3 State observer approaches

The observer problems from control theory are similar to back analysis or inversion techniques. To the best of our knowledge, control theoretical approaches of information reconstruction has never been applied in the context of landslides. However, many of these methodologies' applications may be found in hydrological systems, overland flow, meteorology, oceanography, and a variety of other fields. When some internal information of the system is derived from exterior (directly available) measurements, the observer problem inevitably emerges in a system approach. In general, one cannot use as many sensors as signals of interest characterizing system behavior (due to cost, technological constraints, and so on), mainly because such signals can be of various types: they typically include time-varying signals characterizing the system (state variables), constant ones (parameters), and unmeasured external signals (disturbances). Internal information is required for a variety of reasons, including modeling (identification), monitoring (fault detection), and driving (control) the system. These methods are generally based on a model (dynamical model). According to [Besançon2007], observer problems can be solved either via *optimization* techniques or via direct *observer design*.

2.3.3.1 Adjoint-based optimization

It is a gradient-based optimization method in which the derivative information is derived using an adjoint or co-state equation from a mathematical standpoint. These approaches, also known as optimal control theory, have their origins in the traditional calculus of variations and were developed in the 1950s and 1960s to optimize dynamical systems, particularly for the optimal control of rocket and satellite flight paths [Bryson1975, Stengel1986]. During the 1970s, adjoint-based optimization techniques were introduced in numerical reservoir simulation for computer-assisted 'history matching,' i.e., model parameter estimation through parameter adjustment until the model output matches measured pressures and fluid rates in the wells [Chen1974, Chavent1975]. The Lagrangian multiplier method is used in this approach to connect the system dynamics and the cost function, which is commonly defined as the least square error between simulation values and measurements. The adjoint state approach is then used to minimize the objective functional, so as to obtain the adjoint system and gradients for the parameters of interest and the initial state. With gradients, parameters and initial states are modified (iterative process) until measurement and model output match.

This strategy is effective in solving observer or estimating difficulties in numerous research. Reservoir characteristics are determined using well pressure data for hypothetical and existing Saudi Arabian reservoirs [Chen1974] for reservoir systems represented by a single-phase flow equation. Using five-year pressure and production data, the authors [Chavent1975] used an adjoint-based optimization method to predict permeability distribution. The approach is tested on a semi-realistic field model that is part of a 9×19 grid with ten production wells. For recorded periodic values of water surface height at a particular station, both constant and position-dependent parameters (bottom friction and water depth) are approximated using a hydrodynamical tidal flow model [Das1991]. In [Nguyen2014], an optimal estimation of initial condition based on the adjoint approach is proposed for overland flow depicted by a one-dimensional Saint-Venant equation. The Banzioumbou Tondi Kiboro catchment in Niger is then extended to estimate Manning roughness and Horton infiltration coefficients [Nguyen2015]. The adjoint approach is used in [Ding2005, Atanov Genadii1999, Ramesh2000, Chen1999] to estimate the manning roughness coefficient in an open channel flow. [Nguyen2016a] proposed state and parameter estimation problems for 1D hyperbolic PDEs that reflect traffic and overland flow, while [Nguyen2018] extended the method to switching 1D hyperbolic PDEs. A brief survey on the parameter estimation (inverse) problem in meteorology and oceanography in view applications of 4D variational data is given in Parameters estimation in meteorology and oceanography [Navon1998]. A review on adjoint-based optimization of multi-phase flow (e.g., optimal recovery of hydrocarbons from subsurface reservoirs) through porous media is given [Jansen2011].

2.3.3.2 Observer design

A state observer or state estimator is a system in control theory that estimates the internal state of a given real system based on observations of the real system's input and output. It is usually computer-implemented and serves as the foundation for many practical applications. It can also aid in estimating model parameters by treating unknown parameters as constant state variables. An observer is a model-based, measurement-based, closed-loop information reconstructor that depends on a model with online adaption based on available measurements and aims at information reconstruction [Besançon2007]. An observer is a well-known tool for state estimation as well as joint state and parameter estimation (starting with the famous *Kalman Filter*), as well as joint state and parameter estimation (e.g. with the *Extended Kalman Filter*). In recent years, it has also been extended to

systems with distributed dynamics (described by Partial Differential Equations (PDE)), with examples in open channel level control [Besançon2008] or monitoring [Bedjaoui2009], backstepping boundary observer for a class of linear first-order hyperbolic systems with spatially-varying parameters [Di Meglio2013], robust state estimation based on a boundary output injection for a class of convection-diffusion-reaction systems [Besançon2013], matrix inequality-based observer for transport-reaction systems [Schaum2014], backstepping adaptive observer-based state and parameter estimation for hyperbolic systems with uncertain boundary parameters and its application to underbalanced drilling [Di Meglio2014], adaptive observer for coupled linear hyperbolic PDEs with unknown boundary parameters based on swapping [Anfinsen2016] up to very recent results based on so-called high-gain technique [Kitsos2022, Kitsos2021]. Extensions to coupled ODE-PDE (combining Oedinary and Partial Differential Equations) can also be found, as in the case of a class of nonlinear ODE-PDE cascade system [Ahmed-Ali2015], and boundary observer based on the Volterra integral transformation for hyperbolic PDE-ODE cascade systems [Hasan2016].

Summary on information reconstruction

- Based on landslide monitoring data and models, it is essential to reconstruct information that can be beneficial to produce early warnings.
- This information could be a geometrical and mechanical parameter, some threshold, statistical or physical criterion.
- The choice of information reconstruction scheme itself depends on the landslide model under consideration and data collected using landslide monitoring.

2.4 Conclusions

Landslide monitoring, modeling, and information reconstruction schemes are the three vital ingredients for landslides forecasting. In the past few decades, with technical upgrades in landslide monitoring, our understanding of complex physical phenomena taking place on-site has also improved, i.e., the advancement in landslide modeling studies. Like landslide monitoring and modeling, with improved computational power and data processing algorithms, the efficiency of landslide forecasting can be improved. With time all these three aspects will keep improving. This manuscript proposes a *cross-disciplinary approach* for landslides investigation, associating landslide models from *Geophysics and Control theoretical tools* for information reconstruction.

3

Calculus of variations for estimation in ODE-PDE landslide models with discrete-time asynchronous measurements

Motivated by some landslide models, and related estimation challenges, this chapter presents an optimal estimation method for state and parameter in a special ODE-PDE coupled system based on the adjoint method for discrete-time asynchronous measurements. This system is described by a pair of coupled Ordinary Differential Equation (ODE) and Partial Differential Equation (PDE), with a mixed boundary condition for the PDE. The coupling appears both in the ODE and in the Neuman boundary condition of the PDE. For this system, initial conditions or state variables and some empirical parameters are assumed to be unknown and need to be estimated. The Lagrangian multiplier method is used to connect the dynamics of the system and the cost function defined as the least square error between the simulation values and the available measurements. The adjoint state method is applied to the objective functional to get the adjoint system and the gradients with respect to parameters and initial state. The cost functional is optimized, employing the steepest descent method to estimate parameters and initial state. Two illustrative examples corresponding to two different landslide models validate the presented optimal estimation approach. The first one is about state and parameter estimation in an extended sliding-consolidation landslide model, and the second one is in the viscoplastic sliding-consolidation landslide model. The material of this chapter corresponds to the paper [Mishra2022a].

3.1 Introduction

Landslide is a geological hazard responsible for about 17% of all casualties from natural hazards [Chae2017]. It also poses a significant threat to the exposed region's ecosystem, infrastructure, and economy. A landslide Early Warning System (EWS) can help reduce life and economic losses by facilitating timely corrective measures. These EWS's rely on models (data-driven and physically-based) to predict landslide occurrence considering different triggering factors such as rainfall, displacement/velocity, and material properties. The current study is mainly motivated by research work on landslide displacement/velocity forecasting [Bernardie2014b, Herrera2013b, Corominas2005b], in which beforehand forecasting process, unknown parameters are estimated first (back analysis) from historical data using some applied mathematical tools, for instance, Sequential Quadratic Programming (SQP) and non-linear regression. This approach is called 'history matching', i.e., model parameter estimation through matching the model output with measurements [Chen1974, Chavent1975]. In some landslide models, Partial Differential Equations (PDE) appear in conjunction with Ordinary Differential Equation (ODE) termed as coupled ODE-PDE systems [Iverson2005b]. Apart from landslides many, more systems are modeled as ODE-PDE systems (see for instance [Zainea2007] for power converters connected to transmission lines, and references therein).

Recently, we proposed an adjoint method to estimate unknown material parameters for the extended sliding-consolidation model of landslide based on synthetic data [Mishra2020c]. The present chapter extends this previous work, where along with material parameters, the initial excess pore pressure distribution is estimated for two landslide models, namely the extended sliding-consolidation model and viscoplastic sliding-consolidation model. Both models depict a sliding type of slope movement and are based on a mechanism of opposition to landslide down-slope movement by basal Coulomb friction, viscosity for the second model, and regulation through basal pore fluid pressure feedback. A major difference between the two models is their applicability, where the extended sliding-consolidation model can represent diverse rates of landslide motions while the viscoplastic sliding-consolidation model (with additional viscous force) can mainly depict slow persistent movement. The motion of the slide block (velocity/displacement) and excess pore pressure evolution are described as ODE and PDE (diffusion equation), respectively. The output of the models depends on initial excess pore pressure distribution, geometrical parameters, and material properties of landslides, out of which we assume that initial excess pore pressure distribution and some material properties (viscosity, friction, and dilatancy angle) are unknown and need to be estimated. Apart from these models, some more parameter-rich complex models represent variety of mass movements [McDougall2017, Iverson2016, Frank2015, Liu2016, Johnson2016, Pradhan2014b]. Back analysis for such models requires extensive spatial data [Chae2017]; therefore, this chapter focuses on relatively simple landslide models depicting sliding behavior.

The calculus of variations-based adjoint method has been a vastly used concept for more than 250 years and is employed in various applied mathematics problems. A brief survey of the history and applications of variational calculus is shown in the work of Ferguson [Ferguson2004]. A large number of studies have illustrated the effectiveness of this approach to solve observer or estimation problems, for instance, reservoir parameters estimation from well pressure data [Chen1974]; permeability distribution estimation given flow production data [Chavent1975]; estimation of the water depth and bottom friction coefficient in the tidal flow model [Das1991]; state and parameter estimation in switched 1D hyperbolic PDEs [Nguyen2018], traffic flow [**?**], overland flow [Nguyen2014] and a real hydrological system [Nguyen2016c]; parameters estimation in meteorology and oceanography [Navon1998]; estimation of the initial condition and parameters in overland flow

for actual field data on the Tondi Kiboro catchment [Nguyen2015]; and estimation of the Manning roughness coefficient in an open channel flow [Ding2005, Atanov Genadii1999, Ramesh2000, Chen1999]. A review on adjoint-based optimization of multi-phase flow through porous media is given in [Jansen2011]. Besides applications for observer problems, the adjoint method is also employed in the control design, such as designing the controller for the contaminant releases in rivers [Michael1997a, Michael1997b]; air traffic flow management [Strub2006]; and space shuttle reentry problem [Graichen2008].

In the context of landslides, measurements may be available only at given times, not necessarily uniformly distributed (in time) due to landslide monitoring constraints (i.e., discrete-time asynchronous measurement). We claim that the optimization (adjoint) method can handle the estimation problem in coupled ODE-PDE models of landslides with discrete-time asynchronous measurements. In this procedure, the system and adjoint equations are solved with the so-called Euler [Ascher1998] and Crank-Nicholson [Crank1947] schemes. To obtain optimal parameter values, gradients (obtained by adjoint method) are utilized as descent directions for the steepest descent method [Bartholomew-Biggs2008]. Numerical simulations validate the solution of the work with noisy synthetic observation values given by a system simulation. For better analysis of the solution method, simulations are performed for different noise levels in measurements and distinct initial sets of guessed parameter values.

The chapter is organized as follows: Section 3.2 describes the dynamics of the system and the formulation of the optimal estimation problem. The formulated optimization problem is solved using the adjoint method in Section 3.3. In Section 3.4, two illustrative examples dealing with state and parameter estimation in landslide models validate the effectiveness of the solution method. Some conclusions and perspectives are put forward at the end of the chapter in Section 3.5.

3.2 Problem formulation

3.2.1 System dynamics

Let us consider a special case of ODE-PDE coupled system of state variables $y(t)$ and $u(z,t)$, evolving according to functions f and h of variables t, $y(t)$, some input $I(t)$ but also a vector of parameters $p \in \mathbb{R}^N$ and $u(z,t)$ satisfying a diffusion equation of coefficient V as:

$$\begin{cases} \dot{y} = \frac{dy}{dt} & = f\left[t,p,y(t),u(0,t),I(t)\right], \quad y(0) = y_0 \\ \frac{\partial u(z,t)}{\partial t} & = V\frac{\partial^2 u(z,t)}{\partial z^2}, \quad u(z,0) = u_0^i(z) \\ \frac{\partial u(0,t)}{\partial z} & = h\left[t,p,y(t),u(0,t),I(t)\right], \quad u(Z,t) = u_0^b(t) \end{cases} \tag{3.1}$$

where, spatial variable z and time variable t belong to the set $(z,t) \in [0,Z] \times [0,T]$, function $u_0^b(t)$ is a predefined boundary condition, function $u_0^i(z)$ and y_0 denote initial conditions. In order to shorten the notations, f, h and u will be used instead of functions $f\left[t,p,y(t),u(0,t),I(t)\right]$, $h\left[t,p,y(t),u(0,t),I(t)\right]$ and $u(z,t)$.

3.2.2 Optimal estimation problem

On the basis of system dynamics (3.1), let us consider the problem of estimating time and space evolution of u and time evolution of y from input $I(t)$ and measurements $y_{mea}(t_k)$ when initial conditions $u_0^i(z)$ and parameters $p_q = [p_1 ... p_q ... p_Q] \subseteq p$ are unknown. We use an

approach to minimize the errors between simulated output y and some related observation values at discrete-time $t_l : y_{mea}(t_l)$. Using similar idea as in [**?**] with regard to discrete-space measurements, we tackle constraint of discrete-time measurements by comparing discrete-time asynchronous measurements to simulated output localized at discrete-times t_k via the Dirac-Delta weight δ_A. Technically, we are thus interested in minimizing the cost function J defined as

$$J = \frac{\epsilon_1}{2}\int_0^Z \left\|u_0^i(z) - u_{0_F}^i(z)\right\|^2 dz + \frac{1}{2}\sum_{q=1}^{Q}\epsilon_{2q}\left\|p_q - p_{q_F}\right\|^2 + \frac{\epsilon_3}{2}\sum_{l=1}^{L}\left(\int_0^T \delta_A(t-t_l)y(t)dt - y_{mea}(t_l)\right)^2 \tag{3.2}$$

where, T is the optimization horizon, Q is the number of unknown parameters, $0 \leq t_1 < ... < t_L \leq T$ are measurement times, L is the number of observation values, $y_{mea}(t_l)$ is measured value of $y(t)$ at time t_l, $u_{0_F}^i(z)$ is the guessed value of initial condition, p_{q_F} is the guessed value of parameters. Weighting factors ϵ_1, ϵ_{2q} and ϵ_3 are introduced to adjust the scale of the different terms of the cost function. The term $\delta_A(t-t_l)$ denotes the Dirac-Delta function, described here by a Gaussian function with a very small variance σ^2 as $\delta_A(t-t_l) = e^{-(t-t_l)^2/\sigma^2}$.

3.3 Solution method

3.3.1 Variational analysis

Based on the defined problem statement, the optimal values of p_q and $u_0^i(z)$ must minimize cost function (5.10) subject to system dynamics (3.1) as constraints. To solve this constrained optimization problem, let us consider the Lagrange multipliers $\lambda(t)$ and $\Gamma(z,t)$ that combine both system equations and cost function into a new cost functional L

$$L = J + \int_0^T \lambda(t)\left[\dot{y} - f\right]dt + \int_0^T\int_0^Z \Gamma(z,t)\left(\frac{\partial u}{\partial t} - V\frac{\partial^2 u}{\partial z^2}\right)dzdt \tag{3.3}$$

Using integration by parts, the cost functional can be rewritten as

$$\begin{aligned} L = {} & \frac{\epsilon_1}{2}\int_0^Z \left\|u_0^i(z) - u_{0_F}^i(z)\right\|^2 dz + \frac{1}{2}\sum_{q=1}^{Q}\epsilon_{2q}\left\|p_q - p_{q_F}\right\|^2 + \lambda(T)y(T) - \lambda(0)y(0) \\ & + \frac{\epsilon_3}{2}\sum_{l=1}^{L}\left(\int_0^T \delta_A(t-t_l)y(t)dt - y_{mea}(t_l)\right)^2 - \int_0^T y(t)\dot{\lambda}dt - \int_0^T \lambda(t)f dt + V\int_0^T h\Gamma(0,t)dt \\ & + \int_0^Z \left[\Gamma(z,T)u(z,T) - \Gamma(z,0)u(z,0)\right]dz - \int_0^T\int_0^Z u\left(\frac{\partial\Gamma(z,t)}{\partial t} + V\frac{\partial^2\Gamma(z,t)}{\partial z^2}\right)dzdt \\ & + V\int_0^T\left[\frac{\partial\Gamma(Z,t)}{\partial z}u(Z,t) - \frac{\partial\Gamma(0,t)}{\partial z}u(0,t)\right]dt - V\int_0^T \Gamma(Z,t)\frac{\partial u(Z,t)}{\partial z}dt \end{aligned} \tag{3.4}$$

To solve this optimization problem, the adjoint method is used to obtain the adjoint system and establish the gradient of the cost functional with respect to the parameters and initial states. These gradients describe the sensitivity of cost function under the constraints of system dynamics to variation of initial conditions and parameters. First of all, let us compute the first variation of the cost functional with respect to the system variables (y

and u), initial condition $u_0^i(z)$, and parameters p_q. The first variation δL is given as,

$$\begin{aligned}
\delta L = \epsilon_1 \int_0^Z [u_0^i(z) - u_{0_F}^i(z)]\delta u_0^i dz + \sum_{q=1}^{Q} \epsilon_{2q}[p_q - p_{q_F}]\delta p_q + \lambda(T)\delta y(T) - \lambda(0)\delta y(0) \\
+ \epsilon_3 \sum_{l=1}^{L} \int_0^T \delta_A(t-t_l)\left(\int_0^T \delta_A(t-t_l)y(t)dt - y_{mea}(t_l)\right)\delta y dt - \int_0^T \dot{\lambda}\delta y dt \\
- \int_0^T \lambda(t) f_y \delta y dt - \sum_{q=1}^{Q}\int_0^T \lambda(t) f_{p_q} dt \delta p_q - \int_0^T \lambda(t) f_{u(0,t)}\delta u(0,t)dt \\
+ \int_0^Z \Gamma(z,T)\delta u(z,T)dz - \int_0^Z \Gamma(z,0)\delta u(z,0)dz - \int_0^T\int_0^Z [\Gamma_t + V\Gamma_{zz}]\delta u dz dt \\
+ V\int_0^T \frac{\partial \Gamma(Z,t)}{\partial z}\delta u(Z,t)dt - V\int_0^T \frac{\partial \Gamma(0,t)}{\partial z}\delta u(0,t)dt - V\int_0^T \Gamma(Z,t)\delta\frac{\partial u(Z,t)}{\partial z}dt \\
+ V\int_0^T \Gamma(0,t)h_y \delta y dt + V\sum_{q=1}^{Q}\int_0^T \Gamma(0,t)h_{p_q}dt\delta p_q + V\int_0^T \Gamma(0,t)h_{u(0,t)}\delta u(0,t)dt
\end{aligned} \tag{3.5}$$

where we use notation, ν_a for partial derivative of a variable ν w.r.t. argument a : $\frac{\partial \nu}{\partial a}$.

All the terms multiplied by δy and δu in Eq. (3.5) are collected together and set to zero (with $\delta y(0) = 0$ assuming here $y(0)$ is known). This gives the first order optimality condition, or the adjoint system, for adjoint variables $\lambda(t)$ and $\Gamma(z,t)$, obtained from their weak forms, as:

$$\begin{cases}
\dot{\lambda} & = \epsilon_3 \sum_{l=1}^{L} \delta_A(t-t_l)\left(\int_0^T \delta_A(t-t_l)y(t)dt - y_{mea}(t_l)\right) - \lambda(t)f_y + V\Gamma(0,t)h_y, \\
\frac{\partial \Gamma(z,t)}{\partial t} & = -V\frac{\partial^2 \Gamma(z,t)}{\partial z^2}, \\
\frac{\partial \Gamma(0,t)}{\partial z} & = -\frac{1}{V}\lambda(t)f_{u(0,t)} + \Gamma(0,t)h_{u(0,t)}, \qquad \Gamma(Z,t) = 0, \\
\lambda(T) & = 0, \qquad \Gamma(z,T) = 0
\end{cases} \tag{3.6}$$

The gradient of objective functional with respect to parameter p_q, formed by selecting all the terms related to δp_q in Eq. (3.5), is then:

$$L_{p_q} = \epsilon_{2q}(p_q - p_{q_F}) - \int_0^T \lambda(t) f_{p_q} dt + V\int_0^T \Gamma(0,t)h_{p_q}dt \tag{3.7}$$

By using the same method, the gradient with respect to initial condition $u_0^i(z)$ can be obtained from variation in Eq. (3.5) below:

$$\delta L_{\delta u_0^i(z)} = \epsilon_1 \int_0^Z [u_0^i(z) - u_{0_F}^i(z)]\delta u_0^i(z)dz - \int_0^Z \Gamma(z,0)\delta u_0^i(z)dz.$$

With the same weak form argument as before, the gradient is:

$$L_{u_0^i(z)} = \epsilon_1[u_0^i(z) - u_{0_F}^i(z)] - \Gamma(z,0) \tag{3.8}$$

The system dynamics and adjoint equations must be discretized in order to be solved numerically. The considered spatial domain $[0, Z]$ is discretized into a set of smaller sections $[z_m, z_{m+1}]$. Similarly, the gradient of initial condition (3.8) is discretized at every single position z_m, $\forall z_m = m\Delta z$ where $0 < m \leq M-1$ with $\Delta z = Z/M$, M being the number of point, giving:

$$L_{u_0^i(z_m)} = \epsilon_1[u_0^i(z_m) - u_{0_F}^i(z_m)] - \Gamma(z_m,0). \tag{3.9}$$

3.3.2 Numerical implementation

3.3.2.1 Euler method for discretization

The Euler method is based on a truncated Taylor series expansion [Ascher1998], i.e., expansion of y in the neighborhood of $t = t_n$, $\forall t_n = n\Delta t$ where $0 < n \leq N-1$ with $\Delta t = T/N$, N being the number of time steps, gives

$$y_{n+1} := y(t_n + \Delta t) = y(t_n) + \Delta t \frac{dy(t_n)}{dt} + O(\Delta t^2) = y_n + \Delta t f(y_n, t_n) + O(\Delta t^2). \tag{3.10}$$

At each time step, higher order terms $O(\Delta t^2)$ are neglected which induces local truncation error proportional to the square of the step size (Δt), and the global error (error at a given time) is proportional to the step size. The value of variable y at time $t_n + \Delta t$ in Eq. (3.1) is computed as

$$y(t_n + \Delta t) = y_{n+1} = y_n + \Delta t f. \tag{3.11}$$

The Euler method is used for numerical integration of system and adjoint ODEs, both forward and backward in time.

3.3.2.2 Crank-Nicholson method for discretization

The Crank–Nicolson scheme is a finite difference method used for numerically solving the heat equation and similar Partial Differential Equations (PDEs) [Crank1947]. It is a second-order implicit method in time. The time derivative of PDE in Eq. (3.1) are approximated by forward differences and space derivatives by central differences averaged over $n+1$ and n. By denoting $u(z_m + \Delta z, t_n + \Delta t)$ as u_{n+1}^{m+1}, the Crank-Nicholson scheme for discretizing Eq. (3.1) becomes:

$$\frac{u_{n+1}^m - u_n^m}{\Delta t} = \frac{V}{2}\left[\frac{u_{n+1}^{m+1} - 2u_{n+1}^m + u_{n+1}^{m-1}}{\Delta z^2} + \frac{u_n^{m+1} - 2u_n^m + u_n^{m-1}}{\Delta z^2}\right]. \tag{3.12}$$

Rearranging and substituting $r = V\Delta t/2\Delta Z^2$ leads to,

$$-ru_{n+1}^{m+1} + (1+2r)\,u_{n+1}^m - ru_{n+1}^{m-1} = ru_n^{m+1} + (1-2r)\,u_n^m + ru_n^{m-1}. \tag{3.13}$$

The boundary conditions in Eq. (3.1) are approximated as,

$$u_{n+1}^{M-1} = u_0^b(t_{n+1}) \quad \text{and} \quad u_{n+1}^1 - u_{n+1}^0 = \Delta z h(t_{n+1}). \tag{3.14}$$

Now, Eq. (3.13) and (3.14) can be rewritten as a set of simultaneous equations in matrix form as follows:

$$\overbrace{\begin{bmatrix} -1 & 1 & 0 & \dots & 0 & 0 & 0 \\ -r & 1+2r & -r & \dots & 0 & 0 & 0 \\ \dots & \dots & \dots & \dots & \dots & \dots & \dots \\ 0 & 0 & 0 & \dots & -r & 1+2r & -r \\ 0 & 0 & 0 & \dots & 0 & 0 & 1 \end{bmatrix}}^{A} \overbrace{\begin{bmatrix} u_{n+1}^0 \\ u_{n+1}^1 \\ \dots \\ u_{n+1}^{M-2} \\ u_{n+1}^{M-1} \end{bmatrix}}^{X} = \overbrace{\begin{bmatrix} \Delta z h(t_{n+1}) \\ ru_n^2 + (1-2r)\,u_n^1 + ru_n^0 \\ \dots \\ ru_n^{M-1} + (1-2r)\,u_n^{M-2} + ru_n^{M-3} \\ u_0^b(t_{n+1}) \end{bmatrix}}^{B} \tag{3.15}$$

Therefore at each time step t_n, $X = \begin{bmatrix} u_{n+1}^0 & u_{n+1}^1 & \dots & u_{n+1}^{M-2} & u_{n+1}^{M-1} \end{bmatrix}^T = A^{-1}B$ can be computed using minor matrix operation. Notice that, in vector B of equation (3.15) term

$h(t_{n+1})$ depends on y_{n+1} and u_{n+1}. Out of which y_{n+1} can be obtained from solution of ODE (3.11) while for $h(t_{n+1})$ linear in u_{n+1}, term u_{n+1} need to be taken to the left hand side of the equation (3.14) before performing matrix operation.

Truncation error of the scheme is proportional to $O(\Delta t^2) + O(\Delta z^2)$. Although the Crank-Nicholson scheme is unconditionally stable, in the simulations values of Δt and Δz are chosen such that $r < 1$. The Crank-Nicholson method is used for numerical integration of system and adjoint PDEs, both forward and backward in time.

3.3.2.3 Steepest descent method for optimal estimation

We employ a steepest descent method [Bartholomew-Biggs2008] to solve the optimization problem. The gradients L_{p_q} and $L_{u_0^i(z_m)}$ give the descent directions to estimate optimal parameter values p_q^* and initial values $u_0^i(z_m)^*$. We choose constant step sizes γ_{p_q} and $\gamma_{u_0^i}$, which minimize the cost functional L in the descent directions. We use Algorithm 1 below to solve the optimization problem. The algorithm stops when the norm of the gradient is smaller than the chosen tolerance ξ_{p_q} and $\xi_{u_0^i}$. Notice that computing gradients require solving both system (3.1) and adjoint system (3.6) equations.

Algorithm 1: Optimal parameter and initial value estimation

Input: Model input $I(t)$ & Measurements $y(t_k)$
Guessed parameter and initial values, p_{q_F} & $u^i_{0_F}(z_m)$
Set initial parameter and state values, p_{q_0} $u^i_{0_0}(z_m)$
Step sizes, γ_{p_q} & $\gamma_{u_0^i}$
Gradient tolerances, ξ_{p_q} & $\xi_{u_0^i}$
Stop_flag = false
Iteration index k=1
Set $p_q^k = p_{q_0}$ and $u_0^i(z_m)^k = u^i_{0_0}(z_m)$

Output: p_q^*, $u_0^i(z_m)^*$

while *Stop_flag = false* **do**
  Simulate system equations (3.1) with $y(0)$, $u_0^i(z_m)^k$, p_q^k, & $u_0^i(z_m)^k$;
  Simulate the adjoint system equation (3.6) (backward in time);
  Compute gradients $L^k_{p_q}$, $L^k_{u_0^i(z_m)}$ using (3.7) & (3.9);
  if $\left|L^k_{p_q}\right| \leq \xi_{p_q}$ & $\left|L^k_{u_0^i(z_m)}\right| \leq \xi_{u_0^i}$ **then**
    Stop_flag = true;
  else
    $p_q^{k+1} = p_q^k$ - $\gamma_{p_q} L^k_{p_q}$;
    $u_0^i(z_m)^{k+1} = u_0^i(z_m)^k$ - $\gamma_{u_0^i} L^k_{u_0^i(z_m)}$;
    $k = k+1$;
  end
  Display p_q, $u_0^i(z_m)$ and J
end
Return p_q^*, $u_0^i(z_m)^*$

3.4 Landslide application examples

3.4.1 Example I: Extended sliding-consolidation model

3.4.1.1 System dynamics

The extended sliding-consolidation model [Iverson2005b] of landslide assumes that a slide block is placed on an inclined surface as shown in Fig. 5.1. This model proposes a mechanism of opposition to slide block down-slope movement by basal Coulomb friction and regulation through basal pore fluid pressure feedback. The model splits total basal pore pressure into two components of: i) imposed pore pressure p_i due to rain infiltration and ii) development of excess pore pressure p_e in response to the dilation or contraction of the basal shear zone. The velocity of the slide block $v(t)$ and excess pore pressure $p_e(z,t)$ (equivalent to $y(t)$ and $u(z,t)$ respectively in Eq. (3.1) evolution (diffusion equation) are described by Eq. (3.16).

$$\begin{aligned}
\dot{v}(t) &= \varphi(t,\phi,\psi)\left\{gcos\psi\left[sin(\theta-\psi)-cos(\theta-\psi)tan\phi\right]+\frac{cos^2\psi tan\phi}{\rho Z}\left[p_i(t)+p_e(0,t)\right]\right\}, \\
&= f(t,\phi,\psi,p_e(0,t),p_i(t)), \qquad v(0)=v_0 \\
\frac{\partial p_e(z,t)}{\partial t} &= D\frac{\partial^2 p_e(z,t)}{\partial z^2}, \qquad p_e(z,0)=p_{e_0} \\
\frac{\partial p_e(0,t)}{\partial z} &= \frac{\rho_w g\psi}{K}v(t)=h(\psi,v), \qquad p_e(Z,t)=0
\end{aligned} \tag{3.16}$$

where $p_i(t)$ is the imposed pore pressure at the slide block base (input to the model), $(z,t)\in[0,Z]\times[0,T]$ with Z as a spatial domain length (slide block thickness), and T is the length of time horizon. ϕ is the friction angle characterizing the mechanical strength of the material, ψ is the dilatancy angle representing volume change of the material when it is subject to deformation, ρ is the soil density, ρ_w is the pore water density, D is the diffusion coefficient ($D>0$), K is the hydraulic conductivity, g is the acceleration due to gravity and θ is the slope angle. In addition, v_0 and p_{e_0} are initial values ($t=0$) of the v and p_e respectively. Finally, $\varphi(t,\phi,\psi)$ is a smooth activation or logistic function given by,

$$\varphi(t,\phi,\psi)=\frac{1}{1+e^{-\xi_{af}[p_i(t)-p_{crit}]}} \tag{3.17}$$

where ξ_{af} is the steepness of activation function and p_{crit} is the critical pore pressure above which slide block starts to accelerate given as [Iverson2005b]

$$p_{crit}=\frac{gcos\psi\left[cos(\theta-\psi)tan\phi-sin(\theta-\psi)\right]}{cos^2\psi tan\phi/\rho Z}. \tag{3.18}$$

The activation function φ smoothly transits between 1 and 0 depending on positive and negative (respectively) values of $p_i(t)-p_{crit}$. ξ_{af} can be used to adjust the transition slope of activation function.

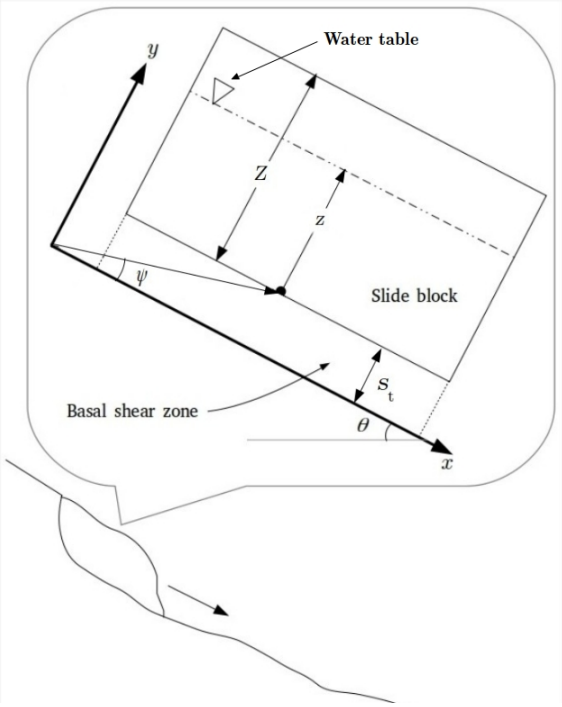

Figure 3.1: Schematic view illustrating geometrical variables used to model slide block motion (shear zone thickness s_t is used only in viscoplastic sliding-consolidation model)

3.4.1.2 Estimation results

To validate the effectiveness of the proposed approach, a synthetic velocity profile $v_{mea}(t)$ is generated by solving the system equations (3.16). The initial values and parameter values used for the simulation are summarized in Table 3.1. The geometrical and material parameters are taken from the literature [Iverson2005b] and correspond to the case of a dense loamy soil. In the simulations, imposed pore pressure is assumed to be sinusoidal in time (with a period of 20 days to represent rainfall variations), oscillating around p_{crit}. Simulated synthetic velocity measurement (with two different cases of additive noises) and pore pressure profiles are shown in Fig. 3.2. Additive noises are white Gaussian noises with signal-to-noise ratios (SNR) 10dB and 20dB, respectively, representing the observation errors.

Here, we are interested in estimating mechanical parameters ψ and ϕ (equivalent to p_q in Eq. (3.1)) along with initial condition p_{e_0} (equivalent to $u_0^i(z)$ in Eq. (3.1)) assuming other mechanical and geometrical parameters, velocity measurement $v_{mea}(t)$ and imposed pore pressure $p_i(t)$ are known. The corresponding cost function is given by Eq. (3.19). Based on the solution method (Section 3.2), adjoint system equations and gradients are obtained (as shown by Eq. (3.20) and (3.21)). Then with the help of model and simulation parameters (steepness of the activation function, step sizes, stopping conditions, and weighting factors) of Table 3.1 and Algorithm 1, simulations are performed. Weighting factors are chosen in order to normalize the different terms of the cost function on a

Table 3.1: Parameter Values: Extended sliding-consolidation model

Parameters	**Value**	**Unit**
Initial velocity, v_0	0.010	mm/s
Initial basal excess pore pressure, p_{e_0}	-0.41	Pa
Time Δt & space Δz step	0.01 & 0.0066	sec & m
Diffusion coefficient, D	3×10^{-3}	m^2/s
Acceleration due to gravity, g	9.8	m/s^2
Slide block thickness, Z	0.65	m
Hydraulic conductivity, K	2×10^{-5}	m/s
Slide block mass ρ & pore water ρ_w density	2000 & 1000	kg/m^3
Plane inclination θ, friction ϕ and dilatancy ψ angle	31, 35 & 6	°
Steepness of activation function, ξ_{af}	100	-
Guessed initial excess pore pressure, $p_{e_{0_F}}$	-0.2	kPa
Guessed friction ϕ & dilatancy ψ_F angle	31 & 4	°
Initial excess pore pressure, p_{e_0}	0	kPa
Initial friction angle, ϕ_0	25, 29, 32	°
Initial dilatancy angle, ψ_0	3, 4, 5	°
Step size, γ_{p_e}	1.1×10^{-4}	-
Step size, γ_ϕ	5×10^{-3}	-
Step size, γ_ψ	1.4×10^{-4}	-
Weighting factor, ϵ_1	1×10^{-12}	-
Weighting factor, (ϵ_{21} & ϵ_{22})	(2.5 & 5) $\times10^{-3}$	-
Weighting factor, ϵ_3	30	-
Stop condition, $\xi_{p_{e_0}}$, ξ_ϕ, ξ_ψ	10^{-2}	-

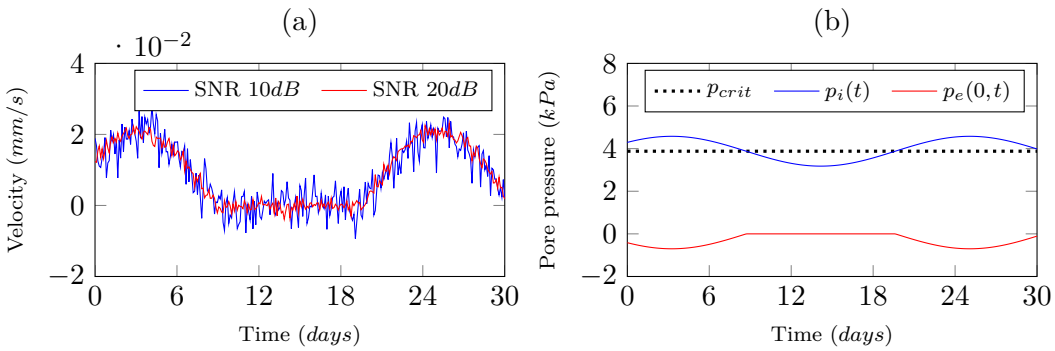

Figure 3.2: Synthetic data: Extended sliding-consolidation model. (a) Synthetic velocity measurement [$v_{mea}(t)$] for two additive noises. (b) Critical [p_{crit}], imposed [$p_i(t)$] and basal excess pore pressure [$p_e(0,t)$]

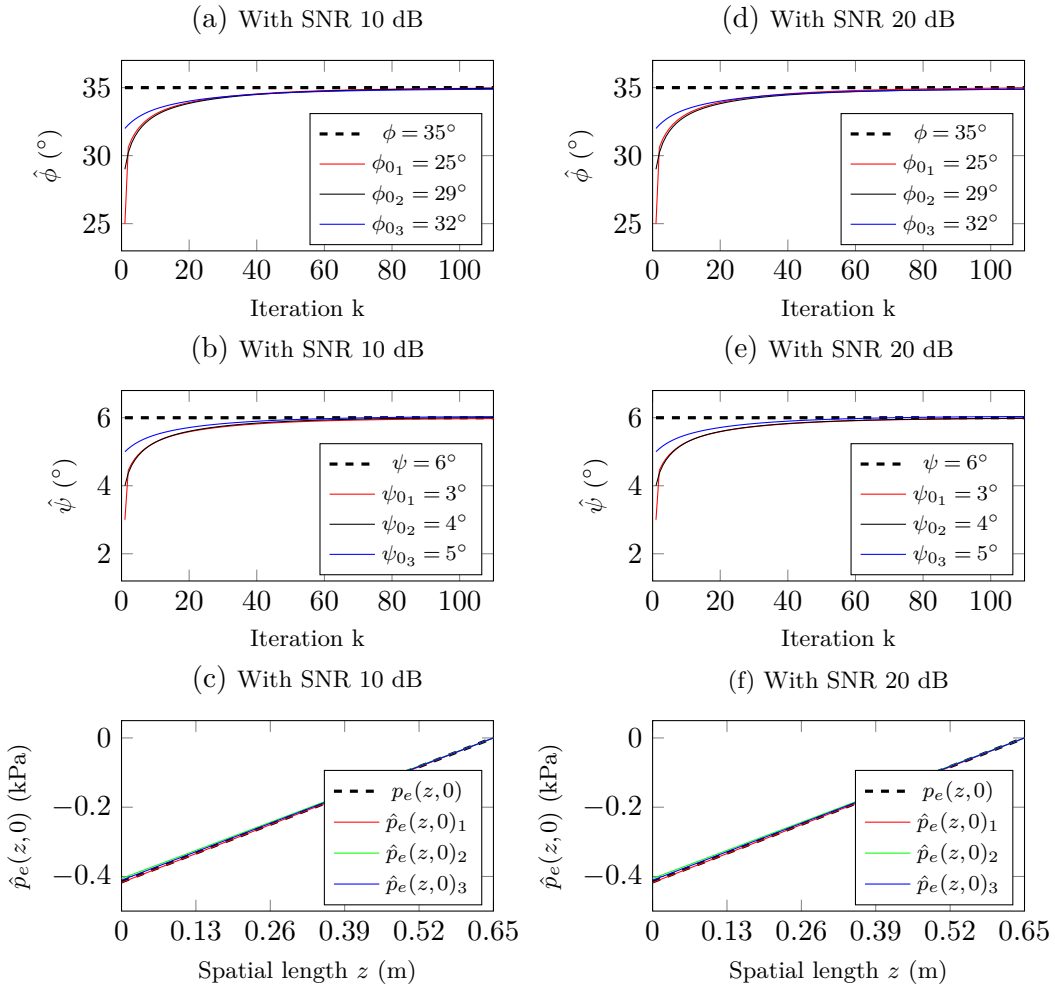

Figure 3.3: Estimation results: Extended sliding-consolidation model. (a)&(d) Evolution of the parameter estimate ($\hat{\phi}$) for velocity measurement with SNR 10 dB and 20 dB respectively, (b)&(e) Evolution of the parameter estimate ($\hat{\psi}$) for velocity measurement with SNR 10 dB and 20 dB respectively, (c)&(f) Estimated initial state [$\hat{p}_e(z,0)$] for velocity measurement with SNR 10 dB and 20 dB respectively.

common scale. They also affect the speed of convergence (number of iterations required) in estimated and actual parameter values and are chosen manually by a trial and error scheme. Notice that, although synthetic data are generated with a time step $\Delta t = 0.01$ *sec*, only asynchronous measurements are considered in the estimation. It is indeed here, assumed that on alternate days, data are collected after every 30 minutes and 1 hour, i.e., for day one half-hourly and on an hourly basis for day 2. In order to validate the effectiveness of the estimation scheme, six simulations are performed with two distinct noise levels (10 and 20 dB) and three different sets of initial parameter values (estimated values for each simulation are summarised in Table 3.2). One can observe in Fig. 3.3 the estimation results.

Cost function:

$$\begin{aligned} J_1 = &\frac{\epsilon_1}{2}\int_0^Z \left\| p^i_{e_0}(z) - p^i_{e_{0_F}}(z) \right\|^2 dz + \frac{\epsilon_{21}}{2}\left\|\phi - \phi_F\right\|^2 + \frac{\epsilon_{22}}{2}\left\|\psi - \psi_F\right\|^2 \\ &+ \frac{\epsilon_3}{2}\sum_{l=1}^{L}\left(\int_0^T \delta_A(t-t_l)v(t)dt - v_{mea}(t_l)\right)^2 \end{aligned} \tag{3.19}$$

Adjoint system:

$$\begin{aligned} &\dot{\lambda}_1 = \epsilon_3 \sum_{l=1}^{L}\delta_A(t-t_l)\left(\int_0^T \delta_A(t-t_l)v(t)dt - v_{mea}(t_l)\right) + \frac{D\rho_w g\psi}{K}\Gamma_1(0,t), \quad \lambda_1(T) = 0 \\ &\frac{\partial \Gamma_1(z,t)}{\partial t} = -D\frac{\partial^2 \Gamma_1(z,t)}{\partial z^2}, \qquad \Gamma_1(z,T) = 0 \\ &\frac{\partial \Gamma_1(0,t)}{\partial z} = -\frac{1}{D}\lambda_1(t) f_{p_e(0,t)}, \qquad \Gamma_1(Z,t) = 0 \end{aligned} \tag{3.20}$$

Gradients:

$$\begin{aligned} &\frac{\partial L_1}{\partial p_{e_0}(z_m)} = \epsilon_1[p_{e_0}(z_m) - p_{e_{0_F}}(z_m)] - \Gamma_1(z_m,0) \\ &\frac{\partial L_1}{\partial \phi} = \epsilon_{21}(\phi - \phi_F) - \int_0^T \lambda_1(t) f_\phi dt \\ &\frac{\partial L_1}{\partial \psi} = \epsilon 22(\psi - \psi_F) + \frac{D\rho_w g}{K}\int_0^T \Gamma_1(0,t)v(t)dt - \int_0^T \lambda_1(t) f_\psi dt \end{aligned} \tag{3.21}$$

Estimated initial condition and parameter values indeed converge to respective real values with small bias. These estimation biases are possibly caused by the truncation errors of numerical schemes (Section 3.3) and/or due to noise in measurements. Note that, initial value v_0 is taken from v_{mea} which itself is noisy. Even with the presence of noise in measurements and numerical errors, the results obtained are quite satisfactory in the sense of relative error in estimation (see Table 3.2). The relative errors between the real values of variables and estimated ones are very small given the noise level. For similar set of initial parameter values and 20dB noise level in measurement estimation results are more accurate as compared to high noise level (10dB) scenario (see Table 3.2). It is also observed that the closer the initial parameters for the estimation are to the actual ones, the more accurate the estimation is. In addition, the lower the measurement noise level is, the more accurate the estimation results are (see Table 3.2). Note that, initial excess pore pressure is being estimated for all z i.e., $p_e(z,0)$ but in Table 3.2 only estimated initial basal excess pore pressure $[\hat{p}_e(0,0)]$ is mentioned.

Table 3.2: Initial and estimated Values: Extended sliding-consolidation model

Sr. no.	Noise SNR (dB)	Initial values ϕ_0, ψ_0, p_{e_0} (°, °, kPa)	Estimated values $\hat{\phi}$ (°)	Error (%)	$\hat{\psi}$ (°)	Error (%)	$\hat{p}_e(0,0)$ (kPa)	Error (%)
1	10	25, 3, 0	34.90	0.28	5.96	0.67	-0.413	0.73
2	10	29, 4, 0	34.92	0.22	5.96	0.67	-0.411	0.24
3	10	32, 5, 0	34.93	0.20	5.97	0.50	-0.409	0.24
4	20	25, 3, 0	34.91	0.25	5.97	0.50	-0.412	0.48
5	20	29, 4, 0	34.92	0.22	5.97	0.50	-0.412	0.48
6	20	32, 5, 0	34.94	0.17	5.98	0.34	-0.411	0.24

3.4.2 Example II: Viscoplastic sliding-consolidation model

3.4.2.1 System dynamics

The viscoplastic sliding-consolidation model is formulated based on the similar mechanism as the extended sliding-consolidation model with two modifications: i) a term related to viscous force $(-\eta v(t)/s_t)$ which opposes landslide down-slope movement is added, ii) to depict slow-moving landslides, the acceleration term $\dot{v}$ is neglected, as inertia effects are expected to remain small compared to other forces in the momentum balance. A similar setting without basal pore fluid pressure feedback (simplified viscoplastic sliding model) is presented in [Mishra2021]. We extended this model by including diffusion equation (PDE) for excess pore pressure evolution to obtain an ODE-PDE coupled system:

$$\begin{aligned}
\dot{d} &= \varphi(t,\phi,\psi)\left\{\frac{\rho s_t Z}{\eta}\left[sin(\theta-\psi)-cos(\theta-\psi)tan\phi\right]+\frac{s_t tan\phi cos\psi}{\eta}\left[p_i(t)+p_e(0,t)\right]\right\} \\
&= f(\phi,\psi,\eta/s_t,p_e(0,t),p_i(t)), \quad d(0)=d_0 \\
\frac{\partial p_e(z,t)}{\partial t} &= D\frac{\partial^2 p_e(z,t)}{\partial z^2}, \qquad p_e(z,0)=p_{e_0} \\
\frac{\partial p_e(0,t)}{\partial z} &= \frac{\rho_w g\psi v}{K} = h(\phi,\psi,\eta/s_t,p_e(0,t),p_i(t)) = \frac{\rho_w g\psi}{K}f, \quad p_e(Z,t)=0
\end{aligned} \tag{3.22}$$

where, $d(t)$ is slide block displacement, s_t is the shear zone thickness (see in Fig. 5.1), η is the viscosity, and φ is the activation function (3.17).

3.4.2.2 Estimation results

A synthetic displacement $d_{mea}(t)$ time-series is computed by solving (3.22) for initial and parameter values given in Table 3.3. The geometrical and mechanical parameters of Minor Creek landslide with gravelly sand clay are taken from the literature [Iverson2005b]. Similar to Example I (Section 3.4.1), imposed pore pressure is assumed sinusoidal (with a period of 300 days to represent seasonal variation in imposed pore pressure) oscillating around p_{crit} computed using Eq. (3.18). Simulated synthetic displacement time-series (with noises) and pore pressure profiles are shown in Fig. 3.4.

In this example we are estimating mechanical parameters ψ, ϕ and η/s_t along with initial condition $p_e(z,0)$ assuming other mechanical and geometrical parameters, displacement measurement d_{mea} and imposed pore pressure $p_i(t)$ are known, i.e., optimizing cost function (3.23). Note that, in this example, parameters η and s_t are clubbed together to form a single parameter η/s_t since they cannot be estimated independently. It is also

Table 3.3: Parameters values: Viscoplastic sliding-consolidation model

Parameters	**Value**	**Unit**
Initial displacement, d_0	0.12	m
Initial basal excess pore pressure, p_{e_0}	-2.69	kPa
Simulation time, T	360	days
Time step, Δt	1800	s
Space step, Δz	0.12	m
Diffusion coefficient, D	1×10^{-5}	m^2/s
Acceleration due to gravity, g	9.8	m/s^2
Slide block thickness, Z	6	m
Hydraulic conductivity, K	5×10^{-8}	m/s
Plane inclination angle, θ	15	$^\circ$
Slide block mass density, ρ	2200	kg/m^3
Pore water density, ρ_w	1000	kg/m^3
Friction angle, ϕ	15	$^\circ$
Dilatancy angle, ψ	3	$^\circ$
Viscosity, η	10^8	Pa.s
Shear zone thickness, s_t	0.1	m
Steepness of activation function, ξ_{af}	500	-
Guessed initial excess pore pressure, $p_{e_{0_F}}$	-1	kPa
Guessed friction angle, ϕ_F	12.5	$^\circ$
Guessed dilatancy angle, ψ_F angle	2	$^\circ$
Guessed viscosity/shear zone thickness, $(\eta/s_t)_F$	8×10^8	Pa.s/m
Initial excess pore pressure, p_{e_0}	0	kPa
Initial friction angle, ϕ_0	10.5, 12.5, 13.5	$^\circ$
Initial dilatancy angle, ψ_0	1.5, 2, 2.5	$^\circ$
Initial viscosity/shear zone thickness, $(\eta/s_t)_0$	$(7,8,9) \times 10^8$	Pa.s/m
Step size, γ_{p_e}	$1.1{\times}10^{-4}$	-
Step size, γ_ϕ	$2.5{\times}10^{-4}$	-
Step size, γ_ψ	$7{\times}10^{-5}$	-
Step size, γ_{η/s_t}	$1.4{\times}10^{-4}$	-
Weighting factor, ϵ_1	$1{\times}10^{-12}$	-
Weighting factor, ϵ_{21}	$2.5{\times}10^{-3}$	-
Weighting factor, ϵ_{22}	$5{\times}10^{-3}$	-
Weighting factor, ϵ_{23}	$1{\times}10^{-16}$	-
Weighting factor, ϵ_3	10	-
Stop condition, $\xi_{p_{e_0}}$, ξ_ϕ, ξ_ψ, ξ_{η/s_t}	10^{-2}	-

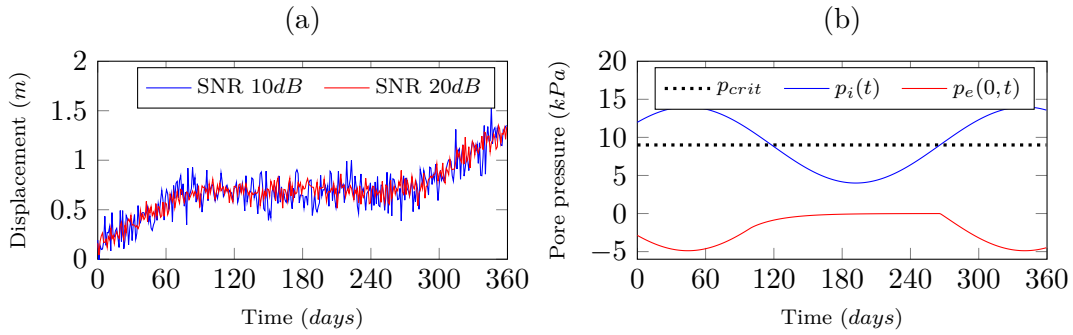

Figure 3.4: Synthetic data: Viscoplastic sliding-consolidation model. (a) Displacement measurement $[d_{mea}(t)]$ for two additive noises. (b) Critical $[p_{crit}]$, imposed $[p_i(t)]$ and basal excess pore pressure $[p_e(0,t)]$

because it would not be possible to estimate them independently. Similarly to the previous example, asynchronous measurements with four and two data points a day are assumed for the estimation scheme. In this example as well, simulations are (for model and simulation parameters Table 3.3, adjoint system equations and gradients given by Eq. (3.24) and (3.25)) performed six times with different noise levels and distinct initial parameter values (estimated values for each simulation are summarised in Table 3.4). Estimation results can be seen in Fig. 3.5. In comparison to the previous example, error between actual and estimated parameters (see Table 3.4) are a little bit higher (but $< 5\%$) as we are estimating one additional parameter. Similarly to the previous example, it is observed that lower noise level in the measurement and closer initial parameter values to the actual ones yield more accurate estimation results (see Table 3.4). In addition, the number of iterations required to reach convergence in this example is about 120 while in previous example around 110 iterations were needed. The number of iterations required depends on weighting factors ϵ and step sizes γ (Table 3.3) which are chosen on trial and error basis. Simulation results in Fig. 3.5(c) & (g) also shows that for the simulation parameters of Table 3.3 convergence in parameter estimates $\hat{\eta}/s_t$ is faster then the other parameters.

Cost function:

$$J_2 = \frac{\epsilon_1}{2}\int_0^Z \left\| p^i_{e_0}(z) - p^i_{e_{0_F}}(z) \right\|^2 dz + \frac{\epsilon_{21}}{2}\left\|\phi - \phi_F\right\|^2 + \frac{\epsilon_{22}}{2}\left\|\psi - \psi_F\right\|^2 + \frac{\epsilon_{23}}{2}\left\|(\eta/s_t) - (\eta/s_t)_F\right\|^2 + \frac{\epsilon_3}{2}\sum_{l=1}^{L}\left(\int_0^T \delta_A(t-t_l)d(t)dt - d_{mea}(t_l)\right)^2 \tag{3.23}$$

Adjoint system:

$$\begin{aligned}
\dot{\lambda}_2 &= \epsilon_3 \sum_{l=1}^{L} \delta_A(t-t_l)\left(\int_0^T \delta_A(t-t_l)v(t)dt - v_{mea}(t_l)\right), && \lambda_2(T) = 0 \\
\frac{\partial \Gamma_2(z,t)}{\partial t} &= -D\frac{\partial^2 \Gamma_2(z,t)}{\partial z^2}, && \Gamma_2(z,T) = 0 \\
\frac{\partial \Gamma_2(0,t)}{\partial z} &= -\frac{1}{D}\lambda_2(t) f_{p_e(0,t)} + \frac{\rho_w g}{K}\Gamma_2(0,t) f_{p_e(0,t)}, && \Gamma_2(Z,t) = 0
\end{aligned} \tag{3.24}$$

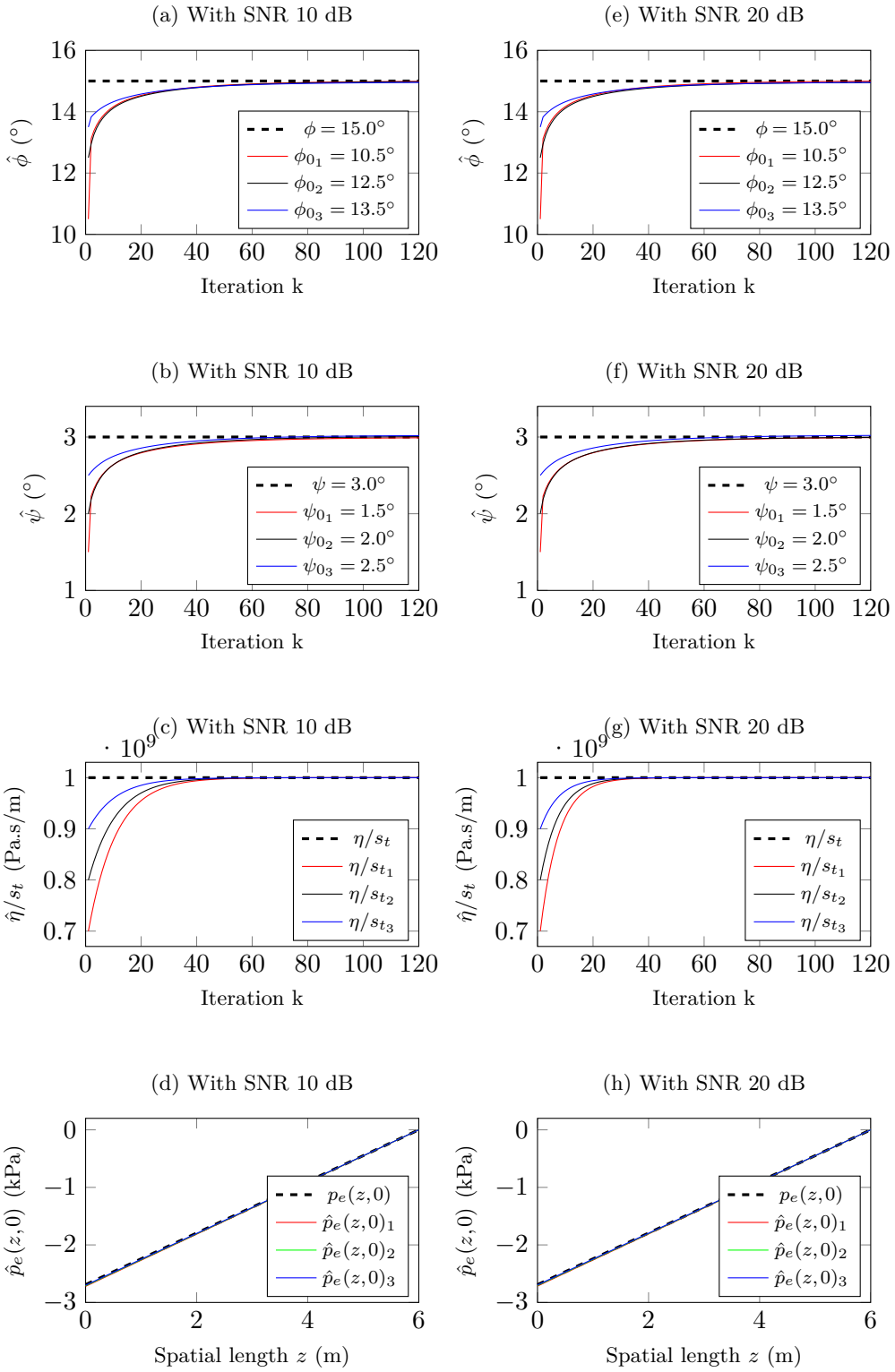

Figure 3.5: Estimation results: Viscoplastic sliding-consolidation model. (a)&(e) Evolution of the parameter estimate ($\hat{\phi}$) for displacement measurement with SNR 10 dB and 20 dB respectively, (b)&(f) Evolution of the parameter estimate ($\hat{\psi}$) for displacement measurement with SNR 10 dB and 20 dB respectively, (c)&(g) Evolution of parameter estimate $\hat{\eta}/s_t$ for displacement measurement with SNR 10 dB and 20 dB respectively, (d)&(h) Estimated initial state $[\hat{p}_e(z,0)]$ for displacement measurement with SNR 10 dB and 20 dB respectively.

Gradients:

$$\begin{aligned}
\frac{\partial L_2}{\partial p_{e_0}(z_m)} &= \epsilon_1[p_{e_0}(z_m) - p_{e_{0_F}}(z_m)] - \Gamma_2(z_m, 0) \\
\frac{\partial L_2}{\partial(\eta/s_t)} &= \epsilon_{23}[(\eta/s_t) - (\eta/s_t)_F] - \int_0^T \lambda_2(t) f_{\eta/s_t} dt + \frac{D\rho_w g}{K} \int_0^T \Gamma_2(0,t) f_{\eta/s_t} dt \\
\frac{\partial L_2}{\partial \phi} &= \epsilon_{21}(\phi - \phi_F) + \frac{D\rho_w g}{K} \int_0^T \Gamma_2(0,t) f_\phi dt - \int_0^T \lambda_2(t) f_\phi dt \\
\frac{\partial L_2}{\partial \psi} &= \epsilon_{22}(\psi - \psi_F) + \frac{D\rho_w g}{K} \left[\int_0^T \Gamma_2(0,t) f dt + \int_0^T \Gamma_2(0,t) f_\psi dt \right] - \int_0^T \lambda_2(t) f_\psi dt
\end{aligned} \tag{3.25}$$

Table 3.4: Estimated Values: Viscoplastic sliding-consolidation model

Sr. no.	**Noise SNR** (dB)	**Initial values** ϕ_0,ψ_0,η/s_{t_0},p_{e_0} (°, °, GPa.s/m, kPa)	**Estimated values**							
			$\hat{\phi}$ (°)	Error (%)	$\hat{\psi}$ (°)	Error (%)	$\hat{\eta}/s_t$ (GPa.s/m)	Error (%)	$\hat{p}_e(0,0)$ (kPa)	Error (%)
1	10	10.5, 1.5, 0.7, 0	14.90	0.66	2.95	1.67	0.996	0.4	−2.81	4.46
2	10	12.5, 2.0, 0.8, 0	14.91	0.60	2.95	1.67	0.996	0.4	−2.73	1.48
3	10	13.5, 2.5, 0.9, 0	14.92	0.54	2.96	1.34	0.997	0.3	−2.77	2.97
4	20	10.5, 1.5, 0.7, 0	14.93	0.47	2.97	1.00	0.997	0.3	−2.72	1.11
5	20	12.5, 2.0, 0.8, 0	14.93	0.47	2.98	0.67	0.998	0.2	−2.71	0.74
6	20	13.5, 2.5, 0.9, 0	14.94	0.40	2.98	0.67	0.998	0.2	−2.70	0.37

3.5 Conclusions

This chapter has proposed and validated an optimal approach for state and parameter estimation in landslide motion models based on the adjoint method and the steepest descent approach. Firstly, a generic case of the ODE-PDE coupled model has been presented. Secondly, the initial state and parameter estimation problem has been formulated as an optimization problem from discrete-time asynchronous observation values using the Lagrange multiplier approach. Then the adjoint method has been introduced to obtain gradients of the cost functional and the adjoint equations. These gradients were then utilized as descent directions for the steepest descent method to get optimal parameter values. The differential equations of both system and adjoint systems have been discretized and solved numerically utilizing Euler and Crank-Nicholson method. Lastly, the proposed solution method has been validated with synthetically generated noisy data for extended sliding-consolidation and viscoplastic sliding-consolidation models of landslide. The optimal values of the initial state and parameters have been shown to be well estimated for both examples. In the simulation results, it is observed that relative error and iterations required in estimation for the second example are slightly larger in comparison to the first example, as one additional parameter is being estimated in this second case.

The performance of the estimation process (convergence) can be improved by using the inexact line search method [Shi2004] to choose step sizes γ_{p_q} and $\gamma_{u_0^i}$ instead of constant ones. In both examples, it is observed that the lesser the noise level in measurement

and closer the initial parameter values to the actual parameter values, the more accurate estimates are obtained from the proposed approach. A validation with field data is in progress to evaluate the applicability of the presented method to the Super-Sauze landslide data taken from the literature. The proposed approach could be extended to more complex landslide models. Finally, for the cases in which imposed pore pressure will not be known, proposed approach can be extended to coupled hydrological landslide models [Iverson2000].

4

Observer design for state and parameter estimation in a landslide model

This chapter presents an observer-based state and parameter estimation for the extended sliding-consolidation model of a landslide. This system is described by a pair of coupled Ordinary Differential Equation (ODE) and Partial Differential Equation (PDE), with a mixed boundary condition for the PDE. The coupling appears both in the ODE and in the Neuman boundary condition of the PDE. The observer consists of a copy of the PDE part of the system and Kalman-like observer for the ODE. It is shown to ensure exponential convergence of the state and parameter estimates by means of Lyapunov tool. Finally, a simulation result of the extended sliding-consolidation model is presented to illustrate the effectiveness of the proposed observer. The material of this chapter corresponds to the paper [Mishra2020a].

4.1 Introduction

A landslide or slope destabilization is a gravity-driven downslope movement of rock, debris, or soil near earth's surface caused by heavy precipitation, flood, earthquakes, substantial snowmelt, or human activities such as construction work. Over the last decade, climate change [Gariano2016] and rapid urbanization [Nyambod2010] have increased the frequency of occurrence of landslides. This, in turn, grabbed the attention towards the implementation of early warning systems (EWS) to take timely actions to reduce human and economic losses in advance of hazardous events [Krøgli2018]. One of the significant components of EWS is environmental monitoring and forecasting [UN/ISDR2006]. Environmental monitoring and forecasting are tools to assess the current status of an environment and establish the trends in environmental parameters. Information or data collected with the help of environmental monitoring are processed and often used in the assessment of risks related to the environment, e.g., weather forecast provides better predictions for tropical storms, hurricanes, and severe weather. In the past few years, developments in satellite remote sensing of the surface and atmosphere of the earth, numerical modeling, and data assimilation have improved the accuracy of weather forecasting.

Similarly, for anticipation of the hazards associated with landslide, a physics-based dynamical model, landslide monitoring, and heterogeneous data handling play a vital role. These physics-based dynamical models, e.g., sliding-consolidation model [Hutchinson1986], extended sliding-consolidation model [Iverson2005a] and viscoplastic sliding-consolidation model [Bernardie2014a, Herrera2013a, Corominas2005a] are sensitive to the initial conditions and parameters of the system. These sensitivities can be taken into account by simulating a model and iteratively adjusting the initial conditions and parameter values to obtain consistency with measured data, i.e., by adjoint method [Nguyen2016b]. Another efficient approach is to run a model over a time and continually fine-tune it to synchronize with incoming data, i.e., Kalman filter like approach. Therefore, a comprehensive evaluation of landslide hazards involves multi-dimensional problems, which require a multi-disciplinary approach viz. geophysics, mechanics, signal/data processing, dynamical systems, control theory, and information technologies.

In this context, the present chapter proposes an observer design for state and parameter estimation in an extended sliding-consolidation of a landslide with full convergence analysis. The key feature of this model is mechanical feedback, which might be responsible for the diverse rates of landslide motion (from steady creeping motion to runaway acceleration). This model is made of an Ordinary Differential Equation (ODE) coupled with a Partial Differential Equation (PDE) subject to mixed boundary conditions, with the PDE state entering into the ODE dynamics, and the ODE state affecting the Neuman boundary of the PDE. The observer design relies on a measurement on the ODE. Notice that observer is known to be an efficient tool for state estimation, or joint state and parameter estimation (starting with the famous Extended Kalman Filter). In recent years, it has also been extended to systems with distributed dynamics, with examples in open channel level control [Besançon2008] or monitoring [Bedjaoui2009], backstepping boundary observer for a class of linear first-order hyperbolic systems with spatially-varying parameters [Di Meglio2013], robust state estimation based on a boundary output injection for a class of convection-diffusion-reaction systems [Besançon2013], matrix inequality-based observer for transport-reaction systems [Schaum2014], backstepping adaptive observer-based state and parameter estimation for hyperbolic systems with uncertain boundary parameters and its application to underbalanced drilling [Di Meglio2014], adaptive observer for coupled linear hyperbolic PDEs with unknown boundary parameters based on swapping [Anfinsen2016], and even with extension to coupled ODE-PDE like in the case of high-gain type observer for a class of nonlinear ODE-PDE cascade systems [Ahmed-Ali2015], and boundary ob-

server based on the Volterra integral transformation for hyperbolic PDE-ODE cascade systems [Hasan2016]. In the present chapter, the coupled PDE-ODE observer problem under consideration is addressed by basically combining a copy of PDE dynamics with a Kalman-like observer for the ODE.

The structure of the chapter is as follows: A landslide model depicting landslide behavior and the problem statement is given in Section 4.2. Section 4.3 presents the proposed observer with full convergence analysis. In Section 4.4, the simulation results demonstrate the effectiveness of the proposed observer. Finally, some conclusions and future directions of the work are discussed in Section 4.5.

4.2 Problem Formulation

Extended sliding-consolidation model

The extended sliding-consolidation model [Iverson2005a] is based on a representation of the landslide as a rigid block overlying a thin shear zone, where landslide (slide block) motion is opposed by basal Coulomb friction and regulated by basal pore fluid pressure. For the analysis purpose, the model assumes two components of basal pore pressure: i) imposed pore pressure p_i due rain infiltration and ii) development of excess pore pressure p_e in response to dilation or contraction of the basal shear zone. The motion of the slide block and excess pore pressure evolution are described by Eq.(4.1) and (4.2) respectively.

Momentum equation

$$\begin{aligned}\frac{d^2u_x}{dt^2} = \frac{dv_x}{dt} &= gcos\psi\,[sin(\theta-\psi) - cos(\theta-\psi)tan\phi] \\ &+ \frac{cos^2\psi tan\phi}{\rho Z}\{p_i(0,t) + p_e(0,t)\}\end{aligned} \tag{4.1}$$

Excess pore pressure diffusion equation

$$\begin{aligned}\frac{\partial p_e(z,t)}{\partial t} &= D\frac{\partial^2 p_e(z,t)}{\partial z^2} \\ \frac{\partial p_e(0,t)}{\partial z} &= \frac{\rho_w g\psi}{K}v_x, \\ p_e(Z,t) &= 0\end{aligned} \tag{4.2}$$

where ϕ: friction angle (mechanical strength),
ψ: dilatancy angle of the material,
ρ: soil density,
ρ_w: pore water density,
D: diffusion coefficient,
K: hydraulic conductivity,
g: acceleration due to gravity,
θ: sliding angle,
$u_x(t)$ and $v_x(t)$: displacement and velocity of the slide block respectively (along x-axis),
$p_i(0,t)$: imposed pore pressure at the slide block base,
$p_e(z,t)$: excess pore pressure distribution,
$\partial p_e(0,t)/\partial z = \rho_w g\psi v_x/K$: Neuman boundary condition,
and $p_e(Z,t) = 0$: Dirichlet boundary condition of the excess pore pressure diffusion equation.
$z \in [0, Z]$ with Z the spatial domain length (slide block thickness), and $t \geqslant 0$ is the time. In

addition, v_{x_0} and p_{e_0} are initial values of v_x and p_e respectively. Coordinate z translates with the base of the slide block such that with dilation or contraction of shear zone the base of the slide block is always located at $z = 0$ as shown in Fig. 4.1.

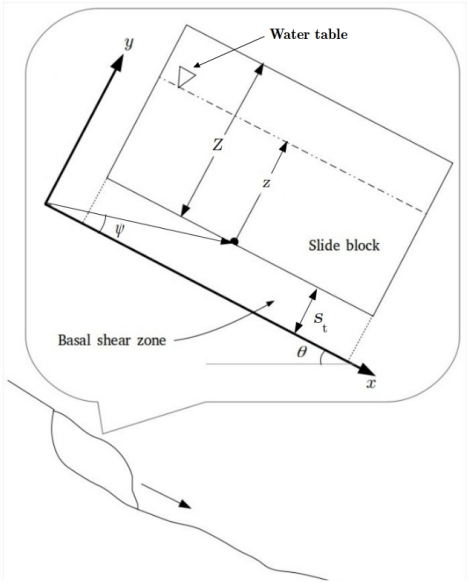

Figure 4.1: The coordinate systems, geometric variables and material property of the slide block

In this model, rate of landslide motion depends on the dilatancy angle (ψ), which is generally difficult to measure. Also, this model is sensitive to the friction angle (ϕ) of the soil. Assuming that the other parameters can be obtained from some knowledge on soil characteristics and landslide geometry, this chapter is thus concerned with the estimation of ϕ and ψ, along with the system state variables v_x and $p_e(x,t)$. This will be done assuming further some known imposed pore pressure time series, as well as some measured velocity time series.

4.3 Observer-based state and Parameter Estimation

4.3.1 Normalized and transformed system equations

In order to address the observer problem, let us first normalize the system equations by introducing dimensionless variables defined as

$$\begin{aligned} z^* = \frac{z}{Z}, \quad t^* = \frac{t}{Z^2/D}, \quad v_x^* = \frac{v_x}{g(Z^2/D)}, \\ p_i^* = \frac{p_i}{\rho_w g Z} \quad \& \quad p_e^* = \frac{p_e}{\rho_w g Z}. \end{aligned} \tag{4.3}$$

Then, consider a transformation

$$\bar{p}_e^*(z^*,t^*) = \left[\frac{K/g}{\psi(Z^2/D)}\right] p_e^*(z^*,t^*) \tag{4.4}$$

and set

$$\begin{aligned} f_0 &= cos\psi\left[sin(\theta-\psi) - cos(\theta-\psi)tan\phi\right], \\ f_1 &= \frac{\rho_w}{\rho} cos^2\psi tan\phi \quad \& \quad f_2 = \left(\frac{Z^2/D}{K/g}\right)\psi f_1 \end{aligned} \tag{4.5}$$

where f_0, f_1 and f_2 are augmentative states depending on the parameter values i.e. $\dot{f}_0 = \dot{f}_1 = \dot{f}_2 = 0$. Now, substituting (4.3), (4.4), and (4.5) in (4.1) and (4.2) gives following system equations (Note that from now on notation ' $\dot{\text{L}}$ ' denotes d/dt^*):

$$\begin{aligned} \begin{bmatrix} \dot{v}_x^* \\ \dot{f}_0 \\ \dot{f}_1 \\ \dot{f}_2 \end{bmatrix} &= \overbrace{\begin{bmatrix} 0 & 1 & p_i^*(0,t^*) & \bar{p}_e^*(0,t^*) \\ 0 & 0 & 0 & 0 \\ 0 & 0 & 0 & 0 \\ 0 & 0 & 0 & 0 \end{bmatrix}}^{\mathrm{A}(t^*)} \begin{bmatrix} v_x^* \\ f_0 \\ f_1 \\ f_2 \end{bmatrix} \\ y &= C\begin{bmatrix} v_x^* & f_0 & f_1 & f_2 \end{bmatrix}^\top \end{aligned} \tag{4.6}$$

$$\begin{aligned} \frac{\partial \bar{p}_e^*(z^*,t^*)}{\partial t^*} &= \frac{\partial^2 \bar{p}_e^*(z^*,t^*)}{\partial z^{*2}} \\ \frac{\partial \bar{p}_e^*(0,t^*)}{\partial z^*} &= v_x^* \\ \bar{p}_e^*(1,t^*) &= 0 \end{aligned} \tag{4.7}$$

where $C = \begin{bmatrix} 1 & 0 & 0 & 0 \end{bmatrix}$. This new form will be used for observer design. Here system transformation simplifies system equations while normalization helps to define space domain as $0 \leq z^* \leq 1$, which will facilitate the convergence proof of observer.

4.3.2 Observer Design

For the sake of clarity, let us recall some notations, Poincaré's inequality, Agmon's inequality and definition of regular persistence which will be used later in the convergence proof of the proposed scheme.

Notations

For a given $x \in \mathbb{R}^n$, $\|x\|$ and $\|x\|_{H_1}$ denotes its usual Euclidean norm and H_1 norm respectively.

Poincaré's inequality

Let $g = g(x)$ be continously differentiable function on $[0,1]$ with $g(0) = 0$ or $g(1) = 0$, then [Besançon2013]

$$\int_0^1 g^2(x)dx \leq \frac{1}{\pi^2}\int_0^1 g_x^2(x)dx < \int_0^1 g_x^2(x)dx$$

where g_x is the first order derivative of g w.r.t. x.

Agmon's inequality

For a function $g(x) \in H_1$ on $[0,1]$ following inequality holds [Krstic2008]

$$\max_{x\in[0,1]} |g(x)|^2 \leq 2\sqrt{\int_0^1 g(x)^2 dx}\sqrt{\int_0^1 g_x(x)^2 dx}.$$

Regular persistence

For regularly persistent $p_i^*(0,t^*)$ and initial conditions in system (4.6)-(4.7), $\exists\, T>0$, $\alpha>0$, $t_0^*>0$ such that [Besançon1996]

$$\int_{t^*}^{t^*+T} \phi^\top(\tau,t^*)C^\top C\phi(\tau,t^*)d\tau \geq \alpha I \quad \forall t^* \geq t_0^* \tag{4.8}$$

where $\phi(\tau,t^*)$ is the state transition matrix of (4.6).

Lemma 1 *Consider the following disturbed Lyapunov equations:*

$$\begin{aligned}\dot{S}(t^*) &= -\theta S(t^*) - A^\top(t^*)S(t^*) - S(t^*)A(t^*) + C^\top C\\ \dot{\hat{S}}(t^*) &= -\theta \hat{S}(t^*) - \hat{A}^\top(t^*)\hat{S}(t^*) - \hat{S}(t^*)\hat{A}(t^*) + C^\top C\end{aligned} \tag{4.9}$$

with $\hat{A} = A + \Delta$ *and* $S(0) = \hat{S}(0) = S_0$. *Assume that:*

- $A(t^*)$ *is uniformaly bounded.*
- $||\Delta|| \leq \bar{\lambda} e^{-\bar{\xi}t^*}$ *for some* $\bar{\lambda} > 0$ *and* $\bar{\xi} > 0$.

Then there exists $\bar{\theta}_0 > 0$ *such that for all* $\theta > \bar{\theta}_0$, $\forall t^* \geq 0$, $||\bar{S}(t^*) - S(t^*)|| \leq \lambda^* e^{-\xi^* t^*}$ *for some positive* λ^*, ξ^* *(proof can be found in [Besançon1996]).*

The main result can be stated as follows:

Theorem 2 *For system (4.6)-(4.7) with available measurement* $y = v_x^*$, *regularly persistent known imposed pore pressure time series* $p_i^*(0,t^*)$ *and any initial condition, observer (4.10)-(4.11) guarantees that* $\hat{\bar{p}}_e^*(z^*,t^*) - \bar{p}_e^*(z^*,t^*)$, $\hat{v}_x^*(t^*) - v_x^*(t^*)$, $\hat{f}_0(t^*) - f_0$, $\hat{f}_1(t^*) - f_1$, *and* $\hat{f}_2(t^*) - f_2$ *converge to 0 as* $t^* \to \infty$ *for all* $0 \leq z^* \leq 1$, *and* $\theta \geq \theta_0$ *for some* $\theta_0 > 0$.

$$\begin{aligned}\frac{\partial \hat{\bar{p}}_e^*(z^*,t^*)}{\partial t^*} &= \frac{\partial^2 \hat{\bar{p}}_e^*(z^*,t^*)}{\partial z^{*2}}\\ \frac{\partial \hat{\bar{p}}_e^*(0,t^*)}{\partial z^*} &= y,\\ \hat{\bar{p}}_e^*(1,t^*) &= 0\end{aligned} \tag{4.10}$$

$$\begin{bmatrix}\dot{\hat{v}}_x^*\\ \dot{\hat{f}}_0\\ \dot{\hat{f}}_1\\ \dot{\hat{f}}_2\end{bmatrix} = \overbrace{\begin{bmatrix}0 & 1 & p_i^*(0,t^*) & \hat{\bar{p}}_e^*(0,t^*)\\ 0 & 0 & 0 & 0\\ 0 & 0 & 0 & 0\\ 0 & 0 & 0 & 0\end{bmatrix}}^{\hat{A}(t^*)} \begin{bmatrix}\hat{v}_x^*\\ \hat{f}_0\\ \hat{f}_1\\ \hat{f}_2\end{bmatrix} - \hat{S}^{-1}C^\top\left[\hat{v}_x^* - y\right] \tag{4.11}$$

$$\dot{\hat{S}}(t^*) = -\theta\hat{S}(t^*) - \hat{A}(t^*)^\top\hat{S}(t^*) - \hat{S}(t^*)\hat{A}(t^*) + C^\top C$$

Proof. Define estimation errors: $e(z^*,t^*) := \hat{\bar{p}}_e^*(z^*,t^*) - \bar{p}_e^*(z^*,t^*)$ and

$$E(t^*) = \begin{bmatrix} \hat{v}_x^*(t^*) \\ \hat{f}_0(t^*) \\ \hat{f}_1(t^*) \\ \hat{f}_2(t^*) \end{bmatrix} - \begin{bmatrix} v_x^*(t^*) \\ f_0 \\ f_1 \\ f_2 \end{bmatrix}.$$

Then, they satisfy equations:

$$\begin{aligned} e_t(z^*,t^*) &= e_{zz}(z^*,t^*) \\ e_z(0,t^*) &= 0 \\ e(1,t^*) &= 0 \\ e(z^*,0) &= e_0(z^*) \end{aligned} \tag{4.12}$$

and

$$\dot{E} = \left[\hat{A}(t^*) - \hat{S}^{-1}(t^*)C^\top C\right] E + \begin{bmatrix} \left\{\hat{\bar{p}}_e^*(0,t^*) - \bar{p}_e^*(0,t^*)\right\} f_2 \\ 0 \\ 0 \\ 0 \end{bmatrix} \tag{4.13}$$

where e_z and e_{zz} are first and second order derivatives of e w.r.t. z^* respectively, and e_t is the first order derivative of e w.r.t. t^*. Let us study the convergence of both estimation errors by *Lyapunov function approach* separately.

Convergence of $e(z^*,t^*)$:

A candidate Lyapunov function based on the classical energy function is considered as [Krstic2008]:

$$V_1(t^*) := \frac{1}{2}\int_0^1 e^2(z^*,t^*)dz^* + \frac{1}{2}\int_0^1 e_z^2(z^*,t^*)dz^*. \tag{4.14}$$

Differentiating (4.14) w.r.t. t^*, by using integration by parts and (4.12), we get:

$$\begin{aligned} \dot{V}_1(t^*) &= -\int_0^1 e_z^2 dz^* - \int_0^1 e_{zz}^2 dz^* \leq -\int_0^1 e_z^2 dz^* \\ \dot{V}_1(t^*) &\leq -\frac{1}{2}\int_0^1 e_z^2 dz^* - \frac{1}{2}\int_0^1 e_z^2 dz^*. \end{aligned}$$

Finally, by using Poincaré's inequality and (4.14), we obtain $\dot{V}_1(t^*) \leq -V_1(t^*)$ which implies $V_1(t^*) \leq exp(-t^*)V_1(0)$ i.e.,

$$\begin{aligned} &\int_0^1 [e^2(z^*,t^*) + e_z^2(z^*,t^*)]dz^* \\ &\quad \leq exp(-t^*)\left\{\int_0^1 \left[e^2(z^*,0) + e_z^2(z^*,0)\right] dz^*\right\} \\ &\quad \leq exp(-t^*)\left\|e(z^*,0))\right\|_{H_1}^2. \end{aligned} \tag{4.15}$$

Condition above proves that $\int_0^1 e(z^*,t^*)dz^* \to 0$ as $t^* \to \infty$ but this does not imply that $e(z^*,t^*)$ goes to 0 $\forall z^* \in (0,1)$. Therefore, by Agmon's inequality we obtain

$$\begin{aligned} \max_{z^*\in[0,1]} |e(z^*,t^*)|^2 &\leq 2\sqrt{\int_0^1 e^2(z^*,t^*)dz^*}\sqrt{\int_0^1 e_z^2(z^*,t^*)dz^*} \\ &\leq \int_0^1 e^2(z^*,t^*)dz^* + \int_0^1 e_z^2(z^*,t^*)dz^*. \end{aligned}$$

Now, by using (4.15) we get

$$\max_{z^*\in[0,1]} |e(z^*,t^*)|^2 \leq exp(-t^*)\,\|e(z^*,0))\|^2_{H_1}. \tag{4.16}$$

This conclude that $e(z^*,t^*)$ converges to 0 as $t^*\to\infty$ $\forall z^*\in[0,1]$.

Convergence of $E(t^*)$:

Remember first regular persistence (4.8) and its consequence on the following Lyapunov differential equation:

$$\dot{S}(t^*) = -\theta S(t^*) - A^\top(t^*)S(t^*) - S(t^*)A(t^*) + C^\top C, \quad S(0)>0. \tag{4.17}$$

From [Besançon1996] for instance, $\exists\theta_0>0$ such that $\forall\theta\geq\theta_0$, $\exists\alpha_1>0,\alpha_2>0,t_0^*>0:\forall t^*\geq t_0^*$

$$\alpha_1 I \leq S(t^*) \leq \alpha_2 I$$

Notice then that $\hat{A}=A+\Delta$ with $\|\Delta\|$ exponentially vanishing. It results from Lemma 1 that solution of

$$\dot{\hat{S}}(t^*) = -\theta\hat{S}(t^*) - \hat{A}^\top(t^*)\hat{S}(t^*) - \hat{S}(t^*)\hat{A}(t^*) + C^\top C, \quad \hat{S}(0)>0$$

satisfies $\left\|\hat{S}(t^*)-S(t^*)\right\| \leq \lambda e^{-\xi t^*}$ for $\lambda>0$, $\xi>0$ and θ large enough. From this, θ can be chosen so that $\hat{S}(t^*)$ also satisfies boundedness of the form

$$\hat{\alpha}_1 I \leq \hat{S}(t^*) \leq \hat{\alpha}_2 I, \quad \forall t^*\geq t_0^*, \hat{\alpha}_1,\hat{\alpha}_2>0. \tag{4.18}$$

Hence, we can consider a candidate Lyapunov function as:

$$V_2(t^*) := E(t^*)^\top \hat{S}(t^*)E(t^*). \tag{4.19}$$

Firstly, differentiating (4.19) w.r.t. time, using (4.11) and (4.13) we get

$$\begin{aligned}
\dot{V}_2(t^*) &= 2E(t^*)^\top\hat{S}(t^*)\dot{E}(t^*) + E(t^*)^\top\dot{\hat{S}}(t^*)E(t^*) \\
&= -\theta E(t^*)^\top\hat{S}(t^*)E(t^*) + 2E(t^*)^\top\hat{S}(t^*)\begin{bmatrix} e(0,t^*)f_2 \\ 0 \\ 0 \\ 0 \end{bmatrix} \\
&\leq -\theta V_2 + 2\|E\|\left\|\hat{S}(t^*)\right\||e(0,t^*)|\,f_2
\end{aligned}$$

Then, from (4.16), (4.18) and (4.19) we obtain

$$\dot{V}_2(t^*) \leq -\theta V_2 + 2\sqrt{V_2(t^*)/\hat{\alpha}_2}\hat{\alpha}_2 exp(-t^*)\,\|e(0,0))\|^2_{H_1} f_2$$

Now, dividing both sides of the equation by $2\sqrt{V_2(t^*)}$ we get

$$\frac{\mathrm{d}}{\mathrm{d}t^*}\sqrt{V_2(t^*)} \leq -\frac{\theta}{2\hat{\alpha}_2}\sqrt{V_2(t^*)} + \sqrt{\hat{\alpha}_2}exp(-t^*)\,\|e(0,0))\|^2_{H_1} f_2.$$

Integrating both sides of the equation gives

$$\begin{aligned}
\sqrt{V_2(t^*)} &\leq exp\left(-\frac{\theta}{2\hat{\alpha}_2}t^*\right)\sqrt{V_2(0)} \\
&+ \int_0^{t^*} exp\left(-\frac{\theta}{2\hat{\alpha}_2}(t^*-\tau)\right)\sqrt{\hat{\alpha}_2}exp(-\tau)\,\|e(0,0))\|^2_{H_1} f_2 d\tau
\end{aligned}$$

which implies that $\sqrt{V_2(t^*)}$ exponentially decays to zero and so $E(t^*)\to 0$ as $t^*\to\infty$.

4.4 Simulation Results

4.4.1 Measured velocity time-series

To validate the effectiveness of the designed observer, a slide block velocity time-series is generated by solving the system equations (4.1)-(4.2), and then white Gaussian noise is added to it (Signal to noise ratio = 20 dB). The parameter values [Iverson2005a] and initial values used for the simulation are indicated in Table 4.1 (Initial values are chosen differently than initial values for the observer to validate the performance). The momentum equation (4.1) is solved by a stepwise analytical method, and the numerical solution of the pore pressure diffusion equation (4.2) is obtained with the Crank-Nicolson method. In the simulations, imposed pore pressure time-series $p_i(0,t)$ representing rainfall variations is assumed as shown in Fig 4.2. The value of imposed pore pressure assumed to be greater than or equal to p_{crit} given as

$$p_{crit} = \frac{gcos\psi\,[cos(\theta-\psi)tan\phi - sin(\theta-\psi)]}{cos^2\psi tan\phi/\rho Z},$$

which corresponds to the value of pore pressure above which slide block starts to accelerate. Simulated excess pore pressure and velocity time series (with noise) are shown in Fig. 4.2 and Fig. 4.3 respectively. At each time step of solving (4.1)-(4.2) variables t, $p_i(0,t)$ and $v_x(t)$ are normalized using (4.3), so as to obtain t^*, $p_i^*(0,t^*)$ and $v_x^*(t^*)$ which act as input to observer.

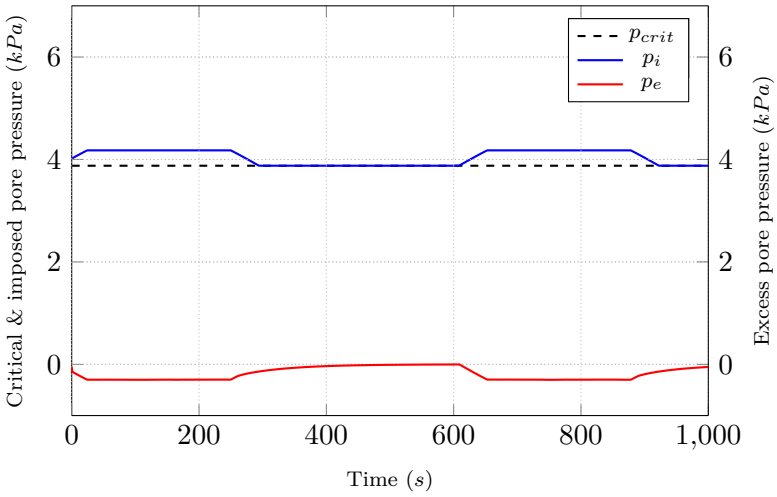

Figure 4.2: Critical, imposed pore pressure and simulated excess pore pressure

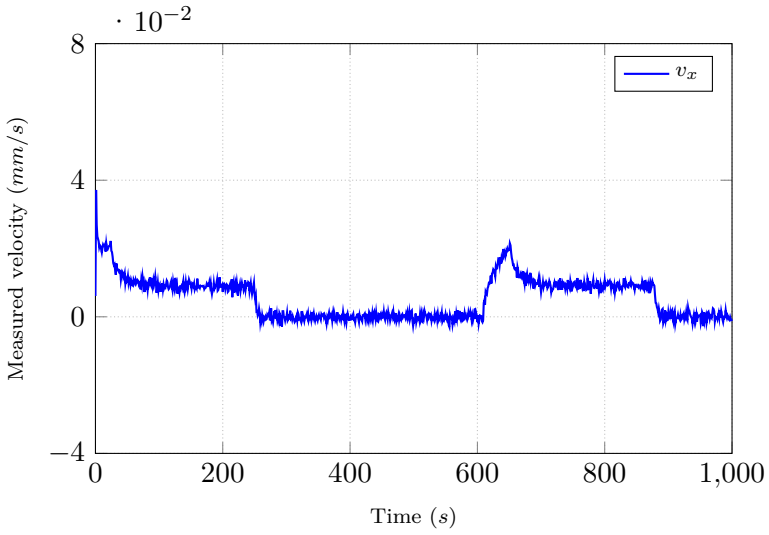

Figure 4.3: Synthetic measured velocity time-series

Table 4.1: Parameter Values

Parameters	**Value**	**Unit**
Initial velocity, v_0	2.4×10^{-2}	mm/s
Initial excess pore pressure, p_{e_0}	-46.6	Pa
Simulation time, T	1000	s
Time step, Δt	0.01	s
Space step, Δz	0.0066	m
Diffusion coefficient, D	3×10^{-3}	m^2/s
Acceleration due to gravity, g	9.8	m/s^2
Slide block thickness, Z	0.65	m
Hydraulic conductivity, K	2×10^{-5}	m/s
Plane inclination angle, θ	31	deg
Slide block mass density, ρ	2000	kg/m^3
Pore water density, ρ_w	1000	kg/m^3
Friction angle, ϕ	**35**	deg
Dilatancy angle, ψ	**6**	deg

4.4.2 Observer results

In the simulation result, we are interested in the estimation of friction angle ϕ, dilatancy angle ψ, velocity of the slide block v_x, and basal excess pore pressure $p_e(0,t)$ assuming other parameter values and imposed pore pressure are known along with synthetic slide block velocity measurement. For initial states given in Table 4.2 (chosen such that initial guess for the ϕ and ψ are 55° and 3° respectively), observer (4.10)-(4.11) gives, estimates of the slide block velocity $\hat{v}_x^*$, excess pore pressure $\hat{\bar{p}}_e^*(z,t)$, augmentative states $\hat{f}_0$, $\hat{f}_1$

and $\hat{f}_2$. Notice that for observer (4.10)-(4.11) space step $\Delta z^* = \frac{\Delta z}{Z} = 0.01$ and time step

Table 4.2: Initial states for the observer

State	**Value**
Initial velocity, $\hat{v}_x^*(0)$	0
Initial excess pore pressure, $\hat{p}_e^*(z^*,0)$	0
Initial augmentative state, $\hat{f}_0(0)$	-0.7895
Initial augmentative state, $\hat{f}_1(0)$	0.7114
Initial augmentative state, $\hat{f}_2(0)$	2.5691×10^6

$\Delta t^* = \frac{\Delta t}{Z^2/D} = 7.1 \times 10^{-5}$. Based on estimates from observer, at each time step firstly dilatancy angle $\hat{\psi}$ and mechanical strength $\hat{\phi}$ are reconstructed by using Eq. (4.20) and (4.21) respectively.

$$\hat{\psi}(t^*) = \frac{\hat{f}_2(t^*)}{\hat{f}_1(t^*)} \times \left(\frac{K/g}{Z^2/D}\right) \tag{4.20}$$

$$\hat{\phi}(t^*) = tan^{-1}\left[\frac{\rho \hat{f}_1(t^*)}{\rho_w cos^2 \hat{\psi}(t^*)}\right] \tag{4.21}$$

Then, basal excess pore pressure $\hat{p}_e^*(0,t^*)$ is obtained by inverse transformation

$$\hat{p}_e^*(0,t^*) = \left[\frac{Z^2/D}{K/g}\right] \hat{\psi}(t^*)\hat{p}_e^*(0,t^*). \tag{4.22}$$

Observer (4.10)-(4.11) is solved for simulation time $T^* = \frac{T}{Z^2/D} = 7.1$. After completion of the simulation, all desired estimates $\hat{\psi}(t)$, $\hat{\phi}(t)$, $\hat{v}_x(t)$, and $\hat{p}_e(0,t)$ are reconstructed from $\hat{\psi}(t^*)$, $\hat{\phi}(t^*)$, $\hat{v}_x^*(t^*)$, and $\hat{p}_e^*(0,t^*)$ using (4.3).

A convergence of the state and parameter estimates can be seen in Fig. 4.4, Fig. 4.5, Fig. 4.6 and Fig. 4.7. In this simulation, the estimated parameter values are $\psi = 5.97°$ and $\phi = 35.5°$ with the relative error between estimated and desired values 0.5% and 1.42% respectively.

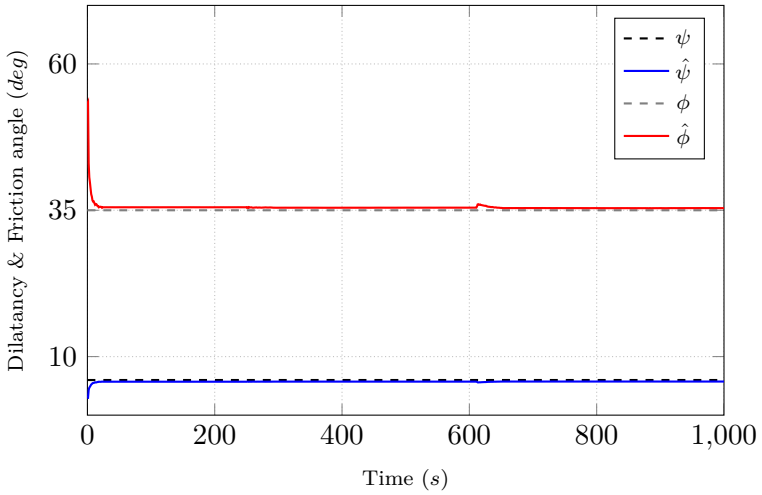

Figure 4.4: Time evolution of the parameter estimate $\hat{\psi}$ & $\hat{\phi}$

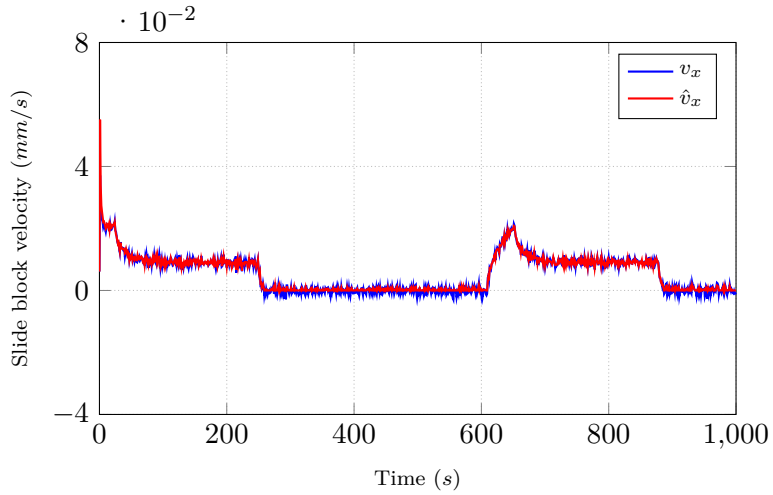

Figure 4.5: Time evolution of the state estimate $\hat{v}_x$

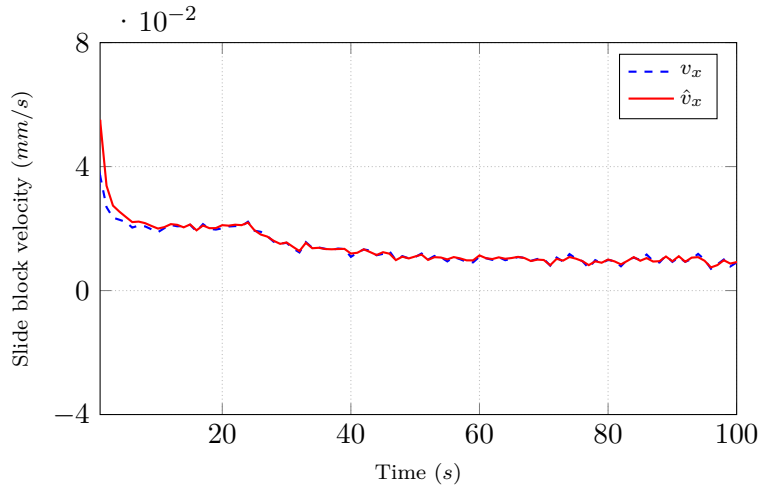

Figure 4.6: Time evolution of the state estimate $\hat{v}_x$ (Zoomed-in)

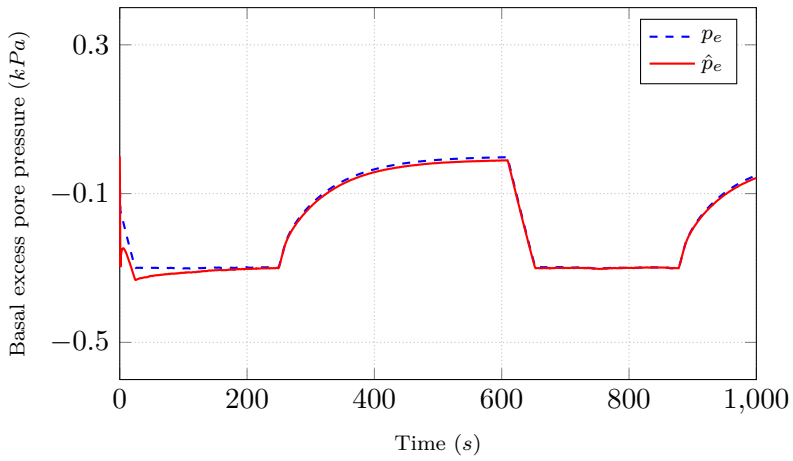

Figure 4.7: Time evolution of the state estimate $\hat{p}_e(0,t)$

4.5 Conclusions and future work

In this chapter, we designed an observer for state and parameter estimation of a landslide. Firstly, we considered the extended sliding-consolidation model depicting a landslide behavior, which is a coupled ODE-PDE system. Secondly, the model is transformed and simplified to utilize the Kalman filter like approach for the observer design. Then the exponential stability of estimation errors has been validated with the help of candidate Lyapunov functional. Lastly, parameter values (friction and dilatancy angle) and states of the system have been well estimated. Based on this result, a future direction for work will be to validate the effectiveness of the designed observer on actual field measurements.

5

Reconstruction and forecasting of landslide displacement using a Kalman filter approach

This work presents an approach for reconstructing displacement patterns and some unknown soil properties of slow-moving landslides, using a special form of so-called Kalman filter or observer. *An observer relies on a model for the prediction step, with online correction based on available measurements. The proposed observer makes use of a simplified viscoplastic sliding model of landslide. In this model, a rigid slide block is assumed to be placed on an inclined surface, where landslide (slide block) destabilizing motion is opposed by sliding resistance constituted by friction, basal pore fluid pressure, cohesion, and viscosity. In order to improve the observer performance, a resetting method is proposed, and to overcome sensitivity to the observer coefficients, a novel tuning method is introduced, considering both actual and synthetic test cases. In this approach, known parameter values (landslide geometrical parameters and some material properties) and water-table height time series are provided as input. The case of Super-Sauze landslide, with data taken from the literature, validates the presented approach. Finally, the observer is extended to forecast displacement pattern assuming that future water-table height time series is known. The material of this chapter corresponds to the paper [Mishra2022b].*

5.1 Introduction

Natural hazards can have severe socio-economic consequences such as substantial cost in life losses, economy, infrastructure, and ecosystem of the affected region. Such disasters need to be detected by Early Warning Systems (EWS) in advance to take timely corrective measures to reduce economic and life losses. One of the essential components of EWS is environmental monitoring and forecasting [UN/ISDR2006]. In the context of landslide hazards, landslide monitoring techniques help determining the stability of the slope and establish the trends in landslide triggering factors, which helps predicting ground movements [Bernardie2014a, Corominas2005a, Herrera2013a].

Monitoring marginally stable slopes provides information on kinematic, hydrological, and climatic variables. These variables play a crucial role in developing landslide models [Buchli2013, Springman2013b], which can then be used for forecasting purposes. There is a large variety of instruments and techniques that typically can be used in landslide monitoring, e.g., Global Positioning System (GPS), photogrammetry, remote sensing (LiDAR, InSAR, etc.), Electrical Resistivity Tomography (ERT), Ground Penetrating Radar (GPR), geotechnical techniques (inclinometers, piezometers, extensometer, Radio Frequency Identification (RFID), Shape Acceleration Arrays (SAA), etc.) [Pecoraro2019, Savvaidis2003, Angeli2000b, Gili2000, Breton2019] and geophysical methods [Larose2015, Bottelin2017]. The most commonly measured parameters are ground displacement, groundwater pressure head and rainfall [Bernardie2014a].

There are two broad categories of models that can be utilized to predict landslide mobility. The phenomenological models employ empirical relationships [Caine1980b, Larsen1993, Guzzetti2008b], probabilistic or statistical approaches [Capparelli2010b, Capparelli2011], or artificial neural network [Bui2020, Yang2019, Mayoraz2002], to establish a relation between soil movement and landslide-inducing factors, e.g., rainfall, water table fluctuations. However, as these models lack in time aspects of landslides, they are unable to predict the impact of changes in landslide-controlling condition [Westen2004b]. Secondly, there are mechanics-based models, which are governed by laws of physics representing physical processes controlling landslide occurrence [Dikshit2019, Kim2016, Pradhan2014a, Teixeira2014, Alvioli2014a, Ali2014b, Herrera2013a, Van Asch2007, Corominas2005a, Angeli1998, Asch1990, Hutchinson1986]. Some combined statistical-mechanical models are also developed for the investigation of landslide displacement, pore water pressure, and rainfall in order to define the possible cause for the triggers, the responses of the slope, and to predict the slope kinematics [Bernardie2014a]. In this paper we rely on physically-based landslide models depicting sliding behavior. As complex landslide models [Frank2015, Liu2016] require extensive spatial data for estimation and prediction purposes [Chae2017].

Physically-based landslide models are sensitive to initial conditions and parameters (constant one or time-varying). Some of the parameters (geometrical parameters and material properties) are generally obtained by field observations, laboratory, and in situ tests, while other unknown parameters need to be estimated with the help of inversion techniques. The most used approach to estimate the unknown parameters is by minimizing the difference between measured displacement and displacement computed with the help of the model. Several optimization schemes exist to estimate unknown parameters such as sequential quadratic programming (SQP) [Bernardie2014a] and non-linear regression [Corominas2005a, Herrera2013a]. Both methods are adapted for the optimization of non-linear dynamical systems; which can give sub-optimal solution, i.e., different sets of estimated parameters can exist depending on optimization initiation. This might provide faulty displacement forecasts. Apart from optimization methods (deterministic approach), probabilistic back analysis can also be used [Zuo2020]. Once the unknown parameters are estimated, the model equation can be solved to forecast displacements

patterns [Bernardie2014a].

These sensitivities to initial conditions and parameters can be taken care of by simulating a model iteratively adjusting parameter values to obtain consistency with measured data, i.e. iterative approach. Second efficient approach is to run a model over time and continually fine-tune it to synchronize with measured data, as in the so-called Kalman filter (or 'observer') approach [Kalman1960]. Both of these approaches have been studied for the extended sliding consolidation model of a landslide and synthetically generated data, in [Mishra2020d] for iterative scheme (and 'adjoint method'), and for continuous scheme (and observer design) in [Mishra2020b]. Based on those studies, we found that a continuous scheme can be more suitable for the case of time-varying parameters. Therefore, Kalman filter approach will be considered here for the Super-Sauze landslide data taken from [Bernardie2014a].

In comparison to the previous study [Mishra2020b], for improved performance to reconstruct displacement pattern and unknown parameters from displacement and pore pressure/water table height measurements, the present paper first proposes the use of a technique corresponding to a 'discrete-time exponential forgetting factor observer' [Ţiclea2013, Ţiclea2009]. Secondly, a resetting method (in the observer) is presented for a better convergence of the estimates. Then, a novel approach of observer coefficients tuning is put forward, considering both actual and synthetic test cases. Finally, the observer is extended to forecast displacement pattern assuming that future water-table height time-series is known.

The structure of the paper is as follows: the considered simplified viscoplastic sliding model of landslide is first given in Section 5.2, together with the corresponding estimation problem, while Section 5.3 presents the proposed reconstruction scheme. In Section 5.4, simulation results demonstrate the effectiveness of the estimation scheme on the Super-Sauze landslide data taken from the literature. Moving forward, Section 5.5 extends the proposed observer for the landslide displacement forecasting purpose. Finally, Section 5.6 provides a conclusion and discusses future directions of the work.

5.2 Simplified viscoplastic sliding model of landslide

The viscoplastic sliding model [Corominas2005a, Herrera2013a, Bernardie2014a] of a landslide assumes a rigid slide block overlying a thin shear zone, as shown in Fig. 5.1. The dynamics is guided by difference between gravity force F_g and resisting forces F_r made of effective friction, cohesion, and viscosity. Net inertia of the block F_i is given by,

$$\begin{aligned} F_i &= \rho H A a(t) = F_g - F_r = \rho H A g \sin\theta \\ &- A\left[\rho H g \cos\theta \tan\phi - p(t)\tan\phi + C + \eta v(t)/s_t\right] \end{aligned} \tag{5.1}$$

where ρ is the soil density, H is the slide block height, A is the slide block base area, $a(t)$ is acceleration of the slide block, g is the acceleration due to gravity, θ is the inclination angle, ϕ is the friction angle, $p(t)$ is pore water pressure at time t, C is the cohesion, η is the viscosity, $v(t)$ is velocity of the slide block, and s_t is the basal shear zone thickness.

For slow-moving landslides the inertia term F_i is expected to remain much smaller than the other terms. Also, assuming a groundwater flow parallel to the slope surface, the pore water pressure can be expressed as [Bernardie2014a],

$$p(t) = \rho_w g \cos^2\theta w_t(t) \tag{5.2}$$

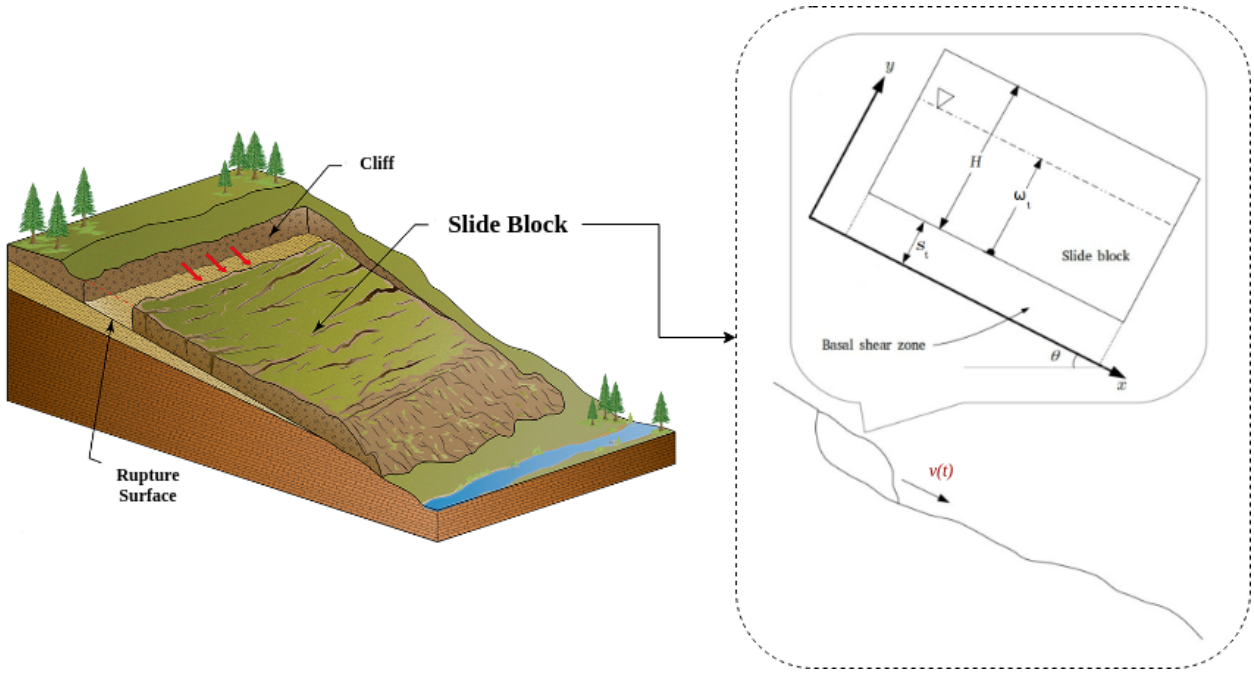

Figure 5.1: Schematic view illustrating geometrical variables used to model slide block motion (graphical representation of landslide on left hand side of the figure is taken from Wyoming State Geological Survey website)

where ρ_w is the pore water density and $w_t(t)$ is water table height as shown in Fig. 5.1. Therefore, substituting (5.2) in (5.1), and rearranging the equation leads to dynamics

$$\begin{aligned}\dot{d} = v(t) = \left(\frac{\rho}{\eta}\right) s_t H g sin\theta - \left(\frac{\rho tan\phi}{\eta}\right) s_t H g cos\theta \\ - \left(\frac{1}{\eta}\right) s_t C + \left(\frac{tan\phi}{\eta}\right) s_t \rho_w g cos^2\theta w_t(t)\end{aligned} \tag{5.3}$$

where d is the displacement of the slide block.

As upslope motion of the rigid slide block is physically impossible, the landslide velocity can not be negative. Such a situation arises whenever water table height $w_t(t)$ goes below a critical water table height w_t^{crit}. From (5.3) the value of w_t^{crit} is evaluated as

$$w_t^{crit} = \frac{C - \rho H g \sin\theta + \rho H g \cos\theta \tan\phi}{\rho_w g \cos^2\theta \tan\phi}. \tag{5.4}$$

When $w_t(t) \leq w_t^{crit}$ landslide dynamics reduces to $\dot{d} = v(t) = 0$.

For known parameter values and water-table height (or pore pressure), time series of displacement can be computed using Eq. 5.3. However some material properties are generally unknown (typically friction angle, cohesion and viscosity) and need to be estimated. In this paper an observer is proposed to estimate friction angle ϕ, and viscosity η from measured displacement $d_{mea}(t)$ and water table height $w_t(t)$, assuming cohesion C is known.

5.3 Reconstruction scheme

5.3.1 Parameter normalization

To address the observer problem, let us first normalize unknown parameter (material property η), by introducing a viscosity scaling factor $\bar{\eta}$ (chosen as a typical viscosity scale) in equation (5.3) as follows:

$$\begin{aligned}\bar{\eta}\dot{d} = &\left(\frac{\bar{\eta}}{\eta}\right) s_t \rho H g sin\theta - \left(\frac{\bar{\eta} tan\phi}{\eta}\right) s_t \rho H g cos\theta \\ &- \left(\frac{\bar{\eta}}{\eta}\right) s_t C + \left(\frac{\bar{\eta} tan\phi}{\eta}\right) s_t \rho_w g cos^2\theta w_t(t).\end{aligned} \tag{5.5}$$

The parameter normalization is introduced to bring parameters of interest in same order of magnitude as friction angle ϕ is dimensionless and usually comprised between 0 and 1.

5.3.2 Model linearization and parameters as augmented states

As η and ϕ are the parameters to be estimated, let us define:

$$\begin{bmatrix}\theta_1 \\ \theta_2\end{bmatrix} := s_t \begin{bmatrix}(\rho H g \sin\theta - C) & -\rho H g \cos\theta \\ 0 & \rho_w g cos^2\theta\end{bmatrix} \begin{bmatrix}\bar{\eta}/\eta \\ \bar{\eta}\tan\phi/\eta\end{bmatrix}. \tag{5.6}$$

This substitution helps in linearizing the model equation. In order to estimate parameters the state vector (vector consisting variables of system) can be extended to accommodate the unknown parameters θ_1 and θ_2 as augmentative states of the model. Substituting (5.6) in (5.5), the model can then be extended by two state variables θ_1, θ_2 with $\dot{\theta}_1 = \dot{\theta}_2 = 0$ (assuming that the parameters will remain constant as the dynamics of the parameters are unknown). Taking into account w_t^{crit} system model reads:

$$\begin{aligned}\dot{d} &= \begin{cases}\frac{\theta_1}{\bar{\eta}} + \frac{\theta_2}{\bar{\eta}} w_t(t) & \text{if } w_t(t) > w_t^{crit} \\ 0 & \text{otherwise}\end{cases} \\ \dot{\theta}_1 &= 0, \quad \dot{\theta}_2 = 0.\end{aligned} \tag{5.7}$$

5.3.3 Model in discrete in time

Instruments incorporated for landslide monitoring collect data with a particular time resolution, e.g., hourly. Therefore, to adapt with discrete measurements, let us express the system dynamics in discrete time,

$$\overbrace{\begin{bmatrix}d^{k+1} \\ \theta_1^{k+1} \\ \theta_2^{k+1}\end{bmatrix}}^{x^{k+1}} = \begin{cases}\overbrace{\begin{bmatrix}1 & \frac{dt}{\bar{\eta}} & \frac{dt}{\bar{\eta}} w_t^k \\ 0 & 1 & 0 \\ 0 & 0 & 1\end{bmatrix}}^{\bar{A}_1^k} \overbrace{\begin{bmatrix}d^k \\ \theta_1^k \\ \theta_2^k\end{bmatrix}}^{x^k}, & \text{if } w_t^k > w_t^{crit} \\ \underbrace{\begin{bmatrix}1 & 0 & 0 \\ 0 & 1 & 0 \\ 0 & 0 & 1\end{bmatrix}}_{\bar{A}_2^k} \underbrace{\begin{bmatrix}d^k \\ \theta_1^k \\ \theta_2^k\end{bmatrix}}_{x^k}, & \text{otherwise}\end{cases} \tag{5.8}$$

where $dt = t^{k+1} - t^k$ is the discrete time step. The measurement model given as

$$y^k = d^k_{mea} = \overbrace{\begin{bmatrix} 1 & 0 & 0 \end{bmatrix}}^{\bar{C}} \overbrace{\begin{bmatrix} d^k \\ \theta_1^k \\ \theta_2^k \end{bmatrix}}^{x^k} + r^k \tag{5.9}$$

where r^k denotes some measurement noise.

5.3.4 Discrete-time exponential forgetting factor observer

Discrete-time exponential forgetting factor observer (or Kalman filtering with forgetting factor) provides least mean-square estimate with an added feature of giving more weight on the most recent measurements employing forgetting factor γ. It optimizes following objective function,

$$\begin{aligned} J_k(\hat{x}_0^k) = \gamma^k (\hat{x}_0^k - \hat{x}_0)^T P_0^{-1} (\hat{x}_0^k - \hat{x}_0) \\ + \sum_{l=0}^{k} \gamma^{k-l} (\hat{y}^l - y^l)^T W^{-1} (\hat{y}^l - y^l) \end{aligned} \tag{5.10}$$

subject to system dynamics

$$\begin{aligned} \hat{x}^{k+1} &= \bar{A}^k \hat{x}^k \\ \hat{y}^k &= \bar{C} \hat{x}^k \end{aligned} \tag{5.11}$$

as constraints, with $\gamma \in (0,1), P_0 = P_0^T > 0, W = W^T > 0$ and where $\hat{x}_0$ denotes the initial guess of the state. The solution of this optimization problem [Ţiclea2013] is provided through measurement update equations:

$$\hat{x}_c^k = \hat{x}_p^k - K^k (\bar{C} \hat{x}_p^k - y^k), \tag{5.12}$$

with

$$K^k = P^k \bar{C}^\intercal (\bar{C} P_p^k \bar{C}^\intercal + W)^{-1}, \tag{5.13}$$

and time update equations,

$$\hat{x}_p^{k+1} = \bar{A}^k \hat{x}_c^k \tag{5.14}$$

$$P^{k+1} = \gamma^{-1} \bar{A}^k [I - K^k \bar{C}] P^k \bar{A}^{k\intercal} + Q \tag{5.15}$$

with initialization P_0, where K^k is the Kalman gain, P is the auto-covariance of state estimation error, W is the auto-covariance of measurement noise r, $\gamma \in (0,1)$ is the forgetting factor, and Q is the process noise auto-covariance matrix.

For dynamics (5.8)-(5.9), observer (5.12)-(5.15) provide estimates of $\hat{d}$, $\hat{\theta}_1$ and $\hat{\theta}_2$. Based on these estimates at each time step firstly $\bar{\eta}/\hat{\eta}$ and $\bar{\eta}\tan\hat{\phi}/\hat{\eta}$ are reconstructed using (5.6)

$$\begin{bmatrix} \bar{\eta}/\hat{\eta} \\ \bar{\eta}\tan\hat{\phi}/\hat{\eta} \end{bmatrix} = \frac{1}{s_t} \begin{bmatrix} \rho H g \sin\theta - C & -\rho H g \cos\theta \\ 0 & \rho_w g cos^2\theta \end{bmatrix}^{-1} \begin{bmatrix} \hat{\theta}_1 \\ \hat{\theta}_2 \end{bmatrix}, \tag{5.16}$$

followed by

$$\hat{\eta} = \frac{\bar{\eta}}{[\bar{\eta}/\hat{\eta}]} \quad \& \quad \hat{\phi} = \tan^{-1}\left(\left[\bar{\eta}\tan\hat{\phi}/\hat{\eta} \right] \times \frac{\hat{\eta}}{\bar{\eta}} \right). \tag{5.17}$$

In the proposed estimation scheme w_t^{crit} plays an important role, which depends on the parameter values, therefore at each step it is estimated using Eq. (5.4)

5.3.5 State estimation error covariance matrix (P) resetting

In practical applications, unknown parameters could be time-varying, affecting the observer's performance, e.g., slow convergence in parameter estimates following abrupt changes in parameter values. This issue can be addressed by detecting such abrupt variations in parameters and resetting state estimation error covariance matrix P. In order to detect abrupt variations Mahalanobis distance [Gnanadesikan1972] between actual and predicted measurements for some previous times (t^{k-m} to t^k), with more weight on the most recent ones, can be calculated as:

$$D^k = \sum_{j=k-m}^{k} \gamma^{k-j} (C^j \hat{x}^j - y^j)^T W^{-1} (C^j \hat{x}^j - y^j) \tag{5.18}$$

For the times when D^j exceeds some threshold ($D^k > \chi^2$), P^k is reset to P_0. This threshold can be obtained from the *chi-square* table [Pearson1900] according to the confidence level of the measurement system. For example, when confidence level is 99% and the dimension of the measurement system vector is 1, the corresponding *chi-square* value is $\chi^2 = 6.635$. Note that there is a possibility of multiple switching one after another time, which could hamper the overall performance of the estimation scheme. Such a scenario is avoided by evading switching for some short duration (e.g., m instances) after the earliest detected switching.

5.3.6 Observer coefficients tuning

Observer coefficients ($P_0, W, Q, \gamma, \chi^2, m$) should be chosen to properly recover model information (See Fig. 5.2). For practical applications, they are manually tuned till proper convergence in estimates are obtained. In such applications, some nominal values of parameters are known, e.g., [Ţiclea2009], which is not the case in this paper. Therefore, a novel approach is introduced, which considers both synthetic and actual data cases to verify the estimates as shown in Fig. 5.3.

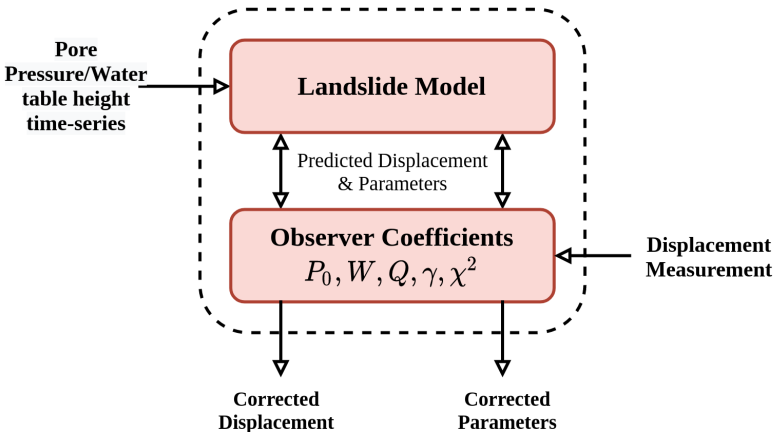

Figure 5.2: Discrete-time exponential forgetting factor observer

In this approach, for the assumed confidence level in the measurement model with a known dimension of the measurement vector, the value of χ^2 is fixed throughout the tuning process. Along with χ^2, P_0 and m are also fixed. P_0 is obtained from its definition with guessed initial states $\hat{x}_0$. m is guessed from some rough initial simulation results on synthetic test cases and can be chosen from the time steps required for first convergence. Once filter coefficients χ^2, P_0 and m are fixed, for some initial Q, γ and W, the estimation scheme is performed on real measurements. For the actual data case, W is manually tuned

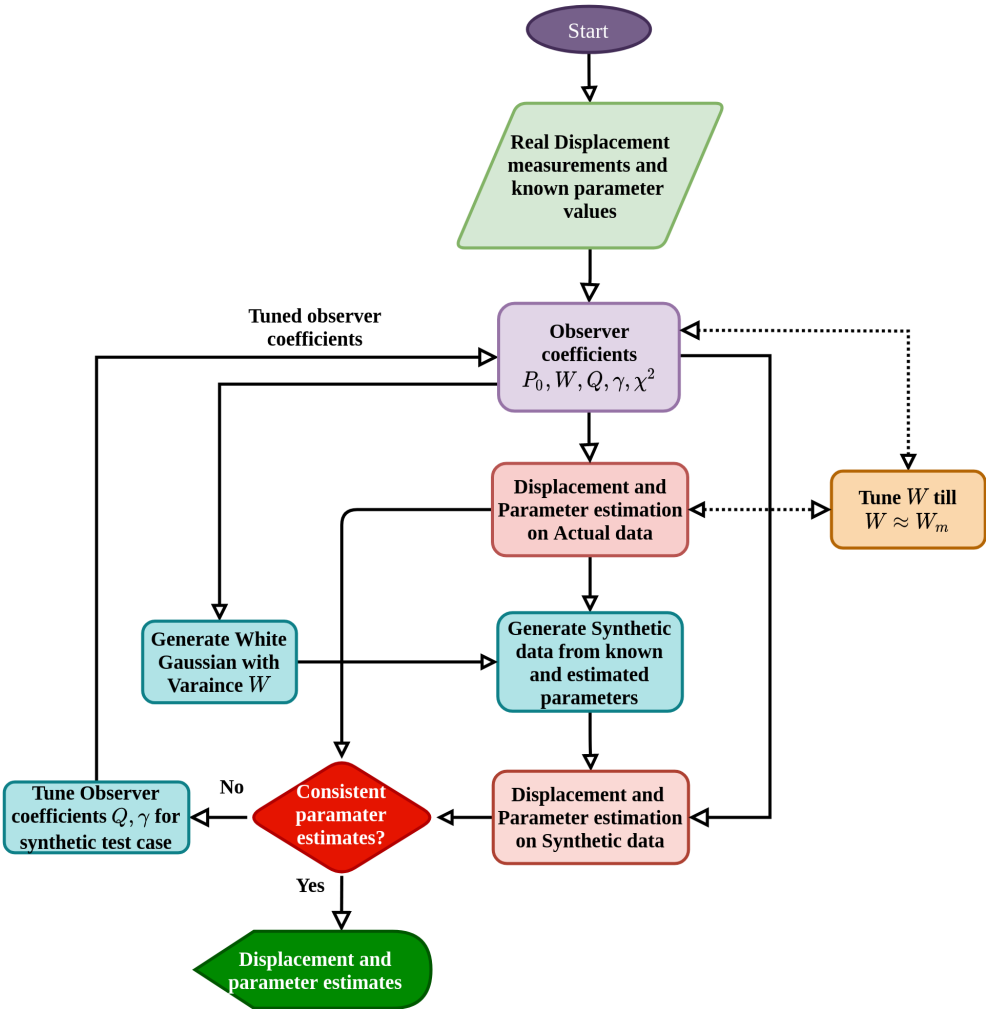

Figure 5.3: Observer coefficients tuning methodology

till $W \approx W_m$ where, W_m is the variance of signal $d_{mea} - \hat{d}$. Then synthetic measurements are generated by solving (5.3) using known parameters, water table height measurements, and estimated parameters (smoothed estimated viscosity and averaged estimated frictional angle) from an actual data case. Now estimation scheme is employed on these synthetic measurements keeping filter coefficients W, γ, and Q same as the actual case. If estimated parameters from both actual case and synthetic test are consistent, filter coefficients tuning process can be stopped; else γ and Q can be tuned with the help of quantitative indicator I_q given as

$$I_q = \sum_{k=1}^{n} \left| \frac{q^k - \hat{q}^k}{q^k} \right| \tag{5.19}$$

where q^k is the parameter of interest (viscosity and friction angle) at time k and $\hat{q}^k$ is corresponding estimated parameter. Indicator I_q provides information on how close the estimated parameters are to the parameters used to generate synthetic test case. Above process of tuning W for actual case followed by γ and Q tuning in synthetic test case is continued till parameter estimates in both cases are consistent to each other, as shown in Fig. 5.3.

5.4 Estimation results

5.4.1 The Super-Sauze landslide data

The Super-Sauze landslide is situated in the French South Alps and monitored by the French Multidisciplinary Observatory of Versant Instabilities (OMIV) for meteorological parameters [meteorological station], slope hydrology [piezometers] and slope kinematics [differential Global Positioning System (GPS): campaigns and permanent receivers, remote Very High-Resolution (VHR) optical cameras, Terrestrial Laser Scanning (TLS)] [Bernardie2014a].

To solve the observer problem, displacement d^k_{mea} and pore water pressure p^k data with time resolution of 2.4 hour (8640 sec) are taken from [Bernardie2014a]. Those data correspond to one of the most active parts of the landslide for a period of high groundwater level from 07/05/1999 to 23/05/1999 (16 days). At that position [location B_2 of Fig. 4 in [Bernardie2014a]], displacement and pore water pressure are measured by a wire extensometer and piezometer, respectively. The piezometer at location B_2 is located at -4m depth while the slip surface is at depth of -9m. In the proposed scheme, water table height time-series w^k_t is required as an input, which is reconstructed from p^k using assumption of groundwater flow parallel to the slope surface (Eq. 5.2) as follows:

$$w^k_t = 5 + p^k/(\rho_w g cos^2\theta).$$

Reconstructed water table height time-series can be seen in Fig. 5.4. The known parameter values are indicated in Table 5.1. Here, the value of $\rho = 1700\ kg/m^3$ is chosen to be the saturated soil density [Malet2005] as the slide block is close to the full saturation level (Fig. 5.4).

Table 5.1: Known geometrical and material parameter values

Parameters	**Value**	**Unit**
Initial block displacement, d_0	0	m
Slide block thickness, H	9	m
Average inclination angle, θ	25	deg
Shear zone thickness, s_t	0.2	m
Acceleration due to gravity, g	9.8	m/s^2
Pore water density, ρ_w	1000	kg/m^3
Cohesion, C	14000	Pa
Slide block mass density, ρ	$1700 - 2140$	kg/m^3

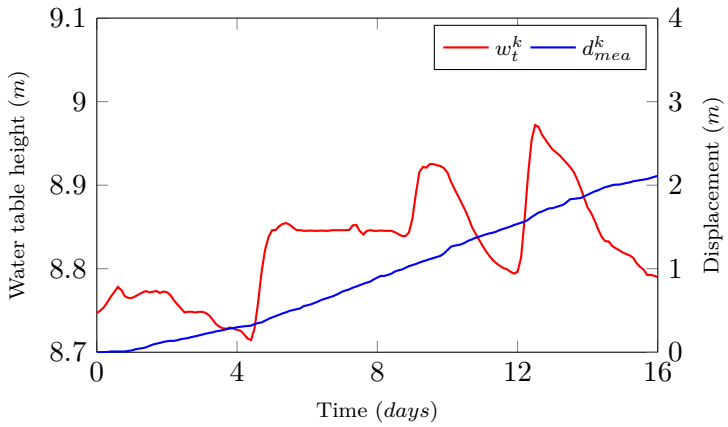

Figure 5.4: Super-Sauze landslide data from 07/05/1999 to 23/05/1999: Displacement measurement d_{mea}^k and reconstructed water table height time-series w_t^k bernardie

5.4.2 Observer results

Displacement pattern $\hat{d}$ along with unknown soil properties ($\hat{\eta}$,$\hat{\phi}$) are reconstructed with the help of proposed estimation scheme (see Section 5.3), for known parameter values (Table 5.1), displacement measurements and water table height time-series (Fig. 5.4). As mentioned in Section 5.3.6, for assumed confidence level (99 %) on measurement systems with dimension equal to 1, the value of χ^2 is set to 6.635. At the same time, the value of m is fixed to 5 (see Section 5.3.6). Initial auto-covariance of state estimation error P_0 is defined as variance of $x_0 - \hat{x}_0$ where, $x_0 = \begin{bmatrix} d_0 & \theta_{1_0} & \theta_{2_0} \end{bmatrix}^T$ (generally assumed to diagonal matrix). Here, the value of d_0 and $\hat{d}_0$ is equal to 0, therefore, the first entry in P_0 is assumed to be W which represents auto-covariance of measurement noise r. Also, as the actual values of θ_1 and θ_2 are not known, other two entries (order of magnitude) are guessed from $\hat{\theta}_1$ and $\hat{\theta}_2$, which are calculated using Eq. (5.6) for assumed η_0 and ϕ_0 to be

10^8 $Pa.s$ and 35° respectively. The matrix P_0 is set to

$$P_0 \approx \begin{bmatrix} W & 0 & 0 \\ 0 & 10000 & 0 \\ 0 & 0 & 100 \end{bmatrix}.$$

For fixed observer coefficients χ^2, m and P_0 with initial $\gamma = 0.95$, $W = 10^{-12}$, and $Q = 10^{-12} I_{3\times3}$ the estimation scheme is performed on real measurements where, $I_{3\times3}$ is the identity matrix of dimension 3. For the actual Super-Sauze case, W is manually tuned till $W \approx W_m$ where, W_m is the variance of $d_{mea} - \hat{d}$. This condition got satisfied for $W = 7.7 \times 10^{-6}$ and $W_m = 7.727 \times 10^{-6}$. For this set of observer coefficients $(\chi^2, m, P_0, \gamma, W, Q)$ obtained estimation results can be seen in Fig. 5.5. In this simulation result, it is observed that friction angle $\hat{\phi}$ is almost constant while viscosity $\hat{\eta}$ varies with time (in correlation with water table height). Therefore to generate synthetic measurements, average value of $\hat{\phi}$ ($\hat{\phi}_{avg}$) and filtered $\hat{\eta}$ ($\hat{\eta}_{fil}$) are utilized (Fig. 5.5). Here to smooth $\hat{\eta}$, the Savitzky-Golay filter is used (Fig. 5.5). Also, in synthetically generated displacement random Gaussian noise with variance W is injected. Now the estimation scheme with similar observer coefficients as in the actual case is employed on the generated synthetic test case, and results can be seen in Fig. 5.6. It is observed that parameter estimates are not converging with $\hat{\phi}_{avg}$ and $\hat{\eta}_{fil}$ (Fig. 5.6(a),(b)). Therefore, γ and Q are tuned with the help of quantitative indicator I_η (see Eq. (5.19)). Notice that, following the sensitivity analysis, it is found that indicator I_η is more sensitive as compared to I_ϕ and I_d to observer coefficient variation. This is because the friction angle is almost constant while displacement is well estimated with measurement update equation (5.12) of the observer.

Based on sensitivity analysis (Table 5.2), for $\gamma = 0.93$ and $Q = 10^{-11} I_{3\times3}$ indicator value $I_\eta = 0.4005$ is the least one. So, for the estimation scheme, values of γ and Q are updated, and simulation results for synthetic and actual cases are obtained. Still, parameter estimates were not consistent; therefore, a process of tuning W for the actual case with condition $W \approx W_m$ and tuning γ and Q with the indicator for a synthetic test case is continued till consistency in parameter estimates were observed. Following this process of observer coefficients tuning for around 6 iterations, consistency in parameter estimates was observed for synthetic test case (Fig. 5.7 (a)-(b)) and actual case (Fig. 5.8 (a)-(b)). In both cases, the average value of the estimated friction angle was found to be equal to 36.77°, while approximately similar variations in estimated viscosity were observed for identical observer coefficients. Here, water-table height is always above critical water-table height ($w_t^k > \hat{w}_t^{crit}$) as shown in Fig. 5.8 (e), i.e., there is no switching in the model as mentioned in Section 5.2. In addition to model switching, state estimation error covariance matrix resetting is proposed in this work for better estimates convergence. This resetting takes place when $D^k > \chi^2$ as shown in Fig. 5.7 (c) and Fig. 5.8 (c), and these switchings can be seen in Fig. 5.7 (f) and Fig. 5.8 (f). Overall, based on results of Fig. 5.7 - Fig. 5.8, estimates for both actual case and synthetic test case are approximately consistent with each other.

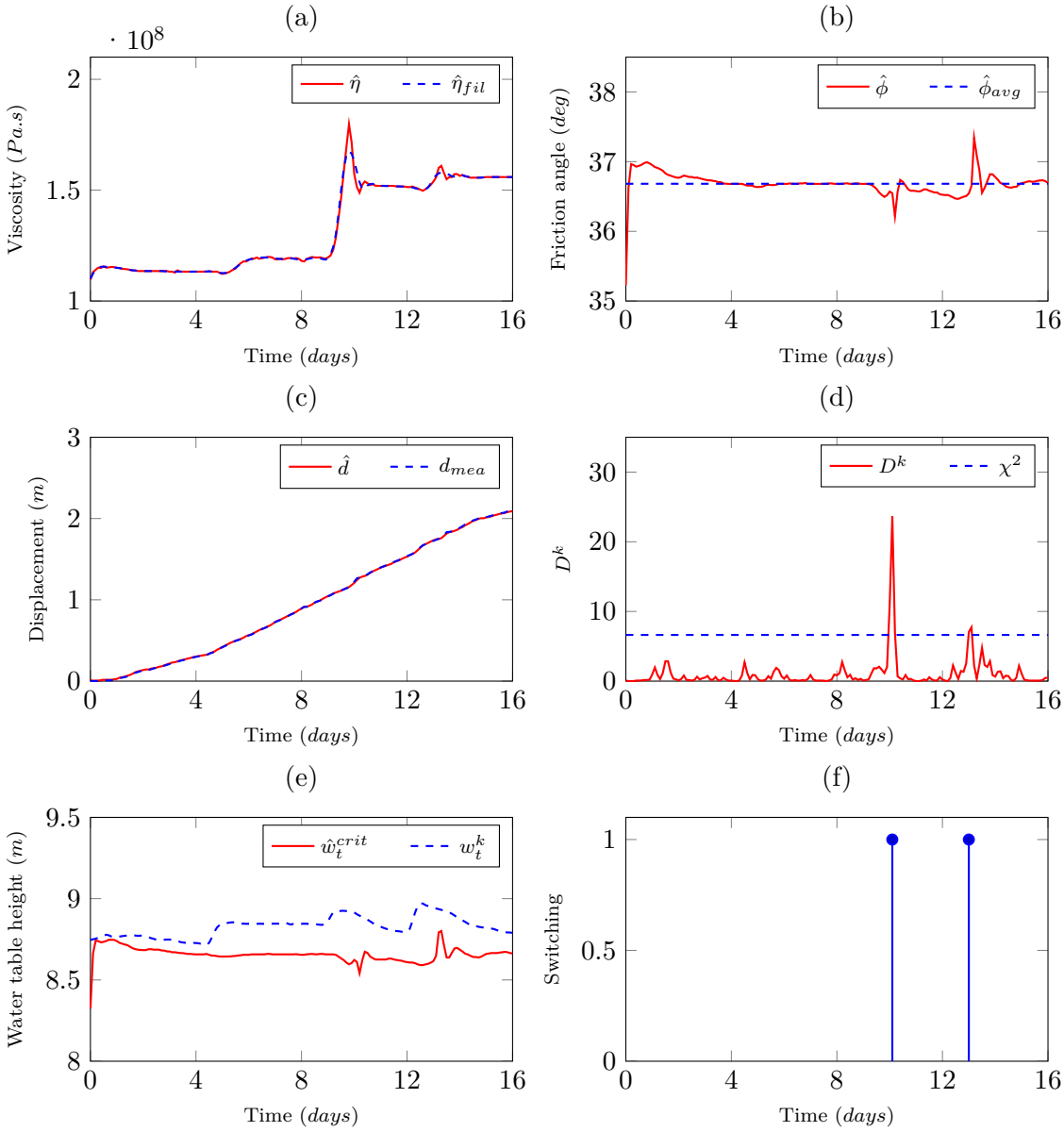

Figure 5.5: Initial estimation results for Super-Sauze case with observer coefficients $\gamma = 0.95$, $W = 7.7 \times 10^{-6}$, $Q = 10^{-12} I_{3\times3}$: *(a)-(b) parameter estimates* ($\hat{\eta}$,$\hat{\phi}$), *filtered viscosity* $\hat{\eta}_{fil}$ *and averaged friction angle* $\hat{\phi}_{avg}$, *(c) Mahalanobis distance between estimated and measured displacement* D^k, *(d) displacement estimate* $\hat{d}$ *and displacement measurement* d_{mea}, *(e) critical water table height estimate* $\hat{w}_t^{crit}$ *and water table height measurement* w_t^k, *(f) Resetting*

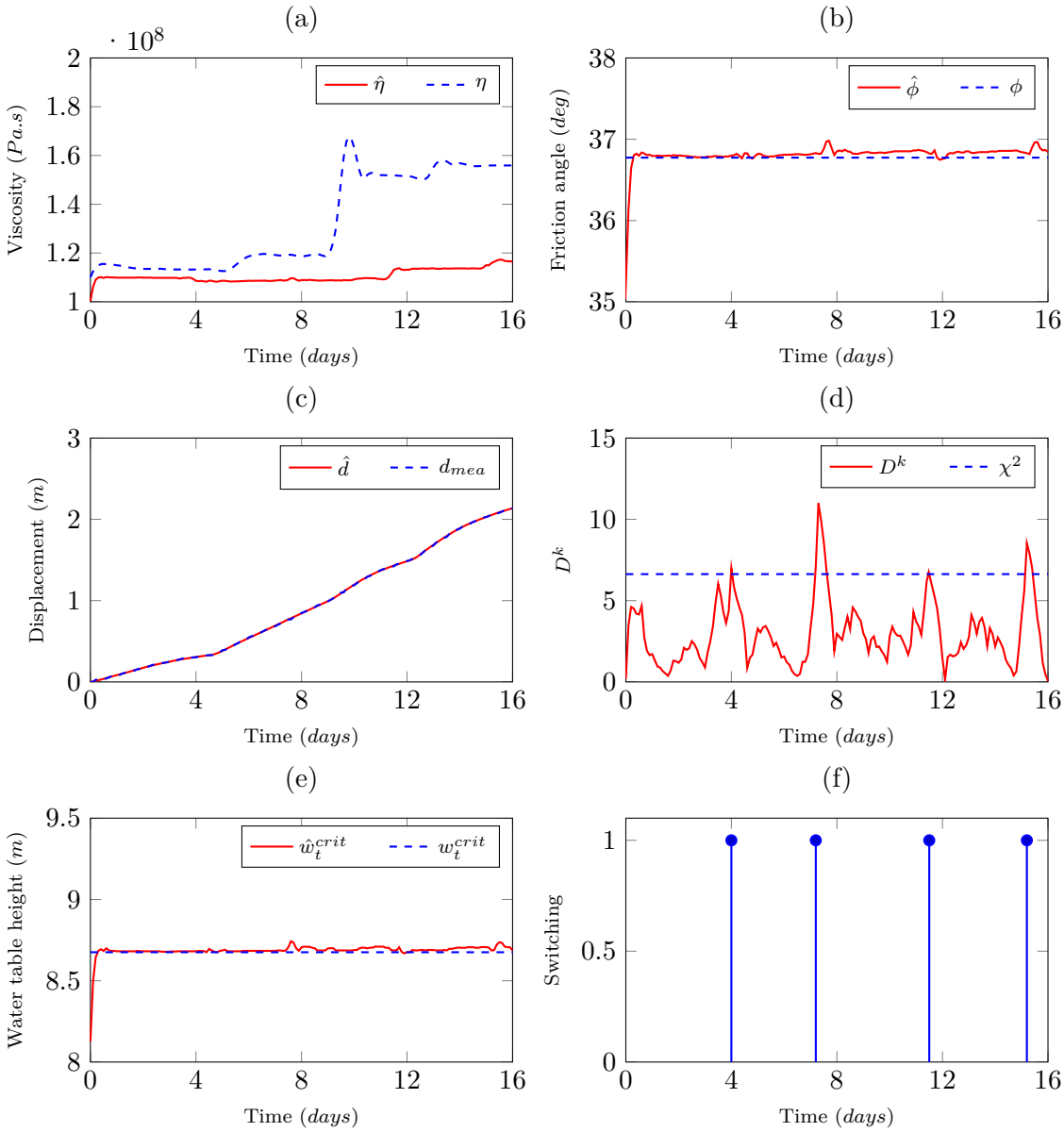

Figure 5.6: Initial estimation results for Super-Sauze synthetic test case with observer coefficients $\gamma = 0.95, W = 7.7 \times 10^{-6}$, $Q = 10^{-12} I_{3\times3}$: (a)-(b) parameter estimates ($\hat{\eta}_{syn}$,$\hat{\phi}_{syn}$), (c) Mahalanobis distance between estimated and synthetic displacement D^k_{syn}, (d) displacement estimate $\hat{d}_{syn}$ and synthetic displacement measurement d_{syn}, (e) critical water table height estimate $\hat{w}_t^{crit}{}_{syn}$, (f) Resetting

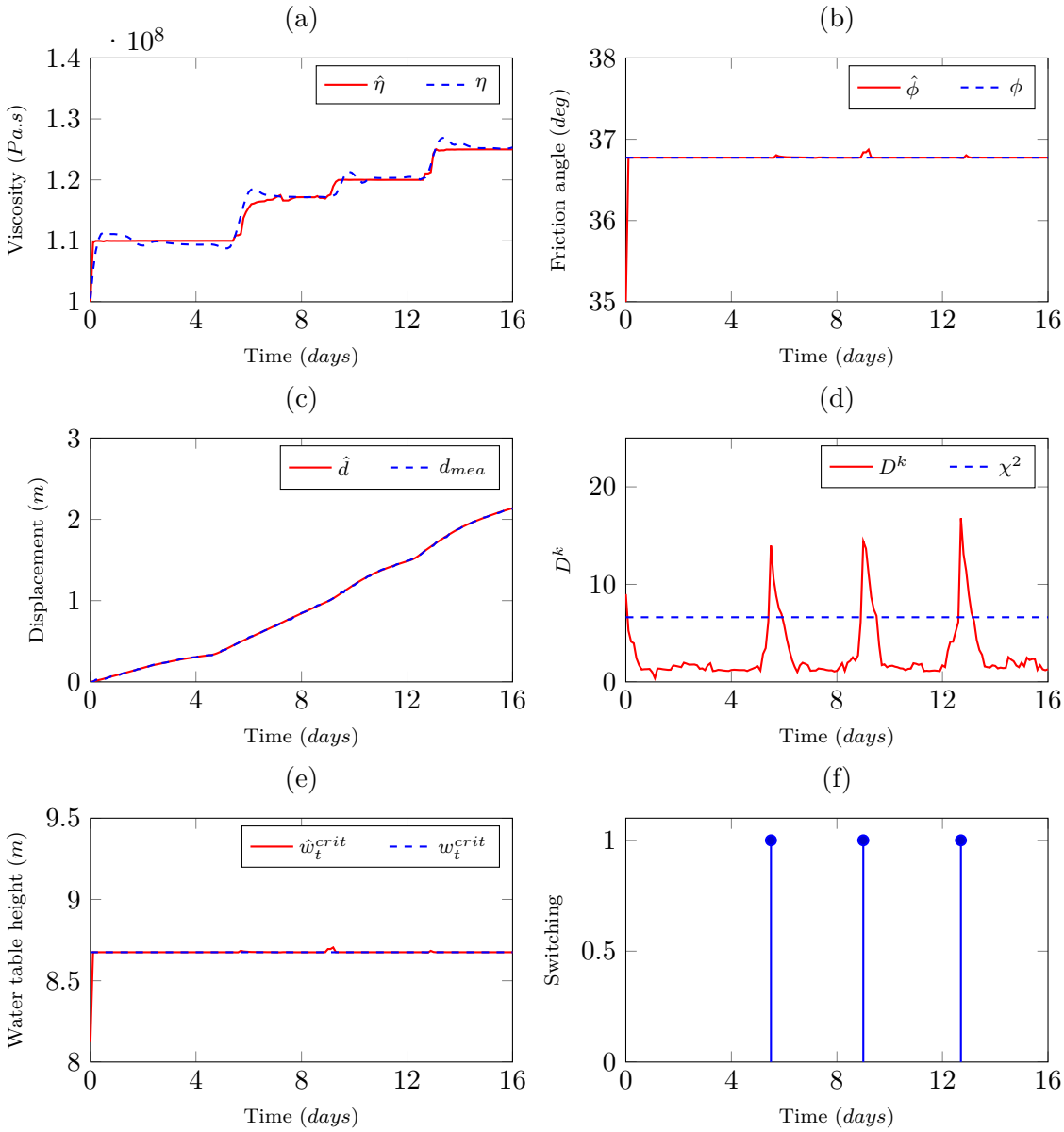

Figure 5.7: Final estimation results for Super-Sauze synthetic test case with observer coefficients $\gamma = 0.9, W = 6 \times 10^{-5}$, $Q = 10^{-11} I_{3\times3}$: (a)-(b) parameter estimates ($\hat{\eta}_{syn}$,$\hat{\phi}_{syn}$), (c) Mahalanobis distance between estimated and synthetic displacement D^k_{syn}, (d) displacement estimate $\hat{d}_{syn}$ and synthetic displacement measurement d_{syn}, (e) critical water table height estimate $\hat{w}_t^{crit}{}_{syn}$, (f) Resetting

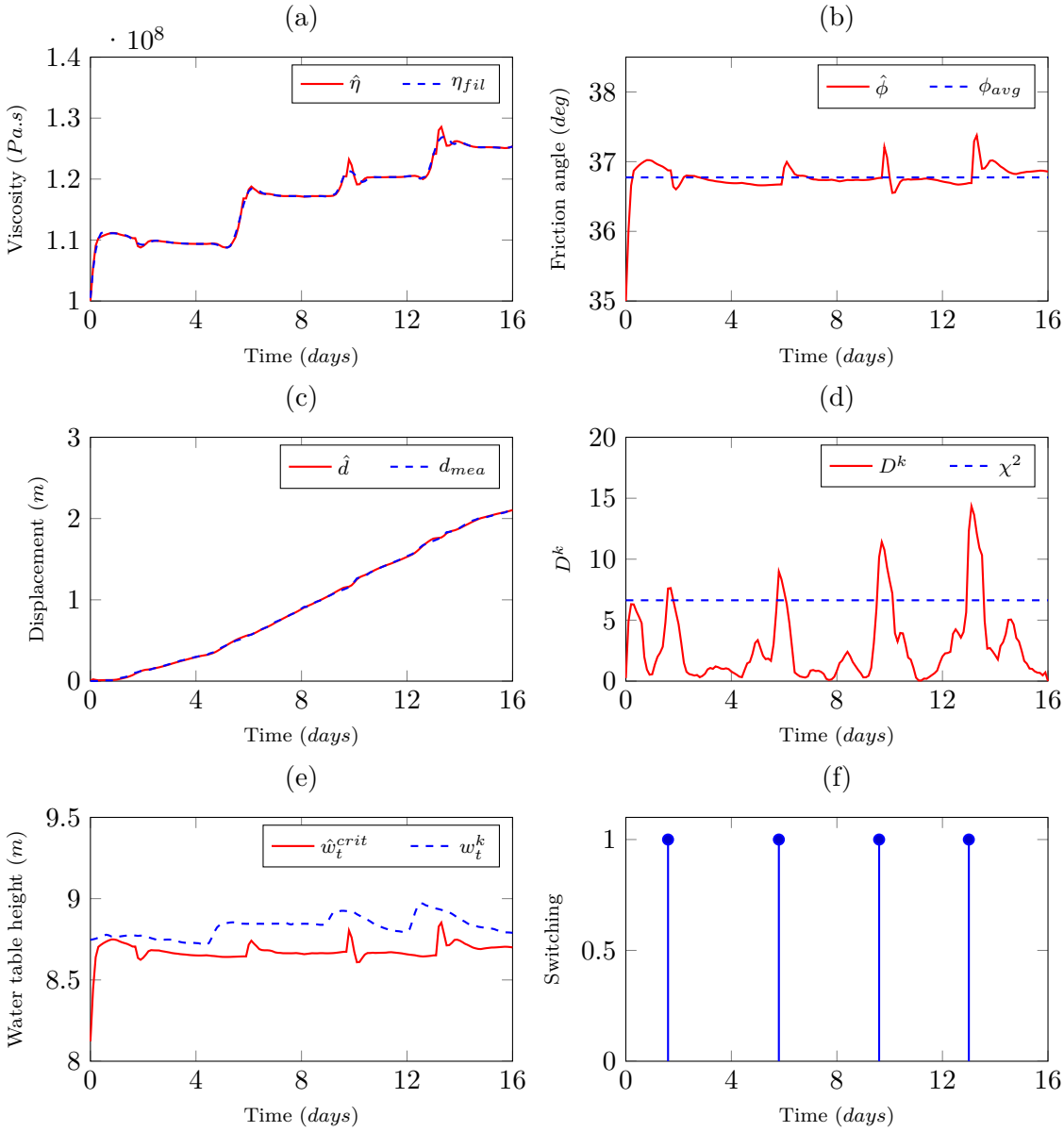

Figure 5.8: Final estimation results for Super-Sauze case with observer coefficients $\gamma = 0.9$, $W = 6 \times 10^{-5}$, $Q = 10^{-11} I_{3\times3}$: *(a)-(b) parameter estimates* ($\hat{\eta}$,$\hat{\phi}$), *filtered viscosity* η_{fil} *and averaged friction angle* ϕ_{avg}, *(c) Mahalanobis distance between estimated and measured displacement* D^k, *(d) displacement estimate* $\hat{d}$ *and displacement measurement* d_{mea}, *(e) critical water table height estimate* $\hat{w}_t^{crit}$ *and water table height measurement* w_t^k, *(f) Resetting*

Table 5.2: Sensitivity analysis for tuning γ and Q

γ/Q	10^{-13}	10^{-12}	10^{-11}	10^{-10}
0.95	0.7768	0.5244	0.4666	0.5628
0.96	0.7666	0.5128	0.4531	0.5534
0.93	0.7628	0.5022	**0.4005**	0.4501
0.92	0.7657	0.6103	0.5130	0.5567

5.5 Landslide displacement forecasting

The reconstruction scheme (Section 5.3) works on the principle of prediction (5.14) followed by correction (5.12) of the information of interest, i.e., at each time step 'k', information is predicted for the next time step '$k+1$' with the help of model (Eq. 5.8) and then corrected based on the measurement. Then, this corrected information helps to predict for the next time step. Here information refers to displacement and parameters, i.e., $\hat{x}^k = \begin{bmatrix} \hat{d}^k & \hat{\theta}_1^k & \hat{\theta}_2^k \end{bmatrix}^T$. Inherently, the proposed scheme can predict information for next time step only. However, with minor update in Eq. (5.14) the prediction horizon can be increased as,

$$\bar{x}_p^{k+l} = \begin{cases} \bar{A}^k \bar{x}_c^k & \text{for} \quad l = 1 \\ \bar{A}^k \bar{x}_p^{k+l-1} & \text{for} \quad l = 2 \quad \text{to} \quad L-1 \end{cases} \tag{5.20}$$

where, L is the prediction horizon.

To validate this extension, for the 16-day Super-Sauze landslide data, the prediction step is initiated after day eight, assuming that water table height time-series is known and at each time step corresponding displacement is being measured. Here, two different prediction horizons are chosen, 1 day ($L = 10$ as step size dt is 2.4 hr) and 2 days ($L = 20$) respectively. In Fig. 5.9 (a)-(c) displacement and parameters forecasts till day 9 and day 10 respectively are presented. As the dynamics of time-varying parameters are unknown, in model equations (5.7) they are assumed constant. Therefore, in simulation results the predicted parameters can seen as constant (Fig. 5.9 (b)-(c)). However, as we move in time, with the measurement update equation of the observer, estimated parameters start varying based on displacement measurement (See Fig. 5.9 (e)-(f)). In the results, it is observed that forecast gets more accurate the closer we are to the actual time (Fig. 5.9 (a)-(c)). This is because of the fact that parameters of model change with time and actual time parameters are being estimated by proposed approach. Fig. 5.9 (d)-(f)) presents moving horizon (1 day and 2 day) predictions, i.e., at instance k forecast of $k+10$ and $k+20$, respectively. As the prediction horizon L is increased accuracy of the forecast reduces. Note that the accuracy of the forecast also depends on the accuracy of the water table height forecast.

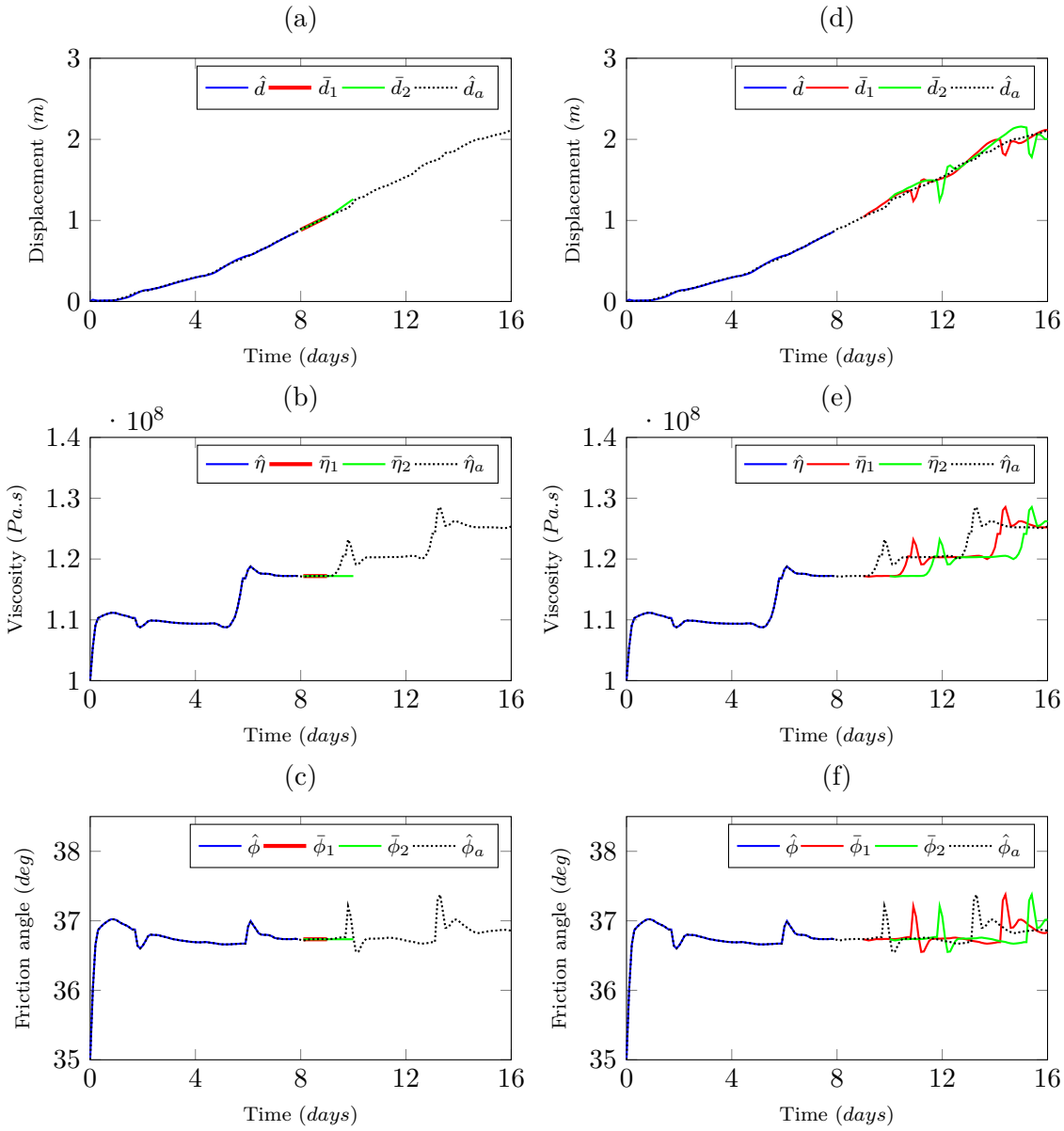

Figure 5.9: Landslide displacement $[\bar{d}]$ and unknown parameters $[\bar{\eta}, \bar{\phi}]$ forecasting: (a) - (c) forecasts with prediction horizon 1 day $[\bar{d}_1, \bar{\eta}_1, \bar{\eta}_1]$ and 2 days $[\bar{d}_2, \bar{\eta}_2, \bar{\eta}_2]$, (d)-(f) forecasts with moving prediction horizon 1 day $[\bar{d}_1, \bar{\eta}_1, \bar{\eta}_1]$ and 2 days $[\bar{d}_2, \bar{\eta}_2, \bar{\eta}_2]$, (a) - (f) estimated displacement, viscosity and friction angle $[\hat{d}_a, \hat{\eta}_a, \hat{\phi}_a]$ from Section 5.4

5.6 Discussion and conclusions

The ability to predict landslide motion is an essential issue for early warnings. Most current alert systems are based on statistical criteria, such as cumulative precipitation thresholds, which inject a degree of uncertainty and make them unreliable. Some alarm systems make use of mechanical models to simulate the kinematic of landslides. However, these models are sensitive to the model parameters (geometrical and material properties of landslide). Knowing all the parameter values, the solution of the model equations can reconstruct complex displacement patterns. However, in many cases, not all the parameters are known. In some studies, preliminary mathematical tools, such as nonlinear regression and sequential quadratic programming, estimate unknown parameters for back analysis. Hence, it is required to utilize a more advanced tool to address the issue.

Therefore, a Kalman filter-like methodology has been proposed, which relies on a simplified viscoplastic sliding model of landslide for both reconstruction and forecasting of displacement and unknown parameters from displacement and water table height measurements. The methodology itself depends on some coefficients. Therefore, a novel method for these coefficients tuning is utilized considering both actual and synthetic test cases, where the coefficients are tuned till the estimation results obtained for both scenarios are consistent with identical coefficients. This methodology is tested for the 16 days Super-Sauze landslide data taken from the literature. The results show that the friction angle ϕ was almost constant while viscosity η varied in correlation to water table height variation for the simulated time.

The presented scheme works on the principle of prediction followed by correction of the information of interest, i.e., at each time step, information is predicted for the next time step and then corrected based on the measurement. This idea of prediction of the next time step is then extended to more time steps with the help of the model equation. To validate this extended scheme, two different prediction horizons are chosen (one day and two days). However, as the dynamics of time-varying parameters are unknown, they are assumed constant for the prediction horizon. As the new measurement arrives correction step takes place, and with these corrected parameters, displacement and parameters are again predicted for the respective prediction horizon. Notice that in the simulation, it is assumed that water table height variation for the prediction horizon is known here. This remains the future work to estimate the water table height variation from precipitation forecasts. Some statistical models are already developed for the water table height prediction from rainfall; however, the focus will remain on a physics-based model.

6

Conclusions and Future Perspectives

This thesis has dealt with the estimation challenges in landslide models. The models under investigation are physically-based landslide models. Given the input (pore water pressure/rainfall) and parameter values (geometrical and material properties), physically-based landslide models can reconstruct and forecast landslide motion. However, it is difficult to collect all those data, and some missing information needs to be reconstructed from available data. This problem can be defined as back analysis, inverse problem, observer problem, or parameter identification issue. After a state-of-the-art about this problem for landslides, this manuscript has proposed an observer design and an optimization-based solution to address the related research question raised in Chapter 1. This chapter lists different thesis outputs, corresponding outcomes and future perspectives as follows:

Thesis Outputs and Outcomes

1. The first output (see Chapter 3) consists of an optimization-based adjoint method for state and parameter estimation in a unique ODE-PDE coupled system for discrete-time asynchronous measurements. In this model, the coupling appears both in the ODE and in the Neuman boundary condition of the PDE. For this system, initial conditions and unknown parameters are estimated for synthetically generated measurements. Firstly the Lagrangian multiplier connects the dynamics of the system and the cost function defined as the least square error between the available (discrete-time asynchronous) measurements and the simulation values. Secondly, the adjoint state method gives the adjoint system equation and the gradients with respect to initial condition and parameters. Then, the cost functional is optimized, employing the steepest descent (iterative) method to estimate parameters and initial state. Finally, The presented approach has been validated for extended sliding-consolidation and viscoplastic sliding-consolidation landslide models.

   For the two examples addressed with optimization, the optimal values of the initial state and parameters (friction angle ϕ, dilatancy angle ψ, and viscosity η) have been well estimated (see Chapter 3). Since one additional parameter is being estimated,

the relative error and iterations required in estimation for the second example are a little higher in contrast to the first example. Using the inexact line search approach to choose step sizes, instead of constant ones can increase the convergence rate. In both cases, it is observed that the proposed methodology produces more accurate estimates for the lower the measurement noise level and the closer the initial parameter values are to the actual parameter values. The key takeaway for the optimization-based method is its scalability; as for the first example, two parameters (ϕ, ψ) have been estimated, and for the second example, three parameters (ϕ, ψ, η). However, this scheme cannot estimate time-varying parameters with a fixed time horizon.

2. The second proposed solution method (see Chapter 4) is an observer-based state and parameter estimation for the extended sliding-consolidation model of a landslide. A copy of the PDE part of the system combined with a Kalman-like observer for the ODE constitutes the observer. The model is transformed and simplified for the observer design to use a Kalman filter-like method. Then, the exponential stability of estimation errors was verified using Lyapunov arguments. Finally, to demonstrate the usefulness of the designed observer, a simulation result of the extended sliding-consolidation model is also shown.

   With the observer-based approach, the system's states and parameter values (friction and dilatancy angle) have been well estimated (see Chapter 4). Also, it is observed that the observer tuning parameter needs to be large enough for better convergence. Note that only two parameters are structurally identifiable for the transformed model, i.e., with an observer design scheme, only two parameters can be estimated. However, this scheme is capable to estimate time-varying parameters.

3. The third output of the thesis (see Chapter 5) presents an approach for reconstructing displacement patterns and some unknown soil properties of slow-moving landslides, using a unique form of so-called *Kalman filter* or observer (discrete-time forgetting factor observer). The proposed observer is based on a simplified landslide viscoplastic sliding model. To increase the observer's performance, a resetting mechanism is presented. The methodology itself depends on some coefficients. Consequently, a novel method for tuning these coefficients is used, which considers both real and synthetic test cases and tunes the coefficients until the estimation results for both cases are consistent with identical coefficients. The input for this method is a time series of water-table heights and known parameter values (landslide geometry parameters and some material qualities). The proposed technique is based on prediction followed by correction of the relevant information, i.e., data is predicted for the next time step and then corrected based on measurement at each time step. With the use of the model equation, the idea of predicting the next time step is then expanded to multiple time steps. Two alternative prediction horizons are used to validate this extended approach (one day and two days). The dynamics of time-varying parameters, on the other hand, are unknown; thus, they are assumed to be constant for the prediction horizon. When a new measurement is received, a correction step is performed, and the corrected parameters are used to forecast displacement and parameters for the respective prediction horizon.

   The case of the Super-Sauze landslide, relying on data from the literature, demonstrates the validity of the proposed method. A set of 16-day Super-Sauze landslide data from the literature has been used to test this methodology. The friction angle ϕ remained nearly constant for the simulated duration while viscosity η fluctuated in conjunction with water table height changes (see Chapter 5).

Thesis Perspectives

1. The applicability of the adjoint-based technique (Chapter 3) to the Super-Sauze landslide data from the literature is now being tested with field data. The proposed approach can be extended to more complicated landslide models. Its extention to time-varying parameters can also be considered.

2. About the observer appraoch (Chapter 4), a future work direction will be to evaluate the effectiveness of the designed observer on actual field measurements. It can be followed by observer design for more complex landslide models for synthetic as well as actual field data.

3. Regarding the third part of the thesis (Chapter 5), it is worth noting that the simulation assumes that the water table height fluctuation for the forecast horizon is known. A study to estimate the water table height fluctuation from precipitation forecasts remains part of the perspectives of the thesis. This issue can be tackled by using some coupled hydrological models. We started investigating this issue based on consolidation models incorporating rainfall as input inspired by Tarzaghi consolidation theory. The proposed methodology can also be applied to some other landslides (the Hollin Hill landslide in England and Harmalière landslide in France) with different data types as a future direction. In particular, preliminary studies and results are ongoing with the Hollin Hill landslides in England, with the help of the British Geological Survey for field data access and related discussions (see Appendix A.1). Based on preliminary results, it is found that for the duration when water table height is close to the critical water table height proposed methodology works well, however for some time intervals proposed scheme is not that efficient. It indicates that some more ingredients (forces) need to be included in the model, followed by an updated information reconstruction scheme.

A Appendix

A.1 The Hollin Hill landslide estimation results using a Kalman filter approach

With a mean slope angle $\theta = 12°$, the Hollin Hill landslide is located south of Terrington, North Yorkshire, UK. The Hollin Hill landslide is a field laboratory that serves as a test location for various monitoring approaches and indicates inland landslides in stiff clays. The landslide is equipped with various monitoring equipment to serve as a research landslide observatory, allowing us to learn more about the factors that cause first-time failure and landslide reactivation. The observatory is made up of the following components: i) two shape arrays (SAA), ii) GPS tracking of 45 marker locations, iii) weather station, and iv) two piezometers (Fig. A.1) [Uhlemann2016]). Apart from these instruments, three clusters of active waveguides monitoring acoustic emission, three inclinometers, and two tiltmeters are employed on-site (Fig. 2.5). Additionally, soil moisture content, bulk conductivity, and temperature are monitored at three separate places, including the backscarp, active lobes, and an area outside the landslide, with sensors set at depths ranging from 0.1 to 6.5 m below ground level [Uhlemann2016]). The tiltmeter, active waveguides, and shape arrays are extremely sensitive to minor movements with a limited spatial resolution and a high temporal resolution. While GPS marker and inclinometer measurements have a low temporal resolution, they can be utilized to identify areas of instability and shear surfaces. The study site can be divided into two lobes, the western and eastern lobe (Fig. A.1). The eastern lobe is a relatively active part of the landslide out of them. As SAA and piezometer are placed close to each other on the eastern lobe (Fig. A.1), we investigate our proposed estimation scheme for eastern lobe data.

A.1.1 Landslide monitoring data

To solve observer problem displacement d^k_{mea} (Fig. A.2) and water table height w^k_t (Fig. A.3) measurements from SAA and piezometer respectively with temporal resolution (dt) of 1 hour (3600 sec) are considered here. This data corresponds to the eastern lobe of the landslide for a period from 01/01/2016 to 01/01/2018, which is provided by British Geological Survey, Nottingham, UK. The known parameter values are indicated in Table A.1 [Uhlemann2016]).

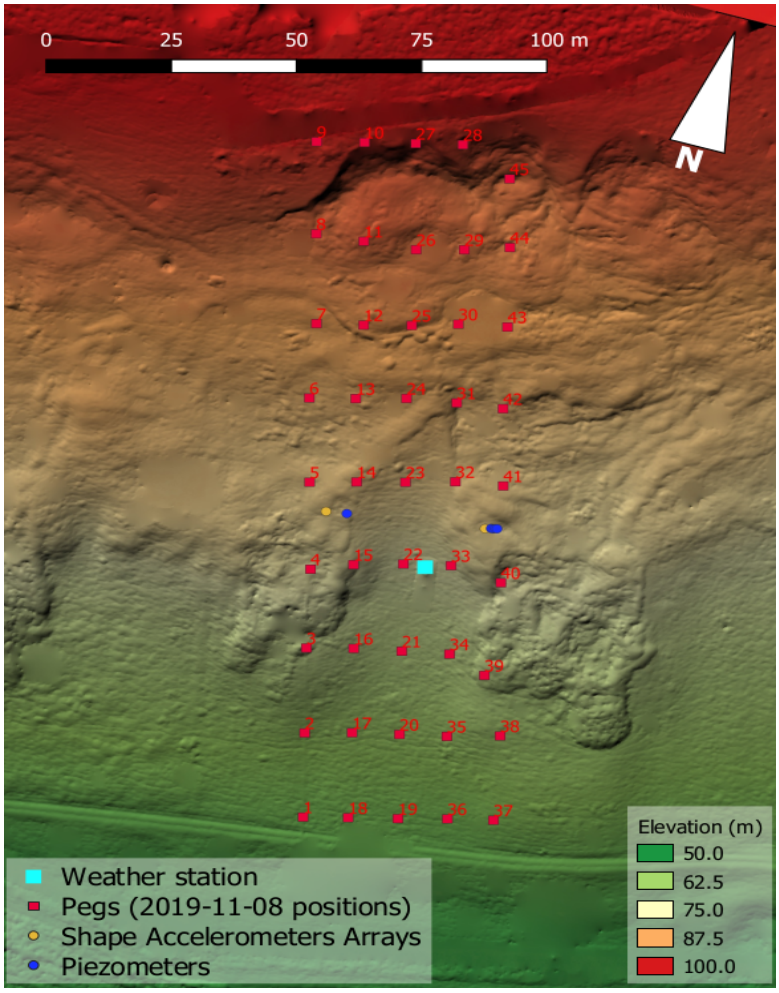

Figure A.1: The Hollin Hill landslide monitoring system (Picture credit: British Geological Survey, Nottingham, UK)

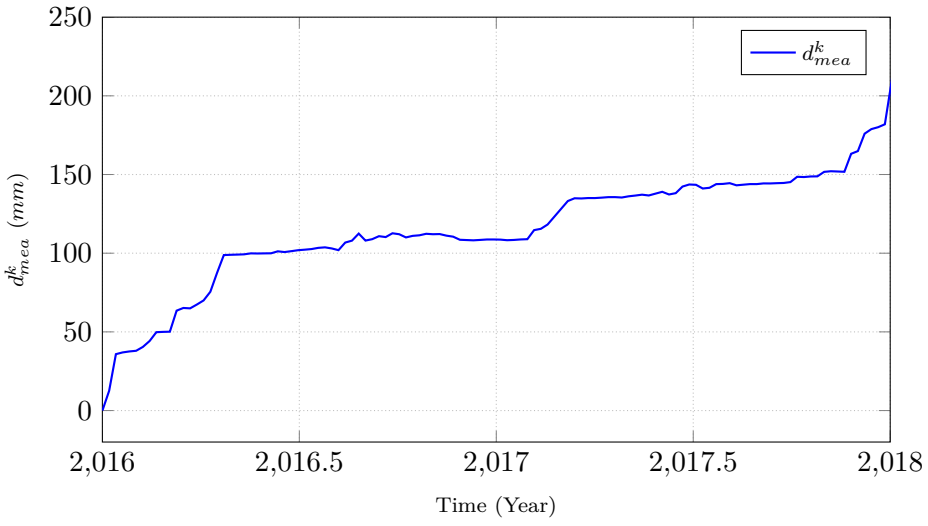

Figure A.2: Displacement d^k_{mea} data (Eastern lobe)

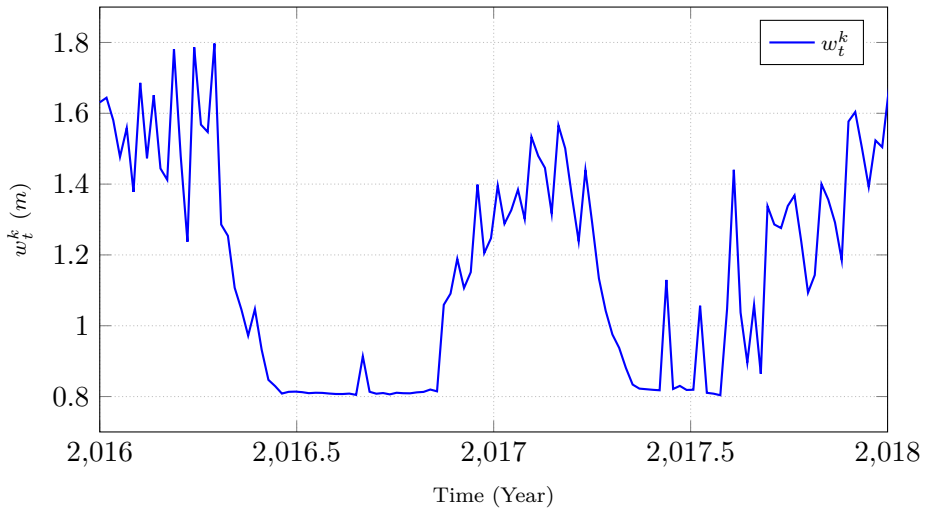

Figure A.3: Water table height w_t^k data (Eastern lobe)

Table A.1: Known geometrical and material parameter values for the Hollin Hill landslide

Parameters	**Value**	**Unit**
Initial block displacement, d_0	0	m
Slide block thickness, H	2	m
Average inclination angle, θ	12	$^\circ$
Acceleration due to gravity, g	9.8	m/s^2
Pore water density, ρ_w	1000	kg/m^3
Slide block mass density, ρ	1750	kg/m^3

A.1.2 Simulation results

Displacement pattern $\hat{d}$ along with unknown soil properties $(\frac{\hat{\eta}}{s_t}, \hat{\phi})$ are reconstructed with the help of proposed estimation scheme (see Section 5.3), for known parameter values (Table A.1), displacement measurements (Fig. A.2) and water table height time-series (Fig. A.3). Note that, for the Hollin Hill landslide cohesion C is not taken into consideration as only two parameters can be estimated, and cohesion is unknown. Also, notice that the preliminary results obtained are with manually tuned observer coefficients $(P_0, W, Q, \gamma, \chi^2, m) = (I_{3\times3}, 5\times10^{-9}, 10^{-11}I_{3\times3}, 0.985, 6.635, 6)$, i.e., without observer coefficients tuning methodology presented in Section 5.3 ($I_{3\times3}$ is identity matrix of rank 3). Estimation results can be seen in Fig. A.4-A.9. Starting with first 140 days of displacement and water table height time-series estimation results are obtained first (Fig. A.4-A.6) followed by whole two years data (Fig. A.7-A.9). The idea is to tune observer coefficients for some initial days using proposed methodology (Section 5.3). Then for tuned observer coefficients, estimation results can be obtained for the whole data (work is under progress). For manually tuned coefficients and initial 140 days data, displacement and unknown parameters have been well reconstructed. It is observed that both friction angle and viscosity/shear zone thickness varies with time. However, similarly to the Super-Sauze landslide case (Fig. 5.8) significant variations in viscosity/shear zone thickness estimate

is observed in comparison to friction angle.

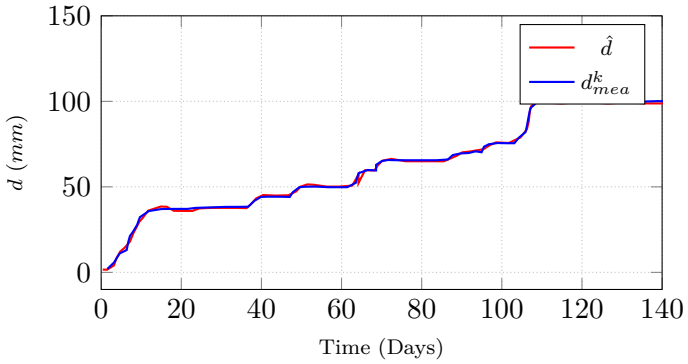

Figure A.4: Displacement estimate $\hat{d}$ for first 140 days

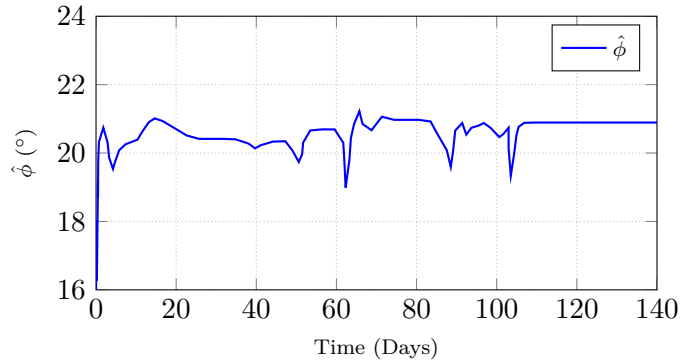

Figure A.5: Friction angle estimate $\hat{\phi}$ for first 140 days

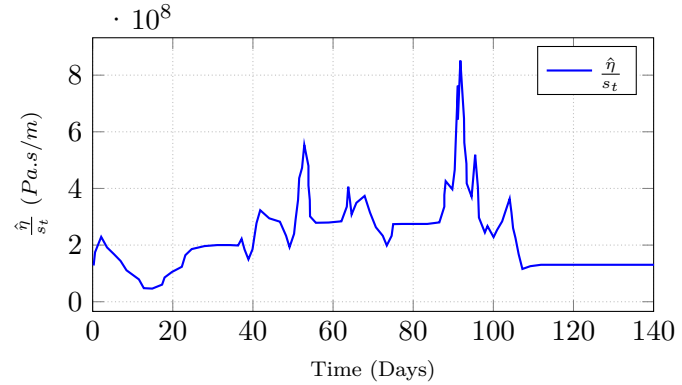

Figure A.6: Viscosity/Shear zone thickness estimate $\frac{\hat{\eta}}{s_t}$ for first 140 days

The estimation scheme is then employed to complete two-year data for the manually tuned observer coefficients. In simulation results, it is observed that information (displacement and unknown parameters) have been well estimated for a majority of times. However, displacement estimates are not converging with displacement data (Fig. A.7) for some instances, i.e., from day 150 to 320 and from day 500 to 550. This is because,

in the assumed landslide model, displacement does not change when water table height is less than critical water table height. However, in data, it appears that some displacement is observed even when water table height is less than critical (≈ 1.45 m). This issue must be translated into unknown parameter estimates as well. It suggests including some more terms in the model which could depict this landslide behavior. It needs to be further investigated.

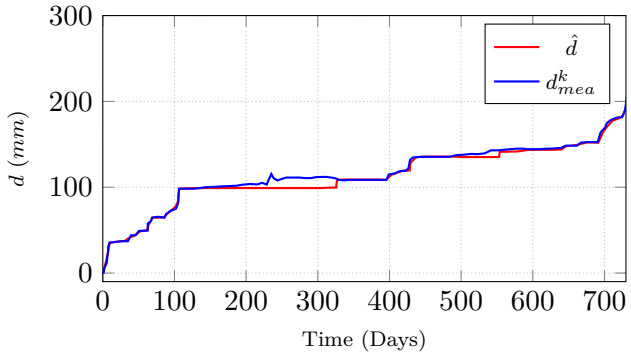

Figure A.7: Displacement estimate $\hat{d}$ for period 2016-2018

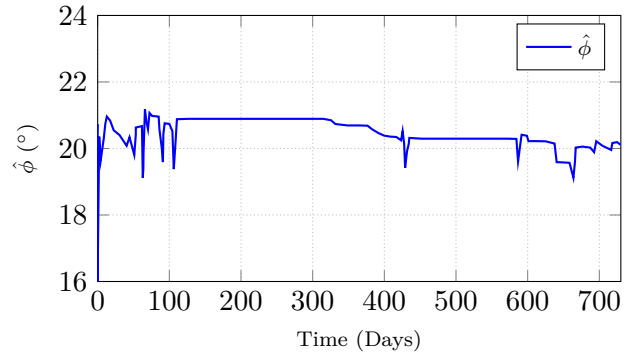

Figure A.8: Friction angle estimate $\hat{\phi}$ for period 2016-2018

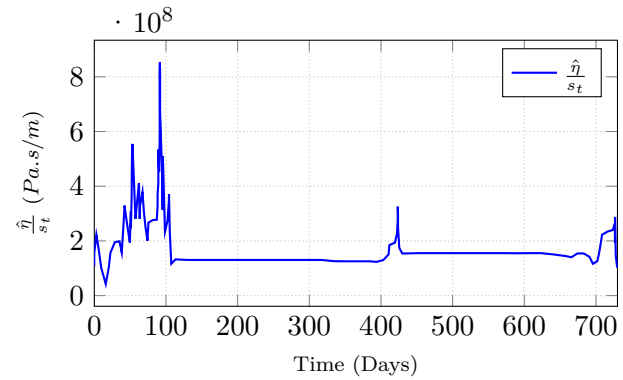

Figure A.9: Viscosity/Shear zone thickness estimate $\frac{\hat{\eta}}{s_t}$ for period 2016-2018

Bibliography

[Abellán2006] A. Abellán, J.M. Vilaplana et J. Martínez. *Application of a long-range Terrestrial Laser Scanner to a detailed rockfall study at Vall de Núria (Eastern Pyrenees, Spain).* Engineering Geology, vol. 88, no. 3-4, pages 136–148, dec 2006.

[Abellán2011] A. Abellán, J. M. Vilaplana, J. Calvet, D. García-Sellés et E. Asensio. *Rockfall monitoring by Terrestrial Laser Scanning – case study of the basaltic rock face at Castellfollit de la Roca (Catalonia, Spain).* Natural Hazards and Earth System Sciences, vol. 11, no. 3, pages 829–841, mar 2011.

[Adam2011] Nico Adam, Fernando Rodriguez Gonzalez, Alessandro Parizzi et Werner Liebhart. *Wide area persistent scatterer interferometry.* In 2011 IEEE International Geoscience and Remote Sensing Symposium. IEEE, jul 2011.

[Adler2003] Robert F. Adler, Christian Kummerow, David Bolvin, Scott Curtis et Chris Kidd. *Status of TRMM Monthly Estimates of Tropical Precipitation.* In Cloud Systems, Hurricanes, and the Tropical Rainfall Measuring Mission (TRMM), pages 223–234. American Meteorological Society, 2003.

[Ahmed-Ali2015] T. Ahmed-Ali, F. Giri, M. Krstic et F. Lamnabhi-Lagarrigue. *Observer design for a class of nonlinear ODE-PDE cascade systems.* Systems & Control Letters, vol. 83, pages 19–27, 2015.

[Aleotti2004] Pietro Aleotti. *A warning system for rainfall-induced shallow failures.* Engineering Geology, vol. 73, no. 3-4, pages 247–265, jun 2004.

[Ali2014a] Abid Ali, Jinsong Huang, A.V. Lyamin, S.W. Sloan, D.V. Griffiths, M.J. Cassidy et J.H. Li. *Simplified quantitative risk assessment of rainfall-induced landslides modelled by infinite slopes.* Engineering Geology, vol. 179, pages 102–116, sep 2014.

[Ali2014b] Abid Ali, Jinsong Huang, A.V. Lyamin, S.W. Sloan, D.V. Griffiths, M.J. Cassidy et J.H. Li. *Simplified quantitative risk assessment of rainfall-induced landslides modelled by infinite slopes.* Engineering Geology, vol. 179, pages 102–116, sep 2014.

[Alvioli2014a] M. Alvioli, Fausto Guzzetti et Mauro Rossi. *Scaling Properties of Rainfall-Induced Landslides Predicted by a Physically Based Model.* Geomorphology, vol. 213, page 38, 05 2014.

[Alvioli2014b] Massimiliano Alvioli, Fausto Guzzetti et Mauro Rossi. *Scaling properties of rainfall induced landslides predicted by a physically based model.* Geomorphology, vol. 213, pages 38–47, may 2014.

[Anfinsen2016] H. Anfinsen, M. Diagne, O. M. Aamo et M. Krstic. *An Adaptive Observer Design for $n+1$ Coupled Linear Hyperbolic PDEs Based on Swapping.* IEEE Transactions on Automatic Control, vol. 61, no. 12, pages 3979–3990, Dec 2016.

[Angeli1998] M.G. Angeli, J. Buma, P. Gasparetto et A. Pasuto. *A combined hillslope hydrology/stability model for low-gradient clay slopes in the Italian Dolomites.* Engineering Geology, vol. 49, no. 1, pages 1–13, 1998.

[Angeli2000a] Maceo-Giovanni Angeli, Alessandro Pasuto et Sandro Silvano. *A critical review of landslide monitoring experiences.* Engineering Geology, vol. 55, no. 3, pages 133–147, feb 2000.

[Angeli2000b] Maceo-Giovanni Angeli, Alessandro Pasuto et Sandro Silvano. *A critical review of landslide monitoring experiences.* Engineering Geology, vol. 55, no. 3, pages 133–147, 2000.

[Apip2010] Apip, Kaoru Takara, Yosuke Yamashiki, Kyoji Sassa, Agung Bagiawan Ibrahim et Hiroshi Fukuoka. *A distributed hydrological–geotechnical model using satellite-derived rainfall estimates for shallow landslide prediction system at a catchment scale.* Landslides, vol. 7, no. 3, pages 237–258, may 2010.

[Arnone2011] E. Arnone, L.V. Noto, C. Lepore et R.L. Bras. *Physically-based and distributed approach to analyze rainfall-triggered landslides at watershed scale.* Geomorphology, vol. 133, no. 3-4, pages 121–131, oct 2011.

[Asch1990] Th.J.W.Van Asch et P.M.B.Van Genuchten. *A comparison between theoretical and measured creep profiles of landslides.* Geomorphology, vol. 3, no. 1, pages 45–55, 1990.

[Asch2007] Th.W.J. Asch, J.-P Malet et L.P.H. Beek. *Techniques, issues and advances in numerical modelling of landslide hazard.* Bulletin de la Societe Geologique de France, vol. 178, 03 2007.

[Ascher1998] Uri M. Ascher et Linda R. Petzold. Computer methods for ordinary differential equations and differential-algebraic equations. Society for Industrial and Applied Mathematics, USA, 1st edition, 1998.

[Atanov Genadii1999] A. Atanov Genadii, G. Evseeva Elena et A. Meselhe Ehab. *Estimation of Roughness Profile in Trapezoidal Open Channels.* Journal of Hydraulic Engineering, vol. 125, no. 3, pages 309–312, 1999.

[Avanzi2009] Giacomo D'Amato Avanzi, Francesco Falaschi, Roberto Giannecchini et Alberto Puccinelli. *Soil slip susceptibility assessment using mechanical–hydrological approach and GIS tech-*

niques: an application in the Apuan Alps (Italy). Natural Hazards, vol. 50, no. 3, pages 591–603, feb 2009.

[Baecher2003] Gregory B. Baecher et John T. Christian. Reliability and statistics in geotechnical engineering. Wiley, 2003.

[Bamler1998] Richard Bamler et Philipp Hartl. *Synthetic aperture radar interferometry.* Inverse Problems, vol. 14, no. 4, pages R1–R54, aug 1998.

[Bardi2014] Federica Bardi, William Frodella, Andrea Ciampalini, Silvia Bianchini, Chiara Del Ventisette, Giovanni Gigli, Riccardo Fanti, Sandro Moretti, Giuseppe Basile et Nicola Casagli. *Integration between ground based and satellite SAR data in landslide mapping: The San Fratello case study.* Geomorphology, vol. 223, pages 45–60, oct 2014.

[Bardi2016] Federica Bardi, Federico Raspini, Andrea Ciampalini, Lene Kristensen, Line Rouyet, Tom Lauknes, Regula Frauenfelder et Nicola Casagli. *Space-Borne and Ground-Based InSAR Data Integration: The Aknes Test Site.* MDPI, AG, vol. 8, no. 3, page 237, mar 2016.

[Baroň2012] Ivo Baroň, David Bečkovský et Lumír Míča. *Application of infrared thermography for mapping open fractures in deep-seated rockslides and unstable cliffs.* Landslides, vol. 11, no. 1, pages 15–27, nov 2012.

[Bartholomew-Biggs2008] Michael Bartholomew-Biggs. The steepest descent method. Springer, 2008.

[Baum2002] Rex L. Baum, William Z. Savage et Jonathan W. Godt. *TRIGRS a Fortran program for transient rainfall infiltration and grid-based regional slope-stability analysis*, 2002.

[Baum2005] Rex L. Baum, Jeffery A. Coe, Jonathan W. Godt, Edwin L. Harp, Mark E. Reid, William Z. Savage, William H. Schulz, Dianne L. Brien, Alan F. Chleborad, Jonathan P. McKenna et John A. Michael. *Regional landslide-hazard assessment for Seattle, Washington, USA.* Landslides, vol. 2, no. 4, pages 266–279, nov 2005.

[Baum2008] Rex L. Baum, William Z. Savage et Jonathan W. Godt. *TRIGRS - A Fortran Program for Transient Rainfall Infiltration and Grid-Based Regional Slope-Stability Analysis, Version 2.0.* Rapport technique, 2008.

[Baum2010] Rex L. Baum, Jonathan W. Godt et William Z. Savage. *Estimating the timing and location of shallow rainfall-induced landslides using a model for transient, unsaturated infiltration.* Journal of Geophysical Research, vol. 115, no. F3, jul 2010.

[Bedjaoui2009] Nadia Bedjaoui, Erik Weyer et Georges Bastin. *Methods for the localization of a leak in open water channels.* Networks & Heterogeneous Media, vol. 4, no. 1556-1801-2009-2-189, pages 189–210, 2009.

[Bennett2016] G. Bennett, S. Miller, J. Roering et D. Schmidt. *Landslides, threshold slopes, and the survival of relict terrain in the wake of the Mendocino Triple Junction.* Geology, vol. 44, 2016.

[Berardino2002] P. Berardino, G. Fornaro, R. Lanari et E. Sansosti. *A new algorithm for surface deformation monitoring based on small baseline differential SAR interferograms.* IEEE Transactions on Geoscience and Remote Sensing, vol. 40, no. 11, pages 2375–2383, nov 2002.

[Berardino2003] Paolo Berardino, Mario Costantini, Giorgio Franceschetti, Antonio Iodice, Luca Pietranera et Vincenzo Rizzo. *Use of differential SAR interferometry in monitoring and modelling large slope instability at Maratea (Basilicata, Italy).* Engineering Geology, vol. 68, no. 1-2, pages 31–51, feb 2003.

[Bernardie2014a] S. Bernardie, N. Desramaut, J.P. Malet, G. Maxime et G. Grandjean. *Prediction of changes in landslide rates induced by rainfall.* Landslides, vol. 12, 2014.

[Bernardie2014b] Séverine Bernardie, Nicolas Desramaut, J.P Malet, Gourlay Maxime et Gilles Grandjean. *Prediction of changes in landslide rates induced by rainfall.* Landslides, vol. 12, 06 2014.

[Berti2000] Matteo Berti, Rinaldo Genevois, R. Lahusen, Alessandro Simoni et Pia Tecca. *Debris flow monitoring in the Acquabona watershed on the Dolomites (Italian Alps).* Physics and Chemistry of the Earth, Part B: Hydrology, Oceans and Atmosphere, vol. 25, pages 707–715, 09 2000.

[Berti2005] M. Berti et A. Simoni. *Experimental evidences and numerical modelling of debris flow initiated by channel runoff.* Landslides, vol. 2, no. 3, pages 171–182, oct 2005.

[Berti2014] Matteo Berti et Alessandro Simoni. *DFLOWZ: A free program to evaluate the area potentially inundated by a debris flow.* Computers & Geosciences, vol. 67, 06 2014.

[Besançon1996] Gildas Besançon, Guy Bornard et Hassan Hammouri. *Observer Synthesis for a Class of Nonlinear Control Systems.* European Journal of Control, vol. 2, no. 3, pages 176–192, 1996.

[Besançon2008] Gildas Besançon, Jean-Francois Dulhoste et Didier Georges. *Nonlinear Observer-Based Feedback for Open-Channel Level Control.* Journal of Hydraulic Engineering, vol. 134, 09 2008.

[Besançon2013] Gildas Besançon, Thang V. Pham et Didier Georges. *Robust state estimation for a class of convection-diffusion-reaction systems.* IFAC Proceedings Volumes, vol. 46, no. 26, pages 203–208, 2013. 1st IFAC Workshop on Control of Systems Governed by Partial Differential Equations.

[Besançon2007] G. Besançon. Nonlinear observers and applications. Springer, 2007.

[Beven1979] K. J. Beven et M. J. Kirkby. *A physically based, variable contributing area model of basin hydrology.* Hydrological Sciences Bulletin, vol. 24, no. 1, pages 43–69, 1979.

[Bianchini2015] Silvia Bianchini, Fabio Pratesi, Teresa Nolesini et Nicola Casagli. *Building Deformation Assessment by Means of Persistent Scatterer Interferometry Analysis on a Landslide-Affected Area: The Volterra (Italy) Case Study.* Remote Sensing, vol. 7, no. 4, pages 4678–4701, apr 2015.

[Bittelli2012] Marco Bittelli, Roberto Valentino, Fiorenzo Salvatorelli et Paola Rossi Pisa. *Monitoring soil-water and displacement conditions leading to landslide occurrence in partially saturated clays.* Geomorphology, vol. 173-174, pages 161–173, nov 2012.

[Bordoni2015] M. Bordoni, C. Meisina, R. Valentino, M. Bittelli et S. Chersich. *Site-specific to local-scale shallow landslides triggering zones assessment using TRIGRS.* Natural Hazards and Earth System Sciences, vol. 15, no. 5, pages 1025–1050, may 2015.

[Bottelin2017] P. Bottelin, L. Baillet, E. Larose, D. Jongmans, D. Hantz, O. Brenguier, H. Cadet et A. Helmstetter. *Monitoring rock reinforcement works with ambient vibrations: La Bourne case study (Vercors, France).* Engineering Geology, vol. 226, pages 136–145, aug 2017.

[Breton2019] Mathieu Le Breton, Laurent Baillet, Eric Larose, Etienne Rey, Philippe Benech, Denis Jongmans, Fabrice Guyoton et Michel Jaboyedoff. *Passive radio-frequency identification ranging, a dense and weather-robust technique for landslide displacement monitoring.* Engineering Geology, vol. 250, pages 1–10, feb 2019.

[Brunetti2010] M. T. Brunetti, S. Peruccacci, M. Rossi, S. Luciani, D. Valigi et F. Guzzetti. *Rainfall thresholds for the possible occurrence of landslides in Italy.* Natural Hazards and Earth System Sciences, vol. 10, no. 3, pages 447–458, mar 2010.

[Bryson1975] A. E. Bryson et Yu-Chi Ho. *Applied Optimal Control: Optimization, Estimation and Control.* Washington: Hemisphere, 1975.

[Brückl2013] E. Brückl, F. K. Brunner, E. Lang, S. Mertl, M. Müller et U. Stary. *The Gradenbach Observatory—monitoring deep-seated gravitational slope deformation by geodetic, hydrological, and seismological methods.* Landslides, vol. 10, no. 6, pages 815–829, jun 2013.

[Buchli2013] Thomas Buchli, Kaspar Merz, Xiaohai Zhou, Wolfgang Kinzelbach et Sarah M. Springman. *Characterization and Monitoring of the Furggwanghorn Rock Glacier, Turtmann Valley, Switzerland: Results from 2010 to 2012.* Vadose Zone Journal, vol. 12, no. 1, page vzj2012.0067, 2013.

[Bui2020] Dieu Tien Bui, Paraskevas Tsangaratos, Viet-Tien Nguyen, Ngo Van Liem et Phan Trong Trinh. *Comparing the prediction performance of a Deep Learning Neural Network model with conventional machine learning models in landslide susceptibility assessment.* CATENA, vol. 188, page 104426, may 2020.

[Burton1998] A. Burton, T. J. Arkell et J. C. Bathurst. *Field variability of landslide model parameters.* Environmental Geology, vol. 35, no. 2-3, pages 100–114, aug 1998.

[Caine1980a] Nel Caine. *The Rainfall Intensity: Duration Control of Shallow Landslides and Debris Flows.* Geografiska Annaler. Series A, Physical Geography, vol. 62, no. 1/2, page 23, 1980.

[Caine1980b] Nel Caine. *The Rainfall Intensity: Duration Control of Shallow Landslides and Debris Flows.* Geografiska Annaler. Series A, Physical Geography, vol. 62, no. 1/2, pages 23–27, 1980.

[Canuti2007] Paolo Canuti, Nicola Casagli, Filippo Catani, Giacomo Falorni et Paolo Farina. *Integration of Remote Sensing Techniques in Different Stages of Landslide Response.* In Progress in Landslide Science, pages 251–260. Springer Berlin Heidelberg, 2007.

[Capparelli2010a] Giovanna Capparelli et Davide Tiranti. *Application of the MoniFLaIR early warning system for rainfall-induced landslides in Piedmont region (Italy).* Landslides, vol. 7, no. 4, pages 401–410, December 2010.

[Capparelli2010b] Giovanna Capparelli et Davide Tiranti. *Application of the MoniFLaIR early warning system for rainfall-induced landslides in Piedmont region (Italy).* Landslides, vol. 7, no. 4, pages 401–410, December 2010.

[Capparelli2011] Giovanna Capparelli et Pasquale Versace. *FLaIR and SUSHI: two mathematical models for early warning of landslides induced by rainfall.* Landslides, vol. 8, no. 1, pages 67–79, March 2011.

[Carrara2008] Alberto Carrara, Giovanni Crosta et Paolo Frattini. *Comparing models of debris-flow susceptibility in the alpine environment.* Geomorphology, vol. 94, no. 3-4, pages 353–378, feb 2008.

[Casagli2005] Nicola Casagli, Riccardo Fanti, Massimiliano Nocentini et Gaia Righini. *Assessing the Capabilities of VHR Satellite Data for Debris Flow Mapping in the Machu Picchu Area (C101-1).* In Landslides, pages 61–70. Springer-Verlag, 2005.

[Casu2006] F. Casu, M. Manzo et R. Lanari. *A quantitative assessment of the SBAS algorithm performance for surface deformation retrieval from DInSAR data.* Remote Sensing of Environment, vol. 102, no. 3-4, pages 195–210, jun 2006.

[Chae2011] Byung-Gon Chae et Man-Il Kim. *Suggestion of a method for landslide early warning using the change in the volumetric water content gradient due to rainfall infiltration.* Environmental Earth Sciences, vol. 66, no. 7, pages 1973–1986, oct 2011.

[Chae2017] Byung-Gon Chae, Hyuck-Jin Park, Filippo Catani, Alessandro Simoni et Matteo Berti. *Landslide prediction, monitoring and early warning: a concise review of state-of-the-art.* Geosciences Journal, vol. 21, no. 6, pages 1033–1070, dec 2017.

[Chandler1999] Jim Chandler. *Effective application of automated digital photogrammetry for geomorphological research.* Earth Surface Processes and Landforms, vol. 24, no. 1, pages 51–63, 1999.

[Chavent1975] G. Chavent, M. Dupuy et P. Lemmonier. *History Matching by Use of Optimal Theory.* Society of Petroleum Engineers Journal, vol. 15, no. 01, pages 74–86, 1975.

[Chelli2006] Alessandro Chelli, Giuseppe Mandrone et Giovanni Truffelli. *Field investigations and monitoring as tools for modelling the Rossena castle landslide (Northern Appennines, Italy).* Landslides, vol. 3, no. 3, pages 252–259, jun 2006.

[Chen1974] W. Chen, G. Gavalas, J. Seinfeld et M. Wasserman. *A New Algorithm for Automatic History Matching.* Society of Petroleum Engineers Journal, vol. 14, no. 06, pages 593–608, 1974.

[Chen1999] Mei-Ling Chen et D. Georges. *Nonlinear optimal control of an open-channel hydraulic system based on an infinite-dimensional model.* In Proceedings of the 38th IEEE Conference on Decision and Control, Phoenix, AZ, USA, volume 5, pages 4313–4318, 1999.

[Chini2011] M. Chini, F. R. Cinti et S. Stramondo. *Co-seismic surface effects from very high resolution panchromatic images: the case of the 2005 Kashmir (Pakistan) earthquake.* Natural Hazards and Earth System Sciences, vol. 11, no. 3, pages 931–943, mar 2011.

[Chleborad2003] Alan F. Chleborad. *Preliminary evaluation of a precipitation threshold for anticipating the occurrence of landslides in the Seattle, Washington, area*, 2003.

[Cho2002] Sung Eun Cho et Seung Rae Lee. *Evaluation of Surficial Stability for Homogeneous Slopes Considering Rainfall Characteristics.* Journal of Geotechnical and Geoenvironmental Engineering, vol. 128, no. 9, pages 756–763, sep 2002.

[Cho2010] Sung Eun Cho. *Probabilistic Assessment of Slope Stability That Considers the Spatial Variability of Soil Properties.* Journal of Geotechnical and Geoenvironmental Engineering, vol. 136, no. 7, pages 975–984, jul 2010.

[Chowdhury2010] R. Chowdhury, P. Flentje et G. Bhattacharya. *Geotechnical Slope Analysis.* CRC Press, 2010.

[Christen2010] Marc Christen, Perry Bartelt et Julia Kowalski. *Back calculation of the In den Arelen avalanche with RAMMS: Interpretation of model results.* Annals of Glaciology, vol. 51, pages 161–168, 05 2010.

[Christen2012] Marc Christen, Yves Bühler, Perry Bartelt, Remco Leine, James Glover, Adrian Schweizer, Christoph Graf, Brian McArdell, Werner Gerber, Yolanda Deubelbeiss, T. Feistl et Axel Volkwein. *Integral hazard management using a unified software environment: numerical simulation tool 'RAMMS' for gravitational natural hazards.* 01 2012.

[Christian1994] John T. Christian, Charles C. Ladd et Gregory B. Baecher. *Reliability Applied to Slope Stability Analysis.* Journal of Geotechnical Engineering, vol. 120, no. 12, pages 2180–2207, dec 1994.

[Chung2016] Ming-Chien Chung, Chih-Hao Tan et Chien-Hsin Chen. *Local rainfall thresholds for forecasting landslide occurrence: Taipingshan landslide triggered by Typhoon Saola.* Landslides, vol. 14, no. 1, pages 19–33, apr 2016.

[Ciampalini2012] Andrea Ciampalini, Francesca Garfagnoli, Benedetta Antonielli, Chiara Del Ventisette et Sandro Moretti. *Photolithological map of the southern flank of the Tindouf Basin (Western Sahara).* Journal of Maps, vol. 8, no. 4, pages 453–464, nov 2012.

[Ciampalini2014] Andrea Ciampalini, Federica Bardi, Silvia Bianchini, William Frodella, Chiara Del Ventisette, Sandro Moretti et Nicola Casagli. *Analysis of building deformation in landslide area using multisensor PSInSAR™ technique.* International Journal of Applied Earth Observation and Geoinformation, vol. 33, pages 166–180, dec 2014.

[Ciampalini2015] Andrea Ciampalini, Federico Raspini, William Frodella, Federica Bardi, Silvia Bianchini et Sandro Moretti. *The effectiveness of high-resolution LiDAR data combined with PSInSAR data in landslide study.* Landslides, vol. 13, no. 2, pages 399–410, dec 2015.

[Ciampalini2016] Andrea Ciampalini, Federico Raspini, Daniela Lagomarsino, Filippo Catani et Nicola Casagli. *Landslide susceptibility map refinement using PSInSAR data.* Remote Sensing of Environment, vol. 184, pages 302–315, oct 2016.

[Coduto2010] D.P. Coduto, M.R. Yeung et W.A. Kitch. Geotechnical Engineering: Principles and Practices. Pearson, New York, 2010.

[Colesanti2003] Carlo Colesanti, Alessandro Ferretti, Claudio Prati et Fabio Rocca. *Monitoring landslides and tectonic motions with the Permanent Scatterers Technique.* Engineering Geology, vol. 68, no. 1-2, pages 3–14, feb 2003.

[Collins2004] Brian D. Collins et Dobroslav Znidarcic. *Stability Analyses of Rainfall Induced Landslides.* Journal of Geotechnical and

Geoenvironmental Engineering, vol. 130, no. 4, pages 362–372, apr 2004.

[Colomina2014] I. Colomina et P. Molina. *Unmanned aerial systems for photogrammetry and remote sensing: A review.* ISPRS Journal of Photogrammetry and Remote Sensing, vol. 92, pages 79–97, jun 2014.

[Comegna2007] Luca Comegna, Luciano Picarelli et Gianfranco Urciuoli. *The mechanics of mudslides as a cyclic undrained–drained process.* Landslides, vol. 4, no. 3, pages 217–232, apr 2007.

[Corominas1996] Jordi Corominas. *The angle of reach as a mobility index for small and large landslides.* Canadian Geotechnical Journal, vol. 33, no. 2, pages 260–271, 1996.

[Corominas1999] Jordi Corominas et José Moya. *Reconstructing recent landslide activity in relation to rainfall in the Llobregat River basin, Eastern Pyrenees, Spain.* Geomorphology, vol. 30, no. 1-2, pages 79–93, oct 1999.

[Corominas2000] J Corominas. *Landslides and climate.* In Proceedings of the 8th International Symposium on Landslides, volume 4, pages 1–33. AA Balkema Cardiff, Wales, 2000.

[Corominas2005a] J. Corominas, J. Moya, A. Ledesma, A. Lloret et J. Gili. *Prediction of ground displacements and velocities from groundwater level changes at the Vallcebre landslide (Eastern Pyrenees, Spain).* Landslides, vol. 2, pages 83–96, 07 2005.

[Corominas2005b] Jordi Corominas, José Moya, Alberto Ledesma, Antonio Lloret et Josep Gili. *Prediction of ground displacements and velocities from groundwater level changes at the Vallcebre landslide (Eastern Pyrenees, Spain).* Landslides, vol. 2, pages 83–96, 07 2005.

[Corominas2013] J. Corominas, C. van Westen, P. Frattini, L. Cascini, J.-P. Malet, S. Fotopoulou, F. Catani, M. Van Den Eeckhaut, O. Mavrouli, F. Agliardi, K. Pitilakis, M. G. Winter, M. Pastor, S. Ferlisi, V. Tofani, J. Hervás et J. T. Smith. *Recommendations for the quantitative analysis of landslide risk.* Bulletin of Engineering Geology and the Environment, nov 2013.

[Corominas2014] Jordi Corominas, C.J. Westen, P. Frattini, Leonardo Cascini, Jean-Philippe, Stavroula Fotopoulou, Filippo Catani, Miet Eeckhaut, Olga Mavrouli, Federico Agliardi, Kyriazis Pitilakis, Mike Winter, Manuel Pastor, Settimio Ferlisi, Veronica Tofani, Javier Hervàs et J.T. Smith. *Recommendations for the quantitative analysis of landslide risk.* Bulletin of Engineering Geology and the Environment, vol. 73, pages 209–263, 05 2014.

[Corsini2005] Alessandro Corsini, A. Pasuto, M. Soldati et A. Zannoni. *Field monitoring of the Corvara landslide (Dolomites, Italy) and its relevance for hazard assessment.* Geomorphology, vol. 66, no. 1-4, pages 149–165, mar 2005.

[Costantini2008] Mario Costantini, Salvatore Falco, Fabio Malvarosa et Federico Minati. *A New Method for Identification and Analysis of Persistent Scatterers in Series of SAR Images.* In IGARSS 2008 - 2008 IEEE International Geoscience and Remote Sensing Symposium. IEEE, jul 2008.

[Crank1947] J. Crank et P. Nicolson. *A practical method for numerical evaluation of solutions of partial differential equations of the heat-conduction type.* Mathematical Proceedings of the Cambridge Philosophical Society, vol. 43, no. 1, page 50–67, 1947.

[Crosetto2008] Michele Crosetto, Erlinda Biescas, Javier Duro, Josep Closa et Alain Arnaud. *Generation of Advanced ERS and Envisat Interferometric SAR Products Using the Stable Point Network Technique.* Photogrammetric Engineering & Remote Sensing, vol. 74, no. 4, pages 443–450, apr 2008.

[Crosetto2016] Michele Crosetto, Oriol Monserrat, María Cuevas-González, Núria Devanthéry et Bruno Crippa. *Persistent Scatterer Interferometry: A review.* ISPRS Journal of Photogrammetry and Remote Sensing, vol. 115, pages 78–89, may 2016.

[Crosta2003] G. B. Crosta et P. Frattini. *Distributed modelling of shallow landslides triggered by intense rainfall.* Natural Hazards and Earth System Sciences, vol. 3, no. 1/2, pages 81–93, apr 2003.

[Crozier1999] Michael J. Crozier. *Prediction of rainfall-triggered landslides: a test of the Antecedent Water Status Model.* Earth Surface Processes and Landforms, vol. 24, no. 9, pages 825–833, 1999.

[Cruden1996a] D. M. Cruden et D. J. Varnes. *Landslides Types and Processes. In: Turner, A.K., Schuster, R.L. (Eds.), Landslides: Investigation and Mitigation.* Transportation Research Board Special Report 247. National Academy Press, WA, pages 36–75, 1996.

[Cruden1996b] D. M. Cruden et D. J. Varnes. *Landslides Types and Processes. In: Turner, A.K., Schuster, R.L. (Eds.), Landslides: Investigation and Mitigation.* Transportation Research Board Special Report 247. National Academy Press, WA, pages 36–75, 1996.

[Dai2002] F.C Dai, C.F Lee et Y.Y Ngai. *Landslide risk assessment and management: An overview.* Engineering Geology, vol. 64, pages 65–87, 04 2002.

[Damiano2012] E. Damiano, L. Olivares et L. Picarelli. *Steep-slope monitoring in unsaturated pyroclastic soils.* Engineering Geology, vol. 137-138, pages 1–12, jun 2012.

[Das1991] S. K. Das et R. W. Lardner. *On the estimation of parameters of hydraulic models by assimilation of periodic tidal data.* Journal of Geophysical Research: Oceans, vol. 96, no. C8, pages 15187–15196, 1991.

[de Luiz Rosito Listo2012] Fabrizio de Luiz Rosito Listo et Bianca Carvalho Vieira. *Mapping of risk and susceptibility of shallow-landslide in the city of*

São Paulo, Brazil. Geomorphology, vol. 169-170, pages 30–44, oct 2012.

[Deline2010] Philip Deline, Massimo Broccolato, Jeannette Noetzli, Ludovic Ravanel et Andrea Tamburini. *The December 2008 Crammont Rock Avalanche, Mont Blanc Massif Area, Italy.* Natural hazards and earth system sciences, vol. 12, page 10388, 04 2010.

[Di Meglio2013] F. Di Meglio, M. Krstic et R. Vazquez. *A backstepping boundary observer for a class of linear first-order hyperbolic systems.* In 2013 European Control Conference (ECC), pages 1597–1602, July 2013.

[Di Meglio2014] F. Di Meglio, Delphine Bresch-Pietri et Ulf Jakob F. Aarsnes. *An adaptive observer for hyperbolic systems with application to UnderBalanced Drilling.* IFAC Proceedings Volumes, vol. 47, no. 3, pages 11391–11397, 2014. 19th IFAC World Congress.

[Dietrich2001] William E. Dietrich, Dino Bellugi et Raphael Real de Asua. *Validation of the Shallow Landslide Model, SHALSTAB, for forest management.* In Water Science and Application, pages 195–227. American Geophysical Union, 2001.

[Dikshit2019] Abhirup Dikshit, Neelima Satyam et Biswajeet Pradhan. *Estimation of Rainfall-Induced Landslides Using the TRIGRS Model.* Earth Systems and Environment, vol. 3, no. 3, pages 575–584, oct 2019.

[Ding2005] Yan Ding et Sam S. Y. Wang. *Identification of Manning's roughness coefficients in channel network using adjoint analysis.* International Journal of Computational Fluid Dynamics, vol. 19, no. 1, pages 3–13, 2005.

[Eisenbeiss2011] Henri Eisenbeiss et Martin Sauerbier. *Investigation of uav systems and flight modes for photogrammetric applications.* The Photogrammetric Record, vol. 26, no. 136, pages 400–421, dec 2011.

[El-Ramly2002] H El-Ramly, N R Morgenstern et D M Cruden. *Probabilistic slope stability analysis for practice.* Canadian Geotechnical Journal, vol. 39, no. 3, pages 665–683, jun 2002.

[Eyers1998] Richard Eyers, John McM. Moore, Javier Hervás et J. G. Liu. *Integrated use of Landsat TM and SPOT panchromatic imagery for landslide mapping: case histories from southeast Spain.* Geological Society, London, Engineering Geology Special Publications, vol. 15, no. 1, pages 133–140, 1998.

[Fannin2001] R.J. Fannin et M.P. Wise. *An empirical-statistical model for debris flow travel distance.* Canadian Geotechnical Journal, vol. 38, pages 982–994, 10 2001.

[Ferguson2004] J. Ferguson. *A brief survey of the history of the calculus of variations and its applications.* In arXiv:math/0402357; 2004, 2004.

[Fernandes2004] Nelson F. Fernandes, Renato F. Guimarães, Roberto A.T. Gomes, Bianca C. Vieira, David R. Montgomery et Harvey Greenberg. *Topographic controls of landslides in Rio de Janeiro: field evidence and modeling.* CATENA, vol. 55, no. 2, pages 163–181, jan 2004.

[Ferrero2008] A. M. Ferrero, G. Forlani, R. Roncella et H. I. Voyat. *Advanced Geostructural Survey Methods Applied to Rock Mass Characterization.* Rock Mechanics and Rock Engineering, vol. 42, no. 4, pages 631–665, jun 2008.

[Ferretti2001] A. Ferretti, C. Prati et F. Rocca. *Permanent scatterers in SAR interferometry.* IEEE Transactions on Geoscience and Remote Sensing, vol. 39, no. 1, pages 8–20, 2001.

[Ferretti2011] Alessandro Ferretti, Alfio Fumagalli, Fabrizio Novali, Claudio Prati, Fabio Rocca et Alessio Rucci. *A New Algorithm for Processing Interferometric Data-Stacks: SqueeSAR.* IEEE Transactions on Geoscience and Remote Sensing, vol. 49, no. 9, pages 3460–3470, sep 2011.

[Fiorucci2011] F. Fiorucci, M. Cardinali, R. Carlà, M. Rossi, A.C. Mondini, L. Santurri, F. Ardizzone et F. Guzzetti. *Seasonal landslide mapping and estimation of landslide mobilization rates using aerial and satellite images.* Geomorphology, vol. 129, no. 1-2, pages 59–70, jun 2011.

[Franceschi2009] Marco Franceschi, Giordano Teza, Nereo Preto, Arianna Pesci, Antonio Galgaro et Stefano Girardi. *Discrimination between marls and limestones using intensity data from terrestrial laser scanner.* ISPRS Journal of Photogrammetry and Remote Sensing, vol. 64, no. 6, pages 522–528, nov 2009.

[Frank2015] Florian Frank, Brian McArdell, Christian Huggel et Andreas Vieli. *The importance of entrainment and bulking on debris flow runout modeling: Examples from the Swiss Alps.* Natural Hazards and Earth System Sciences, vol. 15, pages 2569–2583, 11 2015.

[Franks1999] C. A. M. Franks. *Characteristics of some rainfall-induced landslides on natural slopes, Lantau Island, Hong Kong.* Quarterly Journal of Engineering Geology and Hydrogeology, vol. 32, no. 3, pages 247–259, aug 1999.

[Frattini2004] Paolo Frattini, Giovanni B. Crosta, Nicoletta Fusi et Paolo Dal Negro. *Shallow landslides in pyroclastic soils: a distributed modelling approach for hazard assessment.* Engineering Geology, vol. 73, no. 3-4, pages 277–295, jun 2004.

[Fredlund1996] D G Fredlund, Anqing Xing, M D Fredlund et S L Barbour. *The relationship of the unsaturated soil shear strength to the soil-water characteristic curve.* Canadian Geotechnical Journal, vol. 33, no. 3, pages 440–448, 1996.

[Fredlund2011] Delwyn Fredlund, Daichao Sheng et Jidong Zhao. *Estimation of soil suction from the soil-water characteristic curve.* Canadian Geotechnical Journal, vol. 48, pages 186–198, 02 2011.

[Frodella2015] William Frodella, Francesco Fidolini, Stefano Morelli et Veronica Pazzi. *Application of Infrared Thermography for landslide mapping: the Rotolon DSGDS case study.* Rendiconti online della Società Geologica Italiana, vol. 35, pages 144–147, apr 2015.

[Frodella2016] William Frodella, Andrea Ciampalini, Giovanni Gigli, Luca Lombardi, Federico Raspini, Massimiliano Nocentini, Cosimo Scardigli et Nicola Casagli. *Synergic use of satellite and ground based remote sensing methods for monitoring the San Leo rock cliff (Northern Italy).* Geomorphology, vol. 264, pages 80–94, jul 2016.

[Frodella2017] William Frodella, Giovanni Gigli, Stefano Morelli, Luca Lombardi et Nicola Casagli. *Landslide Mapping and Characterization through Infrared Thermography (IRT): Suggestions for a Methodological Approach from Some Case Studies.* Remote Sensing, vol. 9, no. 12, page 1281, dec 2017.

[Froude2018] M. Froude et D. Petley. *Global fatal landslide occurrence from 2004 to 2016.* Natural Hazards and Earth System Sciences, vol. 18, pages 2161–2181, 2018.

[Fruneau1996] B. Fruneau, J. Achache et C. Delacourt. *Observation and modelling of the Saint-Étienne-de-Tinée landslide using SAR interferometry.* Tectonophysics, vol. 265, no. 3-4, pages 181–190, nov 1996.

[García2010] A. García, A. Hördt et M. Fabian. *Landslide monitoring with high resolution tilt measurements at the Dollendorfer Hardt landslide, Germany.* Geomorphology, vol. 120, no. 1-2, pages 16–25, aug 2010.

[Gariano2016] Stefano Luigi Gariano et Fausto Guzzetti. *Landslides in a changing climate.* Earth-Science Reviews, vol. 162, pages 227–252, 2016.

[Ghiglia1994] Dennis C. Ghiglia et Louis A. Romero. *Robust two-dimensional weighted and unweighted phase unwrapping that uses fast transforms and iterative methods.* Journal of the Optical Society of America A, vol. 11, no. 1, page 107, jan 1994.

[Gigli2009] G. Gigli, F. Mugnai, L. Leoni et N. Casagli. *Analysis of deformations in historic urban areas using terrestrial laser scanning.* Natural Hazards and Earth System Sciences, vol. 9, no. 6, pages 1759–1761, nov 2009.

[Gigli2011] Giovanni Gigli et Nicola Casagli. *Semi-automatic extraction of rock mass structural data from high resolution LIDAR point clouds.* International Journal of Rock Mechanics and Mining Sciences, vol. 48, no. 2, pages 187–198, feb 2011.

[Gigli2012a] G. Gigli, W. Frodella, F. Mugnai, D. Tapete, F. Cigna, R. Fanti, E. Intrieri et L. Lombardi. *Instability mechanisms affecting cultural heritage sites in the Maltese Archipelago.* Natural Hazards and Earth System Sciences, vol. 12, no. 6, pages 1883–1903, jun 2012.

[Gigli2012b] Giovanni Gigli, Stefano Morelli, Simone Fornera et Nicola Casagli. *Terrestrial laser scanner and geomechanical surveys for the rapid evaluation of rock fall susceptibility scenarios.* Landslides, vol. 11, no. 1, pages 1–14, dec 2012.

[Gili2000] Josep A. Gili, Jordi Corominas et Joan Rius. *Using Global Positioning System techniques in landslide monitoring.* Engineering Geology, vol. 55, no. 3, pages 167–192, 2000.

[Gnanadesikan1972] R. Gnanadesikan et J. R. Kettenring. *Robust Estimates, Residuals, and Outlier Detection with Multiresponse Data.* Biometrics, vol. 28, no. 1, pages 81–124, 1972.

[Godt2008] J.W. Godt, R.L. Baum, W.Z. Savage, D. Salciarini, W.H. Schulz et E.L. Harp. *Transient deterministic shallow landslide modeling: Requirements for susceptibility and hazard assessments in a GIS framework.* Engineering Geology, vol. 102, no. 3-4, pages 214–226, dec 2008.

[Godt2009] Jonathan W. Godt, Rex L. Baum et Ning Lu. *Landsliding in partially saturated materials.* Geophysical Research Letters, vol. 36, no. 2, pages n/a–n/a, jan 2009.

[Gokceoglu2000] C. Gokceoglu, H. Sonmez et M. Ercanoglu. *Discontinuity controlled probabilistic slope failure risk maps of the Altindag (settlement) region in Turkey.* Engineering Geology, vol. 55, no. 4, pages 277–296, mar 2000.

[Gopi2007] S. Gopi. Advanced surveying: total station, GIS and Remote Sensing. Pearson Education India, 2007.

[Gorsevski2006] Pece V. Gorsevski, Paul E. Gessler, Jan Boll, William J. Elliot et Randy B. Foltz. *Spatially and temporally distributed modeling of landslide susceptibility.* Geomorphology, vol. 80, no. 3-4, pages 178–198, oct 2006.

[Graichen2008] Knut Graichen et Nicolas Petit. *A continuation approach to state and adjoint calculation in optimal control applied to the reentry problem.* IFAC Proceedings Volumes, vol. 41, no. 2, pages 14307–14312, 2008. 17th IFAC World Congress.

[Griffiths2011] D.V. Griffiths, Jinsong Huang et Gordon A. Fenton. *Probabilistic infinite slope analysis.* Computers and Geotechnics, vol. 38, no. 4, pages 577–584, jun 2011.

[Griswold2008] J.P. Griswold et R.M. Iverson. *Mobility statistics and automated hazard mapping for debris flows and rock avalanches.* USGS Scientific Investigations Report, 01 2008.

[Guimarães2003] Renato Fontes Guimarães, David R. Montgomery, Harvey M. Greenberg, Nelson Ferreira Fernandes, Roberto Arnaldo Trancoso Gomes et Osmar Abı

lio de Carvalho. *Parameterization of soil properties for a model of topographic controls on shallow landsliding: application to Rio de Janeiro.* Engineering Geology, vol. 69, no. 1-2, pages 99–108, apr 2003.

[Guzzetti2000] Fausto Guzzetti. *Landslide Fatalities and the Evaluation of Landslide Risk in Italy.* Engineering Geology, vol. 58, pages 89–107, 11 2000.

[Guzzetti2007] F. Guzzetti, S. Peruccacci, M. Rossi et C. P. Stark. *Rainfall thresholds for the initiation of landslides in central and southern Europe.* Meteorology and Atmospheric Physics, vol. 98, no. 3-4, pages 239–267, jun 2007.

[Guzzetti2008a] Fausto Guzzetti, Silvia Peruccacci, Mauro Rossi et Colin P. Stark. *The rainfall intensity-duration control of shallow landslides and debris flows: an update.* Landslides, vol. 5, no. 1, pages 3–17, dec 2008.

[Guzzetti2008b] Fausto Guzzetti, Silvia Peruccacci, Mauro Rossi et Colin P. Stark. *The rainfall intensity-duration control of shallow landslides and debris flows: an update.* Landslides, vol. 5, no. 1, pages 3–17, February 2008.

[Guzzetti2012] Fausto Guzzetti, Alessandro Cesare Mondini, Mauro Cardinali, Federica Fiorucci, Michele Santangelo et Kang-Tsung Chang. *Landslide inventory maps: New tools for an old problem.* Earth-Science Reviews, vol. 112, no. 1-2, pages 42–66, apr 2012.

[Harr1987] M. E. Harr. Reliability-based design in civil engineering. McGraw-Hill, New York, 1987.

[Hasan2016] Agus Hasan, Ole Morten Aamo et Miroslav Krstic. *Boundary observer design for hyperbolic PDE-ODE cascade systems.* Automatica, vol. 68, pages 75–86, 2016.

[Herrera2010] Gerardo Herrera, Davide Notti, Juan Carlos García-Davalillo, Oscar Mora, Geraint Cooksley, Mónica Sánchez, Alain Arnaud et Michele Crosetto. *Analysis with C- and X-band satellite SAR data of the Portalet landslide area.* Landslides, vol. 8, no. 2, pages 195–206, sep 2010.

[Herrera2013a] G. Herrera, J. A. Fernandez-Merodo, J. Mulas, M. Pastor, G. Luzi et O. Monserrat. *A landslide forecasting model using ground based* SAR *data: The Portalet case study.* Engineering Geology, vol. 105, pages 220–230, 02 2013.

[Herrera2013b] G. Herrera, Jose Antonio Fernandez-Merodo, J. Mulas, Manuel Pastor, Guido Luzi et O. Monserrat. *A landslide forecasting model using ground based* SAR *data: The Portalet case study.* Engineering Geology, vol. 105, pages 220–230, 02 2013.

[Ho2012] Jui-Yi Ho, Kwan Tun Lee, Tung-Chiung Chang, Zhao-Yin Wang et Yu-Hsun Liao. *Influences of spatial distribution of soil thickness on shallow landslide prediction.* Engineering Geology, vol. 124, pages 38–46, jan 2012.

[Hooper2004] Andrew Hooper, Howard Zebker, Paul Segall et Bert Kampes. *A new method for measuring deformation on volcanoes and other natural terrains using InSAR persistent scatterers.* Geophysical Research Letters, vol. 31, no. 23, dec 2004.

[Hooper2007] A. Hooper, P. Segall et H. Zebker. *Persistent scatterer interferometric synthetic aperture radar for crustal deformation analysis, with application to Volcán Alcedo, Galápagos.* Journal of Geophysical Research, vol. 112, no. B7, jul 2007.

[Huang2006] J.C. Huang, S.J. Kao, M.L. Hsu et J.C. Lin. *Stochastic procedure to extract and to integrate landslide susceptibility maps: an example of mountainous watershed in Taiwan.* Natural Hazards and Earth System Sciences, vol. 6, no. 5, pages 803–815, sep 2006.

[Huggel2009] Christian Huggel, Nikolay Khabarov, Michael Obersteiner et Juan Manuel Ramírez. *Implementation and integrated numerical modeling of a landslide early warning system: a pilot study in Colombia.* Natural Hazards, vol. 52, no. 2, pages 501–518, apr 2009.

[Hungr1995] Oldrich Hungr. *A model for the runout analysis of rapid flow slides, debris flows, and avalanches.* Canadian Geotechnical Journal, vol. 32, pages 610–623, 08 1995.

[Hungr2001] Oldrich Hungr, S. G. Evans, M. J. Bovis et J. N. Hutchinson. *A review of the classification of landslides of the flow type.* Environmental and Engineering Geoscience, vol. 7, no. 3, pages 221–238, 08 2001.

[Hungr2005] Oldrich Hungr, Jordi Corominas et Erik Eberhardt. *Estimating landslide motion mechanisms, travel distance and velocity.* Landslide Risk Management, Taylor and Francis, pages 99–128, 01 2005.

[Hungr2014] O. Hungr, S. Leroueil et L. Picarelli. *The Varnes classification of landslide types, an update.* Landslides, vol. 11, 2014.

[Hussin2012] Haydar Hussin, B. Quan Luna, C.J. Westen, Marc Christen, J.-P Malet et Th.W.J. Asch. *Parameterization of a numerical 2-D debris flow model with entrainment: A case study of the Faucon catchment, Southern French Alps.* Natural Hazards and Earth System Science, vol. 12, pages 3075–3090, 10 2012.

[Hutchinson1986] J. N. Hutchinson. *A sliding-consolidation model for flow slides.* Canadian Geotechnical Journal, vol. 23, no. 2, pages 115–126, 1986.

[Hürlimann2008] Marcel Hürlimann, Dieter Rickenmann, Vicente Medina et Allen Bateman. *Evaluation of approaches to calculate debris-flow parameters for hazard assessment.* Engineering Geology, vol. 102, pages 152–163, 12 2008.

[Intrieri2012] Emanuele Intrieri, Giovanni Gigli, Francesco Mugnai, Riccardo Fanti et Nicola Casagli. *Design and implementation of a landslide early warning system.* Engineering Geology, vol. 147-148, pages 124–136, oct 2012.

[Iverson1998] Richard Iverson, Steve Schilling et James Vallance. *Objective delineation of lahar-inundation hazard zones.* Bulletin of the Geological Society of America, vol. 110, pages 972–984, 08 1998.

[Iverson2000] Richard M. Iverson. *Landslide triggering by rain infiltration.* Water Resources Research, vol. 36, no. 7, pages 1897–1910, jul 2000.

[Iverson2001] Richard Iverson et Roger Denlinger. *Flow of variably fluidized granular masses across three-dimensional terrain I. Coulomb mixture theory.* Journal of Geophysical Research, vol. 106, 01 2001.

[Iverson2005a] R. Iverson. *Regulation of landslide motion by dilatancy and pore pressure feedback.* J. Geophys. Res, vol. 110, 06 2005.

[Iverson2005b] Richard Iverson. *Regulation of landslide motion by dilatancy and pore pressure feedback.* J. Geophys. Res, vol. 110, 06 2005.

[Iverson2016] Richard Iverson et David George. *Modelling landslide liquefaction, mobility bifurcation and the dynamics of the 2014 Oso disaster.* Geotechnique, vol. 66, no. 3, pages 175–187, 2016.

[Jaboyedoff2007] M Jaboyedoff, R Metzger, T Oppikofer, R Couture, M Derron, J Locat et D Turmel. *New insight techniques to analyze rock-slope relief using DEM and 3D-imaging cloud points.* In Rock Mechanics: Meeting Society's Challenges and Demands, pages 61–68. Taylor &amp Francis, may 2007.

[Jaboyedoff2010] Michel Jaboyedoff, Thierry Oppikofer, Antonio Abellán, Marc-Henri Derron, Alex Loye, Richard Metzger et Andrea Pedrazzini. *Use of LIDAR in landslide investigations: a review.* Natural Hazards, vol. 61, no. 1, pages 5–28, oct 2010.

[Jakob2003] Matthias Jakob et Hamish Weatherly. *A hydroclimatic threshold for landslide initiation on the North Shore Mountains of Vancouver, British Columbia.* Geomorphology, vol. 54, no. 3-4, pages 137–156, sep 2003.

[Jakob2007] Matthias Jakob et Oldrich Hungr. Debris-flow hazard analysis, pages 411–443. 12 2007.

[Jakob2012] Matthias Jakob, Scott McDougall, Hamish Weatherly et Neil Ripley. *Debris-flow simulations on Cheekye River, British Columbia.* Landslides, vol. 10, 12 2012.

[James2012] M. R. James et S. Robson. *Straightforward reconstruction of 3D surfaces and topography with a camera: Accuracy and geoscience application.* Journal of Geophysical Research: Earth Surface, vol. 117, no. F3, pages n/a–n/a, aug 2012.

[Jansen2011] J.D. Jansen. *Adjoint-based optimization of multi-phase flow through porous media – A review.* Computers & Fluids, vol. 46, no. 1, pages 40–51, 2011. 10th ICFD Conference Series on Numerical Methods for Fluid Dynamics (ICFD 2010).

[J.E.2005] Cannon S.H.and Gartner J.E. *Wildfire-related debris flow from a hazards perspective.* Debris-flow Hazards and Related Phenomena. Springer Praxis Books. Springer, Berlin, Heidelberg, vol. 98, pages 239–267, 12 2005.

[Jiao2005] Jiu J. Jiao, Xu-Sheng Wang et Subhas Nandy. *Confined groundwater zone and slope instability in weathered igneous rocks in Hong Kong.* Engineering Geology, vol. 80, no. 1-2, pages 71–92, aug 2005.

[Jiao2006] Jiu J. Jiao, Guoping Ding et Chi-Man Leung. *Confined groundwater near the rockhead in igneous rocks in the Mid-Levels area, Hong Kong, China.* Engineering Geology, vol. 84, no. 3-4, pages 207–219, may 2006.

[Johnson2016] Brandon C. Johnson, Charles S. Campbell et H. Jay Melosh. *The reduction of friction in long runout landslides as an emergent phenomenon.* Journal of Geophysical Research: Earth Surface, vol. 121, no. 5, pages 881–889, may 2016.

[Kalman1960] Rudolph Emil Kalman. *A New Approach to Linear Filtering and Prediction Problems.* Transactions of the ASME–Journal of Basic Engineering, vol. 82, no. Series D, pages 35–45, 1960.

[Kean2013] Jason Kean, Scott Mccoy, Gregory Tucker, Dennis Staley et Jeffrey Coe. *Runoff-generated debris flows: Observations and modeling of surge initiation, magnitude, and frequency.* Journal of Geophysical Research, vol. 118, 12 2013.

[Keqiang2009] He Keqiang, Wang Shangqing, Du Wen et Wang Sijing. *Dynamic features and effects of rainfall on landslides in the Three Gorges Reservoir region, China: using the Xintan landslide and the large Huangya landslide as the examples.* Environmental Earth Sciences, vol. 59, no. 6, pages 1267–1274, mar 2009.

[Kim2016] Minseok Kim, Yuichi Onda, Taro Uchida et Jin Kwan Kim. *Effects of soil depth and subsurface flow along the subsurface topography on shallow landslide predictions at the site of a small granitic hillslope.* Geomorphology, vol. 271, 07 2016.

[Kitsos2021] Constantinos Kitsos, Gildas Besancon et Christophe Prieur. *High-gain observer design for some semilinear reaction-diffusion systems: a transformation-based approach.* IEEE Control Systems Letters, vol. 5, no. 2, pages 629–634, April 2021.

[Kitsos2022] Constantinos Kitsos, Gildas Besancon et Christophe Prieur. *High-Gain Observer Design for a Class of Quasi-linear Integro-Differential Hyperbolic Systems - Application to an Epidemic Model.* IEEE Transactions on Automatic Control, vol. 67, no. 1, pages 292 – 303, January 2022.

[Konak2004] G. Konak, A. H. Onur, D. Karakus, H. Köse, Y. Koca et H. Yenice. *Slope stability analysis and slide monitoring by inclinometer readings: Part 2.* Mining Technology, vol. 113, no. 3, pages 171–180, sep 2004.

[Krøgli2018] I. K. Krøgli, G. Devoli, H. Colleuille, S. Boje, M. Sund et I. K. Engen. *The Norwegian forecasting and warning service for rainfall- and snowmelt-induced landslides.* Nat. Hazards Earth Syst. Sci., vol. 18, no. 5, pages 1427–1450, 2018.

[Krstic2008] Miroslav Krstic et Andrey Smyshlyaev. Boundary Control of PDEs: A Course on Backstepping Designs. Society for Industrial and Applied Mathematics, USA, 2008.

[Kurtz2014] Camille Kurtz, André Stumpf, Jean-Philippe Malet, Pierre Gançarski, Anne Puissant et Nicolas Passat. *Hierarchical extraction of landslides from multiresolution remotely sensed optical images.* ISPRS Journal of Photogrammetry and Remote Sensing, vol. 87, pages 122–136, jan 2014.

[Lamri2016] Takfarinas Lamri, Safouane Djemaï, Mohamed Hamoudi, Basem Zoheir, Abderrahmane Bendaoud, Khadidja Ouzegane et Massinissa Amara. *Satellite imagery and airborne geophysics for geologic mapping of the Edembo area, Eastern Hoggar (Algerian Sahara).* Journal of African Earth Sciences, vol. 115, pages 143–158, mar 2016.

[Lanari2004] R. Lanari, O. Mora, M. Manunta, J.J. Mallorqui, P. Berardino et E. Sansosti. *A small-baseline approach for investigating deformations on full-resolution differential SAR interferograms.* IEEE Transactions on Geoscience and Remote Sensing, vol. 42, no. 7, pages 1377–1386, jul 2004.

[Lane2000] S. N. Lane, T. D. James et M. D. Crowell. *Application of Digital Photogrammetry to Complex Topography for Geomorphological Research.* The Photogrammetric Record, vol. 16, no. 95, pages 793–821, apr 2000.

[Larose2015] Eric Larose, Simon Carrière, Christophe Voisin, Pierre Bottelin, Laurent Baillet, Philippe Guéguen, Fabian Walter, Denis Jongmans, Bertrand Guillier, Stéphane Garambois, Florent Gimbert et Chris Massey. *Environmental seismology: What can we learn on earth surface processes with ambient noise?* Journal of Applied Geophysics, vol. 116, pages 62–74, may 2015.

[Larsen1993] Matthew C. Larsen et Andrew Simon. *A Rainfall Intensity-Duration Threshold for Landslides in a Humid-Tropical Envi-*

ronment, Puerto Rico. Geografiska Annaler. Series A, Physical Geography, vol. 75, no. 1/2, pages 13–23, 1993.

[Lee2015] Jung Hyun Lee et Hyuck Jin Park. *Assessment of shallow landslide susceptibility using the transient infiltration flow model and GIS-based probabilistic approach.* Landslides, vol. 13, no. 5, pages 885–903, oct 2015.

[Lepore2013] C. Lepore, E. Arnone, L. V. Noto, G. Sivandran et R. L. Bras. *Physically based modeling of rainfall-triggered landslides: a case study in the Luquillo forest, Puerto Rico.* Hydrology and Earth System Sciences, vol. 17, no. 9, pages 3371–3387, sep 2013.

[Leung2012] Anthony Kwan Leung et Charles Wang Wai Ng. *Seasonal movement and groundwater flow mechanism in an unsaturated saprolitic hillslope.* Landslides, vol. 10, no. 4, pages 455–467, jun 2012.

[Li2013] Wei Chao Li, Lee Min Lee, Hong Cai, Hong Jie Li, F.C. Dai et Ming Long Wang. *Combined roles of saturated permeability and rainfall characteristics on surficial failure of homogeneous soil slope.* Engineering Geology, vol. 153, pages 105–113, feb 2013.

[Li2014] Dian-Qing Li, Xiao-Hui Qi, Kok-Kwang Phoon, Li-Min Zhang et Chuang-Bing Zhou. *Effect of spatially variable shear strength parameters with linearly increasing mean trend on reliability of infinite slopes.* Structural Safety, vol. 49, pages 45–55, jul 2014.

[Li2015] Wei Chao Li, F. C. Dai, Ying Qi Wei, Ming Long Wang, Hong Min et Lee Min Lee. *Implication of subsurface flow on rainfall-induced landslide: a case study.* Landslides, vol. 13, no. 5, pages 1109–1123, aug 2015.

[Liao2010] Zonghu Liao, Yang Hong, Dalia Kirschbaum, Robert F. Adler, Jonathan J. Gourley et Rick Wooten. *Evaluation of TRIGRS (transient rainfall infiltration and grid-based regional slope-stability analysis)'s predictive skill for hurricane-triggered landslides: a case study in Macon County, North Carolina.* Natural Hazards, vol. 58, no. 1, pages 325–339, dec 2010.

[Likos2014] William J. Likos, Ning Lu et Jonathan W. Godt. *Hysteresis and Uncertainty in Soil Water-Retention Curve Parameters.* Journal of Geotechnical and Geoenvironmental Engineering, vol. 140, no. 4, page 04013050, 2014.

[Lin2004] Chao-Yuan Lin, Huang-Mu Lo, Wen-Chieh Chou et Wen-Tzu Lin. *Vegetation recovery assessment at the Jou-Jou Mountain landslide area caused by the 921 Earthquake in Central Taiwan.* Ecological Modelling, vol. 176, no. 1-2, pages 75–81, aug 2004.

[Liu2016] Wen-Cheng Liu et Wei-Che Huang. *CLOSE RANGE DIGITAL PHOTOGRAMMETRY APPLIED TO TOPOGRAPHY*

AND LANDSLIDE MEASUREMENTS. ISPRS - International Archives of the Photogrammetry, Remote Sensing and Spatial Information Sciences, vol. XLI-B5, pages 875–880, jun 2016.

[Lombardi2016] Luca Lombardi, Massimiliano Nocentini, William Frodella, Teresa Nolesini, Federica Bardi, Emanuele Intrieri, Tommaso Carlà, Lorenzo Solari, Giulia Dotta, Federica Ferrigno et Nicola Casagli. *The Calatabiano landslide (Southern Italy): preliminary GB-InSAR monitoring data and remote 3D mapping*. Landslides, vol. 14, no. 2, pages 685–696, nov 2016.

[Lu2003] P. Lu et M. S. Rosenbaum. *Artificial Neural Networks and Grey Systems for the Prediction of Slope Stability*. Natural Hazards, vol. 30, no. 3, pages 383–398, nov 2003.

[Lu2006] Ning Lu et William J. Likos. *Suction Stress Characteristic Curve for Unsaturated Soil*. Journal of Geotechnical and Geoenvironmental Engineering, vol. 132, no. 2, pages 131–142, feb 2006.

[Lu2008] Ning Lu et Jonathan Godt. *Infinite slope stability under steady unsaturated seepage conditions*. Water Resources Research, vol. 44, no. 11, nov 2008.

[Lu2011] Ping Lu, Nicola Casagli, Filippo Catani et Veronica Tofani. *Persistent Scatterers Interferometry Hotspot and Cluster Analysis (PSI-HCA) for detection of extremely slow-moving landslides*. International Journal of Remote Sensing, vol. 33, no. 2, pages 466–489, nov 2011.

[Lu2013] Ning Lu et Jonathan Godt. *Failure surface based stability analysis*. In Hillslope Hydrology and Stability, pages 313–363. Cambridge University Press, 2013.

[Luo2008] Xianqi Luo, Fawu Wang, Zhenhua Zhang et Ailan Che. *Establishing a monitoring network for an impoundment-induced landslide in Three Gorges Reservoir Area, China*. Landslides, vol. 6, no. 1, pages 27–37, sep 2008.

[Luzi2004] G. Luzi, M. Pieraccini, D. Mecatti, L. Noferini, G. Guidi, F. Moia et C. Atzeni. *Ground-based radar interferometry for landslides monitoring: atmospheric and instrumental decorrelation sources on experimental data*. IEEE Transactions on Geoscience and Remote Sensing, vol. 42, no. 11, pages 2454–2466, nov 2004.

[Ma2016] Hai-Rong Ma, Xinwen Cheng, Lianjun Chen, Haitao Zhang et Hongwei Xiong. *Automatic identification of shallow landslides based on Worldview2 remote sensing images*. Journal of Applied Remote Sensing, vol. 10, no. 1, page 016008, feb 2016.

[Macciotta2015] Renato Macciotta, Michael Hendry et C. Derek Martin. *Developing an early warning system for a very slow landslide based on displacement monitoring*. Natural Hazards, vol. 81, no. 2, pages 887–907, dec 2015.

[Malet2002] J.-P Malet, O Maquaire et E Calais. *The use of Global Positioning System techniques for the continuous monitoring of landslides: application to the Super-Sauze earthflow (Alpes-de-Haute-Provence, France).* Geomorphology, vol. 43, no. 1-2, pages 33–54, feb 2002.

[Malet2005] J.-P. Malet, D. Laigle, A. Remaître et O. Maquaire. *Triggering conditions and mobility of debris flows associated to complex earthflows.* Geomorphological hazard and human impact in mountain environments, vol. 66, no. 1, pages 215–235, March 2005.

[Marano2010] K. Marano, D. Wald et T. Allen. *Global earthquake casualties due to secondary effects: A quantitative analysis for improving rapid loss analyses.* Natural Hazards, vol. 52, pages 319–328, 02 2010.

[Marcelino2009] Emerson Vieira Marcelino, Antonio Roberto Formaggio et Eduardo Eiji Maeda. *Landslide inventory using image fusion techniques in Brazil.* International Journal of Applied Earth Observation and Geoinformation, vol. 11, no. 3, pages 181–191, jun 2009.

[Marchi2010] Lorenzo Marchi, Marco Cavalli et Vincenzo D'Agostino. *Hydrogeomorphic processes and torrent control works on a large alluvial fan in the eastern Italian Alps.* Natural Hazards and Earth System Sciences, vol. 10, 03 2010.

[Martelloni2012] G. Martelloni, S. Segoni, R. Fanti et F. Catani. *Rainfall thresholds for the forecasting of landslide occurrence at regional scale.* Landslides, vol. 9, no. 4, pages 485–495, Dec 2012.

[Martha2010] Tapas R. Martha, Norman Kerle, Victor Jetten, Cees J. van Westen et K. Vinod Kumar. *Characterising spectral, spatial and morphometric properties of landslides for semi-automatic detection using object-oriented methods.* Geomorphology, vol. 116, no. 1-2, pages 24–36, mar 2010.

[Martha2012] Tapas R. Martha, Norman Kerle, Cees J. van Westen, Victor Jetten et K. Vinod Kumar. *Object-oriented analysis of multi-temporal panchromatic images for creation of historical landslide inventories.* ISPRS Journal of Photogrammetry and Remote Sensing, vol. 67, pages 105–119, jan 2012.

[Matsushi2006] Yuki Matsushi, Tsuyoshi Hattanji et Yukinori Matsukura. *Mechanisms of shallow landslides on soil-mantled hillslopes with permeable and impermeable bedrocks in the Boso Peninsula, Japan.* Geomorphology, vol. 76, no. 1-2, pages 92–108, jun 2006.

[Mayoraz2002] F Mayoraz et L Vulliet. *Neural networks for slope movement prediction.* Int J Geomech, vol. 2 (2), page 153–173, 2002.

[McCoy2010] Scott McCoy, Jason Kean, Jeffrey Coe, Dennis Staley, Thad Wasklewicz et Gregory Tucker. *Evolution of a natural debris*

flow: In situ measurements of flow dynamics, video imagery, and terrestrial laser scanning. Geology, vol. 38, page 735, 08 2010.

[McDougall2004] Scott McDougall et Oldrich Hungr. *A model for the analysis of rapid landslide motion across three-dimensional terrain.* Canadian Geotechnical Journal - CAN GEOTECH J, vol. 41, pages 1084–1097, 12 2004.

[McDougall2017] Scott McDougall. *2014 Canadian Geotechnical Colloquium: Landslide runout analysis — current practice and challenges.* Canadian Geotechnical Journal, vol. 54, no. 5, pages 605–620, may 2017.

[Meisina2007] C. Meisina et S. Scarabelli. *A comparative analysis of terrain stability models for predicting shallow landslides in colluvial soils.* Geomorphology, vol. 87, no. 3, pages 207–223, jun 2007.

[Meisina2008] Claudia Meisina, Francesco Zucca, Davide Notti, Alessio Colombo, Anselmo Cucchi, Giuliano Savio, Chiara Giannico et Marco Bianchi. *Geological Interpretation of PSInSAR Data at Regional Scale.* Sensors, vol. 8, no. 11, pages 7469–7492, nov 2008.

[Meisina2013] Claudia Meisina, Davide Notti, Francesco Zucca, Massimo Ceriani, Alessio Colombo, Flavio Poggi, Anna Roccati et Andrea Zaccone. *The Use of PSInSAR™ and SqueeSAR™ Techniques for Updating Landslide Inventories.* In Landslide Science and Practice, pages 81–87. Springer Berlin Heidelberg, 2013.

[Melchiorre2011] Caterina Melchiorre et Paolo Frattini. *Modelling probability of rainfall-induced shallow landslides in a changing climate, Otta, Central Norway.* Climatic Change, vol. 113, no. 2, pages 413–436, dec 2011.

[Melosh1987] Jay Melosh. *The mechanics of large rock avalanches.* Geol. Soc. Am. Rev. Eng. Geol., vol. VII, 01 1987.

[Metternicht2005] Graciela Metternicht, Lorenz Hurni et Radu Gogu. *Remote sensing of landslides: An analysis of the potential contribution to geo-spatial systems for hazard assessment in mountainous environments.* Remote Sensing of Environment, vol. 98, no. 2-3, pages 284–303, oct 2005.

[Michael1997a] Piasecki Michael et D. Katopodes Nikolaos. *Control of Contaminant Releases in Rivers. I: Adjoint Sensitivity Analysis.* Journal of Hydraulic Engineering, vol. 123, no. 6, pages 486–492, 1997.

[Michael1997b] Piasecki Michael et D. Katopodes Nikolaos. *Control of Contaminant Releases in Rivers. II: Optimal Design.* Journal of Hydraulic Engineering, vol. 123, no. 6, pages 493–503, 1997.

[Michel2014] Gean Paulo Michel, Masato Kobiyama et Roberto Fabris Goerl. *Comparative analysis of SHALSTAB and SINMAP for*

landslide susceptibility mapping in the Cunha River basin, southern Brazil. Journal of Soils and Sediments, vol. 14, no. 7, pages 1266–1277, mar 2014.

[Miller2008] Daniel Miller et Burnett Kelly. *A probabilistic model of debris-flow delivery to stream channels, demonstrated for the Coast Range of Oregon, USA.* Geomorphology, vol. 94, pages 184–205, 02 2008.

[Mineo2015] S. Mineo, G. Pappalardo, F. Rapisarda, A. Cubito et G. Di Maria. *Integrated geostructural, seismic and infrared thermography surveys for the study of an unstable rock slope in the Peloritani Chain (NE Sicily).* Engineering Geology, vol. 195, pages 225–235, sep 2015.

[Mineo2016] S. Mineo et G. Pappalardo. *The Use of Infrared Thermography for Porosity Assessment of Intact Rock.* Rock Mechanics and Rock Engineering, vol. 49, no. 8, pages 3027–3039, apr 2016.

[Mishra2020a] Mohit Mishra, Gildas Besançon, Guillaume Chambon et Laurent Baillet. *Observer design for state and parameter estimation in a landslide model.* IFAC-PapersOnLine, vol. 53, no. 2, pages 16709–16714, 2020. 21th IFAC World Congress.

[Mishra2020b] Mohit Mishra, Gildas Besançon, Guillaume Chambon et Laurent Baillet. *Observer design for state and parameter estimation in a landslide model.* IFAC-PapersOnLine, vol. 53, no. 2, pages 16709–16714, 2020. 21th IFAC World Congress.

[Mishra2020c] Mohit Mishra, Gildas Besançon, Guillaume Chambon et Laurent Baillet. *Optimal parameter estimation in a landslide motion model using the adjoint method.* In 2020 European Control Conference (ECC), pages 226–231, 2020.

[Mishra2020d] Mohit Mishra, Gildas Besançon, Guillaume Chambon et Laurent Baillet. *Optimal parameter estimation in a landslide motion model using the adjoint method.* In 2020 European Control Conference (ECC), pages 226–231, 2020.

[Mishra2021] Mohit Mishra, Gildas Besançon, Guillaume Chambon et Laurent Baillet. *Combined state and parameter estimation for a landslide model using Kalman filter.* IFAC-PapersOnLine, 19th IFAC Symposium on System Identification SYSID 2021, vol. 54, no. 7, pages 304–309, 2021.

[Mishra2022a] Mohit Mishra, Gildas Besançon, Guillaume Chambon et Laurent Baillet. *Calculus of variations for estimation in ODE-PDE landslide models with discrete-time asynchronous measurements.* International Journal of Control (submitted), 2022.

[Mishra2022b] Mohit Mishra, Gildas Besançon, Guillaume Chambon et Laurent Baillet. *Reconstruction and forecasting of landslide displacement using a Kalman filter approach.* Landslides (submitted), 2022.

[Mondini2011] A.C. Mondini, F. Guzzetti, P. Reichenbach, M. Rossi, M. Cardinali et F. Ardizzone. *Semi-automatic recognition and mapping of rainfall induced shallow landslides using optical satellite images*. Remote Sensing of Environment, vol. 115, no. 7, pages 1743–1757, jul 2011.

[Mondini2014] A. C. Mondini, A. Viero, M. Cavalli, L. Marchi, G. Herrera et F. Guzzetti. *Comparison of event landslide inventories: the Pogliaschina catchment test case, Italy*. Natural Hazards and Earth System Sciences, vol. 14, no. 7, pages 1749–1759, jul 2014.

[Monserrat2014] O. Monserrat, M. Crosetto et G. Luzi. *A review of ground-based SAR interferometry for deformation measurement*. ISPRS Journal of Photogrammetry and Remote Sensing, vol. 93, pages 40–48, jul 2014.

[Montgomery1994] David R. Montgomery et William E. Dietrich. *A physically based model for the topographic control on shallow landsliding*. Water Resources Research, vol. 30, no. 4, pages 1153–1171, apr 1994.

[Montgomery2002] David R. Montgomery, William E. Dietrich et John T. Heffner. *Piezometric response in shallow bedrock at CB1: Implications for runoff generation and landsliding*. Water Resources Research, vol. 38, no. 12, pages 10–1–10–18, dec 2002.

[Montrasio2008] L. Montrasio et R. Valentino. *A model for triggering mechanisms of shallow landslides*. Natural Hazards and Earth System Sciences, vol. 8, no. 5, pages 1149–1159, oct 2008.

[Montrasio2009] Lorella Montrasio, Roberto Valentino et Gian Luca Losi. *Rainfall-induced shallow landslides: a model for the triggering mechanism of some case studies in Northern Italy*. Landslides, vol. 6, no. 3, pages 241–251, jun 2009.

[Montrasio2011] L. Montrasio, R. Valentino et G. L. Losi. *Towards a real-time susceptibility assessment of rainfall-induced shallow landslides on a regional scale*. Natural Hazards and Earth System Sciences, vol. 11, no. 7, pages 1927–1947, jul 2011.

[Mora2003] O. Mora, J.J. Mallorqui et A. Broquetas. *Linear and nonlinear terrain deformation maps from a reduced set of interferometric sar images*. IEEE Transactions on Geoscience and Remote Sensing, vol. 41, no. 10, pages 2243–2253, oct 2003.

[Moreiras2005] S. Moreiras. *Climatic effect of ENSO associated with landslide occurrence in the Central Andes, Mendoza Province, Argentina*. Landslides, vol. 2, pages 53–59, 2005.

[Morelli2012] Stefano Morelli, Samuele Segoni, Goffredo Manzo, Leonardo Ermini et Filippo Catani. *Urban planning, flood risk and public policy: The case of the Arno River, Firenze, Italy*. Applied Geography, vol. 34, pages 205–218, may 2012.

[Naef2006] D. Naef, D. Rickenmann, P. Rutschmann et B. W McArdell. *Comparison of flow resistance relations for debris flows using a one-dimensional finite element simulation model.* Natural Hazards and Earth System Sciences, vol. 6, no. 1, pages 155–165, feb 2006.

[Navon1998] I. M. Navon. *Practical and theoretical aspects of adjoint parameter estimation and identifiability in meteorology and oceanography.* Dynamics of Atmospheres and Oceans, vol. 27, no. 1, pages 55–79, 1998.

[Navratil2013] Oldrich Navratil, Frédéric Liébault, Hervé Bellot, Eric Travaglini, Joshua Theule, Guillaume Chambon et Dominique Laigle. *High-frequency monitoring of debris-flows propagation in the Réal Torrent, Southern French Alps.* Geomorphology, vol. 201, 11 2013.

[Ng1998] C. W. W. Ng et Q. Shi. *Influence of rainfall intensity and duration on slope stability in unsaturated soils.* Quarterly Journal of Engineering Geology and Hydrogeology, vol. 31, no. 2, pages 105–113, may 1998.

[Nguyen2014] Van Tri Nguyen, Didier Georges et Gildas Besancon. *Optimal state estimation in an overland flow model using the adjoint method.* 2014 IEEE Conference on Control Applications (CCA), pages 2034–2039, 2014. 2014 IEEE Conference on Control Applications (CCA).

[Nguyen2015] V. T. Nguyen, D. Georges, G. Besancon et I. Zin. *Application of adjoint method for estimating Manning-Strickler coefficient in Tondi Kiboro catchment.* In 2015 IEEE Conference on Control Applications (CCA), pages 551–556, 2015.

[Nguyen2016a] Van Tri Nguyen, Didier Georges et Gildas Besançon. *State and parameter estimation in 1-D hyperbolic PDEs based on an adjoint method.* Automatica, vol. 67, pages 185–191, 2016.

[Nguyen2016b] Van Tri Nguyen, Didier Georges et Gildas Besançon. *State and parameter estimation in 1-D hyperbolic PDEs based on an adjoint method.* Automatica, vol. 67, pages 185–191, 2016.

[Nguyen2016c] Van Tri Nguyen, Didier Georges, Gildas Besançon et Isabella Zin. *Parameter estimation of a real hydrological system using an adjoint method.* IFAC-PapersOnLine, vol. 49, no. 13, pages 300–305, 2016. 12th IFAC Workshop on Adaptation and Learning in Control and Signal Processing ALCOSP 2016.

[Nguyen2018] Van Tri Nguyen, Didier Georges et Gildas Besancon. *Calculus of variations approach for state and parameter estimation in switched 1-D hyperbolic PDEs.* Optimal Control Applications and Methods, Wiley, vol. 39, no. 3, pages 1182–1201, 2018. Optimal Control Applications and Methods, Wiley.

[Nolesini2016] Teresa Nolesini, William Frodella, Silvia Bianchini et Nicola Casagli. *Detecting Slope and Urban Potential Unstable Areas*

by Means of Multi-Platform Remote Sensing Techniques: The Volterra (Italy) Case Study. Remote Sensing, vol. 8, no. 9, page 746, sep 2016.

[Nyambod2010] Emmanuel M. Nyambod. *Environmental Consequences of Rapid Urbanisation: Bamenda City, Cameroon.* Journal of Environmental Protection, vol. 1, pages 15–23, 2010.

[O'Brien1993a] J. O'Brien, P. Julien et W. Fullerton. *Two-Dimensional Water Flood and Mudflow Simulation.* Journal of Hydraulic Engineering-asce - J HYDRAUL ENG-ASCE, vol. 119, 02 1993.

[O'Brien1993b] J. O'Brien, P. Julien et W. Fullerton. *Two-Dimensional Water Flood and Mudflow Simulation.* Journal of Hydraulic Engineering-asce - J HYDRAUL ENG-ASCE, vol. 119, 02 1993.

[O'Connor2021] Kevin M. O'Connor et Charles H. Dowding. GeoMeasurements by pulsing TDR cables and probes. CRC Press, nov 2021.

[O'Loughlin1986] E. M. O'Loughlin. *Prediction of Surface Saturation Zones in Natural Catchments by Topographic Analysis.* Water Resources Research, vol. 22, no. 5, pages 794–804, may 1986.

[Pack1998] Robert Pack, David Tarboton et C. Goodwin. *The SINMAP approach to terrain stability mapping. Procedeengs of the 8th congress of the international association of engineering geology, Vancouver, British Columbia.* Canada, pages 21–25, 01 1998.

[Palis2016] Edouard Palis, Thomas Lebourg, Emmanuel Tric, Jean-Philippe Malet et Maurin Vidal. *Long-term monitoring of a large deep-seated landslide (La Clapiere, South-East French Alps): initial study.* Landslides, vol. 14, no. 1, pages 155–170, apr 2016.

[Pappalardo2016] G. Pappalardo, S. Mineo, S. Perriello Zampelli, A. Cubito et D. Calcaterra. *InfraRed Thermography proposed for the estimation of the Cooling Rate Index in the remote survey of rock masses.* International Journal of Rock Mechanics and Mining Sciences, vol. 83, pages 182–196, mar 2016.

[Park2001] H Park et T.R West. *Development of a probabilistic approach for rock wedge failure.* Engineering Geology, vol. 59, no. 3-4, pages 233–251, apr 2001.

[Park2005] Hyuck-Jin Park, Terry R. West et Ik Woo. *Probabilistic analysis of rock slope stability and random properties of discontinuity parameters, Interstate Highway 40, Western North Carolina, USA.* Engineering Geology, vol. 79, no. 3-4, pages 230–250, jul 2005.

[Park2013] Hyuck Jin Park, Jung Hyun Lee et Ik Woo. *Assessment of rainfall-induced shallow landslide susceptibility using a GIS-based probabilistic approach.* Engineering Geology, vol. 161, pages 1–15, jul 2013.

[Parker2014] Amy L. Parker, Juliet Biggs et Zhong Lu. *Investigating long-term subsidence at Medicine Lake Volcano, CA, using multi-temporal InSAR.* Geophysical Journal International, vol. 199, no. 2, pages 844–859, sep 2014.

[Pazzi2015] Veronica Pazzi, Stefano Morelli, Francesco Fidolini, Elvis Krymi, Nicola Casagli et Riccardo Fanti. *Testing cost-effective methodologies for flood and seismic vulnerability assessment in communities of developing countries (Dajç, northern Albania).* Geomatics, Natural Hazards and Risk, vol. 7, no. 3, pages 971–999, feb 2015.

[Pearson1900] Karl F.R.S. Pearson. *On the criterion that a given system of deviations from the probable in the case of a correlated system of variables.* The London, Edinburgh, and Dublin Philosophical Magazine and Journal of Science, vol. 50, no. 302, pages 157–175, 1900.

[Pecoraro2019] Gaetano Pecoraro, Michele Calvello et Luca Piciullo. *Monitoring strategies for local landslide early warning systems.* Landslides, vol. 16, no. 2, pages 213–231, February 2019.

[Petley2002] David N. Petley, Mark H. Bulmer et William Murphy. *Patterns of movement in rotational and translational landslides.* Geology, vol. 30, no. 8, pages 719–722, 08 2002.

[Petley2005] D.N. Petley, F. Mantovani, M.H. Bulmer et A. Zannoni. *The use of surface monitoring data for the interpretation of landslide movement patterns.* Geomorphology, vol. 66, no. 1-4, pages 133–147, mar 2005.

[Petley2007] D. N. Petley, G. J. Hearn, A. Hart, N. J. Rosser, S. A. Dunning, K. Oven et W. A. Mitchell. *Trends in landslide occurrence in Nepal.* Natural Hazards, vol. 43, no. 1, pages 23–44, 2007.

[Petley2012] David Petley. *Global patterns of loss of life from landslides.* Geology, vol. 40, no. 10, pages 927–930, oct 2012.

[Pieraccini2003] M. Pieraccini, N. Casagli, G. Luzi, D. Tarchi, D. Mecatti, L. Noferini et C. Atzeni. *Landslide monitoring by ground-based radar interferometry: A field test in Valdarno (Italy).* International Journal of Remote Sensing, vol. 24, no. 6, pages 1385–1391, jan 2003.

[Pirulli2010] Marina Pirulli. *On the use of the calibration-based approach for debris-flow forward-analyses.* Natural Hazards and Earth System Sciences, vol. 10, 05 2010.

[Pradhan2014a] Ananta Pradhan et Yun-Tae Kim. *Application and comparison of shallow landslide susceptibility models in weathered granite*

soil under extreme rainfall events. Environmental earth sciences, 10 2014.

[Pradhan2014b] Ananta Man Singh Pradhan et Yun-Tae Kim. *Application and comparison of shallow landslide susceptibility models in weathered granite soil under extreme rainfall events*. Environmental Earth Sciences, vol. 73, no. 9, pages 5761–5771, nov 2014.

[Pradhan2019] S. P. Pradhan et Tariq Siddique. Mass wasting: An overview, pages 3–20. Springer International Publishing, Cham, 2019.

[Prochaska2008] Adam Prochaska, Paul Santi, Jerry Higgins et Susan Cannon. *Debris-flow runout predictions based on the Average Channel Slope (ACS)*. Engineering Geology, vol. 98, pages 29–40, 04 2008.

[qiang Dou2014] Hong qiang Dou, Tong chun Han, Xiao nan Gong et Jie Zhang. *Probabilistic slope stability analysis considering the variability of hydraulic conductivity under rainfall infiltration–redistribution conditions*. Engineering Geology, vol. 183, pages 1–13, dec 2014.

[Rahardjo2007] H. Rahardjo, T. H. Ong, R. B. Rezaur et E. C. Leong. *Factors Controlling Instability of Homogeneous Soil Slopes under Rainfall*. Journal of Geotechnical and Geoenvironmental Engineering, vol. 133, no. 12, pages 1532–1543, dec 2007.

[Raia2014] S. Raia, M. Alvioli, M. Rossi, R. L. Baum, J. W. Godt et F. Guzzetti. *Improving predictive power of physically based rainfall-induced shallow landslide models: a probabilistic approach*. Geoscientific Model Development, vol. 7, no. 2, pages 495–514, mar 2014.

[Ramesh2000] R. Ramesh, Datta Bithin, Bhallamudi S. Murty et A. Narayana. *Optimal Estimation of Roughness in Open-Channel Flows*. Journal of Hydraulic Engineering, vol. 126, no. 4, pages 299–303, 2000.

[Reichenbach1998] P. Reichenbach, M. Cardinali, P. De Vita et F. Guzzetti. *Regional hydrological thresholds for landslides and floods in the Tiber River Basin (central Italy)*. Environmental Geology, vol. 35, no. 2-3, pages 146–159, aug 1998.

[Reid2016] Mark Reid, Jeffrey Coe et Dianne Brien. *Forecasting inundation from debris flows that grow volumetrically during travel, with application to the Oregon Coast Range, USA*. Geomorphology, vol. 273, 07 2016.

[Remondino2012] F. Remondino, L. Barazzetti, F. Nex, M. Scaioni et D. Sarazzi. *UAV photogrammetry for mapping and 3D modeling - current status and future perspectives*. The International Archives of the Photogrammetry, Remote Sensing and Spatial Information Sciences, vol. XXXVIII-1/C22, pages 25–31, sep 2012.

[Revellino2004] Paola Revellino, Oldrich Hungr, Francesco Guadagno et Stephen Evans. *Velocity and runout simulation of destructive debris flows and debris avalanches in pyroclastic deposits, Campania region, Italy.* Environmental Geology, vol. 45, pages 295–311, 09 2004.

[Rickenmann1999] Dieter Rickenmann. *Empirical Relationships for Debris Flows.* Natural Hazards, vol. 19, pages 47–77, 01 1999.

[Rickenmann2005] Dieter Rickenmann. *Runout prediction methods.* In Debris-flow Hazards and Related Phenomena, pages 305–324. Springer Berlin Heidelberg, 2005.

[Rickenmann2006] D. Rickenmann, Dominique Laigle, Brian McArdell et Johannes Hübl. *Comparison of 2D debris-flow simulation models with field events.* Computational Geosciences, vol. 10, pages 241–264, 05 2006.

[Rickenmann2016] Dieter Rickenmann. *Debris-Flow Hazard Assessment and Methods Applied in Engineering Practice.* International Journal of Erosion Control Engineering, vol. 9, pages 80–90, 08 2016.

[Riley2013] Karin Riley, Rebecca Bendick, Kevin Hyde et Emmanuel Gabet. *Frequency-magnitude distribution of debris flows compiled from global data, and comparison with post-fire debris flows in the western US.* Geomorphology, vol. 191, page 118–128, 06 2013.

[Robinson2003] D. A. Robinson, S. B. Jones, J. M. Wraith, D. Or et S. P. Friedman. *A Review of Advances in Dielectric and Electrical Conductivity Measurement in Soils Using Time Domain Reflectometry.* Vadose Zone Journal, vol. 2, no. 4, page 444, 2003.

[Rose2007] N.D. Rose et Oldrich Hungr. *Forecasting potential rock slope failure in open pit mines using the inverse-velocity method.* International Journal of Rock Mechanics and Mining Sciences, vol. 44, page 308–320, 02 2007.

[Rosser2005] N.J. Rosser, D.N. Petley, M. Lim, S.A. Dunning et R.J. Allison. *Terrestrial laser scanning for monitoring the process of hard rock coastal cliff erosion.* Quarterly Journal of Engineering Geology and Hydrogeology, vol. 38, no. 4, pages 363–375, nov 2005.

[Rossi2013] G. Rossi, F. Catani, L. Leoni, S. Segoni et V. Tofani. *HIRESSS: a physically based slope stability simulator for HPC applications.* Natural Hazards and Earth System Sciences, vol. 13, no. 1, pages 151–166, jan 2013.

[Rosso2006] Renzo Rosso, Maria Cristina Rulli et Giovanni Vannucchi. *A physically based model for the hydrologic control on shallow landsliding.* Water Resources Research, vol. 42, no. 6, jun 2006.

[Rudolf1999] H. Rudolf, D. Leva, D. Tarchi et A.J. Sieber. *A mobile and versatile SAR system.* In IEEE 1999 International Geoscience and Remote Sensing Symposium. IGARSS'99 (Cat. No.99CH36293). IEEE, 1999.

[Rupp2018] Stefan Rupp, Annika Wohlers et Bodo Damm. *Long-term relationship between landslide occurrences and precipitation in southern Lower Saxony and northern Hesse.* Zeitschrift für Geomorphologie, vol. 61, 06 2018.

[Salciarini2006] Diana Salciarini, Jonathan W. Godt, William Z. Savage, Pietro Conversini, Rex L. Baum et John A. Michael. *Modeling regional initiation of rainfall-induced shallow landslides in the eastern Umbria Region of central Italy.* Landslides, vol. 3, no. 3, pages 181–194, may 2006.

[Santoso2011] Anastasia M. Santoso, Kok-Kwang Phoon et Ser-Tong Quek. *Effects of soil spatial variability on rainfall-induced landslides.* Computers & Structures, vol. 89, no. 11-12, pages 893–900, jun 2011.

[Sassa1985] K. Sassa. *The mechanism of debris flow.* pages 1173–1176, 01 1985.

[Sasso2014] S. F. Dal Sasso, A. Sole, S. Pascale, F. Sdao, A. Bateman Pinzòn et V. Medina. *Assessment methodology for the prediction of landslide dam hazard.* Natural Hazards and Earth System Sciences, vol. 14, no. 3, pages 557–567, mar 2014.

[Savage2004] W Savage, J Godt et R Baum. *Modeling time-dependent areal slope stability.* In Landslides: Evaluation and Stabilization/Glissement de Terrain: Evaluation et Stabilisation, Set of 2 Volumes, pages 23–36. CRC Press, jun 2004.

[Savvaidis2003] P. Savvaidis. *Existing Landslide Monitoring Systems and Techniques.* In -, 2003.

[Scaioni2014] Marco Scaioni, Laura Longoni, Valentina Melillo et Monica Papini. *Remote Sensing for Landslide Investigations: An Overview of Recent Achievements and Perspectives.* Remote Sensing, vol. 6, no. 10, pages 9600–9652, oct 2014.

[Scaioni2015] Marco Scaioni, Tiantian Feng, Ping Lu, Gang Qiao, Xiaohua Tong, Ron Li, Luigi Barazzetti, Mattia Previtali et Riccardo Roncella. *Close-Range Photogrammetric Techniques for Deformation Measurement: Applications to Landslides.* In Modern Technologies for Landslide Monitoring and Prediction, pages 13–41. Springer Berlin Heidelberg, 2015.

[Schaum2014] Alexander Schaum, Jaime A. Moreno, Emilia Fridman et Jesus Alvarez. *Matrix inequality-based observer design for a class of distributed transport-reaction systems.* International Journal of Robust and Nonlinear Control, vol. 24, no. 16, pages 2213–2230, 2014.

[Scheidl2009] Christian Scheidl et Dieter Rickenmann. *Empirical prediction of debris-flow mobility and deposition on fans.* Earth Surface Processes and Landforms, vol. 35, pages 157 – 173, 01 2009.

[Schilling1998] Steve Schilling. *LAHARZ; GIS programs for automated mapping of lahar-inundation hazard zones.* U.S. Geological Survey Open-File Report, pages 98–638, 01 1998.

[Schmidt2008] J. Schmidt, G. Turek, M. P. Clark, M. Uddstrom et J. R. Dymond. *Probabilistic forecasting of shallow, rainfall-triggered landslides using real-time numerical weather predictions.* Natural Hazards and Earth System Sciences, vol. 8, no. 2, pages 349–357, 2008.

[Shi2004] Zhen-Jun Shi et Jie Shen. *A gradient-related algorithm with inexact line searches.* Journal of Computational and Applied Mathematics, vol. 170, no. 2, pages 349–370, 2004.

[Shou2005] Keh-Jian Shou et Ying-Liang Chen. *Spatial risk analysis of Li-shan landslide in Taiwan.* Engineering Geology, vol. 80, no. 3-4, pages 199–213, aug 2005.

[Shou2009] K. Shou, Y. Chen et H. Liu. *Hazard analysis of Li-shan landslide in Taiwan.* Geomorphology, vol. 103, no. 1, pages 143–153, jan 2009.

[Simoni2004] A. Simoni, M. Berti, M. Generali, C. Elmi et M. Ghirotti. *Preliminary result from pore pressure monitoring on an unstable clay slope.* Engineering Geology, vol. 73, no. 1-2, pages 117–128, may 2004.

[Simoni2011] Alessandro Simoni, Maria Mammoliti et Matteo Berti. *Uncertainty of debris flow mobility relationships and its influence on the prediction of inundated areas.* Geomorphology, vol. 132, pages 249–259, 09 2011.

[Singhroy1998] V Singhroy, K.E Mattar et A.L Gray. *Landslide characterisation in Canada using interferometric SAR and combined SAR and TM images.* Advances in Space Research, vol. 21, no. 3, pages 465–476, jan 1998.

[Sirangelo1996] Beniamino Sirangelo et Pasquale Versace. *A real time forecasting model for landslides triggered by rainfall.* Meccanica, vol. 31, no. 1, pages 73–85, feb 1996.

[Sirangelo2002] B. Sirangelo et Giovanni Braca. *Identification of Hazard Conditions For Mud Flow Occurrence By Hydrological Model.* Engineering Geology, vol. 73, pages 3750–, 01 2002.

[Slob2005] Siefko Slob, Bart van Knapen, Robert Hack, Keith Turner et John Kemeny. *Method for Automated Discontinuity Analysis of Rock Slopes with Three-Dimensional Laser Scanning.* Transportation Research Record: Journal of the Transportation Research Board, vol. 1913, no. 1, pages 187–194, jan 2005.

[Song2016] Young-Suk Song, Byung-Gon Chae et Jintae Lee. *A method for evaluating the stability of an unsaturated slope in natural terrain during rainfall.* Engineering Geology, vol. 210, no. C, pages 84–92, 2016.

[Sorbino2009] Giuseppe Sorbino, Carlo Sica et Leonardo Cascini. *Susceptibility analysis of shallow landslides source areas using physically based models.* Natural Hazards, vol. 53, no. 2, pages 313–332, sep 2009.

[Sosio2007] Rosanna Sosio, Giovanni Crosta et P. Frattini. *Field observations, rheologucal testing and numerical modeling of a debris-flow event.* Earth Surface Processes and Landforms, vol. 32, pages 290 – 306, 02 2007.

[Sosio2008] Rosanna Sosio, Giovanni Crosta et Oldrich Hungr. *Complete dynamic modeling calibration for the Thurwieser rock avalanche (Italian Central Alps).* Engineering Geology, vol. 100, pages 11–26, 06 2008.

[Spampinato2011] Letizia Spampinato, Sonia Calvari, Clive Oppenheimer et Enzo Boschi. *Volcano surveillance using infrared cameras.* Earth-Science Reviews, vol. 106, no. 1-2, pages 63–91, may 2011.

[Springman2013a] S.M. Springman, A. Thielen, P. Kienzler et S. Friedel. *A long-term field study for the investigation of rainfall-induced landslides.* Géotechnique, vol. 63, no. 14, pages 1177–1193, nov 2013.

[Springman2013b] S.M. Springman, A. Thielen, P. Kienzler et S. Friedel. *A long-term field study for the investigation of rainfall-induced landslides.* Géotechnique, vol. 63, no. 14, pages 1177–1193, 2013.

[Stengel1986] R. F. Stengel. *Stochastic Optimal Control: Theory and Application.* New York: Wiley, vol. 91, no. 910, page 499–499, 1986.

[Stevens2000] William R. Stevens et Bill E. Zehrbach. *Inclinometer Data Analysis for Remediated Landslides.* In Geotechnical Measurements. American Society of Civil Engineers, jul 2000.

[Strozzi2006] T. Strozzi, U. Wegmuller, H.R. Keusen, K. Graf et A. Wiesmann. *Analysis of the Terrain Displacement Along a Funicular by SAR Interferometry.* IEEE Geoscience and Remote Sensing Letters, vol. 3, no. 1, pages 15–18, jan 2006.

[Strub2006] Issam S. Strub et Alexandre M. Bayen. *Continuous adjoint method for Air Traffic Flow Management.* In Proceedings of the 45th IEEE Conference on Decision and Control, pages 101–106, 2006.

[Sturzenegger2009] M. Sturzenegger et D. Stead. *Quantifying discontinuity orientation and persistence on high mountain rock slopes and large landslides using terrestrial remote sensing techniques.* Natural Hazards and Earth System Sciences, vol. 9, no. 2, pages 267–287, mar 2009.

[Tapete2015] Deodato Tapete, Stefano Morelli, Riccardo Fanti et Nicola Casagli. *Localising deformation along the elevation of linear structures: An experiment with space-borne InSAR and RTK GPS on the Roman Aqueducts in Rome, Italy.* Applied Geography, vol. 58, pages 65–83, mar 2015.

[Tarchi1997] D. Tarchi, E. Ohlmer et A. Sieber. *Monitoring of Structural Changes by Radar Interferometry.* Research in Nondestructive Evaluation, vol. 9, no. 4, pages 213–225, jan 1997.

[Tarchi2003] Dario Tarchi, Nicola Casagli, Riccardo Fanti, David D. Leva, Guido Luzi, Alessandro Pasuto, Massimiliano Pieraccini et Sandro Silvano. *Landslide monitoring by using ground-based SAR interferometry: an example of application to the Tessina landslide in Italy.* Engineering Geology, vol. 68, no. 1-2, pages 15–30, feb 2003.

[Teixeira2014] Manuel Teixeira, Carlos Bateira, F. Marques et Bianca Vieira. *Physically based shallow translational landslide susceptibility analysis in Tibo catchment, NW of Portugal.* Landslides, 05 2014.

[Ter-Stepanian2000] George Ter-Stepanian. *Quick clay landslides: Their enigmatic features and mechanism.* Bulletin of Engineering Geology and the Environment, vol. 59, pages 47–57, 09 2000.

[Terhorst2009] Birgit Terhorst et Roger Kreja. *Slope stability modelling with SINMAP in a settlement area of the Swabian Alb.* Landslides, vol. 6, no. 4, pages 309–319, sep 2009.

[Terlien1995] Mark T. J. Terlien, Cees J. Van Westen et Theo W. J. van Asch. *Deterministic Modelling in Gis-Based Landslide Hazard Assessment.* In Geographical Information Systems in Assessing Natural Hazards, pages 57–77. Springer Netherlands, 1995.

[Terlien1998] Mark T. J. Terlien. *The determination of statistical and deterministic hydrological landslide-triggering thresholds.* Environmental Geology, vol. 35, no. 2-3, pages 124–130, aug 1998.

[Teza2012] Giordano Teza, Gianluca Marcato, Eugenio Castelli et Antonio Galgaro. *IRTROCK: A MATLAB toolbox for contactless recognition of surface and shallow weakness of a rock cliff by infrared thermography.* Computers & Geosciences, vol. 45, pages 109–118, aug 2012.

[Teza2014] Giordano Teza, Gianluca Marcato, Alessandro Pasuto et Antonio Galgaro. *Integration of laser scanning and thermal imaging in monitoring optimization and assessment of rockfall hazard: a case history in the Carnic Alps (Northeastern Italy).* Natural Hazards, vol. 76, no. 3, pages 1535–1549, dec 2014.

[Thiebes2014] Benni Thiebes, Rainer Bell, Thomas Glade, Stefan Jäger, Julia Mayer, Malcolm Anderson et Liz Holcombe. *Integration of a limit-equilibrium model into a landslide early warning system.* Landslides, vol. 11, no. 5, pages 859–875, October 2014.

[Ţiclea2009] Alexandru Ţiclea et Gildas Besançon. *State and parameter estimation via discrete-time exponential forgetting factor observer.* In 15th IFAC Symposium on System Identification, SYSID, pages 1370–1374, Saint Malo, France, January 2009.

[Ţiclea2013] Alexandru Ţiclea et Gildas Besançon. *Exponential forgetting factor observer in discrete time.* Systems & Control Letters, vol. 62, no. 9, pages 756–763, 2013.

[Tofani2013] V. Tofani, S. Segoni, A. Agostini, F. Catani et N. Casagli. *Technical Note: Use of remote sensing for landslide studies in Europe.* Natural Hazards and Earth System Sciences, vol. 13, no. 2, pages 299–309, feb 2013.

[Topp1980] G. C. Topp, J. L. Davis et A. P. Annan. *Electromagnetic determination of soil water content: Measurements in coaxial transmission lines.* Water Resources Research, vol. 16, no. 3, pages 574–582, jun 1980.

[Toyos2007] Guillermo Toyos, Paul Cole, Alicia Felpeto et Joan Marti. *A GIS-based methodology for hazard mapping of small volume pyroclastic flows.* Natural Hazards, vol. 41, pages 99–112, 04 2007.

[Tsai2009] Tung-Lin Tsai et Hsin-Fa Chen. *Effects of degree of saturation on shallow landslides triggered by rainfall.* Environmental Earth Sciences, vol. 59, no. 6, pages 1285–1295, mar 2009.

[Tsai2014] Tung-Lin Tsai, Ping-Yu Tsai et Pei-Jhang Yang. *Probabilistic modeling of rainfall-induced shallow landslide using a point-estimate method.* Environmental Earth Sciences, vol. 73, no. 8, pages 4109–4117, sep 2014.

[Tsaparas2002] I Tsaparas, H Rahardjo, D.G Toll et E.C Leong. *Controlling parameters for rainfall-induced landslides.* Computers and Geotechnics, vol. 29, no. 1, pages 1–27, jan 2002.

[Uhlemann2016] S. Uhlemann, A. Smith, J. Chambers, N. Dixon, T. Dijkstra, E. Haslam, P. Meldrum, A. Merritt, D. Gunn et J. Mackay. *Assessment of ground-based monitoring techniques applied to landslide investigations.* Geomorphology, vol. 253, pages 438–451, jan 2016.

[UN/ISDR2006] UN/ISDR. *Developing Early Warning Systems: A checklist.* EWC III Third International Conference on Early Warning, From concept to action, 2006.

[Van Asch2007] Th.W.J. Van Asch, L.P.H. Van Beek et T.A. Bogaard. *Problems in predicting the mobility of slow-moving landslides.* Engineering Geology, vol. 91, no. 1, pages 46–55, 2007. Slope Transport Processes and Hydrology. A tribute to Jan Nieuwenhuis.

[van Genuchten1980] M. Th. van Genuchten. *A Closed-form Equation for Predicting the Hydraulic Conductivity of Unsaturated Soils.* Soil Science

Society of America Journal, vol. 44, no. 5, pages 892–898, sep 1980.

[van Westen2005] C.J. van Westen, T.W.J. van Asch et R. Soeters. *Landslide hazard and risk zonation—why is it still so difficult?* Bulletin of Engineering Geology and the Environment, vol. 65, no. 2, pages 167–184, dec 2005.

[Ventisette2011] C. Del Ventisette, E. Intrieri, G. Luzi, N. Casagli, R. Fanti et D. Leva. *Using ground based radar interferometry during emergency: the case of the A3 motorway (Calabria Region, Italy) threatened by a landslide.* Natural Hazards and Earth System Sciences, vol. 11, no. 9, pages 2483–2495, sep 2011.

[Vieira2010] B. C. Vieira, N. F. Fernandes et O. A. Filho. *Shallow landslide prediction in the Serra do Mar, São Paulo, Brazil.* Natural Hazards and Earth System Sciences, vol. 10, no. 9, pages 1829–1837, 2010.

[Wang2021] H. Wang, C. Li et B. Sun. *Parameter design of ground-based SAR interferometry for landslide deformation measurement.* In IET International Radar Conference (IET IRC 2020). Institution of Engineering and Technology, 2021.

[Werner2003] C. Werner, U. Wegmuller, T. Strozzi et A. Wiesmann. *Interferometric point target analysis for deformation mapping.* In IGARSS 2003. 2003 IEEE International Geoscience and Remote Sensing Symposium. Proceedings (IEEE Cat. No.03CH37477). IEEE, 2003.

[Westen2000] Van Westen et J. Cees. *The Modelling Of Landslide Hazards Using GIS.* Surveys in Geophysics, vol. 21, no. 2, pages 241–255, March 2000.

[Westen2004a] C Van Westen. *Geo-Information tools for landslide risk assessment: an overview of recent developments.* In Landslides: Evaluation and Stabilization/Glissement de Terrain: Evaluation et Stabilisation, Set of 2 Volumes, pages 39–56. CRC Press, jun 2004.

[Westen2004b] C.J. Westen. *Geo-Information tools for landslide risk assessment: an overview of recent developments.* In 9th International Symposium on Landslides, Rio de Jeneiro, 06 2004.

[Wheeler2003] S. Wheeler, Radhey Sharma et M. Buisson. *Coupling of Hydraulic Hysteresis and Stress–strain Behavior in Unsaturated Soils.* Geotechnique, vol. 53, pages 41–54, 01 2003.

[White1996] I. D. White, D. N. Mottershead et S. J. Harrison. Environmental systems: An introductory text. Chapman & Hall, 1996.

[Wieczorek2005] Gerald F. Wieczorek et Thomas Glade. *Climatic factors influencing occurrence of debris flows.* In Debris-flow Hazards and Related Phenomena, pages 325–362. Springer Berlin Heidelberg, 2005.

[Wolter2014] Andrea Wolter, Doug Stead et John J. Clague. *A morphologic characterisation of the 1963 Vajont Slide, Italy, using long-range terrestrial photogrammetry.* Geomorphology, vol. 206, pages 147–164, feb 2014.

[Wu1995] Weimin Wu et Roy C. Sidle. *A Distributed Slope Stability Model for Steep Forested Basins.* Water Resources Research, vol. 31, no. 8, pages 2097–2110, aug 1995.

[Wu2005] Jian-Hong Wu, Hung-Ming Lin, Der-Her Lee et Shih-Chieh Fang. *Integrity assessment of rock mass behind the shotcreted slope using thermography.* Engineering Geology, vol. 80, no. 1-2, pages 164–173, aug 2005.

[Xie2004] Mowen Xie, Tetsuro Esaki et Guoyun Zhou. *GIS-Based Probabilistic Mapping of Landslide Hazard Using a Three-Dimensional Deterministic Model.* Natural Hazards, vol. 33, no. 2, pages 265–282, oct 2004.

[Yang2019] Beibei Yang, Kunlong Yin, Suzanne Lacasse et Zhongqiang Liu. *Time series analysis and long short-term memory neural network to predict landslide displacement.* Landslides, vol. 16, no. 4, pages 677–694, jan 2019.

[Yilmaz2009] Işık Yilmaz et Inan Keskin. *GIS based statistical and physical approaches to landslide susceptibility mapping (Sebinkarahisar, Turkey).* Bulletin of Engineering Geology and the Environment, vol. 68, no. 4, pages 459–471, jan 2009.

[Yin2010] Yueping Yin, Hongde Wang, Youlong Gao et Xiaochun Li. *Real-time monitoring and early warning of landslides at relocated Wushan Town, the Three Gorges Reservoir, China.* Landslides, vol. 7, no. 3, pages 339–349, may 2010.

[Zainea2007] M. Zainea, A. van der Schaft et J. Buisson. *Stabilizing control for power converters connected to transmission lines.* In 2007 American Control Conference, pages 3476–3481, 2007.

[Zhang2007] L. L. Zhang, L. M. Zhang et W. H. Tang. *Rainfall-induced slope failure considering variability of soil properties.* In Risk and Variability in Geotechnical Engineering, pages 215–220. Thomas Telford Publishing, jan 2007.

[Zhou2003] G. Zhou, T. Esaki, Y. Mitani, M. Xie et J. Mori. *Spatial probabilistic modeling of slope failure using an integrated GIS Monte Carlo simulation approach.* Engineering Geology, vol. 68, no. 3-4, pages 373–386, mar 2003.

[Zhou2020] G. Zhou, T. Esaki, Y. Miani et J. Mori. *Slope failure prediction using a spatial probabilistic modeling approach integrated with Monte Carlo simulation and GIS.* In Rock Stress, pages 425–431. CRC Press, dec 2020.

[Zhu2013] H. Zhu, L.M. Zhang, L.L. Zhang et C.B. Zhou. *Two-dimensional probabilistic infiltration analysis with a spatially*

varying permeability function. Computers and Geotechnics, vol. 48, pages 249–259, mar 2013.

[Zimmermann1997] Markus Zimmermann, Peter Mani et H. Romang. *Magnitude-frequency aspects of alpine debris flows.* Eclogae Geologicae Helvetiae, vol. 90, pages 415–420, 01 1997.

[Zizioli2013] D. Zizioli, C. Meisina, R. Valentino et L. Montrasio. *Comparison between different approaches to modeling shallow landslide susceptibility: a case history in Oltrepo Pavese, Northern Italy.* Natural Hazards and Earth System Sciences, vol. 13, no. 3, pages 559–573, mar 2013.

[Zuo2020] Shi Zuo, Lianheng Zhao, Dongping Deng, Zhibin Wang et Zhigang Zhao. *Reliability back analysis of landslide shear strength parameters based on a general nonlinear failure criterion.* International Journal of Rock Mechanics and Mining Sciences, vol. 126, page 104189, feb 2020.

List of Figures

List of Tables

Introduction de la thèse en Français

Le contexte de la thèse

Modélisation des glissements de terrain

Un glissement de terrain, également caractérisé par la déstabilisation d'une pente, est un mouvement descendant de roches, de débris ou de sol sous l'effet de la gravité, près de la surface de la terre, résultant de fortes précipitations, d'inondations, de tremblements de terre, d'une fonte des neiges importante ou d'activités humaines comme la construction (Fig. A.10). Les glissements de terrain sont devenus plus fréquents ces dernières années en raison du changement climatique et de l'urbanisation croissante. Ils peuvent avoir de graves effets socio-économiques, notamment des coûts importants en termes de vies humaines, d'infrastructures, d'économie et d'écosystème de la région. Les glissements de terrain présentent différents types et vitesses de mouvement, allant de la reptation lente à l'accélération catastrophique rapide. Dans les catastrophes les plus destructrices, les roches, les débris ou le sol peuvent s'écouler à des vitesses de plusieurs dizaines de mètres par an, causant des ravages sur les infrastructures, l'économie et l'écosystème de la région.

Figure A.10: Un glissement de terrain recouvre un circuit dans la ville de Nihonmatsu, préfecture de Fukushima, nord-est du Japon, dimanche 14 février 2021. Le fort séisme a secoué les zones sismiques des préfectures de Fukushima et de Miyagi samedi en fin de journée, déclenchant des glissements de terrain et provoquant des coupures de courant pour des milliers de personnes. [Hironori Asakawa/Kyodo News]

D'autre part, les glissements de terrain à évolution lente peuvent avoir des vitesses typiques allant de quelques millimètres à plusieurs mètres par an. Les glissements de terrain lents font rarement des victimes, mais ils peuvent endommager considérablement les infrastructures publiques et privées. Les glissements de terrain lents et persistants

peuvent parfois conduire à une accélération catastrophique ; les glissements de terrain argileux, par exemple, sont sujets à ces transitions. Les solutions traditionnelles de gestion des risques de glissement de terrain consistent à éviter la construction d'infrastructures dans les zones vulnérables en se basant sur les cartes des risques de glissement de terrain, à stabiliser les pentes instables (modification de la géométrie des glissements, drainage de l'eau) et à ériger des structures de protection. Cependant, des infrastructures sont encore construites sur ou à proximité de glissements de terrain majeurs en raison d'un manque de sensibilisation aux risques. La stabilisation des pentes peut s'avérer coûteuse dans de tels cas, et le déplacement de la population vers des endroits plus stables peut générer des problèmes socio-économiques importants. La mise en œuvre d'un système d'alerte précoce (SAP) dans ces scénarios peut aider à prendre des mesures rapides pour réduire les pertes humaines et économiques avant les événements dangereux. Le service de surveillance et d'alerte est un élément essentiel du SAP. Pour l'anticipation/estimation des risques associés au modèle dynamique basé sur la physique des glissements de terrain, la surveillance des glissements de terrain et l'assimilation des données jouent un rôle essentiel.

Notre point de départ est donc que les modèles dynamiques basés sur la physique sont sensibles aux conditions initiales et aux paramètres du système. La simulation d'un modèle et la modification itérative des conditions initiales et des valeurs des paramètres pour obtenir une cohérence avec les données mesurées peuvent rendre compte de ces sensibilités. Une autre méthode efficace peut consister à faire tourner un modèle dans le temps et à l'affiner pour le synchroniser avec les mesures actualisées. Les modèles de glissement de terrain peuvent alors aider à la prévision une fois que ces sensibilités ont été traitées. *En conséquence, ce manuscrit propose une approche interdisciplinaire pour l'étude des glissements de terrain, qui est l'objectif général du projet Risk@UGA, en associant des modèles de glissement de terrain issus de la géophysique et des outils théoriques de contrôle pour la reconstruction de l'information.*

Projet interdisciplinaire "Risk@UGA"

Le travail de doctorat présenté dans cette thèse a été développé dans le cadre d'un projet " Risque " de l'Université Grenoble Alpes. Avec pour devise *"Managing risk for a more resilient world"*, ce projet a été lancé en 2018 pour développer la recherche transversale et l'innovation scientifique dans le domaine de la gestion des catastrophes et des risques, spécifiquement dans les zones rendues vulnérables en raison d'une forte interdépendance entre les humains, les risques naturels ou technologiques. En plus du bassin grenoblois, le projet a abordé sur d'autres territoires vulnérables tels que la région de Beyrouth (Liban), Port-au-Prince (Haïti), ou encore le Pérou et le Népal. Le projet visait également à proposer un institut du risque au sein de l'Université Grenoble Alpes.

Challenges

L'objectif principal du projet était de contribuer à l'atténuation proactive des risques de catastrophe et de développer une culture du risque. Il était dédié à un défi global et régional, fondamental pour les décennies à venir, en raison de l'augmentation de la population mondiale avec une densification souvent anarchique des zones urbanisées, de l'impact croissant de l'homme sur les écosystèmes, mais aussi de l'émergence de nouveaux risques induits par le changement climatique et le développement technologique.

Interdisciplinarité

Le projet a fédéré une centaine de chercheurs appartenant à 15 laboratoires de recherche issus des sciences humaines et sociales, des sciences de l'information et des systèmes, des

géosciences et des sciences de l'ingénieur. Les défis scientifiques que sont la collecte et le traitement de données hétérogènes, la modélisation de phénomènes complexes et en cascade, la prise de décision multi-objectifs, l'évaluation ou la définition de schémas de gouvernance des risques nécessitent des approches véritablement globales et interdisciplinaires.

Organisation du projet

Le projet propose une approche scientifique innovante pour répondre aux défis suivants :

- Gérer l'hétérogénéité des données par une approche participative
- Intégration des événements rares ou émergents et des effets en cascade
- Passer d'une approche statique/réactive de la gestion des risques à une approche proactive/dynamique
- D'une part, concevoir des stratégies appropriées pour la réduction des risques de catastrophes (outre une évaluation pertinente des vulnérabilités et des cultures locales) et pour la communication, d'autre part mieux gérer les risques et renforcer la culture du risque.

Visibilité internationale

Le projet s'inscrivait pleinement dans le cadre de la conférence des Nations Unies de Sendai sur la prévention des risques de catastrophes en 2015, qui encourage les pays à mieux prévenir et à anticiper les risques de catastrophes. Il visait à devenir un interlocuteur privilégié des acteurs de la gestion des risques en France et à l'étranger, notamment sur les cinq sites d'étude sélectionnés (sphère économique, pouvoirs publics, organisations humanitaires, milieu universitaire, ou réseaux de centres de risques). Le projet offre une contribution solide à la fois pour la structure et la visibilité de l'Université Grenoble Alpes en matière d'évaluation et de gestion des risques en proposant un institut de gestion des risques unique en France. Le projet Risk encourage le développement de nouvelles méthodologies interdisciplinaires par les équipes de recherche afin de mieux travailler ensemble et de transférer les résultats de la recherche aux parties prenantes et aux décideurs concernés. Il participe aussi activement au renforcement du cursus interdisciplinaire en gestion des risques.

Question de recherche et objectifs

La principale question de recherche directrice de ce travail a été formulée comme suit:

> *"Comment reconstruire les informations manquantes nécessaires aux modèles de glissement de terrain pour prévoir les mouvements de masse à partir des mesures disponibles ?"*

Pour répondre à cette question, les sous-questions suivantes ont été identifiées:

- Quel est l'état de l'art concernant les différentes techniques de surveillance des glissements de terrain et leurs contraintes en termes de résolution temporelle et spatiale, les

différentes études de modélisation statistique et physique des glissements de terrain, et la variété des outils utilisés pour la reconstruction des informations manquantes (rétroanalyse) à partir des mesures ?

- Qu'est-ce que les outils de contrôle et de systèmes peuvent apporter dans le contexte de cette thèse : l'utilisation d'une apprache hors ligne basée sur l'optimisation, des techniques en ligne basées sur un observateur d'état et des outils de prédiction ?

En réponse aux questions de recherche, le premier objectif de cette thèse est de comprendre les différentes techniques de suivi des glissements de terrain et leurs contraintes. Le second objectif est la sélection de modèles mécaniques de glissements de terrain basés sur les mesures disponibles dans un cadre de système dynamique. Ces deux objectifs constituent l'état de l'art de ce travail. En suivant l'état de l'art sur la surveillance et la modélisation des glissements de terrain, la rétro-analyse (problème inverse) pour l'identification des paramètres inconnus à partir des données disponibles doit être étudiée par une solution basée sur l'optimisation et la conception d'observateurs. Enfin, des approches basées sur des observateurs pour la surveillance dynamique et l'évaluation du mouvement des glissements de terrain doivent être développées sur la base des mesures et des modèles disponibles.

Plan du manuscrit

La structure du manuscrit est la suivante:

- La partie actuelle de la thèse présente un bref aperçu du contexte, du projet transdisciplinaire Risk@UGA, de la question de recherche et des objectifs de la thèse.

- En gardant à l'esprit l'objectif global de la thèse, le chapitre 2 donne un aperçu d'une revue de la littérature sur les différentes techniques de surveillance des glissements de terrain et leurs contraintes, les études de modélisation des glissements de terrain, des modèles statistiques aux modèles physiques, et les techniques d'inversion pour l'identification des paramètres.

- En réponse à la question de recherche sur la reconstruction de l'information, une méthode adjointe basée sur l'optimisation pour l'estimation (paramètres inconnus et condition initiale) dans les modèles de glissement de terrain avec des mesures synthétiques asynchrones en temps discret est proposée dans le chapitre 3. Le système étudié est présenté comme une paire d'équations différentielles ordinaires (ODE) et d'équations différentielles partielles (PDE) couplées. Le multiplicateur de Lagrange est introduit pour relier la dynamique du système et la fonction de coût formulée comme l'erreur des moindres carrés entre les valeurs de simulation et les mesures disponibles. La méthode adjointe est utilisée pour obtenir le système adjoint et les gradients par rapport aux paramètres et à l'état initial. Enfin, la fonction de coût est optimisée à l'aide de la méthode de descente la plus abrupte. Ce chapitre valide la méthode proposée pour l'estimation de l'état et des paramètres à l'aide de deux exemples d'application de glissement de terrain : i) modèle étendu de glissement-consolidation et ii) modèle viscoplastique de glissement-consolidation, et en utilisant des données synthétiques.

- Dans le chapitre 4, comme alternative "continue" à l'approche d'optimisation, un observateur pour l'estimation de l'état et des paramètres dans un modèle étendu de glissement-consolidation est conçu. L'observateur consiste en une copie de la partie PDE du système et en un observateur de type Kalman pour l'ODE. Dans ce

chapitre, l'outil de Lyapunov est utilisé pour assurer la convergence exponentielle des estimations de l'état et des paramètres. À la fin du chapitre, des résultats de simulation sont présentés pour illustrer l'efficacité de l'observateur conçu, toujours sur la base de données synthétiques.

- En considérant un modèle simplifié, une approche par filtre de Kalman pour la reconstruction et la prévision du déplacement des glissements de terrain est présentée au chapitre 5 avec des données synthétiques et de terrain réel (tirées de la littérature). L'observateur proposé s'appuie sur un modèle viscoplastique simplifié de glissement de terrain. Les performances de l'observateur sont améliorées par l'utilisation d'une méthode de réinitialisation, et pour surmonter la sensibilité aux coefficients de l'observateur, une nouvelle méthode de réglage est proposée, qui prend en compte les cas d'essai réels et synthétiques. L'approche est également étendue à la prévision du déplacement des glissements de terrain. En utilisant une approche similaire, certains résultats préliminaires avec les données du glissement de terrain de Hollin Hill sont présentés dans l'annexe A.1.

- Les conclusions générales et les perspectives d'avenir sont enfin présentées dans le chapitre 6.

Liste des publications

1. Mishra, M., Besançon, G., Chambon, G., and Baillet, L. (2021). "Calculus of variations for estimation in ODE-PDE landslide models with discrete-time asynchronous measurements". (soumis dans l'International Journal of Control)

2. Mishra, M., Besançon, G., Chambon, G., and Baillet, L. (2021). "Reconstruction and forecasting of landslide displacement using a Kalman filter approach". (soumis dans le Journal Landslides)

3. Mishra, M., Besançon, G., Chambon, G., and Baillet, L. (2021). "Combined state and parameter estimation for a landslide model using Kalman filter". 19th IFAC Symposium on System Identification SYSID 2021, 54(7), 304-309.

4. Mishra, M., Besançon, G., Chambon, G., Baillet, L., Watlet, A., Whiteley, J. S., Boyd, J. P., and Chambers, J. E. (2021). "Application of Kalman filter to reproduce displacement pattern along with the unknown soil properties of slow-moving landslides". EGU General Assembly 2021, Online, 19-30 Apr 2021, EGU21-9396, doi:10.5194/egusphere-egu21-9396.

5. Mishra, M., Besançon, G., Chambon, G., and Baillet, L. (2020). "Observer design for state and parameter estimation in a landslide model". 21th IFAC World Congress, 53(2), 16709-16714, doi:10.1016/j.ifacol.2020.12.1116.

6. Mishra, M., Besançon, G., Chambon, G., and Baillet, L. (2020). "Optimal parameter estimation in a landslide motion model using the adjoint method". In 2020 European Control Conference (ECC), 226-231, doi:10.23919 ECC51009.2020.9143819.

Notez que les chapitres 3, 4, 5 étant fortement basés sur certains des articles ci-dessus, ils sont présentés de manière autonome.

Modeling and information reconstruction from landslide monitoring data

Résumé

Un glissement de terrain est un mouvement sur pente descendante d'une partie du sol, de débris, ou de roche de surface, entraîné par la gravité. On peut trouver une certaine hétérogénéité dans les mouvements de ce type, comme dans leurs vitesses d'évolution, allant du glissement lent à l'accélération catastrophique. Ces deux scénarios constituent une menace pour la population, les infrastructures, l'écosystème et l'économie de la région exposée. La stratégie traditionnelle de gestion des risques de glissement de terrain suggère d'éviter de construire de nouvelles infrastructures dans une telle région sur la base de cartes des aléas. Cependant, avec le changement climatique et l'urbanisation rapide, cette stratégie semble difficile à tenir. Par conséquent, les Systèmes d'Alerte Précoce (SAP) sont la voie à suivre pour prendre des mesures correctives en temps opportun afin de réduire les pertes en vies humaines et économiques. Ces SAP s'appuient sur des systèmes de surveillance des glissements de terrain, des modèles de glissements de terrain, et des algorithmes de reconstruction d'informations. Dans ce contexte difficile de surveillance et de prévision des glissements de terrain, le travail présenté dans cette thèse vise à définir un modèle dynamique des glissements de terrain basé sur la physique, développer des méthodes d'identification des paramètres inconnus, et contribuer à l'évaluation des risques par des techniques d'observateurs à partir des mesures disponibles. Cela nécessite une approche multidisciplinaire, s'appuyant ici sur des concepts issus d'une part de la géophysique et d'autre part de la théorie du contrôle, pour la définition d la structure du modèle et les méthodes de résolution des problèmes d'observateurs (ou d'identification des paramètres), respectivement. En bref, l'idée est d'analyser les changements dans les variables de glissement de terrain et dans les paramètres mécaniques avant ou pendant un mouvement.

Mots-clés : Dynamique des glissements de terrain, Système ODE-PDE couplé, Estimation d'état et de paramètres, Optimisation, Mesures asynchrones en temps discret, Filtre de Kalman, Conception d'observateur, Réglage d'observateur, Prédiction de déplacement

Abstract

Landslide is a gravity-driven downslope movement of soil, debris, or rock near the earth's surface. It can display heterogeneity in rates and movement types, ranging from creeping motion to catastrophic acceleration. Both scenarios pose a threat to the exposed region's people, infrastructure, ecosystem, and economy. Traditional landslide risk management strategy suggests avoiding building new infrastructure in such a region based on hazard maps. However, with climate change and rapid urbanization, this strategy seems challenging to implement. Therefore, Early Warning Systems (EWS) are way forward to take timely corrective measures to reduce life and economic losses. These EWS's rely on landslide monitoring systems, landslide models, and information reconstruction schemes. In this challenging context of landslide monitoring and forecasting, the present work aims to define a physics-based dynamical model of landslides, unknown parameters identification, and observer-based hazard evaluation from available measurements. This requires a multi-disciplinary approach, i.e., concepts from geophysics on the one hand and control theory on the other hand, for model structure definition and solution methods for observer problems (or parameter identification), respectively. In short, the idea is to analyze the changes in landslide variables and mechanical parameters prior to or while in a motion.

Keywords : Landslide dynamics, Coupled ODE-PDE system, State and parameter estimation, Optimization, Discrete-time asynchronous measurements, Observer design, Kalman filter, Observer tuning, Displacement forecasting